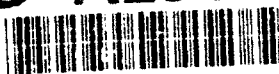


AD-A284 193

Dist: -A

		Form Approved OMB No. 0704-0188	
<small>Public reporting burden for this document is estimated to average 1 hour per response, including the time for reviewing instructions, searching existing data sources, gathering and maintaining the data needed, reviewing existing data sources, and completing and reviewing the collection of information. Send comments regarding this burden estimate or any other aspect of this collection of information, including suggestions for reducing this burden, to Washington Headquarters Services, Directorate for Information Operations and Reports, 1215 Jefferson Davis Highway, Suite 1204, Arlington, VA 22202-4302, and to the Office of Management and Budget, Paperwork Reduction Project (0704-0188), Washington, DC 20503.</small>			
1. AGENCY USE ONLY (Leave blank)		2. REPORT DATE 30 June 94	
		3. REPORT TYPE AND DATES COVERED Annual Technical, 1 June 93- 31 May 94	
4. TITLE AND SUBTITLE Characterization of heterogeneities controlling transport and fate of pollutants in unconsolidated sand and gravel aquifers: Third year report		5. FUNDING NUMBERS  G  AFOSR-91-0298 3484-D-7	
6. AUTHOR(S)  C. D. McElwee and J. J. Butler, Jr.		7. PERFORMING ORGANIZATION NAME(S) AND ADDRESS(ES) Kansas Geological Survey The University of Kansas 1930 Constant Avenue Lawrence, KS	
8. SPONSORING/MONITORING AGENCY NAME(S) AND ADDRESS(ES) AFOSR/NL Building 410 Bolling AFB DC 20332-6448		9. PERFORMING ORGANIZATION REPORT NUMBER KGS OFR 94-32 AFOSR-TR-94 0474	
10. SUPPLEMENTARY NOTES		11. SPONSORING/MONITORING AGENCY REPORT NUMBER AFOSR - 91-0298	
12a. DISTRIBUTION / AVAILABILITY STATEMENT Available from Publication Office of Kansas Geological Survey  A		12b. DISTRIBUTION CODE  OFR 94-32	
13. ABSTRACT (Maximum 200 words) The purpose of this project is to evaluate promising methodologies for characterization of heterogeneities in hydraulic conductivity. The major thrusts of this year's work were an assessment of well tests in heterogeneous formations and preparation for a series of induced-gradient tracer tests. The theoretical components of this effort included development of a general model for slug tests in partially penetrating wells, an assessment of the viability of conventional slug-test methods, modeling investigations of pulse tests in heterogeneous formations, and an analysis of appropriate designs for a tracer-test monitoring well array. The field component of this work emphasized slug tests. Practical guidelines for the design, performance, and analysis of slug tests, which should considerably improve the quality of resulting parameter estimates, have been proposed. A unified slug-test model incorporating the effects of nonlinearities, inertia, viscosity, changing casing radii, and velocity distributions has been developed to explain anomalous data from wells in formations of high hydraulic conductivity. Additional field work included drilling and sampling activities; laboratory analysis of sampled cores; an aqueous geochemistry study; construction and installation of multilevel sampling wells; and experimentation with a new single-well tracer test method. Overall, the research of year three produced results of considerable practical significance.			
14. SUBJECT TERMS Heterogeneities, alluvial aquifers, slug tests, site characterization, pollutant transport, pulse testing		15. NUMBER OF PAGES 237	
16. SECURITY CLASSIFICATION OF REPORT U		17. SECURITY CLASSIFICATION OF THIS PAGE U	
18. SECURITY CLASSIFICATION OF ABSTRACT U		19. LIMITATION OF ABSTRACT	

NSN 7540-01-280-5500

DTIC QUALITY INSPECTED 3

Standard Form 298 (Rev. 2-89)  
Prescribed by ANSI Std. Z39-18  
298-102

CHARACTERIZATION OF HETEROGENEITIES CONTROLLING TRANSPORT  
AND FATE  
OF POLLUTANTS IN UNCONSOLIDATED SAND AND GRAVEL AQUIFERS:  
THIRD YEAR REPORT

A research project of the  
University Research Initiative  
Research Initiation Program  
U.S. Department of Defense

Carl D. McElwee and James J. Butler, Jr.  
Kansas Geological Survey  
The University of Kansas

with

Gwendolyn L. Macpherson  
Department of Geology  
The University of Kansas

Geoffrey C. Bohling, Christine M. Mennicke, Terrance Huettl  
Matthias Zenner, Zafar Hyder, Wenzhi Liu, and Micheal Orcutt  
Kansas Geological Survey  
The University of Kansas

Accession For	
NTIS CRA&I	✓
DTIC TAB	
Unannounced	
Justification	
By	
Distribution /	
Availability Codes	
Dist	Avail and/or Special
A-1	

236107

94-29075



June, 1994

DTIC QUALITY INSPECTED 3

94 9 06 106

## ABSTRACT

A considerable body of research has shown that large-scale spatial variations (heterogeneities) in hydraulic conductivity play an important role in controlling the movement of a contaminant plume in the subsurface. Quantifying these heterogeneities, however, can be a very difficult task. If we are to improve our capabilities for predicting the fate and transport of pollutants in the subsurface, it is critical that we develop methodology that enables a more accurate characterization of hydraulic conductivity variations to be obtained. The purpose of the research of this project is to evaluate, through both theoretical and field experiments, promising methodologies for the characterization of heterogeneities in hydraulic conductivity.

As with earlier years of this research, a major focus of the work during year three was an assessment of the type of information that can be obtained from well tests in heterogeneous formations. This effort had both theoretical and field components. The theoretical components included further development of a semianalytical solution to a general mathematical model describing the flow of groundwater in response to a slug test in a porous formation, the use of this model to assess the viability of conventional methods for the analysis of response data from slug tests, and analytical and numerical modeling investigations of the viability of pulse testing in radially nonuniform formations. Although the pulse testing work is still of a rather preliminary nature, results of considerable practical significance were obtained from the theoretical analyses using the new slug-test solution.

The field components of this study of well tests in heterogeneous formations again concentrated on slug tests. Although the slug test has the potential to provide very useful information about the transmissive and storage properties of a formation, considerable care must be given to all phases of test design, performance, and analysis if the potential of the technique is to be fully realized. In an attempt to improve the reliability of parameter estimates obtained from a program of slug tests, a series of practical guidelines for slug tests were proposed on the basis of the field and theoretical investigations of this research. Results of slug tests at most of the wells in the alluvial aquifer at the Geohydrologic Experimental and Monitoring Site (GEMS) indicate that tests in the sand and gravel section at GEMS are being affected by mechanisms not accounted for in the conventional theory on which the standard methods for slug-test data analysis are based. We have developed a general unified model incorporating the effects of nonlinearities, inertia, viscosity, changing casing radii, and velocity distributions to

explain the anomalous behavior observed at GEMS. Application of this model to several sets of data from slug tests at GEMS produced very promising results.

A sizable component of research efforts this year was directed at preparations for a series of induced-gradient tracer test that will complete this phase of our research on the characterization of spatial variations in hydraulic conductivity. Twenty-four multilevel sampling wells (17 sampling ports per well) were constructed and fifteen of these wells were installed during an intensive field effort. Sampling well locations were based on a theoretical investigation of appropriate designs for the tracer-test monitoring well array. Various designs were assessed using a numerical streamline-tracing algorithm that was coupled with an analytical solution describing conservative transport along streamlines.

As in the first two years of this research, a significant amount of the work in year three was directed at increasing our knowledge of the subsurface at GEMS. This work included continued drilling and sampling activities at GEMS; continued laboratory analysis of the cores obtained with the KGS bladder sampler; a continuing study of the aqueous geochemistry of the alluvium and underlying bedrock at GEMS; and experimentation with a new single-well tracer test method that involves using a wireline logging system and an electrically conductive tracer to delineate vertical variations in hydraulic conductivity and porosity. These characterization efforts, which have continued throughout this project, are directed towards the development of a detailed picture of the subsurface at GEMS, so that we can better assess the results of the hydraulic and tracer tests that are being performed as part of this research.

A considerable amount of acquisition, construction, and modification of equipment took place during the third year of this project in support of the research effort. The equipment included a high capacity air compressor for pumping small-diameter wells, two 10-channel peristaltic pumps for water-quality sampling, a field cart to hold the peristaltic pumps and associated equipment during sampling, a well-head apparatus for the performance of pressurized slug tests, and three additional computers for data processing and analysis. In addition, as a result of the prolonged waterlogging of GEMS that occurred due to the heavy rains in the spring and summer of 1993, access to all portions of GEMS was significantly improved during this year.

An extension period has been requested to complete this phase of our research on the characterization of spatial variations in hydraulic conductivity. Tasks to be completed during this extension period include the following: the performance of a series of induced-gradient tracer tests at GEMS, the completion of the laboratory analysis of all remaining core samples from the site, the completion of the field verification of the



general unified model for the analysis of slug tests performed in high conductivity formations, and the completion of the first phase of the field investigation of pulse tests.

The research team for this project is composed of professional staff from the Kansas Geological Survey and the Department of Geology of the University of Kansas. One indication of the level of activity of this research team is the four peer-reviewed publications concerning this research that were accepted or published during the period covered by this report. Additional manuscripts are currently undergoing peer review. Three graduate students (two funded by this project) and one KGS staff member are using aspects of the work of this project for their thesis research. Additional graduate students are benefitting from this project as a result of the establishment of a computer laboratory for graduate students in hydrogeology and the incorporation of material from this work into courses at the University of Kansas taught by members of the research team.

#### **Acknowledgment**

This research was sponsored in part by the Air Force Office of Scientific Research, Air Force Systems Command, USAF, under grant number AFOSR 91-0298. The views and conclusions contained in this document are those of the authors and should not be interpreted as necessarily representing the official policies, either expressed or implied, of the Air Force Office of Scientific Research or of the U.S. Government. The U.S. Government is authorized to reproduce and distribute reprints for Governmental purposes notwithstanding any copyright notation thereon.

## **TABLE OF CONTENTS\***

### **I. INTRODUCTION**

- A. Research Objectives**
- B. Brief Outline of Report**

### **II. THEORETICAL INVESTIGATIONS OF WELL TESTS**

#### **IN HETEROGENEOUS MEDIA**

- A. Slug Tests in Partially Penetrating Wells**
- B. Pulse-Testing in Heterogenous Formations**
- C. Numerical Simulation of Induced Gradient Tracer Tests**

### **III. FIELD INVESTIGATIONS OF MULTILEVEL SLUG TESTS**

- A. Improving the Reliability of Parameter Estimates Obtained From Slug Tests**
- B. A General Nonlinear Model for Analysis of Slug-Test Data**

### **IV. SITE CHARACTERIZATION ACTIVITIES**

- A. Drilling and Sampling Activities**
- B. Laboratory Activities**
- C. Aqueous Geochemistry at GEMS**
- D. Wireline Logging Activities-An Evaluation of a Borehole Induction Single-Well Tracer Test to Characterize the Distribution of Hydraulic Properties in an Alluvial Aquifer**

### **V. CONSTRUCTION PROJECTS AND EQUIPMENT PURCHASES**

### **VI. PERSONNEL AND PRODUCTIVITY ISSUES**

- A. Published and Planned Papers**
- B. List of Participating Personnel**
- C. Interactions With Other Research Groups**
- D. Teaching Activities**

### **VII. SUMMARY OF YEAR THREE RESEARCH AND OUTLOOK FOR THE EXTENSION PRIOD**

- A. Summary of Research in Year Three**
- B. Outlook for Research in the Extension Period**

### **VIII. REFERENCES**

### **IX. APPENDICES**

- A. Derivation of Partially Penetrating Slug-Test Solution**
- B. Numerical Inversion Procedures**

\* - Note that pages are numbered according to section and subsection.

## I. INTRODUCTION

### A. RESEARCH OBJECTIVES

The accurate prediction of the transport and fate of pollutants in aquifers is one of the most difficult and pressing problems in hydrogeology today. Physical, chemical, and microbial processes all play major roles in controlling contaminant movement in the subsurface. Before we can begin to understand the influence of the chemical and biological side of this problem, however, we must fully understand the role of physical processes and, specifically, the influence of the physical hydrogeological properties. Many researchers now recognize (e.g., Molz et al., 1989) that if we are to improve our predictive capabilities for subsurface transport, we must first improve our capabilities for measuring and describing conditions in the subsurface. That is the focus of the research described in this report. The specific objective of this research is to assess the potential of advanced well-testing technology for providing more accurate estimates of spatial variations in the physical properties that control contaminant plume movement in saturated porous media. Although effective porosity is clearly an important consideration, the major emphasis of this work is on characterizing spatial variations (heterogeneities) in hydraulic conductivity.

Ideally, heterogeneities in hydraulic conductivity must be studied and characterized at several different scales in order to understand their influence on the movement of a contaminant plume. Although theoretical modeling work is an important element of any study of the influence of spatial variations in hydraulic conductivity on contaminant movement, a rigorous study of this subject must have a major field component. A field site at which researchers at the University of Kansas can pursue work on the effects of heterogeneities in flow properties on subsurface transport has been set up as part of this research. The specific site of the field effort is the Geohydrologic Experimental and Monitoring Site (GEMS), which is located just north of Lawrence, Kansas on land owned by the University of Kansas Endowment Association. Figure 1 is a map showing the location of GEMS and some of the major features at the site. GEMS overlies approximately 70 feet (21.3 m) of Kansas River valley alluvium. These recent unconsolidated sediments overlie and are adjacent to materials of Pleistocene and Pennsylvanian age. A cross-sectional view of the subsurface at one of the well nests at GEMS is shown in Figure 2. The alluvial facies assemblage at this site consists of approximately 35 feet (10.7 m) of clay and silt overlying 35 feet (10.7 m) of sand and gravel. The stratigraphy is a complex system of stream-channel sand and overbank deposits. The general nature of the stratigraphy would lead one to expect that a

considerable degree of lateral and vertical heterogeneity in hydraulic conductivity would be found in the subsurface at GEMS. Although analyses of sampled cores do indicate considerable variability in hydraulic conductivity within the sand and gravel interval, it is not yet clear how the variability at the small scale of a core translates into variability at larger scales.

In the third year of this research, a large amount of work was again directed at the use of slug tests to describe spatial variations in hydraulic conductivity. The analysis of response data from slug tests at GEMS has turned out to be considerably more challenging than expected. It is clear from our work that conventional methodology for the analysis of slug-test data is not adequate when dealing with very high conductivity media, wells that are only partially screened across an anisotropic formation, wells with disturbed zones created by drilling or development activities, and layered media. Since the slug test has become the most common technique for estimation of hydraulic conductivity at sites of groundwater contamination, we have expended much more effort on this phase of the project than was originally anticipated. However, this research has produced a number of very interesting results of practical significance, so we feel that it has been a profitable redirection of effort. Probably the result of most practical significance has been the definition of a series of guidelines for the design, performance, and analysis of slug tests that should considerably improve the quality of parameter estimates obtained using this technique.

As a result of the redirection of our efforts, the work on pulse tests has not progressed as far as originally expected. Last year, we started work on pulse tests in three areas: 1) multiwell slug tests, where the excitation consists of a single pulse (slug); 2) hydraulic tomography in a steady-state flow field; and 3) an analytical solution for propagation of sinusoidal signals in heterogeneous formations. In the third year of this research, we continued a theoretical investigation of the use of pulse tests in heterogeneous aquifers. Both analytical and numerical approaches were explored in an attempt to assess whether discrete zones in heterogeneous formations could be characterized with pulsing (sinusoidally varying) signals.

This year, a considerable amount of additional work has again been directed at increasing our knowledge of the subsurface at GEMS. This effort has involved continued drilling and sampling of the alluvium at GEMS, continued laboratory analysis of sampled cores, further analysis of the aqueous geochemistry at GEMS, and experimentation with a new single-well tracer test method that involves using a wireline logging system and an electrically conductive tracer to delineate vertical variations in hydraulic conductivity and porosity. These characterization efforts are directed at providing the detailed information

that will allow us to better assess the quality of the information provided by the various well-testing approaches evaluated in this work. The ultimate goal of these characterization efforts is to describe the site in enough detail that it effectively becomes an underground laboratory at which new technology can be evaluated.

A sizable component of our activities this year was directed at preparations for the series of induced-gradient tracer tests that will occur in the final phase of this research. These activities included the construction of twenty four multilevel sampling wells (17 sampling ports per well), a theoretical investigation of the appropriate design for the tracer-test monitoring well array, and an intensive field effort to install the multilevel sampling wells. Fifteen of the twenty four multilevel sampling wells have now been installed and developed. The remaining nine wells will be installed in the near future.

## **B. BRIEF OUTLINE OF REPORT**

The remainder of this report is divided into six major sections, each of which is essentially a self-contained unit. Pages, figures, and equations are labelled by section and, when warranted, by subsection for the convenience of the reader. Note that a number of the subsections of this report are essentially the text of articles that have been or will shortly be submitted for publication.

Section II describes theoretical work directed at developing a better understanding of the type of information that can be obtained from a variety of field techniques applied in heterogeneous media. The first subsection deals with slug tests in partially penetrating wells. The second subsection assesses the viability of pulse testing using a sinusoidally varying signal for the investigation of heterogeneous formations. The final subsection summarizes our activities directed at the design of a monitoring well array for the planned series of induced-gradient tracer tests.

Section III primarily describes further field investigations using slug tests. The first subsection summarizes many of the conclusions of our field and theoretical research on slug tests. The main goal of this subsection is to present a series of practical field guidelines that should help improve the reliability of parameter estimates obtained from slug tests. In the second subsection, a general nonlinear model for slug tests that accounts for the major mechanisms thought to be affecting the GEMS slug-test data is presented. The application of this model to several sets of data from slug tests at GEMS demonstrates the potential of the approach.

Section IV primarily describes activities directed at increasing our knowledge of the subsurface at GEMS. After a description of the drilling and sampling activities that occurred over the last year at GEMS, work in the KGS core measurement laboratory is

discussed. Further results of the aqueous geochemistry study at GEMS are described in the third subsection. The section concludes with a report on experiments with a new single-well tracer test method using a wireline logging system and an electrically conductive tracer to delineate vertical variations in hydraulic conductivity and effective porosity.

Section V describes new equipment that was built or purchased during the third year of this project and how it enhances various aspects of the research.

Section VI describes the personnel of the research team that has been organized to pursue this work, and lists relevant publications of the team over the last year. The section concludes with a discussion of the interactions with other research groups and teaching activities that have occurred during the last year.

Section VII summarizes the research of this report and briefly outlines the work planned for the requested extension period.

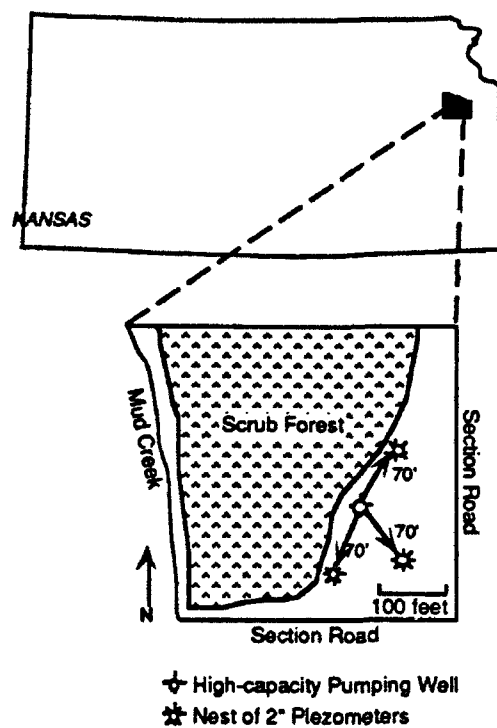


Figure 1 - Location map for the Geohydrologic Experimental and Monitoring Site (GEMS).

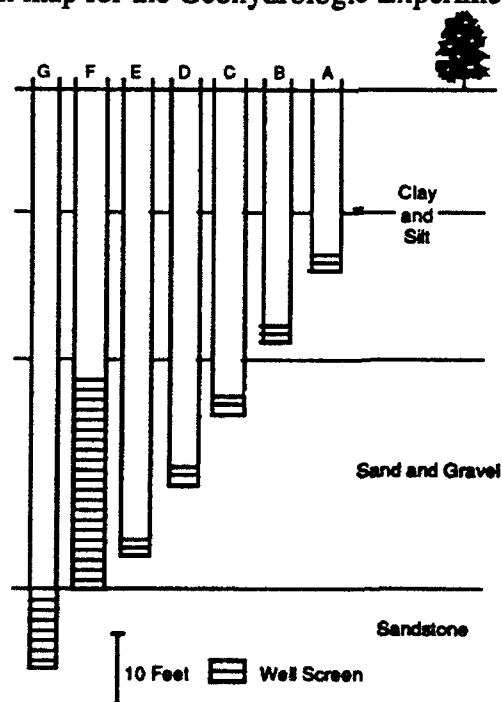


Figure 2. A typical well nest cross-section

## **II. THEORETICAL INVESTIGATIONS OF WELL TESTS IN HETEROGENEOUS MEDIA**

### **A. SLUG TESTS IN PARTIALLY PENETRATING WELLS**

#### **Abstract**

In this section, a semianalytical solution to a mathematical model describing the flow of groundwater in response to a slug test in a confined or unconfined porous formation is presented. The model incorporates the effects of partial penetration, anisotropy, finite-radius well skins, and upper and lower boundaries of either a constant-head or an impermeable form. This model is employed to assess the magnitude of the error that is introduced into hydraulic conductivity estimates through use of currently accepted practices (i.e. Hvorslev (1951) and Cooper et al. (1967)) for the analysis of slug-test response data. The magnitude of the error arising in a variety of commonly faced field configurations is the basis for practical guidelines for the analysis of slug-test data that can be utilized by field practitioners.

#### **Introduction**

The slug test is one of the most commonly used techniques by hydrogeologists for estimating hydraulic conductivity in the field (Kruseman and de Ridder, 1989). This technique, which is quite simple in practice, consists of measuring the recovery of head in a well after a near instantaneous change in water level at that well. Approaches for the analysis of the recovery data collected during a slug test are based on analytical solutions to mathematical models describing the flow of groundwater to/from the test well. Over the last thirty years, solutions have been developed for a number of test configurations commonly found in the field. Chirlin (1990) summarizes much of this past work.

In terms of slug tests in confined aquifers, one of the earliest proposed solutions was that of Hvorslev (1951), which is based on a series of simplifying assumptions concerning the slug-induced flow system (e.g., negligible specific storage, finite effective radius, etc.). Much of the work following Hvorslev has been directed at removing one or more of these simplifying assumptions. Cooper et al. (1967) developed a fully transient solution for the case of a slug test in a well fully screened across a confined aquifer. Moench and Hsieh (1985) extended the solution of Cooper et al. to the case of a fully penetrating well with a finite radius well skin. A number of workers (e.g., Dougherty and Babu, 1984; Hayashi et al., 1987) have developed solutions for slug tests



in wells partially penetrating isotropic, confined aquifers. Butler and McElwee (1990) presented a solution for slug tests in wells partially penetrating confined aquifers that incorporates the effects of anisotropy and a finite-radius skin at the test well. In most field applications, the methods of Hvorslev (1951) or Cooper et al. (1967) are employed. The error that is introduced into hydraulic conductivity estimates by employing these models in conditions where their assumptions are inappropriate has not yet been fully evaluated. Note that Nguyen and Pinder (1984) proposed a method for the analysis of data from slug tests in wells partially penetrating confined aquifers that has received a fair amount of use. Recently, however, Butler and Hyder (1993) have shown that the parameter estimates obtained using this approach must be viewed with considerable skepticism owing to an error in the analytical solution upon which the model is based.

In terms of slug tests in unconfined aquifers, solutions for the mathematical model describing flow in response to the induced disturbance are difficult to obtain because of the nonlinear nature of the model in its most general form. Currently, most field practitioners use the technique of Bouwer and Rice (Bouwer and Rice, 1976; Bouwer, 1989), which employs empirical relationships developed from steady-state simulations using an electrical analog model, for the analysis of slug tests in unconfined flow systems. Dagan (1978) presents an analytical solution based on assumptions similar to those of Bouwer and Rice (1976). Amoozegar and Warrick (1986) summarize related methods employed by agricultural engineers. All of these techniques result from the application of several simplifying assumptions to the mathematical description of flow to a well in an unconfined aquifer (e.g., negligible specific storage, finite effective radius, representation of the water table as a constant-head boundary, etc.). As with the confined case, the ramifications of these assumptions have not yet been fully evaluated.

In this paper, a semianalytical solution to a mathematical model describing the flow of groundwater in response to an instantaneous change in water level at a well screened in a porous formation is presented. The model incorporates the effects of partial penetration, anisotropy, finite-radius well skins of either higher or lower permeability than the formation as a whole, and upper and lower boundaries of either a constant-head or an impermeable form. This model can be employed for the analysis of data from slug tests in a wide variety of commonly met field configurations in both confined and unconfined formations. Although packers are not explicitly included in the formulation, earlier numerical work has shown that such a model can also be used for the analysis of multilevel slug-test data when packers of moderate length (0.75 meters or longer) are employed (e.g., Bliss and Rushton, 1984; Butler et al., 1994a).

The major purpose of this paper is to use this solution to quantify the error that

is introduced into parameter estimates as a result of using currently accepted practices for the analysis of response data from slug tests. The magnitude of the error arising in a variety of commonly met field configurations will serve as the basis for practical guidelines that can be utilized by field practitioners. Although such an investigation of parameter error could be carried out using either a numerical or analytical model, the analytical model described in the previous paragraph is employed here in order to provide a convenient alternative for data analysis when the error introduced by conventional approaches is deemed too large for a particular application.

### Statement of Problem

The problem of interest here is that of the head response, as a function of  $r$ ,  $z$ , and  $t$ , produced by the instantaneous introduction of a pressure disturbance into the screened or open section of a well. For the purposes of this initial development, the well will be assumed to be located in the confined aquifer shown in Figure II.A.1. Note that, as shown on Figure II.A.1, there is a well skin of radius  $r_w$  that extends through the full thickness of the aquifer. The skin has transmissive and storage properties that may differ from the formation as a whole. Flow properties are assumed uniform within both the skin and formation, although the vertical ( $K_z$ ) and radial ( $K_r$ ) components of hydraulic conductivity may differ.

The partial differential equation representing the flow of groundwater in response to an instantaneous change in water level at a central well screened in a porous formation is the same for both the skin and the aquifer and can be written as

$$\frac{\partial^2 h_i}{\partial r^2} + \frac{1}{r} \frac{\partial h_i}{\partial r} + \left( \frac{K_{zi}}{K_{ri}} \right) \frac{\partial^2 h_i}{\partial z^2} = \left( \frac{S_{wi}}{K_{ri}} \right) \frac{\partial h_i}{\partial t} \quad (1)$$

where

$h_i$  = head in zone  $i$ , [L];

$S_{wi}$  = specific storage of zone  $i$ , [1/L];

$K_{zi}$ ,  $K_{ri}$  = vertical and radial components, respectively, of the hydraulic conductivity of zone  $i$ , [L/T];

$t$  = time, [T];

$r$  = radial direction, [L];

$z$  = vertical direction,  $z=0$  at the top of the aquifer and increases downward, [L];

$i$  = zone designator, for  $r \leq r_w$ ,  $i=1$ , and for  $r_w \leq r$ ,  $i=2$ ;

$r_w$  = screen radius, [L];  
 $r_s$  = outer radius of skin, [L].

The initial conditions can be written as

$$h_1(r, z, 0) = h_2(r, z, 0) = 0, \quad r_w < r < \infty, \quad 0 \leq z \leq B \quad (2)$$

$$\begin{aligned} h_1(r_w, z, 0) &= H_0, \quad d \leq z \leq d+b \\ &= 0, \quad \text{elsewhere} \end{aligned} \quad (3)$$

where

$B$  = aquifer thickness, [L];

$H_0$  = height of initial slug, equal to level of water in well at  $t=0$  ( $H(0)$ ), [L];

$d$  = distance from the top of the aquifer to the top of the screen, [L];

$b$  = screen length, [L].

The boundary conditions are the following:

$$h_2(\infty, z, t) = 0, \quad t > 0, \quad 0 \leq z \leq B \quad (4)$$

$$\frac{\partial h_1(r, 0, t)}{\partial z} = \frac{\partial h_1(r, B, t)}{\partial z} = 0, \quad r_w < r < \infty, \quad t > 0 \quad (5)$$

$$\frac{1}{b} \int_d^{d+b} h_1(r_w, z, t) dz = H(t), \quad t > 0 \quad (6)$$

$$2\pi r_w K_{r1} \frac{\partial h_1(r_w, z, t)}{\partial r} = \frac{\pi r_c^2}{b} \frac{dH(t)}{dt} \square(z), \quad t > 0 \quad (7)$$

where

$r_c$  = radius of well casing, casing and screen do not have to be of equal radius, [L];

$\square(z)$  = boxcar function = 0,  $z < d$ ,  $z > b+d$ ,  
= 1, elsewhere;

$H(t)$  = level of water in well, [L].

In order to ensure continuity of flow between the skin and the formation, auxiliary conditions at the skin-formation boundary ( $r=r_{sk}$ ) must also be met:

$$h_1(r_{sk}, z, t) = h_2(r_{sk}, z, t), \quad 0 \leq z \leq B, \quad t > 0 \quad (8)$$

$$K_{r1} \frac{\partial h_1(r_{sk}, z, t)}{\partial r} = K_{r2} \frac{\partial h_2(r_{sk}, z, t)}{\partial r}, \quad 0 \leq z \leq B, \quad t > 0 \quad (9)$$

Equations (1)-(9) approximate the flow conditions of interest here. Appendix A provides the details of the solution derivation. In summary, the approach employs a series of integral transforms (Laplace transform in time and a finite Fourier cosine transform in the  $z$  direction) to obtain functions in transform space that satisfy the transform-space analogues of (1)-(9). The transform-space function that is obtained for the head in a partially penetrating well with a finite-radius well skin in an anisotropic confined aquifer can be written in a non-dimensional form as

$$\Phi(p) = \frac{\frac{\gamma}{\alpha} \Omega}{[1 + \frac{\gamma}{\alpha} p \Omega]} \quad (10)$$

where

$\Phi(p)$  = the nondimensional Laplace transform of  $H(t)$ ;

$p$  = Laplace-transform variable;

$$\alpha = (2r_w^2 S_{s2} b) / r_c^2;$$

$$\gamma = K_{s2} / K_{s1};$$

$$\Omega = \int_{\zeta}^{\zeta+1} (F_c^{-1}(F_c(\omega) f_1)) d\eta;$$

$\omega$  = Fourier-transform variable;

$F_c(\omega)$  = finite Fourier cosine transform of  $\square(z)$ ;

$F_c^{-1}$  = inverse finite Fourier cosine transform;

$$f_1 = \frac{[\Delta_2 K_0(v_1) - \Delta_1 I_0(v_1)]}{v_1 [\Delta_2 K_1(v_1) + \Delta_1 I_1(v_1)]};$$

$$\eta = z/b;$$

$$\zeta = d/b;$$

$$v_i = (\psi_i^2 \omega^2 + R_i p)^{1/2};$$

$$\psi_i = (A_i / a^2)^{1/2};$$

$$A_i = K_{s2} / K_{si};$$

$$a = b / r_w;$$

$$R_i = \gamma \alpha / 2\lambda, i = 1,$$

$$= \alpha / 2, i = 2;$$

$$\lambda = S_{s2} / S_{s1};$$

$$\Delta_1 = K_0(v_1 \xi_{sk}) K_1(v_2 \xi_{sk}) - \left[ \frac{N}{\gamma} \right] K_0(v_2 \xi_{sk}) K_1(v_1 \xi_{sk});$$

$$\Delta_2 = I_0(v_1 \xi_{sk}) K_1(v_2 \xi_{sk}) + \left[ \frac{N}{\gamma} \right] K_0(v_2 \xi_{sk}) I_1(v_1 \xi_{sk});$$

$$N = v_1 / v_2;$$

$$\xi_{w,1} = r_w/r_w$$

For the unconfined case, the upper no-flow boundary condition in eqn. (5) is changed into a constant-head boundary condition, so the upper and lower boundary conditions are rewritten as:

$$h_1(r, 0, t) = 0, \quad r_w < r < \infty, \quad t > 0 \quad (11)$$

$$\frac{\partial h_1(r, B, t)}{\partial z} = 0, \quad r_w < r < \infty, \quad t > 0 \quad (12)$$

Appendix A also provides the details of the solution derivation for the unconfined case. The transform-space function that is obtained for the head in a partially penetrating well with a finite-radius well skin in an anisotropic unconfined aquifer can be written in a non-dimensional form as

$$\Phi_{uc}(p) = \frac{\frac{\gamma}{\alpha} \Omega^*}{[1 + \frac{\gamma}{\alpha} p \Omega^*]} \quad (13)$$

where

$\Phi_{uc}(p)$  = the Laplace transform of the nondimensional form of  $H(t)$  for the unconfined case;

$$\Omega^* = \int_{\xi}^{\xi+1} (F_s^{-1}(F_s(\omega^*)f_1))d\eta;$$

$F_s(\omega^*)$  = modified finite Fourier sine transform of  $\square(z)$ ;

$\omega^*$  = Fourier transform variable for the modified sine transform.

For expressions of the complexity of (10) and (13), the analytical back transformation from transform space to real space is only readily performed under quite limited conditions. In the general case, the transformation is best performed numerically. Numerical evaluation of the Fourier transforms and their inversions were done here using Discrete Fourier Transforms (Brigham, 1974), thereby allowing computationally efficient

Fast Fourier Transform techniques (Cooley and Tukey, 1965) to be utilized. This approach, which is briefly outlined in Appendix B, did not introduce significant error into the inversion procedure. An algorithm developed by Stehfest (1970), which has been found to be of great use in hydrologic applications (Moench and Ogata, 1984), was employed to perform the numerical Laplace inversion.

Several checks were performed in order to verify that (10) and (13) are solutions to the mathematical model outlined here. Substitution of (10) and (13) into the respective transform-space analogues of (1)-(9) and (11)-(12) demonstrated that the proposed solutions honor the governing equation and auxiliary conditions in all cases. In addition, if the test well is assumed to be fully screened across an isotropic, confined aquifer, (10) reduces to the Laplace-space form of the solution of Moench and Hsieh (1985). Likewise, in the no-skin case, (10) reduces to the Laplace-space form of the solution of Cooper et al. (1967). Similarly, if the test well is assumed to be partially screened across an isotropic, confined aquifer, (10) reduces to the Laplace-space form (eqn. (62)) of the solution of Dougherty and Babu (1984). Butler et al. (1993b) describe additional checks performed with a numerical model to verify the solutions proposed here.

### **Ramifications for Data Analysis**

As discussed in the Introduction, the primary purpose of this paper is to evaluate the error that is introduced into parameter estimates through use of currently accepted practices to analyze response data from slug tests performed in conditions commonly faced in the field. This evaluation is carried out by using (10) and (13) to simulate a series of slug tests. The simulated response data are analyzed using conventional approaches. The parameter estimates are then compared to the parameters employed in the original simulations to assess the magnitude of the error introduced into the estimates through use of a particular approach for the data analysis. The simulation and analysis of slug tests were performed in this work using SUPRPUMP, an automated well-test analysis package developed at the Kansas Geological Survey (Bohling and McElwee, 1992).

### **Partial Penetration Effects**

The first factor examined here was the effect of partial penetration on parameter estimates in a homogeneous aquifer (no skin case). Figure II.A.2 displays a plot of the hydraulic conductivity ratio ( $K_{ex}/K_r$ ) versus  $\psi$ , where  $\psi$  is the square root of the anisotropy ratio ( $\sqrt{K_z/K_r}$ ) over the aspect ratio ( $b/r_w$ ), for a configuration in which the

upper and lower boundaries are at such a large distance from the screened interval that they have no effect ( $\beta = B/b = 64$ ,  $\zeta = d/b = 32$ ). In this case, the hydraulic conductivity estimates are obtained using the solution of Cooper et al. (1967), which assumes that the well is fully screened across the aquifer (i.e. flow is purely radial). Figure II.A.2 shows that the error arising from the radial flow assumption diminishes with decreases in  $\psi$ . This is as expected since  $\psi$  reflects the proportion of vertical to radial flow in the slug-induced flow system. Decreases in  $\psi$  correspond to decreases in the anisotropy ratio or increases in the aspect ratio, the effect of both of which is to constrain the slug-induced flow to the interval bounded by horizontal planes at the top and bottom of the well screen (i.e. the proportion of radial flow increases). In addition, Figure II.A.2 shows that the error in the conductivity estimates decreases greatly with increases in  $\alpha$ , the dimensionless storage parameter. This is in keeping with the results of Hayashi et al. (1987) who noted that, for a constant aspect ratio, vertical flow decreases with increases in the storage parameter. Based on Figure II.A.2, it is evident that application of the Cooper et al. solution to data from slug tests performed in conditions where  $\psi$  is less than about 0.003 should introduce little error into the conductivity estimates. For isotropic to slightly anisotropic systems, this  $\psi$  range corresponds to aspect ratios greater than about 250. Only in the case of a very low dimensionless storage parameter will significant error ( $> 25\%$ ) be introduced into the estimates. Note that Figure II.A.2 should be considered an extension of the findings of Hayashi et al. (1987) to the case of slug tests in open wells, a more common configuration for groundwater applications than the shut-in pressurized slug test configuration that they examined.

Currently, the most common method for analysis of slug tests in partially penetrating wells in confined aquifers is that proposed by Hvorslev (1951). Hvorslev developed a model that can be used for the analysis of slug tests performed in a screened interval of finite length in a uniform, anisotropic, vertically unbounded medium. Figure II.A.3a displays a plot analogous to Figure II.A.2 for the case of the Hvorslev model being used to obtain the conductivity estimates. Note that the Hvorslev model requires the use of a "shape factor", which is related to the geometry of the well intake region. The shape factor used in Figure II.A.3a is that for Case 8 described in Hvorslev (1951) and results in the following expression for the radial component of hydraulic conductivity:



$$K_{HV} = \frac{r_c^2 \ln[1/(2\psi) + \sqrt{1+(1/2\psi)^2}]}{2bT_0} \quad (14)$$

where

$K_{HV}$  = estimate for the radial component of hydraulic conductivity obtained using the Hvorslev model;

$T_0$  = basic time lag, time at which a normalized head of .37 is reached.

As the aspect ratio gets large ( $1/2\psi$  gets large), (14) will reduce to Hvorslev's expression for a fully penetrating well (Case 9) if the effective radius (distance beyond which the slug-induced disturbance has no effect on heads) is set equal to the screen length in Case 9. Note that the anisotropy ratio, which appears in the  $\psi$  term, and  $K_{HV}$  are perfectly correlated in (14), so these parameters cannot be estimated independently.

In Figure II.A.3a, all analyses were performed using (14) while assuming that the anisotropy ratio was known. Given the difficulty of reliably estimating the degree of anisotropy in natural systems, this assumption must be considered rather unrealistic. Therefore, the analyses were repeated assuming that the degree of anisotropy was not known. However, since the anisotropy ratio and  $K_{HV}$  cannot be estimated independently, some value for the anisotropy ratio must be assumed for the analysis. This assumption of an arbitrary anisotropy ratio will give rise to an apparent  $\psi$  ( $\psi^*$ ) value, which is the square root of the assumed anisotropy ratio over the aspect ratio. Figure II.A.3b displays results obtained for slug tests analyzed using different  $\psi^*$  values. When considered in order of decreasing magnitude, the  $\psi^*$  curves correspond to aspect ratios of 10, 50, and 200, respectively, for the case of an assumed anisotropy ratio of 1 (a common assumption in field applications). These curves will apply to different aspect ratios when an anisotropy ratio other than one is assumed.

Often, field analyses are performed using the fully penetrating well model of Hvorslev (Case 9). For this approach, some assumption must be made concerning the effective radius of the slug test. In a frequently cited publication, the U.S. Dept. of Navy (1961) recommends that an effective radius of 200 times the well radius be employed. Figure II.A.3c displays the error that is introduced into conductivity estimates when that recommendation is adopted.

Figure II.A.3a indicates that the estimates provided by (14) will be reasonable for moderate to small values of dimensionless storage if the anisotropy ratio is known. At larger  $\alpha$ 's, however, the error introduced into the parameter estimates increases beyond the limit of what is considered reasonable for this investigation ( $\pm 25\%$ ). Note that in

Figure II.A.3a, as in the remaining figures of this paper, the smallest  $\psi$  value plotted is 0.001. This is a result of the relationships shown in Figure II.A.2, which indicate that, except in the case of very small values of dimensionless storage, the Cooper et al. model is the appropriate tool for analysis for  $\psi$  values less than 0.001.

Figure II.A.3b indicates that the quality of the estimates provided by (14) will be dependent on the assumed apparent  $\psi$  ( $\psi^*$ ) value for the case of an unknown anisotropy ratio. This figure demonstrates that for each  $\psi^*$  value there is a range of actual  $\psi$  for which the Hvorslev method will provide reasonable estimates. Although it is difficult to summarize the results of Figure II.A.3b succinctly, it is clear that, if the assumed anisotropy is moderately close to the actual anisotropy (within a factor of 2-3), the Hvorslev estimate will meet the criterion of reasonability employed here ( $\pm 25\%$ ). It can be readily shown that the  $\psi^*$  curves of Figure II.A.3b are related to one another by a simple multiplicative factor. This relationship enables curves for  $\psi^*$  values other than those considered here to be generated by multiplying the  $K_{an}/K_r$  ratio for one of the curves given in Figure II.A.3b by a factor consisting of the natural logarithm term  $(\ln[1/2\psi^* + \sqrt{1+(1/2\psi^*)}])$  from (14) for the curve to be generated over the same term for the curve in Figure II.A.3b. Although several standard references (e.g., Freeze and Cherry, 1979) recommend use of the isotropic form of (14), these results indicate that such an approach is only appropriate in isotropic to slightly anisotropic systems. This recommendation will result in a consistent underprediction of hydraulic conductivity in moderately to strongly anisotropic systems.

Figure II.A.3c indicates that the fully penetrating well model of Hvorslev (using an effective radius of 200 times the well radius) is appropriate in conditions where  $\psi$  is less than about 0.01 for moderate to small values of dimensionless storage. This  $\psi$  range corresponds to an aspect ratio greater than 100 for isotropic systems. For strongly anisotropic systems ( $K_r/K_t$  considerably less than one), the aspect ratios at which the fully penetrating well model becomes appropriate are much smaller. Given the form of the fully penetrating well model of Hvorslev employed here, the curves on Figure II.A.3c correspond to a  $\psi^*$  value of 0.005. From the discussion of the previous paragraph, it should be clear that the curves plotted on Figure II.A.3c can be used to generate all needed  $\psi^*$  curves for common values of the dimensionless storage parameter. Table II.A.1 presents the results from Figure II.A.3c in a tabular form so that the reader can readily generate the curve needed for a particular application. Since the  $\psi^*$  curves can be readily related to one another, the results presented in the remainder of this paper will be for one particular  $\psi^*$  value ( $\psi^* = 0.005$ ), which, as stated above, also corresponds to

the fully penetrating well model of Hvorslev. The tabulated values for all the curves presented here are given in Hyder (1994).

Figures II.A.3a-II.A.3c show that the quality of the Hvorslev estimates deteriorates rapidly as dimensionless storage increases above 0.001. Figure II.A.4 graphically displays the large errors that are introduced into parameter estimates as  $\alpha$  approaches 1 for the same conditions as shown in Figure II.A.3c. Clearly, the Hvorslev model must be used with extreme caution at large values of the dimensionless storage parameter. Since Figure II.A.2 indicates that the Cooper et al. model provides excellent conductivity estimates at large values of dimensionless storage, the Cooper et al. model should always be employed when high values of dimensionless storage are expected. As shown by Chirlin (1989), large values of dimensionless storage will often be reflected in a distinct concave upward curvature in a log head versus time plot. Note that the  $\psi$  curves on Figure II.A.4 become nearly horizontal as  $\alpha$  decreases. Therefore, the results that are discussed in this paper concerning the viability of the Hvorslev model at  $\alpha$  values of  $10^{-5}$  to  $10^{-7}$  are very good approximations for conditions where  $\alpha$  values are smaller than  $10^{-7}$ .

An important goal of this paper is to define guidelines for the field practitioner. Since, in actual field applications, the aspect ratio should be a known quantity, guidelines based on the magnitude of the aspect ratio would be preferred. Although the general lack of information concerning anisotropy and specific storage introduces uncertainty, the results of this section can be used to roughly define such guidelines for the analysis of response data from slug tests in partially penetrating wells. Clearly, at large aspect ratios (greater than 250), the Cooper et al. (1967) model is the most appropriate tool for data analysis. In strongly anisotropic systems ( $K_z/K_r$  considerably less than one), the Cooper et al. model will be applicable at much smaller aspect ratios. Although it is difficult to accurately estimate the degree of anisotropy from slug-test response data, Butler et al. (1993a) present a simple approach that can be used to assess if significant anisotropy is present. In the general case, the fully penetrating well model of Hvorslev (1951) would be the best approach for analyzing response data from wells of aspect ratios between 100 and 250. At smaller aspect ratios, the partially penetrating model of Hvorslev is best in the most general case. However, the most appropriate model for any particular application will depend on the anisotropy ratio and specific storage. If some reasonable estimates can be made about these parameters, Figures II.A.2-II.A.4 and Table II.A.1 can be used to assess which method is most appropriate for that specific application. Note that the model of Cooper et al. should be employed at all aspect ratios when the dimensionless storage parameter is large.

### Boundary Effects

The previous discussion has focussed on the effects of partial penetration in a vertically infinite system. Although one might suspect that most natural systems can be considered as vertically infinite for the purposes of the analysis of response data from slug tests, there may be situations in which the upper and/or lower boundaries of the system influence the response data. Thus, the next factor examined here was the effect of impermeable and constant-head boundaries in the vertical plane on parameter estimates. Figure II.A.5 displays a plot of the hydraulic conductivity ratio versus the normalized distance to a boundary ( $\zeta = d/b$ ). Results are shown for both impermeable and constant-head boundaries. In all cases, an apparent  $\psi$  ( $\psi'$ ) value of 0.005 is used to obtain the conductivity estimates. It is clear from Figure II.A.5 that a boundary will only have a significant effect ( $>25\%$ ) on parameter estimates when the screen is very close to the boundary (i.e.  $\zeta < 1-2$ ) and  $\psi$  is relatively large. If there is any degree of anisotropy in hydraulic conductivity, the influence of the boundary will be considerably lessened. Note that Hvorslev (1951) also proposed a semi-infinite, partially penetrating well model (single impermeable boundary with screen extending to boundary) for slug tests. The equation for estimation of hydraulic conductivity in this case is the same as (14) except  $\psi$  is used instead of  $2\psi$  in the logarithmic term. The circles and triangles on Figure II.A.5 show the estimates that would be obtained using this model for the confined case. Clearly, the semi-infinite variant of the Hvorslev model is only necessary at large  $\psi$  values (wells of small aspect ratios in isotropic aquifers). As the proportion of vertical flow decreases ( $\psi$  gets small), the semi-infinite model becomes slightly inferior to the vertically infinite form of the Hvorslev model. Although all of the parameter estimates in Figure II.A.5 were obtained using the Hvorslev model, the method of Bouwer and Rice (1976) would normally be employed if an unconfined boundary is suspected. Hyder and Butler (in press) provide a detailed discussion of the error introduced into parameter estimates using the Bouwer and Rice model.

The above discussion focusses on results when only a single boundary is influencing parameter estimates. In thin aquifers, one may face conditions when both the upper and lower boundaries are close enough to the screen to be affecting the slug test responses. Figure II.A.6 displays a plot of the hydraulic conductivity ratio versus normalized aquifer thickness ( $\beta = B/b$ ) for the case of a well screen located at the center of the unit. Clearly, in thin confined systems, the Hvorslev model provides estimates considerably less than the actual formation conductivity for relatively large values of  $\psi$ .

In thin unconfined systems, the lower impermeable boundary acts in an opposite manner to the upper constant-head boundary so that the estimates are more reasonable than in the single boundary case.

The results of this section indicate that, except in cases of very thin aquifers ( $\beta < 10$ ), screens located very close to a boundary ( $\zeta < 5$ ), and large values of  $\psi$  ( $> 0.05$ ), the assumption of a vertically infinite system introduces a very small amount of error into the parameter estimates obtained using the Hvorslev model. Thus, the relationships presented in Figures II.A.3 and II.A.4 can be considered appropriate for the vast majority of field applications. Note that no analyses were performed in this section using the Cooper et al. (1967) model. In the previous section, a range of aspect ratios ( $> 250$ ) was defined for which the Cooper et al. model would provide reasonable estimates. Since boundaries in the vertical plane will only introduce sizable errors into parameter estimates when there is a considerable component of vertical flow, the effects of boundaries will be very small if the Cooper et al. model is only applied over the previously defined range.

### Well Skin Effects

The results of the previous sections pertain to the case of slug tests performed in homogeneous formations. Often, however, as illustrated in Figure II.A.1, well drilling and development creates a disturbed, near-well zone (well skin) that may differ in hydraulic conductivity from the formation in which the well is screened. It is important to understand the effect of well skins on conductivity estimates in order to avoid using estimates representative of skin properties to characterize the formation as a whole.

Figure II.A.7a illustrates the effect of a well skin on conductivity estimates obtained using the Hvorslev model ( $\psi^* = 0.005$ ) for a broad range of contrasts between the conductivity of the skin and that of the formation. Clearly, the existence of a well skin can have a dramatic effect on the Hvorslev estimates. In the case of a skin less permeable than the formation, a conductivity estimate differing from the actual formation value by over an order of magnitude can easily be obtained. Figure II.A.7a displays results for the case of a skin whose outer radius is twice that of the well screen ( $\xi_s = r_s/r_w = 2$ ). Figure II.A.7b shows how the results depend on the thickness of the skin for the case of a skin one order of magnitude less conductive than the formation ( $\gamma = 10.0$ ). Note that when the skin radius equals the effective radius assumed in the Hvorslev fully penetrating well model ( $\xi_s = 200$ ), the estimated conductivity will approach that of the skin for small values of  $\psi$ .

Figure II.A.8 displays a plot of a simulated slug test and the best-fit Hvorslev

model, which is representative of all the low-conductivity skin cases shown in Figures II.A.7a-II.A.7b. As can be seen from Figure II.A.8, the Hvorslev model matches the simulated data extremely well. In fact, a large number of additional simulations have shown that the Hvorslev fit for the low-conductivity skin case is almost always better than that for the homogeneous case. This is especially true at small  $\psi$  values (moderate to large aspect ratios) where the response data for the homogeneous case generally will display a distinct concave upward curvature (e.g., Chirlin, 1989).

At moderate to small  $\psi$  values, an underlying assumption of the Hvorslev model is that there is an effective radius beyond which the slug-induced disturbance has no effect on aquifer heads. In the low-conductivity skin case, this assumption is a very close approximation of reality, for almost all of the head drop occurs across the skin; heads in the formation are essentially unaffected by the slug test. Another major assumption of this model is that the specific storage of the formation can be neglected. In most cases, the thickness of the skin is relatively small so the influence of the specific storage of the skin on slug-test responses is essentially negligible. Thus, the assumptions of the Hvorslev model actually appear to be more reasonable in the low-conductivity skin case than in the homogeneous case. So, if one assumes an effective radius equal to the skin radius (e.g.,  $\xi_{sk}=200$  in Figure II.A.7b), the estimated conductivity will be a reasonable approximation of the conductivity of the skin at moderate to small  $\psi$  values. Hyder and Butler (in press) show that a low-conductivity skin has a similar effect on parameter estimates obtained using the Bouwer and Rice (1976) method.

Figure II.A.9 illustrates the effect of a well skin on conductivity estimates obtained using the Cooper et al. model. In general, the effect of a skin on the Cooper et al. model estimates is similar to that seen with the Hvorslev model. Again, the effect of a low-conductivity skin is quite pronounced. If the specific storage is assumed known or constrained to physically realistic values, application of the Cooper et al. model to data from a well with a low-conductivity skin will produce an estimate that is heavily weighted towards the conductivity of the skin. In addition, there will always be a considerable deviation between the best-fit Cooper et al. model and the response data in a manner similar to that shown in Figure II.A.10. At small  $\psi$  values (moderate to large aspect ratios), the combination of an excellent Hvorslev fit and a systematic deviation between the Cooper et al. model and the test data appears to be a very good indication of a low-conductivity skin. At larger  $\psi$  values (lower aspect ratios), however, such a combination is also an indication of a strong component of vertical flow. Note that McElwee and Butler (1992) have proposed an empirical equation that relates the Cooper et al. conductivity estimate to skin and formation properties. The practical use of this

equation is limited, however, since estimation of formation conductivity from the Cooper et al. estimate requires knowledge of skin conductivity and thickness.

In the high-conductivity skin case, as shown in Figures II.A.7a and II.A.9, conductivity estimates will be greater than the formation conductivity as a result of a considerable amount of vertical flow along the more conductive skin. The difference will be greatest at large  $\psi$  values because of the larger proportion of vertical flow under those conditions. Note that the difference between the two high-conductivity skin cases decreases at small  $\psi$  values because of the lessening importance of vertical flow. If the radius of the well screen is set to the nominal screen radius in the analysis, there will always be the offset between the high-conductivity skin cases and the homogeneous case shown at small  $\psi$  values in Figures II.A.7a and II.A.9.

Since there is a very small head drop in the radial direction across a high-conductivity skin, one might expect that parameter estimates for the high-conductivity skin case could be considerably improved by assuming the radius of the well screen equals the radius of the high-conductivity skin. Although such an approach will decrease the offset at small  $\psi$  values displayed in Figures II.A.7a and II.A.9, additional simulations have shown that the gains obtained through this approach are quite modest (less than 10%). The reason for these smaller than might have been expected gains is that an increase in the well radius only influences  $\alpha$  and  $\psi$ . As has been shown in plots in the previous sections, hydraulic conductivity estimates are not strongly affected by moderate changes in these dimensionless variables. The major cause of the differences between the high-conductivity skin and homogeneous cases shown in Figures II.A.7a and II.A.9 is the uncertainty concerning the screen length. Since screen length is a term in the dimensionless time variable ( $\tau$ ), an error in the screen length estimate of a certain magnitude directly translates into an error in the estimated hydraulic conductivity of the same magnitude. Thus, uncertainty about the value to use for the screen length can introduce considerable error into the conductivity estimates. In the case of a partially penetrating well, the high-conductivity skin (e.g., the gravel pack) will normally be of greater length than the well screen. In this situation, the length of the high-conductivity skin, and not the nominal length of the well screen, is the quantity of interest. This larger-than-the-nominal screen length can be termed the "effective screen length" for the purposes of this discussion. In Figures II.A.7a and II.A.9, the high-conductivity skin cases were analyzed assuming that the nominal screen length was the appropriate screen length for the analysis. At large  $\psi$  values, such an approach is clearly incorrect. A more appropriate approach would have been to attempt to estimate the actual effective screen length. If there is an adequate seal in the annulus, the effective screen length

should be the length of the gravel pack up to that seal. However, in cases where the length of the high-conductivity skin is considerably longer than the nominal screen length, such as shown in Figures II.A.7a and II.A.9, the effective screen length will be dependent on the conductivity contrast between the formation and the skin. Further work is required to develop approaches for estimation of the effective screen length in such situations.

### Summary and Conclusions

A semianalytical solution to a model describing the flow of groundwater in response to a slug test in a porous formation has been presented. The primary purpose for the development of this model was to assess the viability of conventional methods for the analysis of response data from slug tests. The results of this assessment can be summarized as follows:

- 1) In a homogeneous aquifer, the Cooper et al. model will provide reasonable estimates (within 25%) of the radial component of hydraulic conductivity for  $\psi$  values less than about 0.003. For isotropic to slightly anisotropic systems, this  $\psi$  range corresponds to aspect ratios greater than about 250 (much smaller aspect ratios for strongly anisotropic formations). In systems with a large dimensionless storage ( $\alpha > 0.01$ ), the Cooper et al. model should provide reasonable estimates at virtually all commonly used aspect ratios. The viability of this model at  $\psi$  less than 0.003 is only in question for configurations with small values of dimensionless storage ( $\alpha < 10^{-6}$ );
- 2) In a homogeneous aquifer, the Hvorslev model (Case 8) will provide reasonable estimates of the radial component of hydraulic conductivity at moderate to small values of dimensionless storage ( $\alpha < 10^{-4}$ ) for a broad range of  $\psi$  values if the magnitude of the anisotropy ratio is known. If the anisotropy ratio is not known, which is the situation commonly faced in the field, the Hvorslev model will provide reasonable estimates if the assumed anisotropy ratio is within a factor of two to three of the actual ratio. A table provided with this paper allows the error introduced by the anisotropy ratio assumption to be readily assessed for any value of the assumed anisotropy. If the effective radius is assigned a value 200 times the well radius, the fully penetrating variant of the Hvorslev model (Case 9) will provide reasonable conductivity estimates for  $\psi$  values less than 0.01;
- 3) Except in cases of large values of  $\psi$  ( $> 0.05$ ), and very thin aquifers ( $\beta < 10$ ) or well screens located very close to a boundary ( $\zeta < 5$ ), boundaries in the vertical plane will have little influence on parameter estimates obtained using conventional approaches. If



the formation has any degree of anisotropy in hydraulic conductivity, the range of conditions over which boundary effects are significant will be further limited. In general, the assumption of a vertically infinite system introduces a very small amount of error into parameter estimates. Relationships developed for vertically infinite systems should thus be appropriate for most field applications;

4) In the case of a low conductivity skin, neither the Hvorslev nor the Cooper et al. model provide reasonable estimates of hydraulic conductivity of the formation. Both approaches will provide estimates that are heavily weighted towards the conductivity of the skin. The underlying assumptions of the Hvorslev model actually appear to be more reasonable in the low-conductivity skin case than in the homogeneous case. At small  $\psi$  values (moderate to large aspect ratios), the combination of an excellent fit of the Hvorslev model to the test data and a systematic deviation between the test data and the Cooper et al. model appears to be a very good indication of a low-conductivity skin;

5) In the case of a high conductivity skin, the Cooper et al. model will provide reasonable estimates of formation conductivity at small  $\psi$  values. The fully penetrating well variant of the Hvorslev model (effective radius 200 times the well radius) will provide viable estimates at  $\psi$  values less than about 0.01. The quality of the estimates for both models can be slightly improved if the radius of the screen is set equal to an approximate skin radius. At  $\psi$  values greater than 0.01, the viability of Hvorslev conductivity estimates will strongly depend on the quality of estimates for the effective screen length. In most cases, the length and radius of the gravel pack should be used in place of the nominal screen length and radius, respectively, for the analysis of the response data.

The results of this assessment indicate that there are many commonly faced field conditions in which the conventional methodology for the analysis of response data from slug tests appears viable. Since the definition of what constitutes a reasonable parameter estimate will be application dependent, the user can consult the figures and table included with this paper to assess if the introduced error is acceptable for a specific application. If it appears that conventional approaches will not provide acceptable parameter estimates for a test in a particular configuration, the model developed here can be used to analyze the response data. Butler et al. (1993a) describe a series of slug tests in both consolidated and unconsolidated formations in which the model described in this article is employed for the data analysis. This model, however, is not a panacea. Considerable experience is required for successful application in configurations with low-conductivity skins or a moderate degree of anisotropy owing to uncertainties introduced by a high degree of parameter correlation.

Note that the results of this study must be considered in the light of the three major assumptions used in the mathematical definition of the slug-test model employed in this work. First, in equation (7), we adopted the commonly employed assumption of a uniform hydraulic gradient along the well screen as a mathematical convenience. In actuality, one would suspect that the gradient would be larger at either end of the screen producing a U-shaped profile in the vertical plane. Butler et al. (1993b), however, have performed detailed simulations with a numerical model to show that the use of this mathematical convenience introduces a negligible degree of error to the results reported here and virtually all practical applications.

Second, in equations (8) and (9), we assumed that the skin fully penetrates the formation being tested. Although this assumption is appropriate for the case of multilevel slug tests performed in a well fully screened across the formation, it is clearly not representative of reality in the general case. For tests in wells with a low-conductivity skin, however, this assumption is of little significance since a low-conductivity skin will not serve as a vertical conduit. In this situation, flow in response to a slug-induced disturbance will be primarily constrained to an interval bounded by horizontal planes at the top and bottom of the well screen. In the case of a high-conductivity skin, this assumption will produce considerably more vertical flow in the skin than would actually occur. Butler et al. (1993b), however, have shown through numerical simulation that a slug test performed in a partially penetrating well with a high conductivity skin that extends to the bottom of the screen is indistinguishable from a slug test performed in a similar configuration in which the well screen terminates against a lower impermeable layer. Thus, for the high conductivity skin cases examined here, the slug tests were simulated assuming that the screen abutted against a lower impermeable layer. Note that this approach is only appropriate for a skin considerably more conductive (i.e. larger by a factor of 2-3) than the formation as a whole. This approach would not be appropriate for the case of a skin of only slightly higher conductivity than the formation.

Third, in equation (11), we assumed that the water table could be represented as a constant-head boundary. Given the small amount of water that is introduced to/removed from a well during a slug test, this assumption is considered reasonable under most conditions. The cases in which this assumption may be suspect are that of a well that is screened across the water table or a well screened over a deeper interval with a gravel pack that extends above the water table. Ongoing numerical and field investigations are currently being undertaken to assess the error that is introduced through this assumption and to suggest approaches for data analysis when that error is deemed unacceptably large (Butler et al., 1994b).

$\psi$	$\alpha=0.1$	$\alpha=0.001$	$\alpha=1.0\text{e-}5$	$\alpha=1.0\text{e-}7$
1.00E-3	3.196	1.249	0.867	0.803
2.23E-3	3.198	1.275	0.950	0.909
3.16E-3	3.203	1.293	1.001	0.964
7.07E-3	3.221	1.374	1.150	1.125
1.00E-2	3.244	1.429	1.233	1.210
2.22E-2	3.330	1.641	1.491	1.470
3.20E-2	3.399	1.774	1.638	1.615
7.10E-2	3.693	2.225	2.108	2.076
1.00E-1	3.920	2.508	2.388	2.347

TABLE 1 - Tabulated values of the conductivity ratio for the plots of Figure II.A.3c

$$(\psi = \sqrt{K_t/K_r} / (b/r_w) ; \alpha = (2r_w^2 S_b b)/r_c^2 ).$$

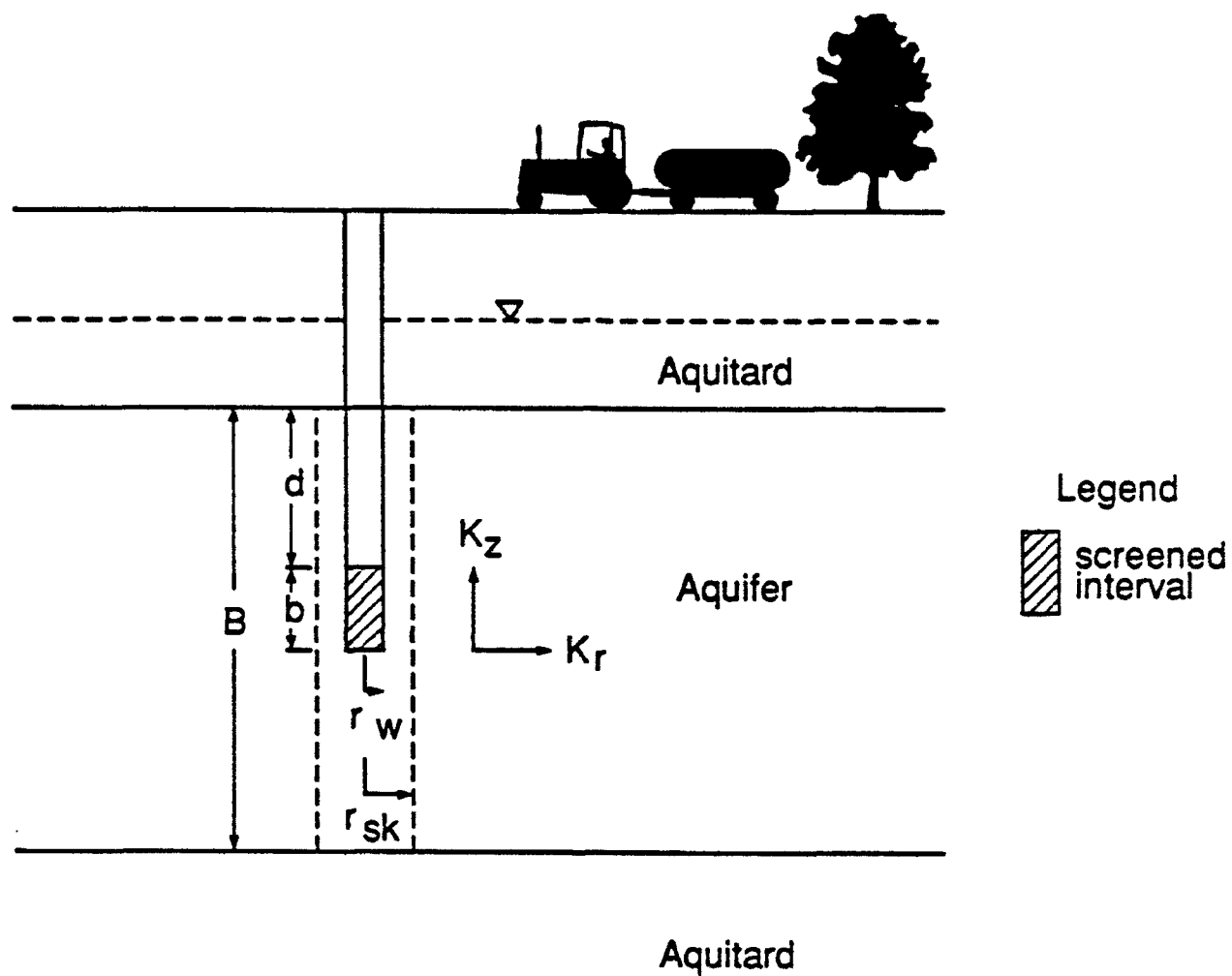


FIGURE II.A.1 - Cross-sectional view of a hypothetical confined aquifer (notation explained in text).

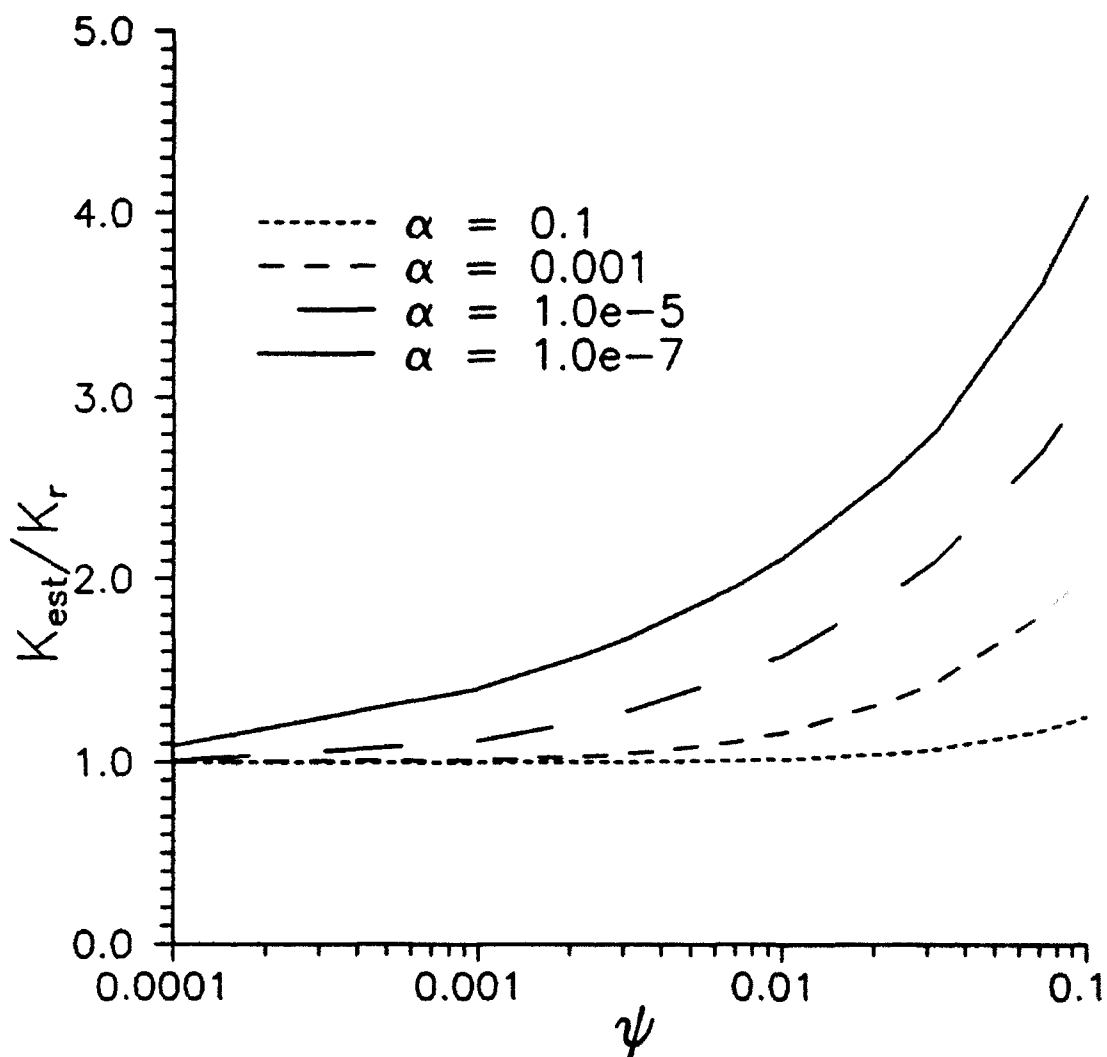


FIGURE II.A.2 - Plot of conductivity ratio (Cooper et al. estimate ( $K_{est}$ ) over actual conductivity ( $K_r$ )) versus  $\psi$  ( $\sqrt{K_r/K_r} / (b/r_w)$ ) as a function of  $\alpha$  ( $(2r_w^2 S_b)/r_e^2$ ) for the case of a well screened near the center of a very thick aquifer ( $\beta = 64$ ,  $\zeta = 32$ ).

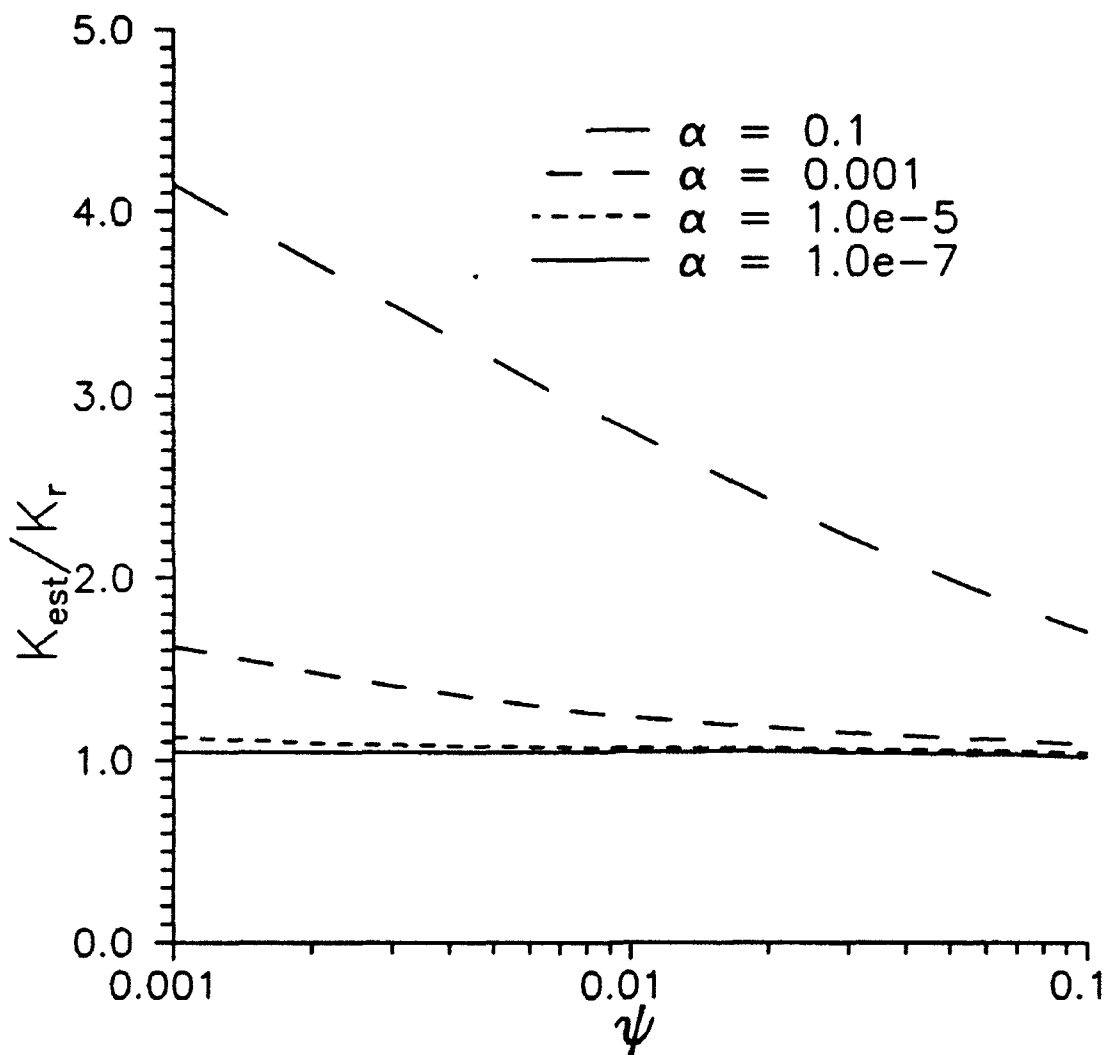
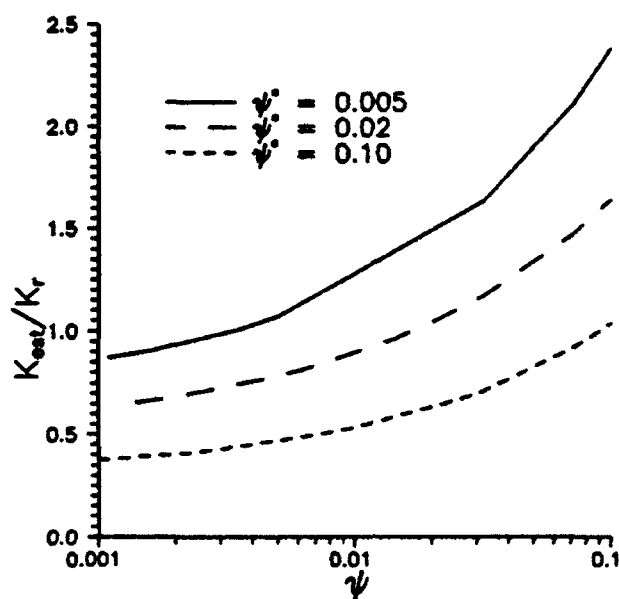
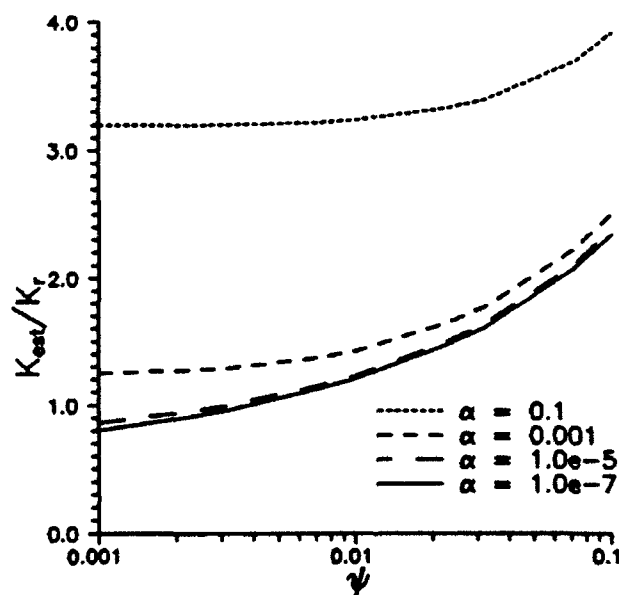


FIGURE II.A.3 - Plot of conductivity ratio (Hvorslev estimate ( $K_{est}$ ) over actual conductivity ( $K_r$ )) versus  $\psi$  ( $\sqrt{K_r/K_t} / (b/r_w)$ ) for the case of a well screened near the center of a very thick aquifer ( $\beta \approx 64$ ,  $\zeta \approx 32$ ): a) Hvorslev estimates obtained with equation (II.A.14) (anisotropy ratio known) as a function of  $\alpha$  ( $(2r_w^2 S_t b)/r_c^2$ );



b) Hvorslev estimates obtained with equation (II.A.14) (anisotropy ratio unknown) as a function of  $\psi^*$  ( $\psi$  term with an assumed anisotropy ratio) for  $\alpha = 1.0e^{-5}$ ;



c) Hvorslev estimates obtained with the fully penetrating well variant of the Hvorslev model (assuming an effective radius of  $200r_w$ ) as a function of  $\alpha$  ( $(2r_w^2 S_b)/r_e^2$ ).

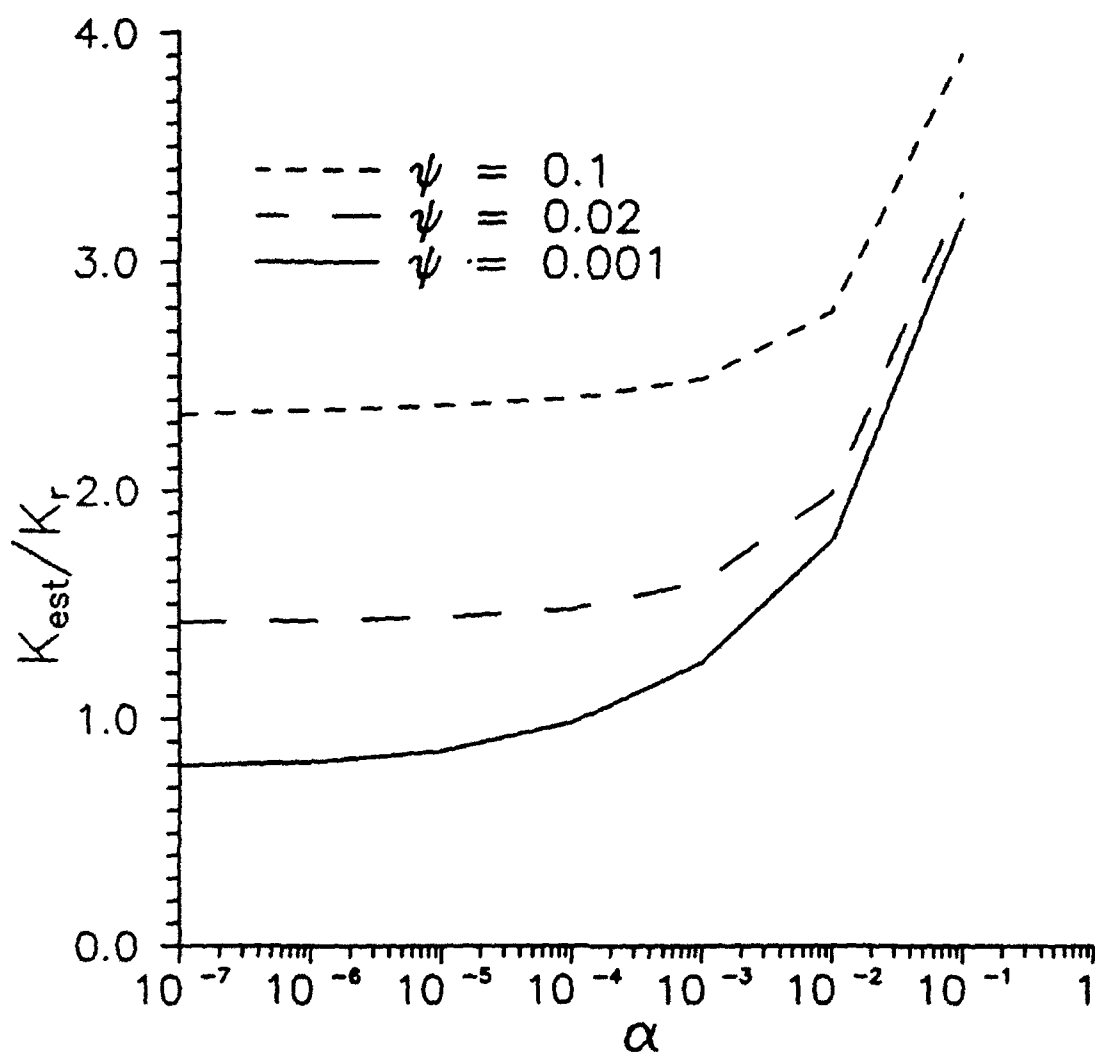


FIGURE II.A.4 - Plot of conductivity ratio (Hvorslev estimate ( $K_{est}$ ) over actual conductivity ( $K_r$ )) versus  $\alpha$  ( $(2r_w^2 S_b)/r_c^2$ ) as a function of  $\psi$  ( $\sqrt{K_r/K_{est}}/(b/r_w)$ ) for the case of a well screened near the center of a very thick aquifer ( $\beta = 64$ ;  $\zeta = 32$ ;  $\psi^* = 0.005$ ).



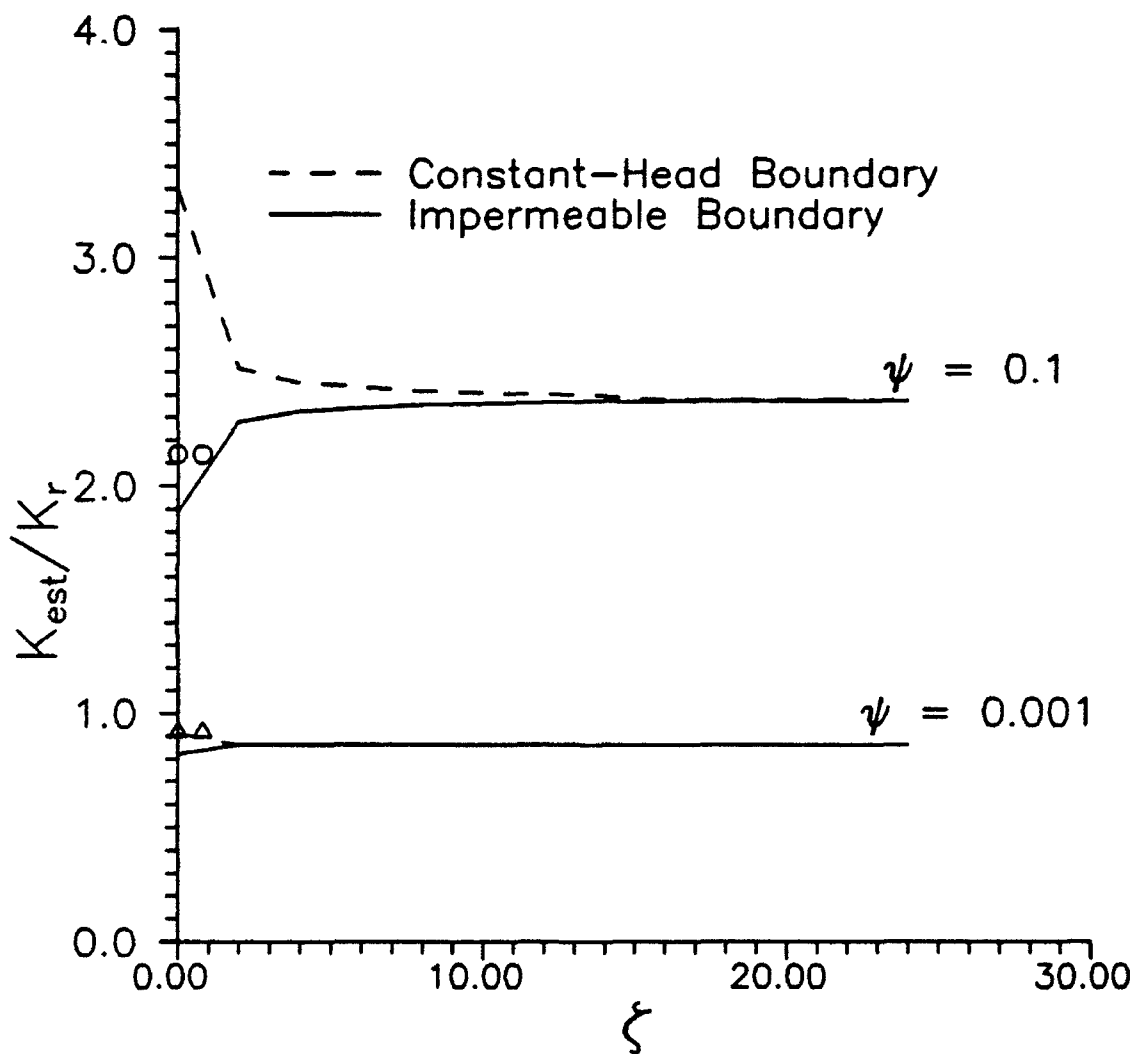


FIGURE II.A.5 - Plot of conductivity ratio (Hvorslev estimate ( $K_{est}$ ) over actual conductivity ( $K_r$ )) versus  $\zeta$  ( $d/b$ ) as a function of  $\psi$  ( $\sqrt{K_z/K_r} / (b/r_w)$ ) (solid lines designate impermeable upper boundary, dashed lines designate constant-head upper boundary; circles and triangles designate estimates obtained using the semi-infinite variant of the Hvorslev model for  $\psi$  values of 0.1 and 0.001, respectively;  $\beta = 64$ ;  $\alpha = 1.0e^{-5}$ ;  $\psi^* = 0.005$ ).

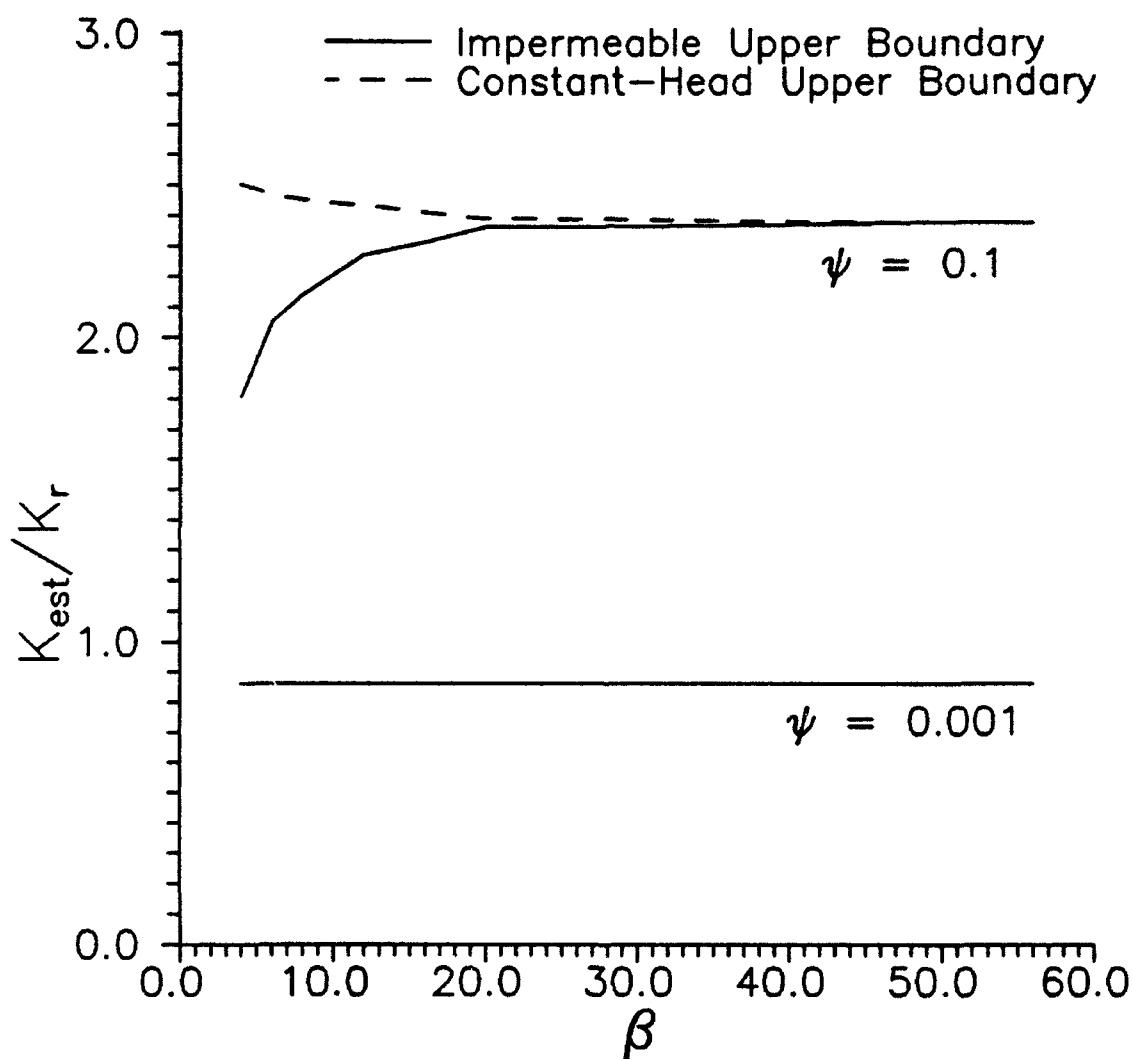


FIGURE II.A.6 - Plot of conductivity ratio (Hvorslev estimate ( $K_{est}$ ) over actual conductivity ( $K_r$ )) versus  $\beta$  ( $B/b$ ) as a function of  $\psi$  ( $\sqrt{K_r/K_t}/(b/r_w)$ ) (solid lines designate impermeable upper boundary, dashed lines designate constant-head upper boundary;  $\alpha = 1.0e^{-5}$ ;  $\psi^* = 0.005$ ).

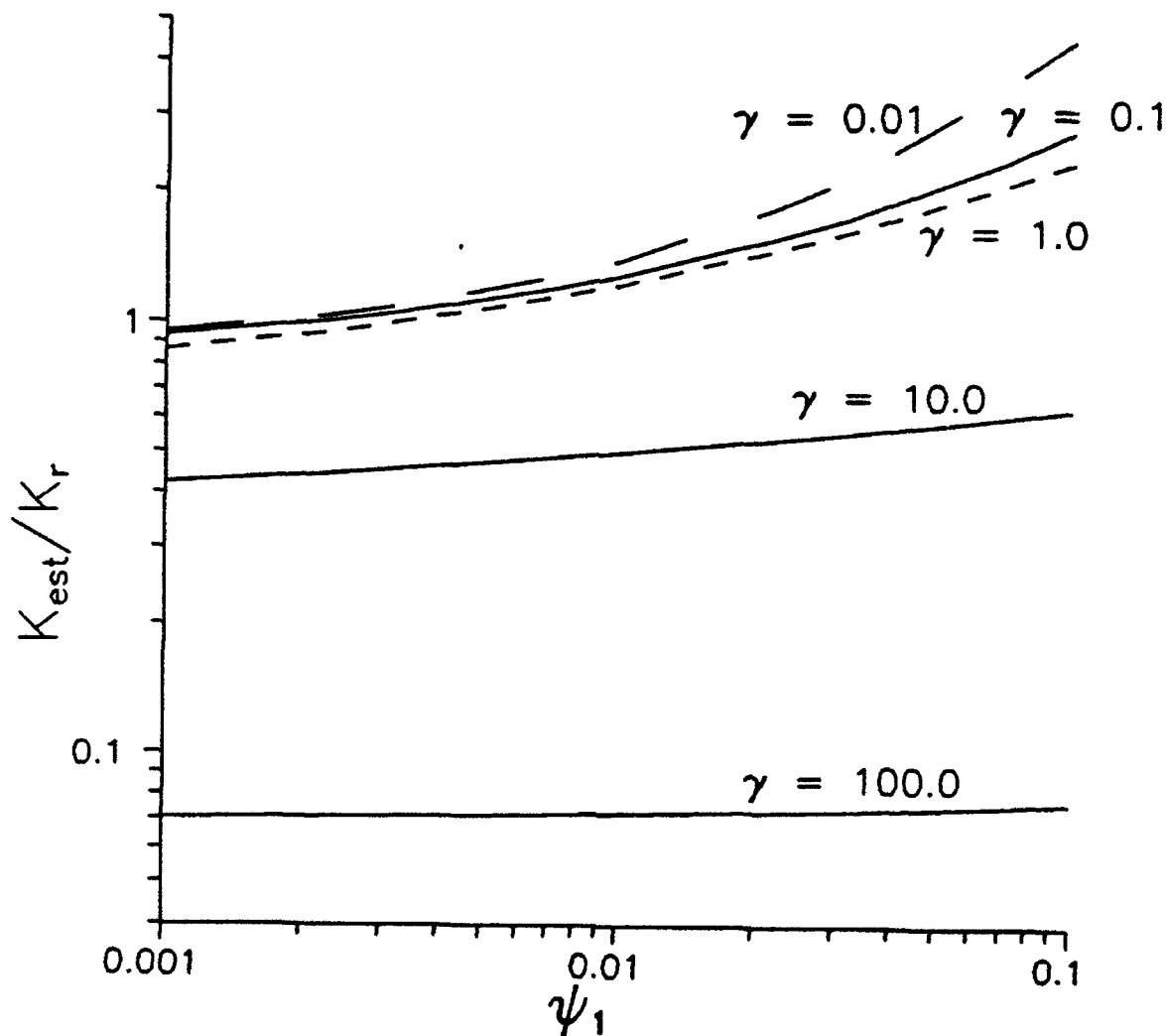
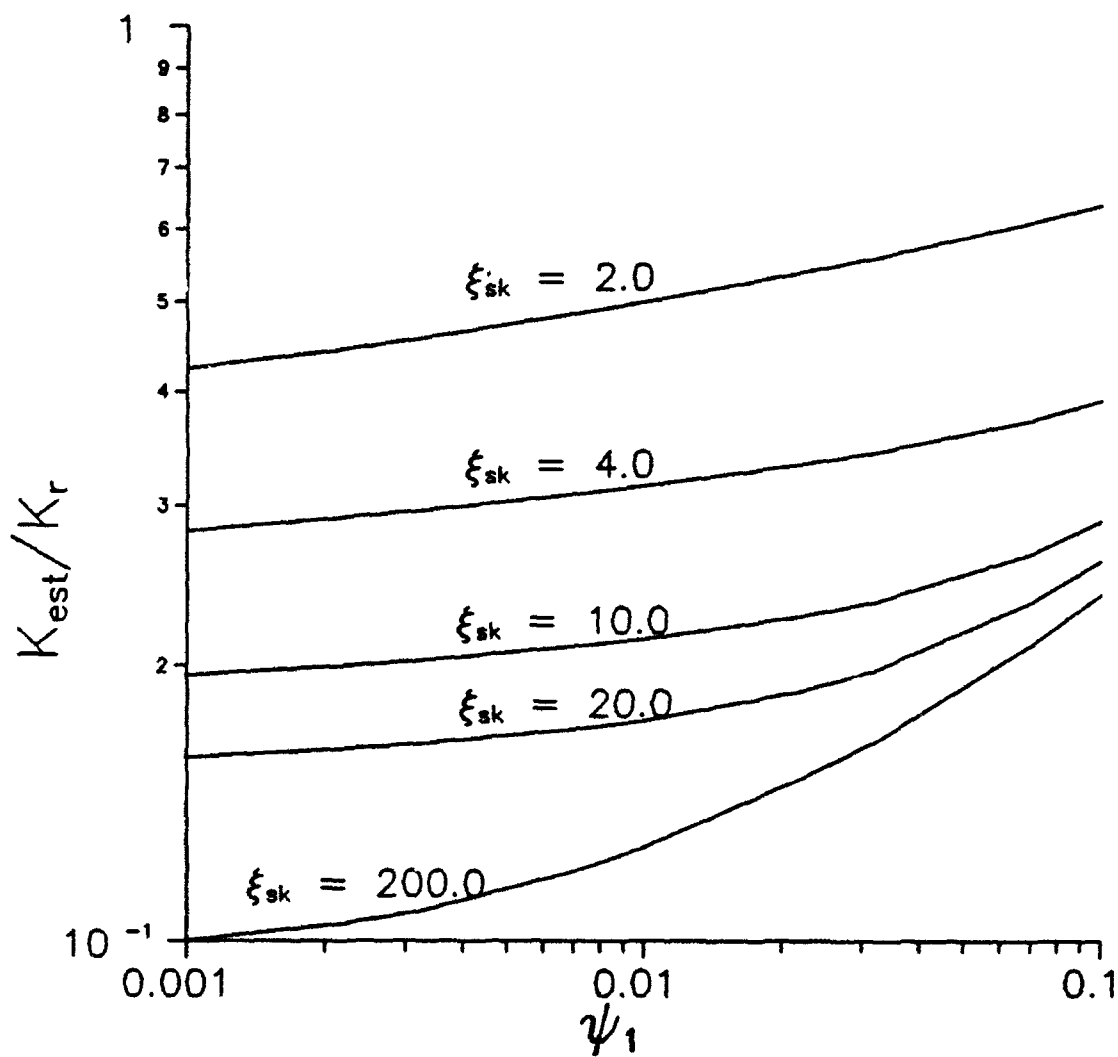


FIGURE II.A.7 - Plot of conductivity ratio (Hvorslev estimate ( $K_{est}$ ) over actual formation conductivity ( $K_r$ )) versus  $\psi_1$  ( $\sqrt{K_{r1}/K_{r1}} / (b/r_w)$ ) for the case of high and low conductivity well skins ( $\beta = 64$ ;  $\zeta = 32$ ;  $\alpha = 1.0e^{-5}$ ;  $\psi^* = 0.005$ ;  $\psi_1 = \psi_2$ ); a) Hvorslev estimates as a function of  $\gamma$  ( $K_{r2}/K_{r1}$ ) for  $\xi_* = 2$ ;



b) Hvorslev estimates as a function of  $\xi_{sk}$  ( $r_{sk}/r_w$ ) for  $\gamma=10.0$ .

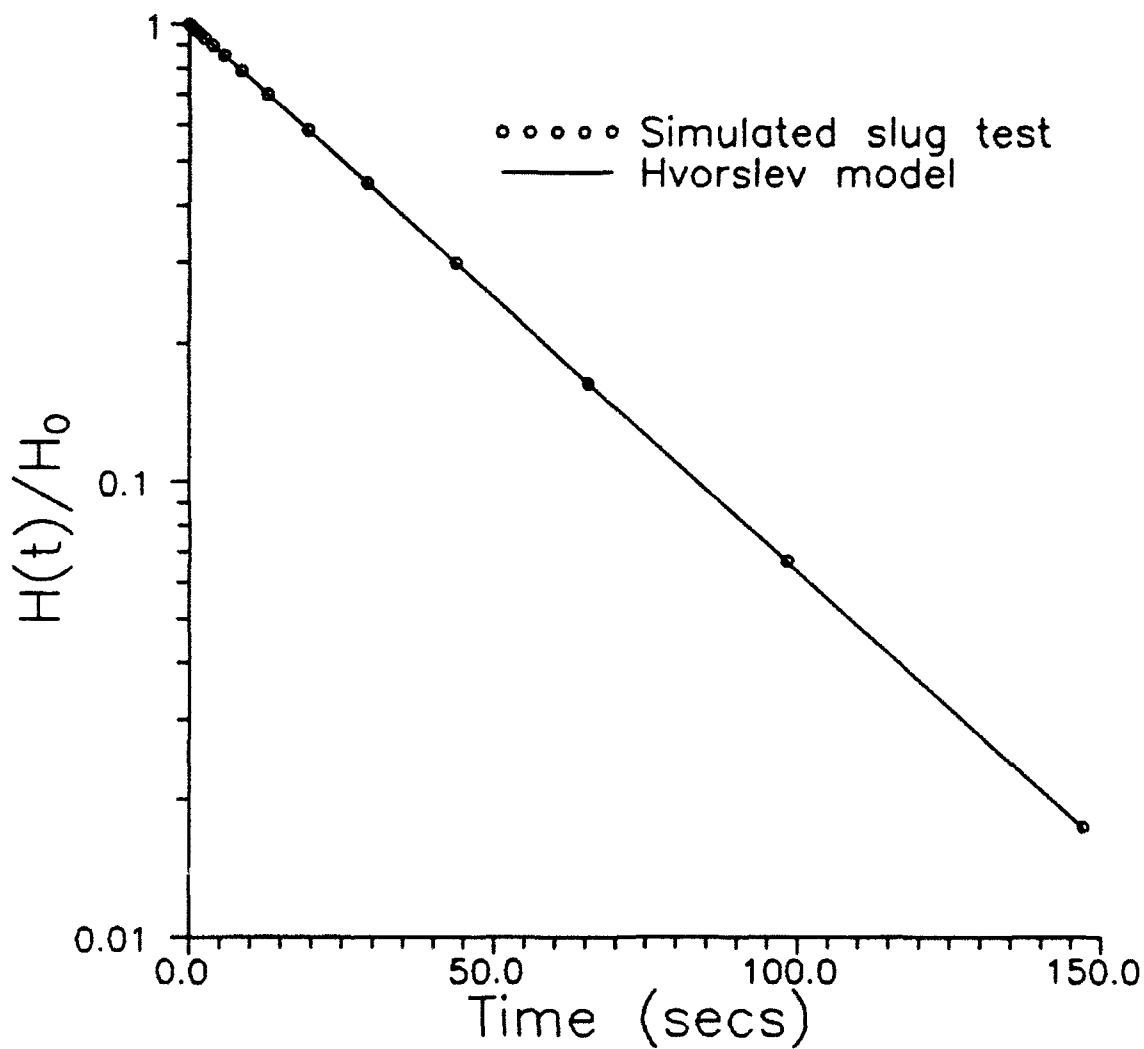


FIGURE II.A.8 - Normalized head versus time plot of simulated slug-test data and the best-fit Hvorslev model for the case of a skin two orders in magnitude less conductive than the formation ( $b/r_w = 50$ ;  $r_{sk} = .10$  m;  $r_w = r_c = 0.05$  m;  $S_{s1} = S_{s2} = 1.0 \times 10^{-5}$  m<sup>-1</sup>;  $K_{r2} = K_{r2} = 0.001$  m/s;  $K_{r1} = K_{r1} = 0.00001$  m/s).

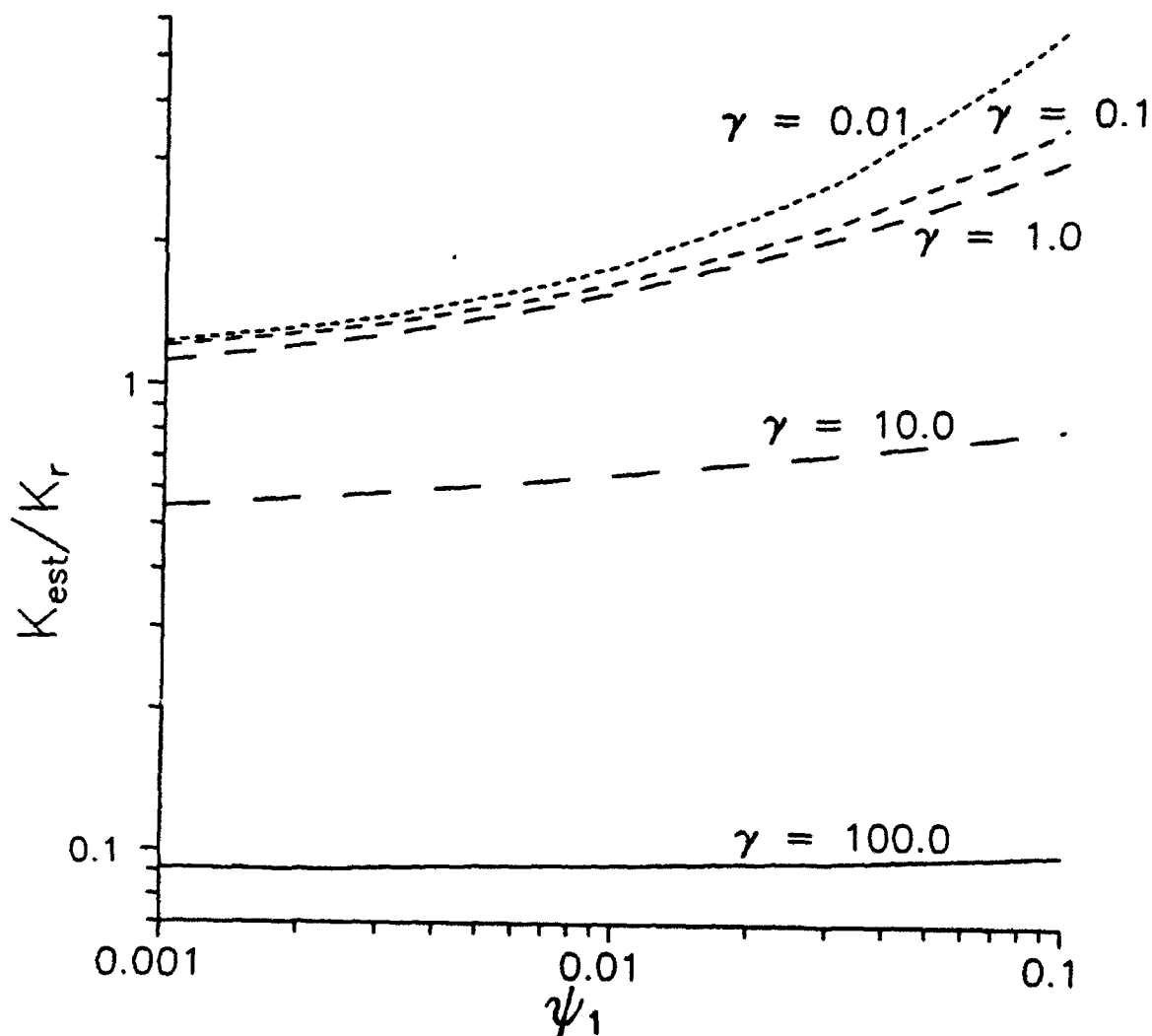


FIGURE II.A.9 - Plot of conductivity ratio (Cooper et al. estimate ( $K_{est}$ ) over actual formation conductivity ( $K_r$ )) versus  $\psi_1$  ( $\sqrt{K_{a1}/K_{r1}}/(b/r_w)$ ) as a function of  $\gamma$  ( $K_{r2}/K_{r1}$ ) for  $\xi_{sk} = 2$  ( $\beta \approx 64$ ;  $\zeta \approx 32$ ;  $\alpha = 1.0e^{-5}$ ;  $\psi_1 = \psi_2$ ).

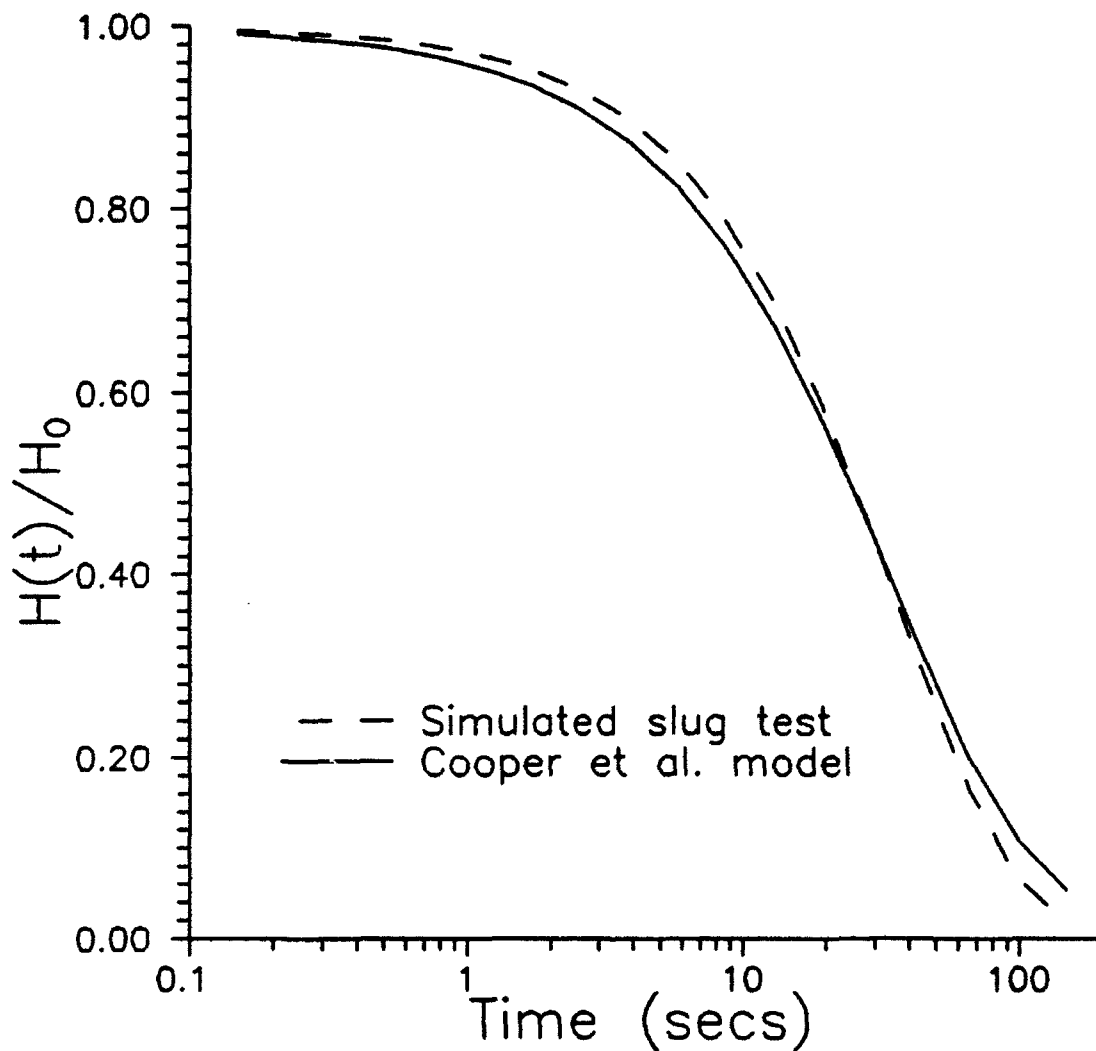


FIGURE II.A.10 - Normalized head versus time plot of simulated slug-test data and the best-fit Cooper et al. model for the case of a skin two orders in magnitude less conductive than the formation ( $b/r_w = 50$ ,  $r_{sk} = .10$  m;  $r_w = r_c = 0.05$  m;  $S_{s1} = S_{s2} = 1.0e-5$  m<sup>-1</sup>;  $K_{r2} = K_{r2} = 0.001$  m/s;  $K_{r1} = K_{r1} = 0.00001$  m/s).

## B. PULSE-TESTING IN HETEROGENEOUS FORMATIONS

### Introduction

In year two of this project we looked at propagating sinusoidal signals using a one-dimensional analytical model with two zones. Traditional inverse methods were used to see if aquifer parameters could be inferred from pulse test data. It was found that the final estimated values could vary considerably depending on the initial estimates. This year we have concentrated on two issues: 1) when extended to the radial case will a sinusoidal signal propagate significant distances, and 2) can the amplitude and phase of the observed signal be used to infer something about heterogeneous aquifers? The work on pulse testing has been extended to the radial case by using numerical solution techniques. The Theis equation has been coupled to an equation describing the borehole. This formulation allows us to answer the first question about propagation distances in the radial model and will be the first subject of this subsection. The question about how diagnostic measurements of amplitude and phase can be when trying to delineate heterogeneities will then be taken up. The preliminary analysis on amplitude and phase was done with the analytical one-dimensional two-zone model developed last year. As a check, these results were evaluated with a numerical model. The numerical model was extended to five zones to see if the results could be generalized.

### Radial Pulse-Test Model

In order to analyze pulse tests with a radial model, we extended an approach of Kabala et al. (1985) who developed a slug-test model based on the momentum equation for the water in the well coupled to the Theis equation for the aquifer. Our approach employs an additional sinusoidal external forcing function representing any desired pumping scheme. The governing ordinary differential equation for the displacement of water ( $x$ , positive upward) in the well with an effective water column ( $H_e$ ) then reads :

$$(H_e + x) \frac{d^2 x}{dt^2} + \beta g \int_0^t \left( \frac{dx}{d\tau} + \frac{Q_0}{\pi r_w^2} \sin(\omega \tau) \right) \frac{e^{-\alpha/(t-\tau)}}{t-\tau} d\tau + gx + \frac{3}{4} \left[ \frac{dx}{dt} \right]^2 = 0 \quad (\text{II.B.1})$$

which is identical to eq. (9) in Kabala et al. ( $g$  is the acceleration of gravity), with the exception of the flow through the screen which is here assumed to be:



$$Q_{screen} = Q_{pumpage} + \pi r_w^2 \frac{dx}{d\tau} = Q_0 \sin(\omega\tau) + \pi r_w^2 \frac{dx}{d\tau} \quad (\text{II.B.2})$$

where  $r_w$  is the well radius and  $Q_0$  is the amplitude of the sinusoidal pumping stress. The quantities  $\alpha$  and  $\beta$  used in equation (II.B.1) are defined as

$$\alpha = \beta S$$

$$\beta = \frac{r_w^2}{4T}$$

where  $S$  is the storage coefficient and  $T$  is the transmissivity.

The numerical solution to equation (II.B.1) can be obtained in an analogous way to that outlined in section (III.B) by means of a point iterative method and yields as the solution  $x$  as a function of time in the well.

$$(H_e + x^n) \frac{x^{n+1,m+1} - 2x^n + x^{n-1}}{\Delta t^2} + \beta g (\text{Term}_1(x^{n+1,m}) + \text{Term}_2) + \frac{3}{4} \left( \frac{x^{n+1,m+1} - x^{n-1}}{2\Delta t} \right) \left( \frac{x^{n+1,m} - x^{n-1}}{2\Delta t} \right) + gx^n = 0 \quad (\text{II.B.3})$$

where  $n$  is the time index and  $m$  is the iteration index.  $\text{Term}_1$  and  $\text{Term}_2$  are two expressions stemming from the discretization of the integral in equation (II.B.1).  $\text{Term}_1$  is dependent on  $x^{n+1,m}$ , the new  $x$  value, whereas  $\text{Term}_2$  is completely known at the beginning of a new time step, since it depends only on old values of  $x$  as shown below. Since equation (II.B.3) is nonlinear and can not be solved explicitly for  $x$ , an iterative solution technique must be used. Multiplying the latter equation by  $(\Delta t)^2$  and solving for  $x^{n+1, m+1}$  the final equation for the solution at time level  $n+1$  becomes

$$\begin{aligned}
 x^{n+1,m+1} = & \frac{(H_e + x^n)(2x^n - x^{n-1}) - (\beta g \text{Term}_2 + g x^n) \Delta t^2}{(H_e + x^n) + \frac{3}{16}(x^{n+1,m} - x^{n-1})} \\
 & + \frac{\frac{3}{16} x^{n-1}(x^{n+1,m} - x^{n-1}) - \beta g \text{Term}_1(x^{n+1,m})}{(H_e + x^n) + \frac{3}{16}(x^{n+1,m} - x^{n-1})}
 \end{aligned} \quad (\text{II.B.4})$$

Equation (II.B.4) must be solved iteratively for  $x$  until there is little change in  $x$  between successive iterations.

The explicit form of the two expressions  $\text{Term}_1$  and  $\text{Term}_2$  can be obtained by discretizing the integral in (II.B.1) as follows :

$$\begin{aligned}
 \int_0^{t_{n+1}} \left( \frac{dx}{d\tau} + \frac{Q_0}{\pi r_w^2} \sin(\omega \tau) \right) \frac{e^{-\alpha/(t_{n+1}-\tau)}}{t_{n+1} - \tau} d\tau \\
 = \sum_{i=0}^n \int_{t_i}^{t_{i+1}} \left( \frac{dx}{d\tau} + \frac{Q_0}{\pi r_w^2} \sin(\omega \tau) \right) \frac{e^{-\alpha/(t_{n+1}-\tau)}}{t_{n+1} - \tau} d\tau \\
 = \frac{1}{2\Delta t} \sum_{i=0}^{n-2} \left[ x^{i+2} - x^i + \frac{Q_0}{\pi r_w^2} \sin(\omega t_{i+1}) \right] \frac{e^{-\left[\frac{\alpha}{(n+1-i-1)\Delta t}\right]}}{(n+1-i-1)} \\
 + \frac{1}{2\Delta t} \left[ x^{n+1} - x^{n-1} + \frac{Q_0}{\pi r_w^2} \sin(\omega t_n) \right] e^{-\frac{\alpha}{\Delta t}}
 \end{aligned} \quad (\text{II.B.5})$$

where we have assumed all  $\Delta t_i$  are equal.

The two terms introduced earlier may now be identified. We must introduce the iteration index  $m$  on the  $x$  at the new time level  $n+1$ .

$$\text{Term}_1(x^{n+1,m}) = \frac{1}{2\Delta t} \left[ x^{n+1,m} - x^{n-1} + \frac{Q_0}{\pi r_w^2} \sin(\omega t_n) \right] e^{-\frac{\alpha}{\Delta t}} \quad (\text{II.B.6})$$

$$Term_2 = \frac{1}{2\Delta t} \sum_{i=0}^{n-2} \left[ x^{i+2} - x^i + \frac{Q_0}{\pi r_w^2} \sin(\omega t_{i+1}) \right] \frac{e^{-\left[\frac{\alpha}{(n+1-i-1)\Delta t}\right]}}{(n+1-i-1)} \quad (II.B.7)$$

With these definitions equation (II.B.4) can be solved for  $x$  in the borehole as a function of time. However, we want to look at the propagation of the wave away from the borehole. In order to do this, we must solve an additional equation (Kabala et al., 1985).

$$s(r,t) = \frac{1}{4\pi T} \int_0^t \left[ \pi r_w^2 \frac{dx}{d\tau} + Q_0 \sin(\omega\tau) \right] \frac{e^{-\left[\frac{r^2 S}{4T(t-\tau)}\right]}}{t-\tau} d\tau \quad (II.B.8)$$

The observation point is at  $r$ , an arbitrary distance from the borehole, and the drawdown ( $s$ ) is given by equation (II.B.8). Since we are using a sinusoidally varying pumpage rate, we would expect the drawdown to be sinusoidal also with an amplitude and phase differing from the signal at the borehole. In general, the solution for this equation would also be done numerically.

Although any arbitrary external discrete forcing function can be used for pumpage, we chose the sinusoidal function outlined above for the first investigations of the behavior of signals transmitted into the aquifer. Figure 1 shows a simulation for which static conditions were initially specified in the borehole (aquifer parameter values are given in Table 1). It can be observed that the peaks of transmitted pulses are phase-shifted with regard to the signal within the well. This is expected according to existing theories (e.g., Streltsova, 1988). Also, the amplitudes decay steadily as one moves away from the well. However, Figure 1 shows that in this case a usable signal has propagated more than 40 meters from the well. This implies that indeed we should be able to propagate sinusoidal signals over significant distances in aquifers.

Finally, the implemented pulse-test code has been validated against SUTRA (Voss, 1984). A precise match of the simulated drawdown with that produced by SUTRA, when specifying equivalent time-dependent boundary flux conditions for the numerical simulator, is shown in Figure 2 (the two curves practically overlaid one another) and confirms that the pulse-test code is working correctly.

### Amplitude and Phase Information

This approach is based upon applying the following homogenous aquifer solution for a propagating sine wave

$$h(x,t) = h_0 \exp(-\sqrt{\frac{S\omega}{2T}}x) \sin(\omega t - \sqrt{\frac{S\omega}{2T}}x) + \text{const.} \quad (\text{II.B.9})$$

to observation data taken from heterogenous aquifers. If we introduce two terms,  $\text{lag} = \sqrt{S\omega / 2T}$  and  $\text{AMP} = h_0 \exp(-\sqrt{S\omega / 2T}x)$ , a plot of  $\ln(\text{AMP}) = \ln(h_0 \exp(-\text{lag} * X_{\text{Obs}})) = \ln(h_0) - \text{lag} * X_{\text{Obs}}$  versus the respective observation location  $X_{\text{Obs}}$  clearly will yield a straight line for a homogenous formation. For a heterogeneous formation, however, the situation might be expected to be different.

Before discussing this approach, some additional analytical manipulations of the two-zone heterogeneous solution presented in McElwee and Butler (1993) will be very useful to understand how the parameters to be estimated (lag and AMP) depend on the observation point location  $x$ . Using the same notation as in section II.E of McElwee and Butler (1993), the analytical solution in the first-zone is

$$\begin{aligned} h_1(x,t) = h_0 e^{-Ax} [(1-F) \sin(\omega t - Ax) + G \cos(\omega t - Ax)] \\ + h_0 e^{Ax} [F \sin(\omega t + Ax) - G \cos(\omega t + Ax)] \end{aligned} \quad (\text{II.B.10})$$

This equation can be rewritten by employing the addition rules for trigonometric functions to yield

$$\begin{aligned} h_1(x,t) = h_0 e^{-Ax} \sqrt{(1-F)^2 + G^2} \sin(\omega t - Ax + \tan^{-1}(\frac{G}{1-F})) \\ + h_0 e^{Ax} \sqrt{F^2 + G^2} \sin(\omega t + Ax - \tan^{-1}(G/F)) \end{aligned} \quad (\text{II.B.11})$$

which shows that the solution in the first zone consists of the superposition of two waves traveling in opposite directions. Equation (II.B.11) can be further manipulated by the cosine law to cast the first-zone solution into a compact form involving only one sine

function term. The respective amplitude factor in front of this trigonometric term becomes

$$AMP = h_0 \sqrt{e^{-2Ax} [(1-F)^2 + G^2] + e^{2Ax} (F^2 + G^2)} \quad (\text{II.B.12})$$

Therefore, the analytical expression for the logarithm of the amplitude for the first zone is

$$\ln(AMP) = \ln(h_0) - Ax + 0.5 \ln[(1-F)^2 + G^2 + e^{4Ax} (F^2 + G^2)] \quad (\text{II.B.13})$$

which shows that there is generally no linear dependence of  $\ln(AMP)$  with respect to the observation location  $x$ . A similar analysis allows us to cast the second-zone solution into the form

$$h_2(x, t) = h_0 e^{-Cx} \sqrt{D^2 + E^2} \sin(\omega t - Cx + \tan^{-1}(\frac{E}{D})) \quad (\text{II.B.14})$$

so that the phase lag and logarithm of the amplitude are given by

$$Lag = -Cx + \tan^{-1}(E/D) \quad (\text{II.B.15})$$

$$\ln(AMP) = \ln(h_0 \sqrt{D^2 + E^2}) - Cx \quad (\text{II.B.16})$$

Equations (II.B.15) and (II.B.16) clearly show that the phase and  $\ln(AMP)$  should plot as straight lines when plotted versus distance for zone 2.

First, we investigated the analytically amenable heterogenous two-zone case. Figures 3 and 4 show the logarithm of the amplitudes  $AMP = h_0 \cdot \exp(-lag \cdot X_{Obs})$  calculated from fitting equation (II.B.9) to the generated two-zone data. The fitted parameters were  $lag = \sqrt{S\omega / 2T}$  and  $h_0$ .  $\omega$  was always kept fixed (assumed known) at the value used to generate the observation data. Table 1 shows the parameter specifications with which the respective two-zone data were generated. It is interesting to note that in each zone the fitted logarithm of the amplitude appears to decay in a linear fashion showing different slopes for both zones which is due to relatively small variations in the transmissivities  $T_1$  and  $T_2$ . The slope of the best fit straight line representing the second zone is identical to

the slope of an equivalent homogenous case (compare Figure 3 and Figure 5) which is in accord with equation (II.B.16), where  $C = \sqrt{S_2 \omega / 2T_2}$  represents the slope within the second zones of Figures 3 and 4. Also, when calculating the amplitude intercept value from equation (II.B.16) at  $x=0m$  we get exactly the same values as those determined in Figures 3 and 14 by fitting. On the other hand, the slope of the best fit straight line representing the first zone is different from that of an equivalent homogenous case (compare Figures 3 and 6). This is again in accord with the analytical solution of the two-zone aquifer indicating that generally we can expect first-zone slopes produced by the suggested fitting procedure to carry information of aquifer zones located further away from the well than where the signal is measured. For the n-zone case the slopes might be expected to carry some weighted information of the hydraulic parameters of those other zones further out from the measurement location. However, an interesting feature of Figures 3 and 4 is that the discrete boundary between zone 1 and zone 2 is easily seen in the plots of the logarithm of the amplitude versus observation distance. This technique could be of good use in some field situations, the main drawback being the necessity of having several observation wells at various distances from the stressed well.

Although not shown here, plots of the phase lag versus observation distance are many times very close to straight line segments with breaks in slope associated with discrete boundaries in aquifer properties. Therefore, plots of phase lag are also good indicators of boundaries and may have some value for field application where sufficient observation wells exist.

In order to investigate whether or not this behavior can also be observed for the one-dimensional n-zone case we resorted to numerical methods and generated oscillatory data for a heterogeneous model aquifer composed of five zones using the finite element program SUTRA (Voss, 1984). Fig. 7 shows the fitted logarithms of the amplitudes versus observation distance which are obtained from fitting the observation data generated with the finite element program. First of all, it should be noted that in more complex systems the overall form of the fitted curve of the logarithm of the amplitude will generally not be stepwise linear. However, the estimation procedure again clearly identifies regions of differing aquifer parameters by showing a significant discontinuity of the slope at the boundaries. In Figure 7, these regions are approximately located at  $x=50m$ ,  $x=120m$ ,  $x=180m$ , and  $x=300m$ . In comparison, the locations of the boundaries of the five aquifer patches had been placed at  $x=50.4m$ ,  $x=116.0m$ ,  $x=180.0m$ , and  $x=304.0m$  for observation data generation with the finite element program. The close reproduction of the boundaries is remarkable. One would suspect that the application of the fitting procedure outlined here might prove very useful in some field applications for

identification of changing aquifer properties and in particular the location of fairly discrete boundaries.

### Conclusions

Presently pulse-testing has exclusively been used for the identification of physical aquifer parameters, specifically for the determination of the spatial distribution of hydraulic diffusivities. Typically, the analysis of pulse test data is based on the analysis of transmitted pulse test signals at one specific observation well assuming a homogenous formation between observation well and pulsed well. A diffusivity value is then assigned to the midpoint of both wells thereby yielding a cartographic interpolation for the hydraulic parameters. Our investigations have revealed the potential of the method to also map the locations of boundaries between aquifer regions having different hydraulic parameters. However, it is necessary to have several observation wells.

The work on pulse testing has been extended to the radial case by using numerical solution techniques. The Theis equation has been coupled to an equation describing the borehole. The purpose was to see if a sinusoidal signal could be transmitted reasonable distances in a radial model. The results of this analysis indicate that a sinusoidal signal generated at a central well can be transmitted large distances relative to those of interest in most contaminant site investigations. The next step was to see if the sinusoidal signal could be analyzed for amplitude and phase to yield some information about heterogeneities it has passed through. The preliminary analysis was done with an analytical, one-dimensional, two-zone model and the results were checked with a numerical model and extended to the case of 5 zones. The preliminary results indicate that plotting amplitude and phase versus distance can yield useful information about heterogeneities, in particular the location of fairly discrete boundaries.

Table 1

Simulation : Fig. :  $T_1$  (m<sup>2</sup>/s) :  $T_2$  (m<sup>2</sup>/s) :  $S_1$  :  $S_2$  :  $X_{Boun.}(m)$

---

No.0	:	1	:	3.0E-2	:	.	:	1.0E-5	:	.	:	.
Case 4	:	3	:	3.0E-2	:	4.9E-2	:	1.0E-5	:	1.0E-5	:	20.0
Case 5	:	4	:	5.9E-2	:	2.9E-2	:	1.0E-5	:	1.0E-5	:	20.0
Case 6	:	5	:	.	:	4.9E-2	:	.	:	1.0E-5	:	.
Case 1	:	6	:	3.0E-2	:	.	:	1.0E-5	:	.	:	.



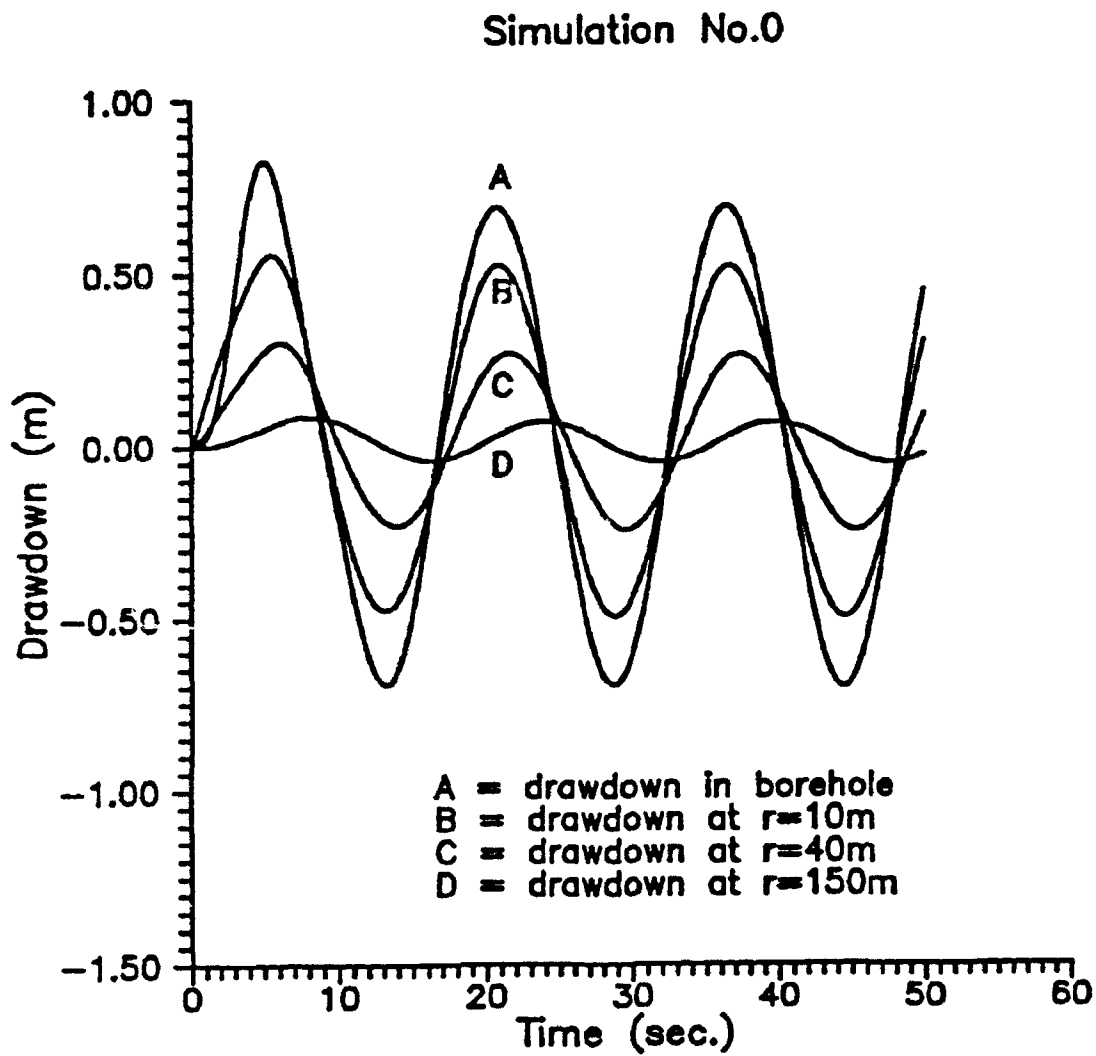


Figure 1. Simulation of pulse test data in a homogenous aquifer with initially static conditions in the borehole.

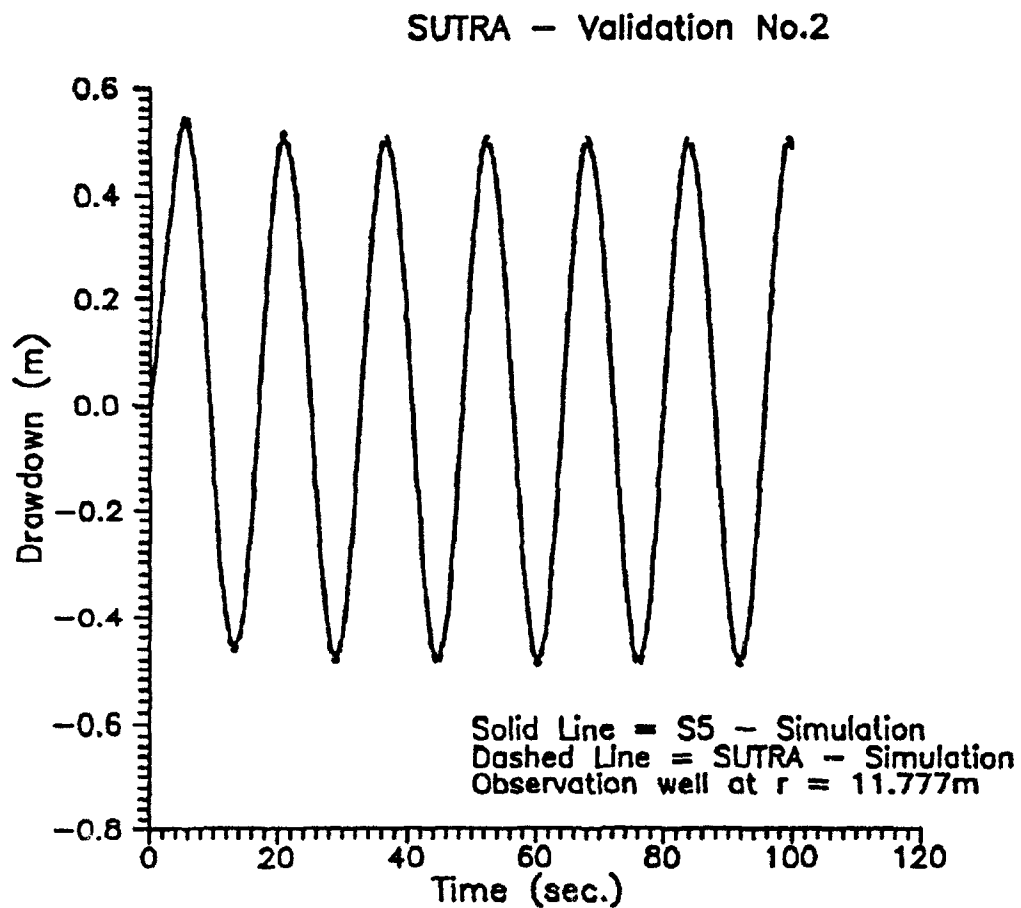


Figure 2. Validation of computer implementation of pulse test program against SUTRA (Voss, 1984).

### Case No.4

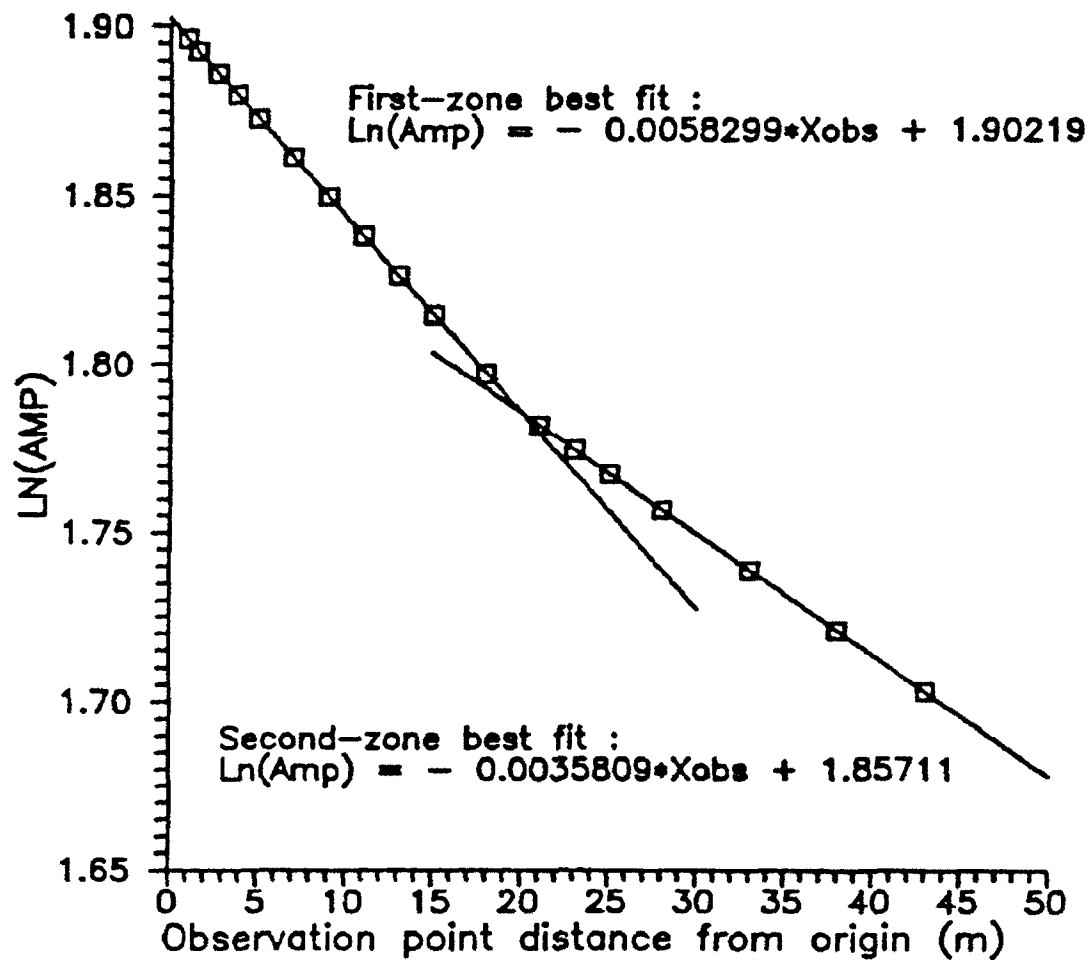


Figure 3. Fitted amplitude  $\text{AMP} = h_0 \cdot \exp(-\text{lag} \cdot X_{\text{obs}})$  versus observation point location for two-zone quasi-steady state data.

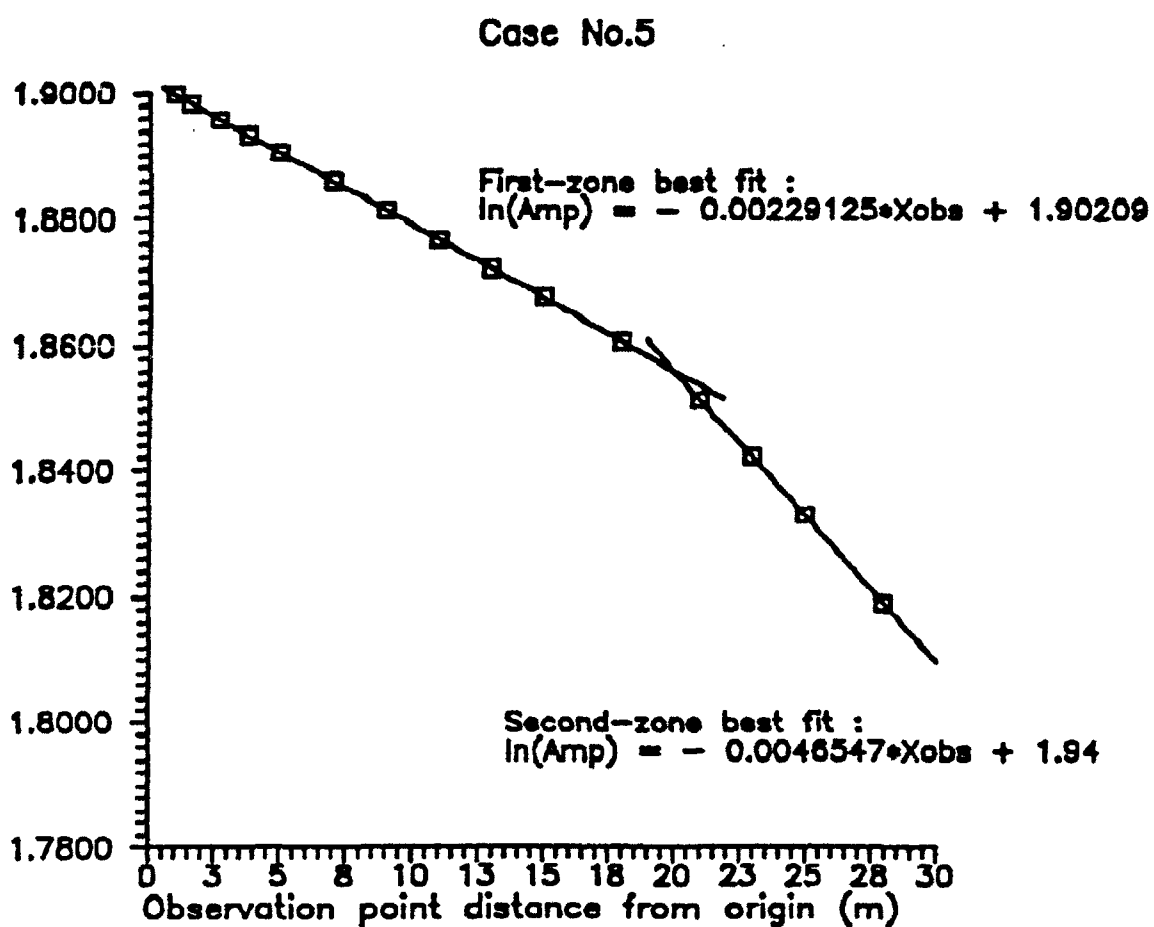


Figure 4. Fitted amplitude  $\text{AMP} = h_0 \cdot \exp(-\text{lag} \cdot X_{\text{obs}})$  versus observation point location for two-zone quasi-steady state data.

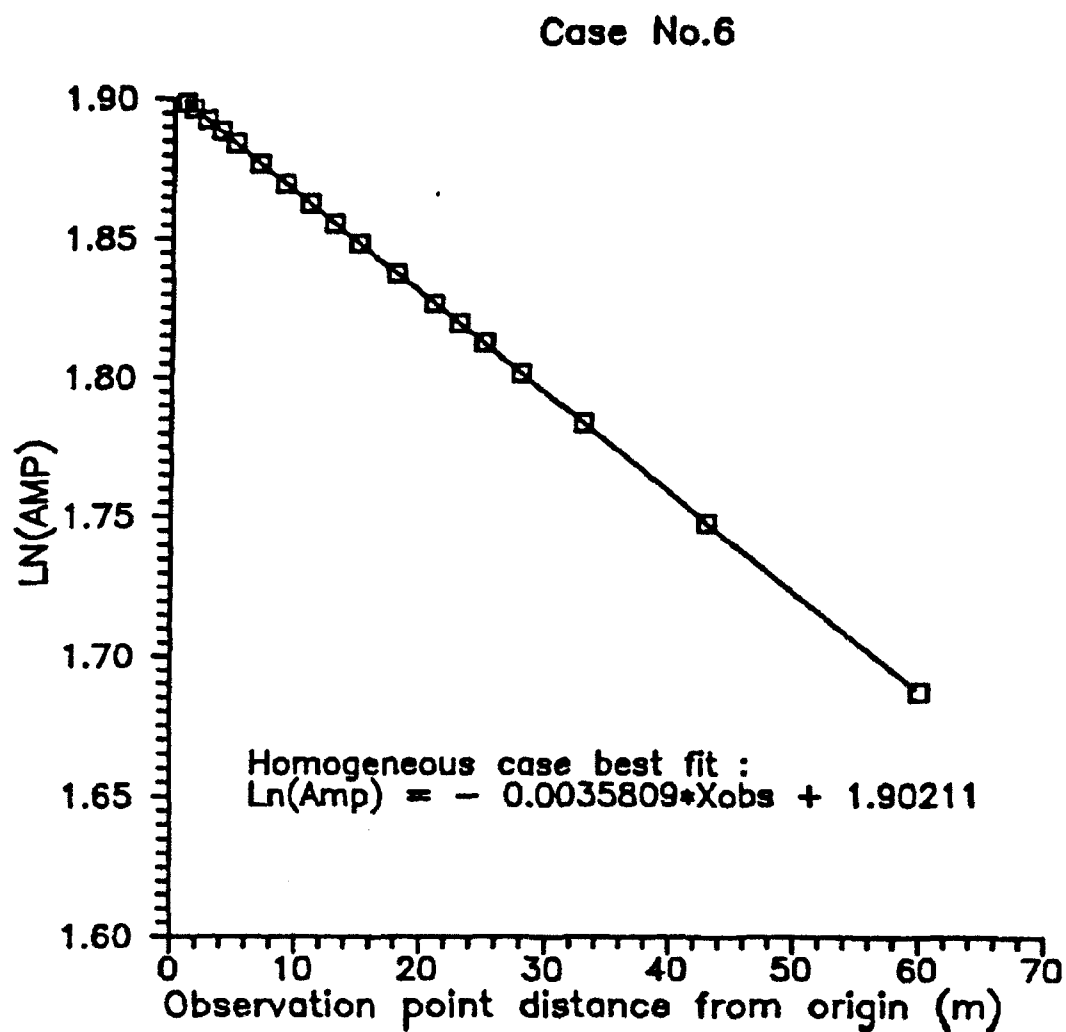


Figure 5. Fitted amplitude  $\text{AMP} = h_0 \cdot \exp(-\text{lag} \cdot X_{\text{obs}})$  versus observation point location for homogenous case data. Physical parameters are the same as for the second zone of two-zone case in figure 3.

Case No.1

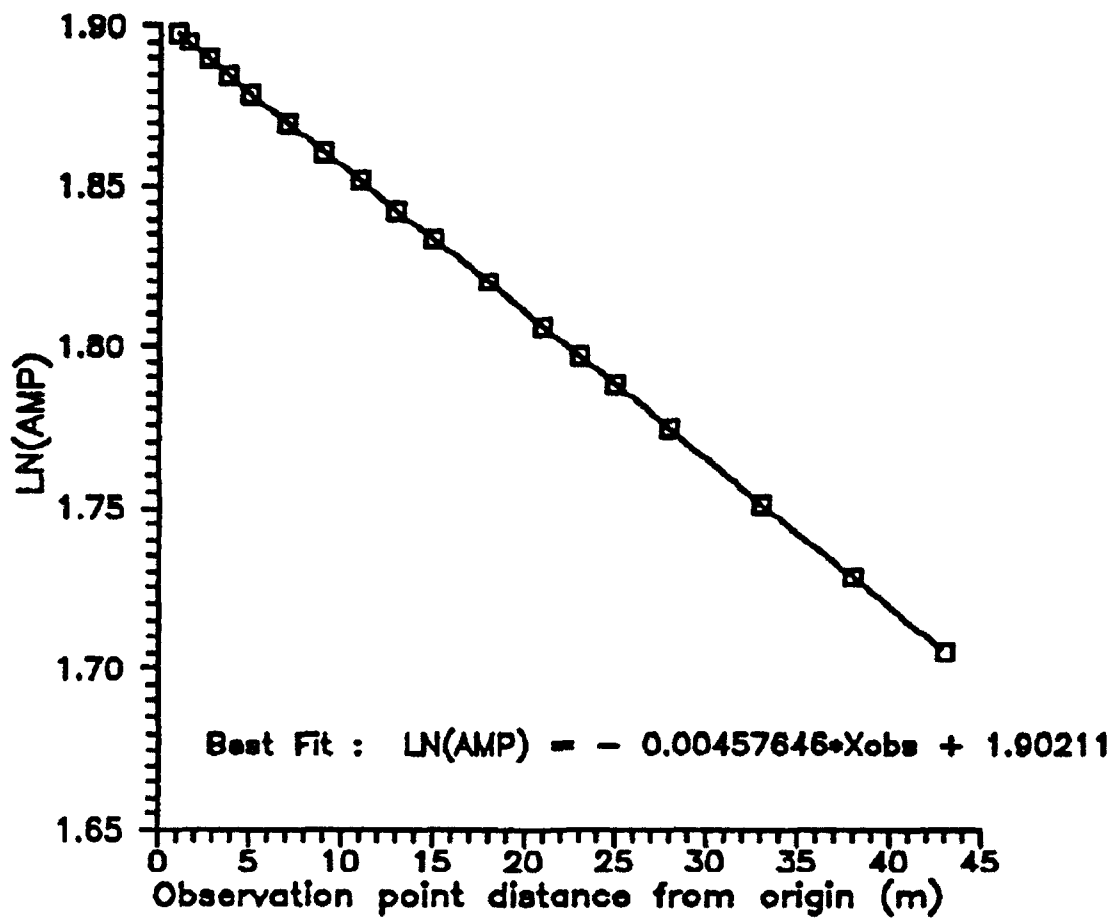


Figure 6. Fitted amplitude  $AMP = h_0 \cdot \exp(-lag \cdot X_{obs})$  versus observation point location for homogenous case data. Physical parameters are the same as for the first zone of two-zone case in figure 3.

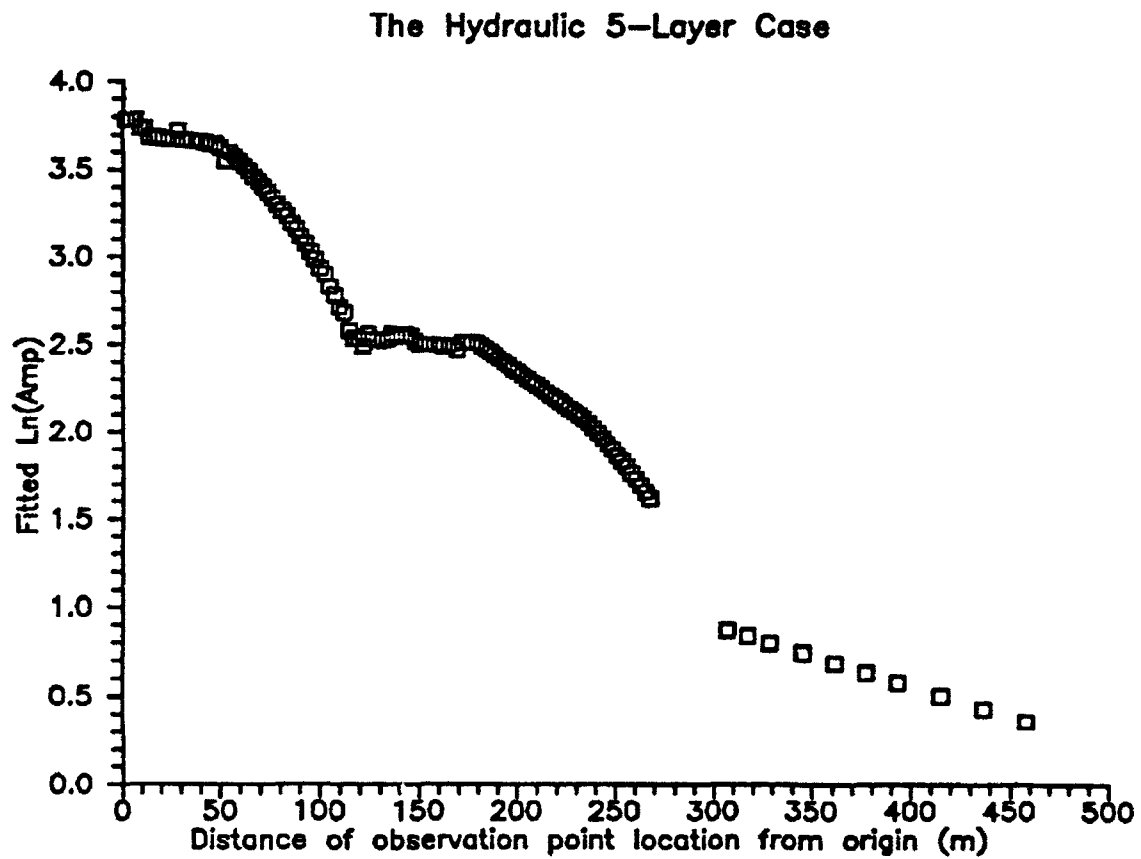


Figure 7. Fitted amplitude  $AMP = h_0 \cdot \exp(-lag \cdot X_{obs})$  versus observation point location for the 5-zone case data generated with SUTRA (Voss 1984).

## C. NUMERICAL SIMULATION OF INDUCED GRADIENT TRACER TESTS

### Introduction

This section presents results of numerical simulations of induced gradient tracer tests. The simulations were performed to address questions regarding the design of an induced gradient test to be performed at the Kansas Geological Survey's Geohydrologic Experimental and Monitoring Site, in the Kansas River valley northeast of the town of Lawrence, KS. The aquifer at the site consists of approximately 35 feet of sand and gravel. This alluvial aquifer is overlain by approximately 35 feet of silt and clay which acts as a semiconfining unit.

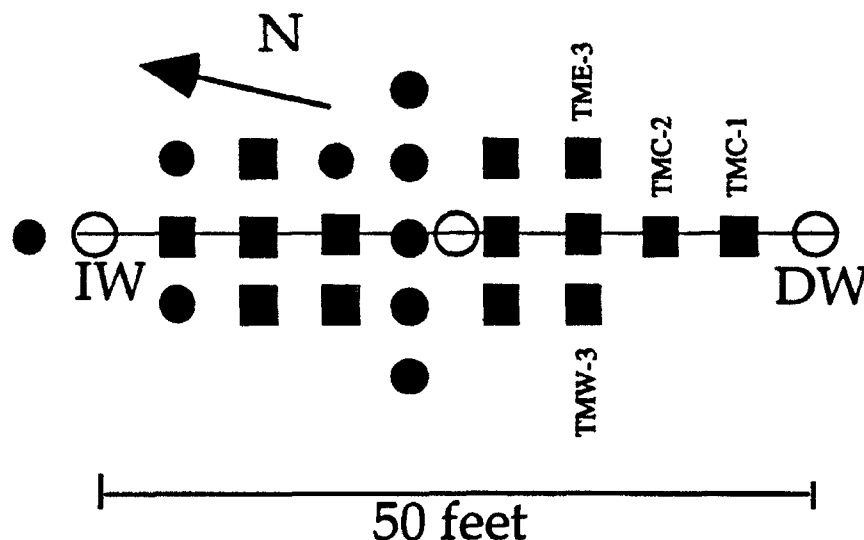
The sampling network for the tracer test will consist of 23 multilevel samplers with 17 sampling ports each. Most of the samplers will have ports every two feet throughout the aquifer thickness. Four of the samplers will be 'detailed' samplers, with ports every foot (except for one two-foot gap to accommodate a coupler between sections of PVC) throughout the bottom 18 feet of the aquifer. Some design questions have been decided by operational logistics. For example, the size of the drill rig limits us to a minimum well spacing of about five feet. The design factors we have some control over are the distance between the injection and pumping wells, width of the network, pumping rate at the discharge well, pumping rate (if any) at the injection well, vertical thickness of the tracer injection zone, the mass of tracer introduced, and whether the tracer is introduced as a pulse or step function at the source. We are trying to develop a network which will allow us to perform tests of several different formats, with both single well convergent and dipole flow regimes, tracer injection over the full aquifer thickness and over certain limited vertical intervals, and possibly two different test scales (requiring an injection well within the sampler network, closer to the discharge well, and another set further away, at the far end of the sampler network). For a given test configuration, important questions to address are: 1) What volume of aquifer is affected by the test? 2) How much mass do we need to introduce to get measurable concentrations throughout the network? 3) How wide does the network need to be in order to contain most of the tracer mass? 4) Will the discharge well be able to capture all the tracer? These questions are addressed using the algorithm of Pollock (1988) to trace streamlines from the injection to discharge wells coupled with a numerical implementation of a solution describing conservative transport along streamlines presented in Welty and Gelhar (1994).

Based on some initial analysis, we have already made some decisions about network design. We are now fairly committed to those decisions, since sampler installation has already begun. The network will be 50 feet long, oriented along the



direction N 20 W. We chose this alignment based on what we thought to be a fairly reliable estimate of the direction of the natural gradient (with the direction of flow being S 20 E). Unfortunately, analysis of additional data has shown that the natural hydraulic gradient at the site is very poorly characterized. A number of measurements taken at more or less at weekly intervals seem to indicate a wildly varying gradient direction. Typical head differences are on the order of a few hundredths of a foot over the horizontal dimensions of the site (a maximum separation of about 135' between piezometer nests). It is possible that the errors in surveyed casing elevations and measured depths to water are of the same magnitude as these head differences, making it impossible to determine the gradient with any accuracy. Most of the estimated gradient magnitudes are in the range  $1 \times 10^{-4}$  to  $1 \times 10^{-3}$  ft/ft, with values greater than  $1 \times 10^{-3}$  often associated with obvious errors in the head measurements. A reasonable average value seems to be about  $3 \times 10^{-4}$  ft/ft. We have used this value in the simulations, for lack of better information. Because of the uncertainty in the gradient direction, we have performed pairs of simulations, one with the natural gradient oriented along the centerline of the tracer test, and a second with the natural gradient perpendicular to the centerline.

The network will be something like that depicted below, where the squares represent those samplers which have been installed as of this writing and the closed circles represent those samplers remaining to be installed.



The detailed samplers will be alternated with the regular samplers along the centerline. The open circles represent injection and discharge wells. The distances between wells

will be about 5 to 5 1/2 feet. The MLS wells will be referenced by row number starting at the discharge well and by C for the centerline and by E or W for east or west of the centerline. The label TM is also used, standing for tracer monitor. A few labels are given in the above diagram for examples. The well represented by the open circle in the middle of the network will be denoted by TMO-1 (O for observation well) and is screened over two different three foot intervals, allowing us to introduce tracer over narrow zones. It will also serve as an observation well for the larger-scale test. It is possible that more than one injection well will be installed at the north end of the network, allowing us to introduce tracer over the entire aquifer thickness and over two limited vertical intervals.

In the simulation of different test scenarios we have employed hydraulic parameters estimated from an earlier pumping test at the site. This and other tests have revealed a significant contribution of leakage from the overlying aquitard. Optimal parameter estimates derived using the leaky artesian function of Hantush and Jacob (1955) are 15.6 ft<sup>2</sup>/min for transmissivity,  $6.84 \times 10^{-4}$  for storage coefficient, and  $2.26 \times 10^{-4}$  ft<sup>-1</sup> for leakage coefficient (square root of  $K'/Tb'$ , where  $K'$  and  $b'$  are the vertical hydraulic conductivity and thickness of the aquitard and  $T$  is the aquifer transmissivity).

### Method of Analysis

This work employs the flowpath-tracing algorithm proposed by Pollock (1988). Pollock developed this algorithm to work with head fields computed by block-centered finite-difference models. The velocity field within each cell is determined by bilinear interpolation of the velocities computed at cell faces. For example the x component of the pore velocity is given by the linear interpolator

$$v_x(x) = v_{x1} + A_x(x - x_1)$$

with

$$A_x = (v_{x2} - v_{x1})/\Delta x$$

where  $v_{x1}$  is the velocity at the left-hand cell face, where  $x = x_1$ ,  $v_{x2}$  is the velocity at the right-hand cell face, and  $\Delta x$  is the cell dimension in the x direction. The cell-face velocities are computed from Darcy's law using the differences between heads in adjacent cells. Schafer-Perini and Wilson (1991) assert that, of a number of proposed methods, bilinear interpolation of cell-face velocities is the only correct, mass-conserving means of computing velocity fields within the cells of block-centered five-point finite-difference models. For further details on the path-tracing algorithm see Pollock (1988). Schafer-

Perini and Wilson (1991) discuss this and other algorithms for tracking contaminant fronts.

We have written a Fortran program to read in a head field computed over a regular two-dimensional grid and compute streamline trajectories using Pollock's algorithm. The user specifies the starting point for each desired streamline and the program traces from this point both backwards and forwards through the flow field, until the streamline reaches a boundary cell or a cell containing a source or sink. The program output includes the (x,y) coordinates of each point where a streamline crosses a cell boundary, the travel times through each cell, and the x and y components of cell-face velocity at each cell boundary along the streamline.

Instead of computing the head field using a finite difference model, we have computed it using the analytical leaky artesian pumping test function of Hantush and Jacob (1955). We computed head values over a regular grid at a time after the solution had reached steady state (about 5000 minutes or 83 hours). The grid ranges from -99 feet to +99 feet with two-foot increments in the x direction and -98 feet to 98 feet with two foot increments in the y direction. The pumping well is located at (x,y) = (25 ft, 0 ft) and the injection well at (-25 ft, 0 ft), each in the center of a grid cell. To incorporate the effects of the natural gradient, we added together the steady-state heads due to pumping/injection and a head field representing the uniform gradient of  $3 \times 10^{-4}$  ft/ft. We were initially unsure of the validity of superposing these two solutions, since the differential equation describing a pumping test under leaky conditions contains a term ( $Ls$ , where  $L$  is the leakage coefficient and  $s$  the drawdown) which is not included in the differential equation describing uniform regional flow. However, both steady state solutions can be regarded as solutions to Poisson's equation, where the right-hand side for the case of the leaky artesian pumping test represents the distributed leakage and the right-hand side for the uniform flow case is zero. Thus, these two solutions can be legitimately superposed.

We have read the output from the path-tracing program into the data analysis package S-Plus and have used them to compute approximate breakthrough curves for any point along one of the computed streamlines, using a numerical implementation of Equations 4, 5, and 7 from Welty and Gelhar (1994). Their Equation 7 describes concentration as a function of displacement along a streamline,  $s$ , and time,  $t$ :

$$c(s,t) = \frac{m}{\rho u(s_0)(4\pi\alpha\omega)^{1/2}} \exp\left[-\frac{(\tau-t)^2}{4\alpha\omega}\right]$$

where  $c$  is a dimensionless mass fraction,  $m$  is the mass per unit cross-sectional area of aquifer at the source ( $s=s_0$ ),  $r$  is the density of the solution,  $u(s_0)$  is the pore velocity at the source, and  $\alpha$  is the longitudinal dispersivity. Transverse horizontal and transverse vertical dispersion are considered negligible in this approach. This is probably a reasonable assumption for many induced gradient tracer tests, since these factors would be expected to become less important as the transport becomes more advectively dominated.  $\tau$  and  $\omega$  are both line integrals along the streamline.  $\tau$  is simply the advective travel time from the source to a point along the streamline, given by Equation 5 of Welty and Gelhar (1994):

$$\tau(s) = \int_0^s \frac{ds}{u(s)}$$

This integral is easily approximated by summing travel times through cells computed using Pollock's algorithm. The integral  $\omega(t)$  accounts for the influence of the varying velocity field on dispersion. It is given by Equation 4 of Welty and Gelhar (1994):

$$\omega(t) = \int_0^{\bar{s}} \frac{ds}{[u(s)]^2}$$

where  $\bar{s}$  is the mean displacement at time  $t$ , found from  $\tau(\bar{s}) = t$ . This integral can be approximated using the output from the path-tracing program by first rewriting it as an integral over time. Since  $ds = udt$ , we can write

$$\omega(t) = \int_0^t \frac{d\tau}{u(\tau)}$$

This integral can be approximated as

$$\hat{\omega}(t) = \sum_i u_i^{-1} \Delta t_i$$

where the index  $i$  runs over the grid cells from the starting point of the streamline up to and including the cell which the streamline exits at time  $t$ ,  $\Delta t_i$  is the travel time through cell  $i$ , and  $u_i^{-1}$  is taken as the average of the inverse velocities at the points where the streamline enters and exits cell  $i$ . As we have implemented this solution,  $\hat{\omega}(t)$  is evaluated only at those times when the streamline exits a cell. Thus the breakthrough

curve at any given point,  $s$ , is built up by computing  $c(s,t)$  at times corresponding to cell-face crossing times for the streamline passing through the point of evaluation. The breakthrough curves could be computed over finer time increments by evaluating  $\hat{w}(t)$  for every desired value of  $t$ , since  $u(t)$  can be expressed at all times, not only at cell-face crossing times, using the analytical expressions presented in Pollock (1988). In addition, it is possible that an analytical expression for  $\hat{w}(t)$  could be developed from the analytical expression for  $u(t)$ , on a cell-by-cell basis. As of this writing, we have not figured out how to perform that integral.

To verify this method of computing breakthrough curves, we have compared the method to Equation 26 of Welty and Gelhar (1994), which describes the response to a pulse input of concentration in a single-well radially convergent test under confined conditions. We have modified this equation to describe breakthrough curves at observation wells other than the discharge well. The primary modifications involve 1) changing the advective travel time to  $V/Q$ , where  $V$  is the volume of aquifer porosity contained between the radial location of the injection well and the radial location of the observation well ( $2\pi(R^2-r^2)nb$ , where  $R$  is the injection radius and  $r$  the observation radius,  $n$  the porosity, and  $b$  the aquifer thickness), rather than the entire volume between the injection and discharge wells, and 2) scaling up the initial mass per unit cross-sectional area,  $m$ , to account for the actual width and thickness of the injection zone. Since Welty and Gelhar are interested only in describing concentrations in the discharge well, they can treat the injected mass as if it were distributed symmetrically over the entire circle of radius  $R$ , rather than over a narrow wedge between the injection and discharge wells. To describe the concentration within this wedge, the initial mass per unit area must be scaled up by  $2\pi/\theta$ , where  $\theta$  is the angular width of the initial injection. In addition, if the tracer is assumed to occupy a thickness,  $\Delta z$ , less than the full aquifer thickness,  $b$ , then the concentrations must also be scaled up by  $b/\Delta z$ . These scaling factors can be quite large in practical situations, implying that even if fairly large concentrations exist in the streamtube containing the tracer, they could be diluted to very small values in the discharge well itself.

Figure 1 shows the advective displacement computed by the path-tracing algorithm versus that computed from  $2\pi(R^2-r^2)nb/Q$  for the case of a radially convergent tracer test with 50 feet between the injection and discharge wells. The discharge well is pumping at  $Q = 60$  gpm and the tracer is assumed to be introduced in a fashion that does not significantly alter the radial flow field. The input to the path-tracing algorithm was actually the steady state head field generated using the leaky artesian function and hydraulic parameters described above. Thus, the flow regime for the path-tracing

algorithm does not exactly match the purely confined flow field assumed in Equation 26 of Welty and Gelhar (1994). The leaky artesian function was employed in this case simply to allow a true steady state solution to be reached. As demonstrated in Figure 1, the advective displacements predicted by the two methods match almost exactly, indicating that the leakage does not contribute a significant volume of flow over the 50 feet between the injection and discharge wells.

Figure 2 compares the breakthrough curves generated using our modified version of Welty and Gelhar's Equation 26 and the numerical method described above, for two observation wells, one 25 feet from the discharge well and the other 7 feet from the discharge well. The concentrations shown are based on a tracer mass of 0.005 kg introduced over a three foot injection thickness and occupying one foot transverse width at the injection radius of 50 m. It is assumed that the vertical thickness of the tracer plume does not change significantly and that measurements have been taken within the zone occupied by tracer. It is clear that there is a significant difference between the two breakthrough curves computed at the 25-foot observation radius. The numerical method overpredicts dispersion relative to Welty and Gelhar's Equation 26. This could result from the discrepancy between the flow regimes, with more dispersion due to velocity variation occurring in the presence of leakage, or simply to inaccuracy of the numerical method, which is based on a fairly crude approximation of the inverse velocity in each cell. Nevertheless, the results are similar enough to consider the numerical method adequate for the purposes of answering design questions regarding magnitude of concentrations expected and approximate time required for the pulse to pass a given point in the network. More rigorous verification of the method would be required before using it for actual tracer test analysis.

The above simulations also answer a critical design question, indicating that we can achieve measurable concentrations of tracer over the proposed network length of fifty feet using a reasonable tracer mass, at least if the tracer is introduced over a relatively small vertical interval, negligible vertical dispersion occurs, and we measure concentrations within the zone occupied by tracer. Clearly, a thicker injection interval will require a proportionally larger amount of mass to achieve the same concentrations in the aquifer. This test format represents a limiting case, since any kind of continuous injection would allow us to introduce more mass than the pulse input simulated here. However, as demonstrated below, continuous injection involving a significant volume of injected water will cause the injected mass to be spread over a larger volume of aquifer, reducing concentrations.

### Streamline Patterns for Different Test Scenarios

Figures 3 through 8 demonstrate the streamline patterns generated using six different test scenarios. The pumping rate at the discharge well, at  $(x,y) = (25 \text{ ft}, 0 \text{ ft})$ , is 60 gallons per minute in all cases, and the magnitude of the natural gradient is  $3 \times 10^{-4}$  ft/ft. The simulations are in pairs, with the natural gradient aligned along the network centerline in the first case and perpendicular to it in the second case. Figures 3 and 4 demonstrate the case of zero pumping rate at the injection well, at  $(x,y) = (-25 \text{ ft}, 0 \text{ ft})$ . For both these figures the starting points for the three streamlines shown are  $(25,0)$ ,  $(25,-0.5)$ , and  $(25,0.5)$ , i.e., at the injection well itself and half a foot to either side. Due to the neglect of transverse dispersion in this analysis, the tracer plume would be expected to occupy a very narrow region, the horizontal width of which would be determined solely by the initial spreading due to tracer injection. It is expected that the effects of transverse dispersion will indeed be small, implying that a fairly narrow network would contain most of the tracer mass. For a single-well convergent test, multilevel samplers would probably not need to be placed any more than a few feet off the network centerline. In the simulation with the gradient perpendicular to the network centerline, the plume is deflected about two feet (maximum) off the centerline. If the plume is only a few feet wide, a significant portion of it could pass between the centerline and off-centerline samplers, if these are too far apart. As mentioned a minimum spacing of about five feet is dictated by drilling logistics. Thus for this format of test we might want to intentionally induce some spreading of the tracer mass upon injection, in order to reduce the risk of losing the pulse between samplers.

Figures 5 and 6 show the streamline patterns generated using a pumping rate of 6 gallons per minute at the injection well, one tenth the pumping rate at the discharge well. In these simulations, the starting points of the streamlines are 39 points evenly spaced on a circle of radius one foot centered on the injection well. Even this small injection rate results in a test that encompasses a much larger volume of aquifer than the zero-injection case, with the possibility of significant tracer mass occurring up to about eight feet to either side of the centerline, for the case with the network centerline aligned with the natural gradient. This test format is somewhat more robust with respect to uncertainty in the direction of the natural gradient. Portions of the tracer plume could be deflected by a few feet by the natural gradient, but clearly a network designed to sample the plume generated by the flow regime depicted in Figure 5 would not miss too much of the plume generated by the flow regime depicted in Figure 6.

Figures 7 and 8 depict the streamlines resulting from a 25 gallon per minute injection rate, with all other factors remaining the same as in Figures 5 and 6. These

figures show fairly clearly the grouping of streamlines resulting from the fact that the source point is embedded in a square cell, with notable gaps between the groups of streamlines emanating from each of the four sides of the cell. It is probably reasonable to mentally interpolate the pattern of streamline density shown by the other streamlines into these gaps, to make up for this artifact of the procedure. Even with the network centerline aligned with the natural gradient, some of the extreme streamlines reach out further than 30 feet from the centerline. A network of this width is not possible with our current resources. With the natural gradient perpendicular to the plume centerline, some of the 'downgradient' streamlines extend almost 50 feet from the plume centerline. Injecting at this rate, therefore, could introduce the possibility of not capturing all the tracer mass with the discharge well. Although all the streamlines converge on the discharge well under the conditions depicted in Figure 8, it is quite possible that non-idealities in the actual flow pattern would result in some tracer mass being transported away from the site given this magnitude of plume spreading due to injection.

#### **Breakthrough Curves for Different Test Scenarios**

Figure 9 shows the advective tracer displacement for the three test scenarios described above with the sampler network aligned along the natural gradient. The results are computed along the centerline between the injection and discharge wells. The starting point for the travel time calculation, in this case, is actually the right edge of the grid cell containing the injection well, one foot to the right of the center of the well. This starting point is used due to the poor representation of the velocity field within the source cell itself. Nevertheless, the computation can be viewed as representing the travel time from the edge of an injected pulse one foot in radius. Clearly, increasing the injection rate leads to significant reductions in the overall time of the tracer test. The advective front reaches the discharge well in approximately 147 hours with a zero injection rate, 112 hours with a 6 gpm injection rate, and 78 hours with a 25 gpm injection rate. Thus, if we perform a dipole test, the injection rate we use will be governed somewhat by the rate at which we can sample ports. We want the test to be completed within a reasonable amount of time (say about a week). At the same time, we do not want the plume to move too fast relative to the rate at which we can take samples. Since we do not yet know how long it will take us to obtain samples from all 17 ports of each sampler, we may have to perform some practice tests before we can determine the optimal injection rate for a dipole test.

Figure 10 shows the breakthrough curves computed midway between the injection and discharge wells, assuming a unit pulse injection of 1 gram per square foot at the



source (one foot from the injection well). Actual concentrations obtained in a pulse input test would be obtained by scaling the concentrations shown according to the actual mass per unit area obtained at a radius of one foot from the injection well. The response to a finite duration injection would be obtained by convolving the unit impulse response shown in Figure 10 with the actual input mass history.

Figure 10 demonstrates that the higher injection rates result in considerably lower concentrations at a given point for the same mass input history. The greater acceleration created by the higher water injection rate results in more dispersion due to velocity variations. Most likely, a continuous mass injection of some duration would be used with the higher (water) injection rates, compensating somewhat for the greater dispersion. Nevertheless, given the limited width of our proposed network and our desire to obtain more detailed information along the network centerline, it would probably be best to use a lower injection rate in any dipole tests that we might perform.

The simulated results can be used to estimate the amount of mass required for a desired concentration at the midpoint of the network. For example, to obtain a concentration of 24 ppm at the midpoint using a single well convergent ("no injection") pulse input test, a mass density of approximately 3 grams/ft<sup>2</sup> would be required at the source, 1 foot from the injection well. Assuming that the tracer injection occurs over the entire aquifer thickness, the pore area represented by this ring is  $2\pi r_0 b n = 2\pi(1\text{ft})(35\text{ft})(0.3) = 66\text{ ft}^2$ . Thus,  $(3\text{ g/ft}^2)(66\text{ ft}^2) = 198\text{ grams}$  of tracer would have to be distributed around this ring in order to obtain the desired concentration 25 feet from the injection well. To obtain a source concentration, one would have to assume that this ring actually occupies a disk of finite radial width with volume  $\pi(r_0^2 - r_i^2)bn$ , where  $r_i$  is the inner radius of the disk, yielding a mass per volume concentration of  $(m)(2\pi r_0 b n)/(\pi(r_0^2 - r_i^2)bn) = 2mr_0/(r_0^2 - r_i^2)$ , where  $m$  is the required mass per unit area. Basically, the difference between  $r_0$  and  $r_i$  needs to be taken small enough to represent a pulse injection, for all practical purposes. Taking  $r_i$  to be 0.9 feet, the required source concentration would be about 32 grams/ft<sup>3</sup>, or 1100 ppm. We will probably need to perform some preliminary experiments to find out how the mechanics of tracer injection affect the initial distribution of mass around the injection well before we make a final decision on the amount of tracer mass to use and how to introduce it.

## Conclusions

We have combined the semi-analytical pathline-tracing algorithm proposed by Pollock (1988) with an analytical solution for advective-dispersive transport along a streamline to compute tracer concentrations at arbitrary points in a tracer test network.

We have used this method to evaluate the efficacy of a proposed sampler network design under different test scenarios. Specifically, we have computed streamline patterns for three different water injection rates (0, 6 and 25 gpm) at an injection well located 50 feet from a discharge well pumping at 60 gpm. For each injection rate, we have performed a pair of simulations, one with a natural gradient of  $3 \times 10^{-4}$  ft/ft aligned along the network centerline, and another with a gradient of the same magnitude aligned perpendicular to the network centerline. These simulations demonstrate the expected width of the tracer cloud for each test scenario. With no pumping at the injection well, the simulations demonstrate that the tracer cloud width is expected to be quite small. In fact, without assuming that the tracer initially occupies some finite width (due to mixing during injection), the method would predict a plume of zero width, due to its neglect of transverse dispersion. In reality, one would expect a fairly narrow plume under this scenario, assuming lateral dispersive processes are indeed negligible. Under these conditions, there is some danger that the plume could pass between the lines of samplers along the centerline and those to either side, if the natural gradient is at a significant angle to the centerline.

The simulations with a 6 gpm injection rate are less affected by the natural gradient. i.e., a network designed for a test with the natural gradient aligned along the network centerline will probably also be appropriate for a test with the gradient at a significant angle to the network centerline. The higher injection rate (25 gpm) induces too much spreading of the tracer plume, introducing the risk of losing some of the tracer due to non-idealities of the flow system. In addition, higher water injection rates induce more dispersion, reducing concentrations in the tracer network.

It appears as if we have chosen a viable network design, despite some errors in our initial assessment of the natural gradient at the site. It is possible that we could use a somewhat larger discharge rate to overcome the effects of the natural gradient to a greater degree. However, we probably cannot pump at any more than 80 gpm from the discharge well that we will be installing. This will probably not change the results greatly from the simulations presented above using 60 gpm. It appears as if a discharge well pumping at 60 gpm will be able to capture the tracer mass as long as we do not introduce too much tracer spreading by using too high a rate of water injection. We still have a number of decisions to make regarding the amount tracer mass to use and how to introduce it. The numerical method of breakthrough curve computation presented above will be valuable in this ongoing work, allowing us to determine expected travel times and concentrations for fairly arbitrary flow configurations.

Figure 1: Advective Displacement for Radially Convergent Test

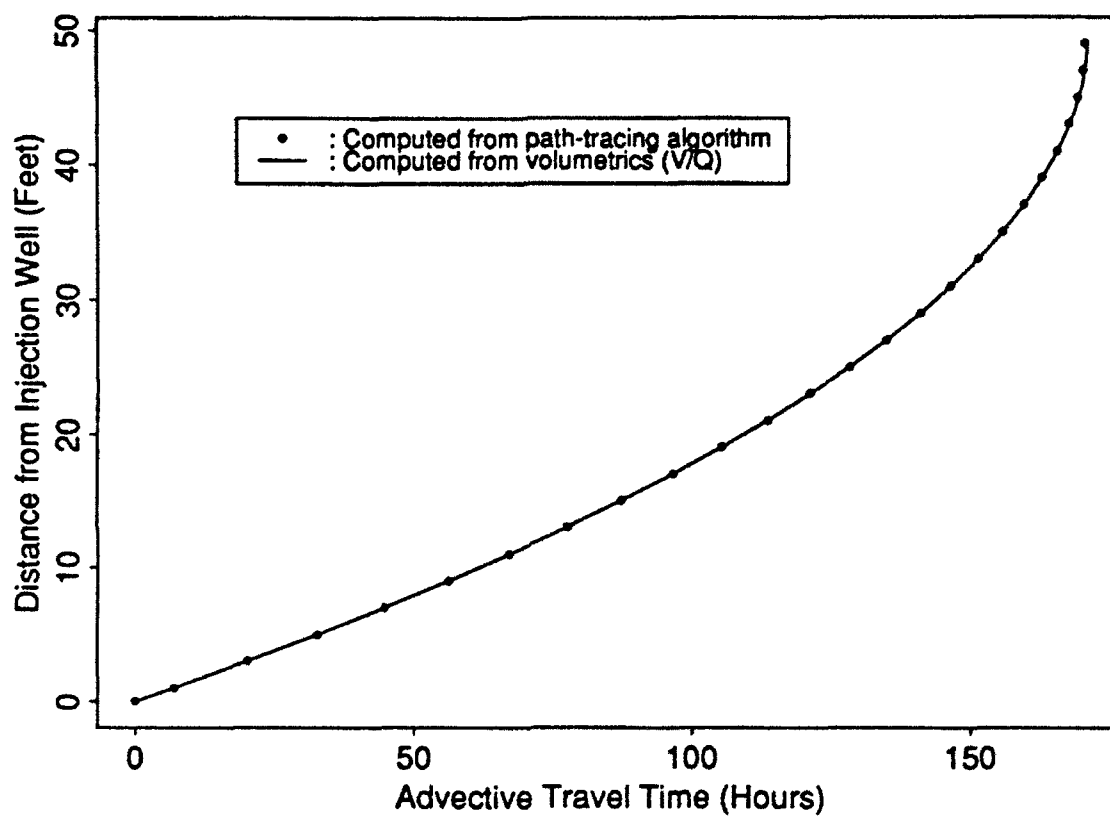


Figure 2: Breakthrough Curves for Radially Convergent Test

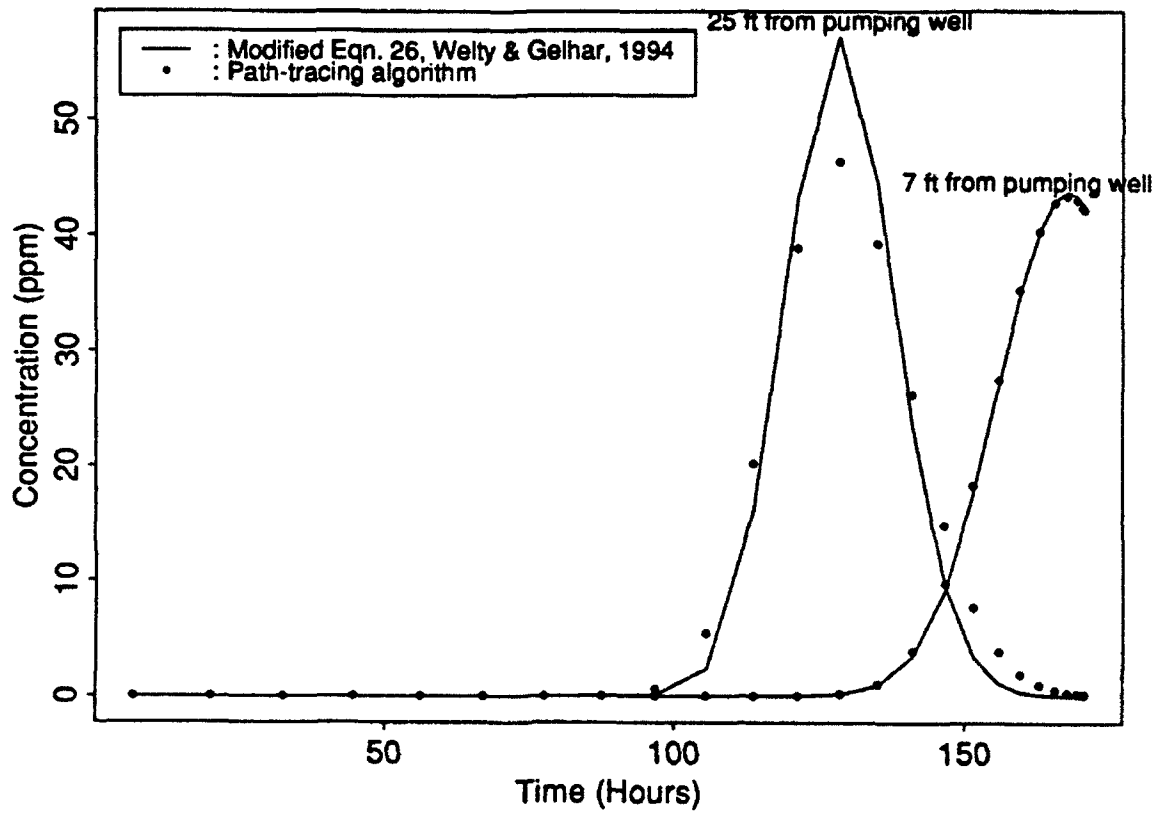


Figure 3: Zero Injection, Gradient Along Centerline

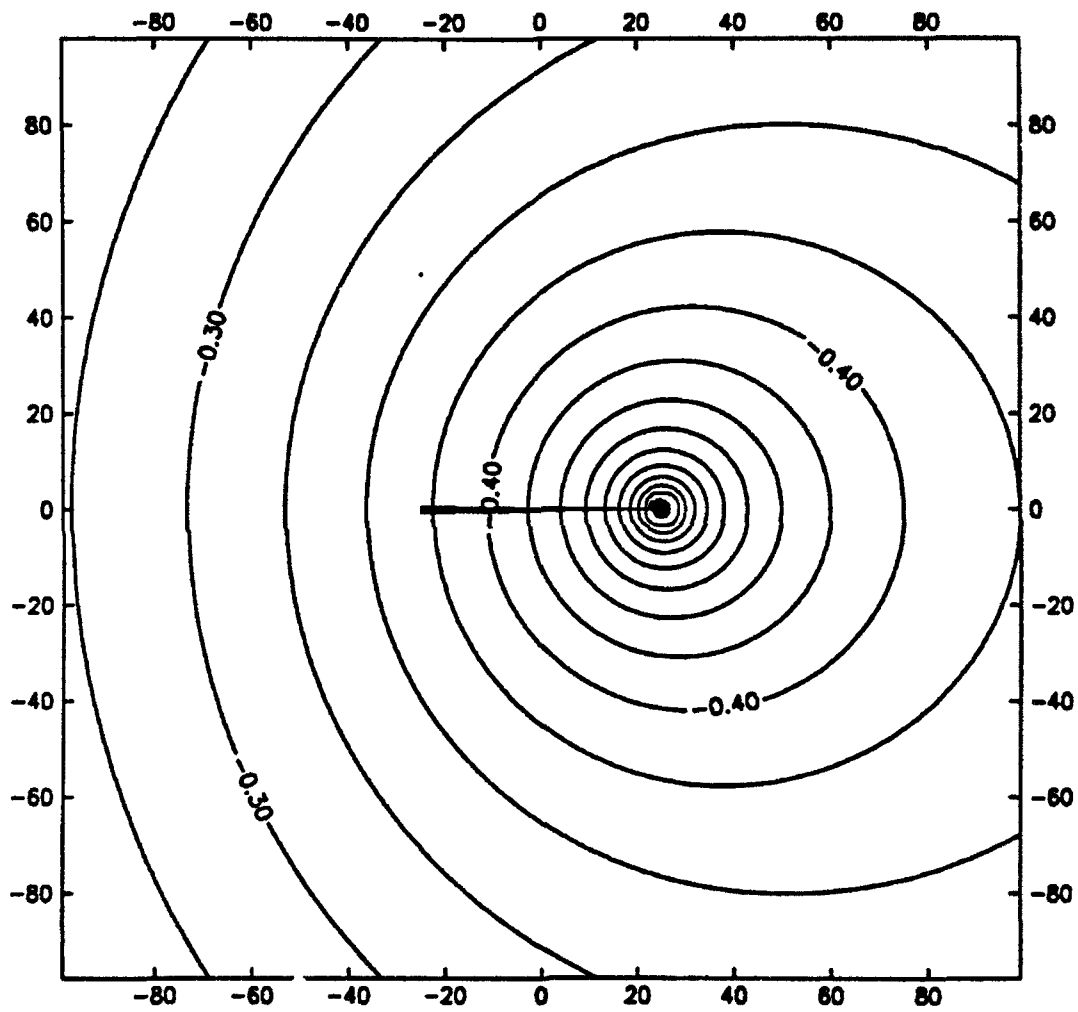


Figure 4: Zero Injection, Gradient Perpendicular to Centerline

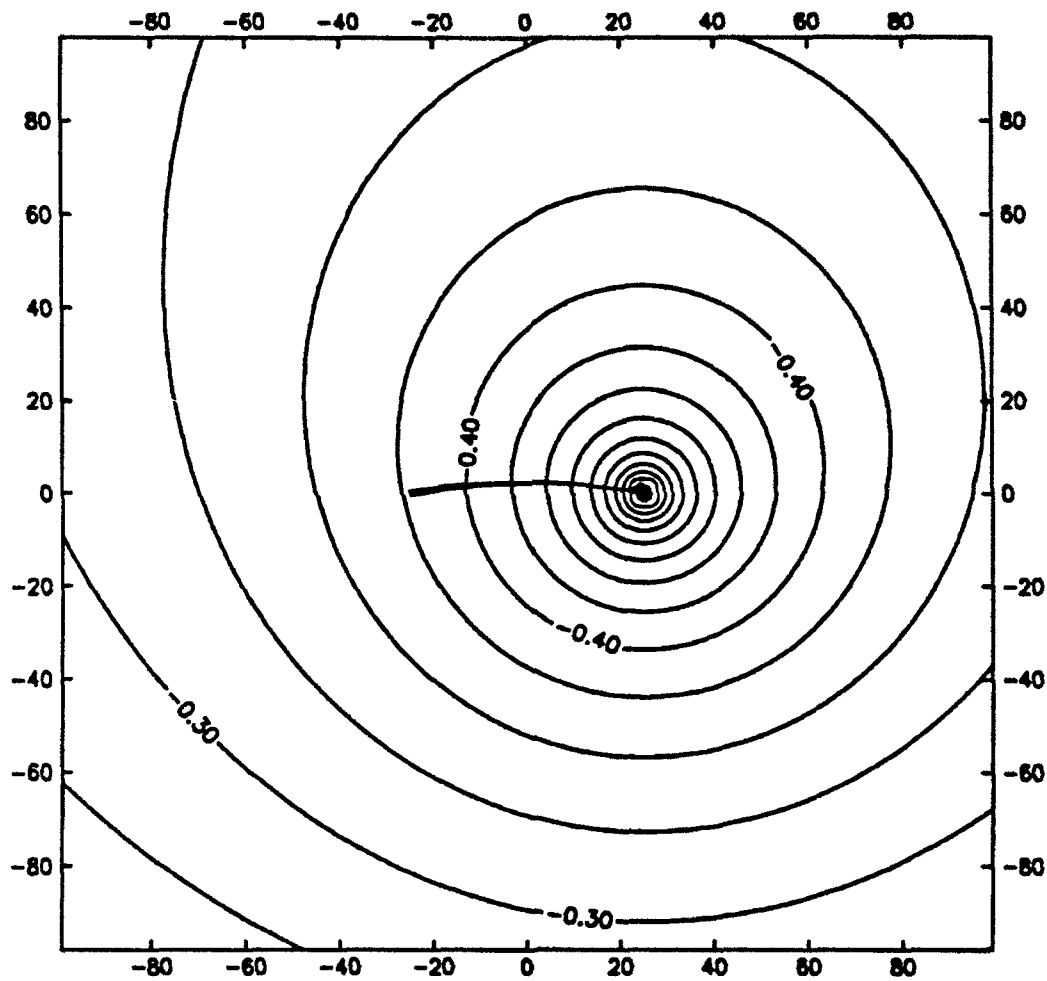


Figure 5: 6 GPM Injection, Gradient Along Centerline

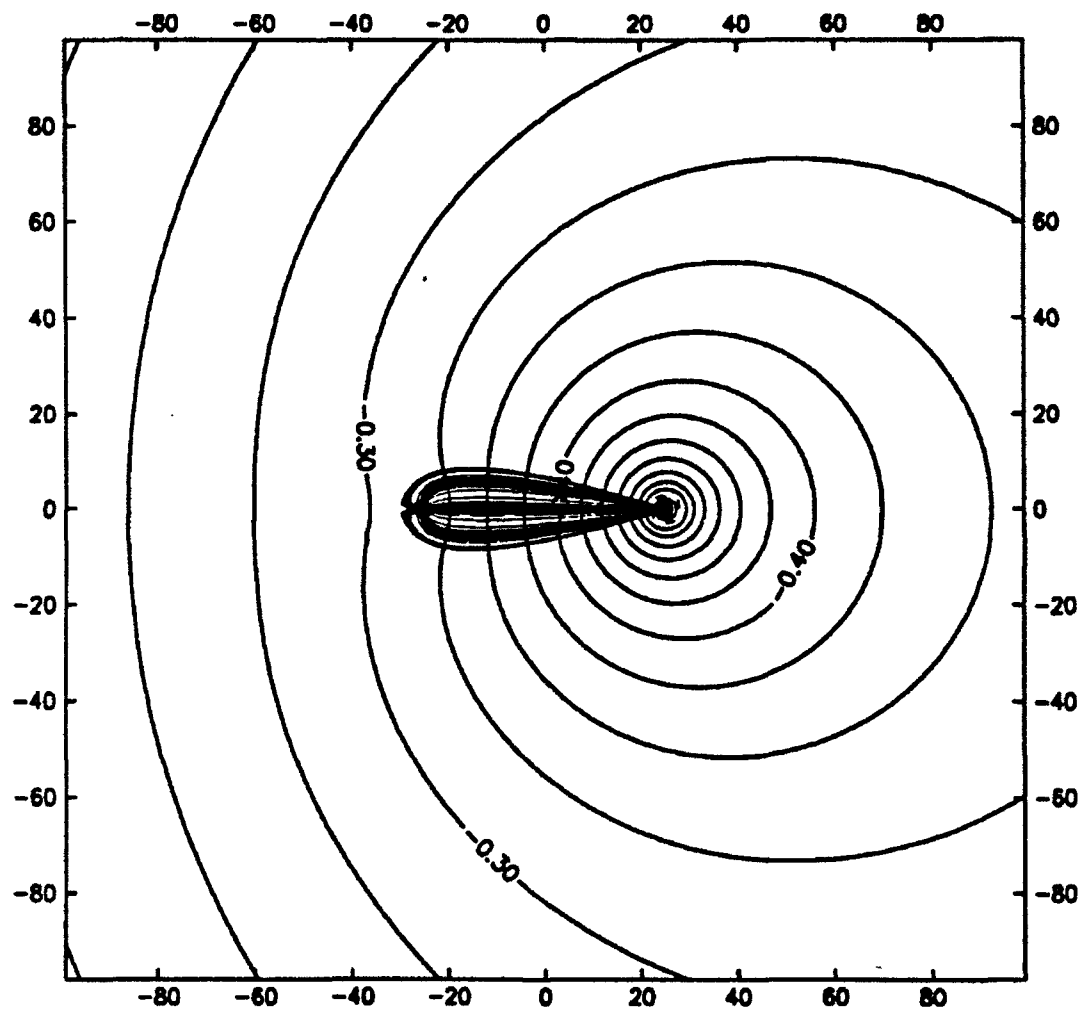


Figure 6: 6 GPM Injection, Gradient Perpendicular to Centerline

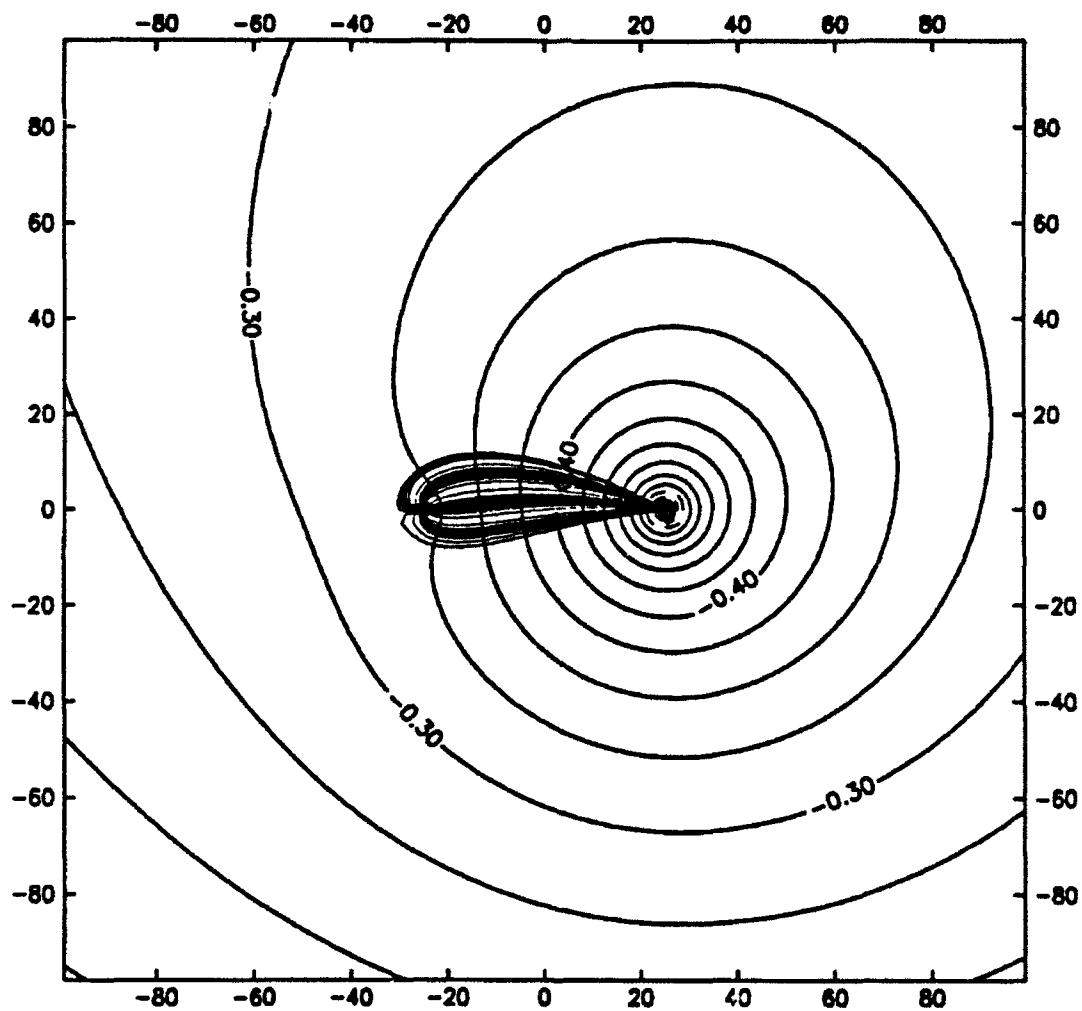




Figure 7: 25 GPM Injection, Gradient Along Centerline

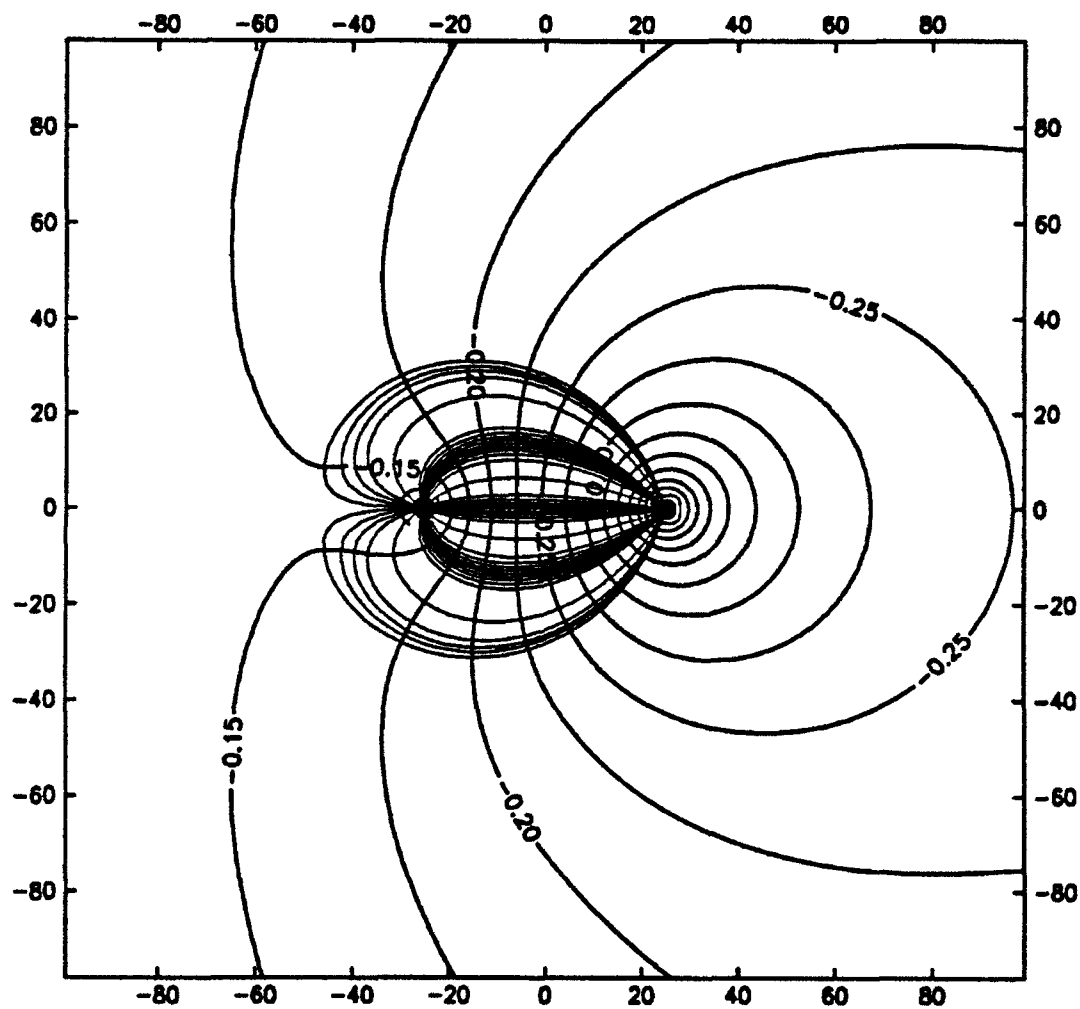


Figure 8: 25 GPM Injection, Gradient Perpendicular to Centerline

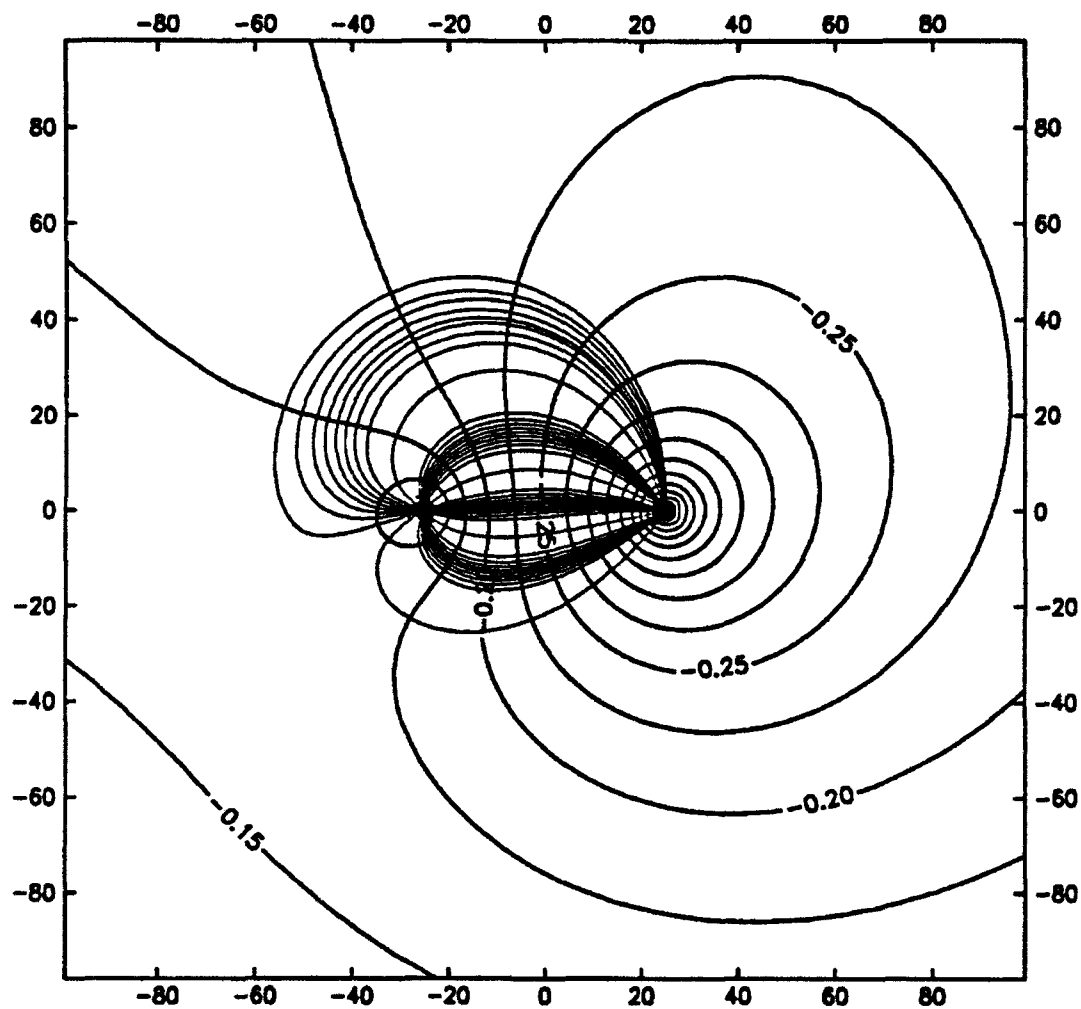


Figure 9: Advective Displacement for Three Test Scenarios

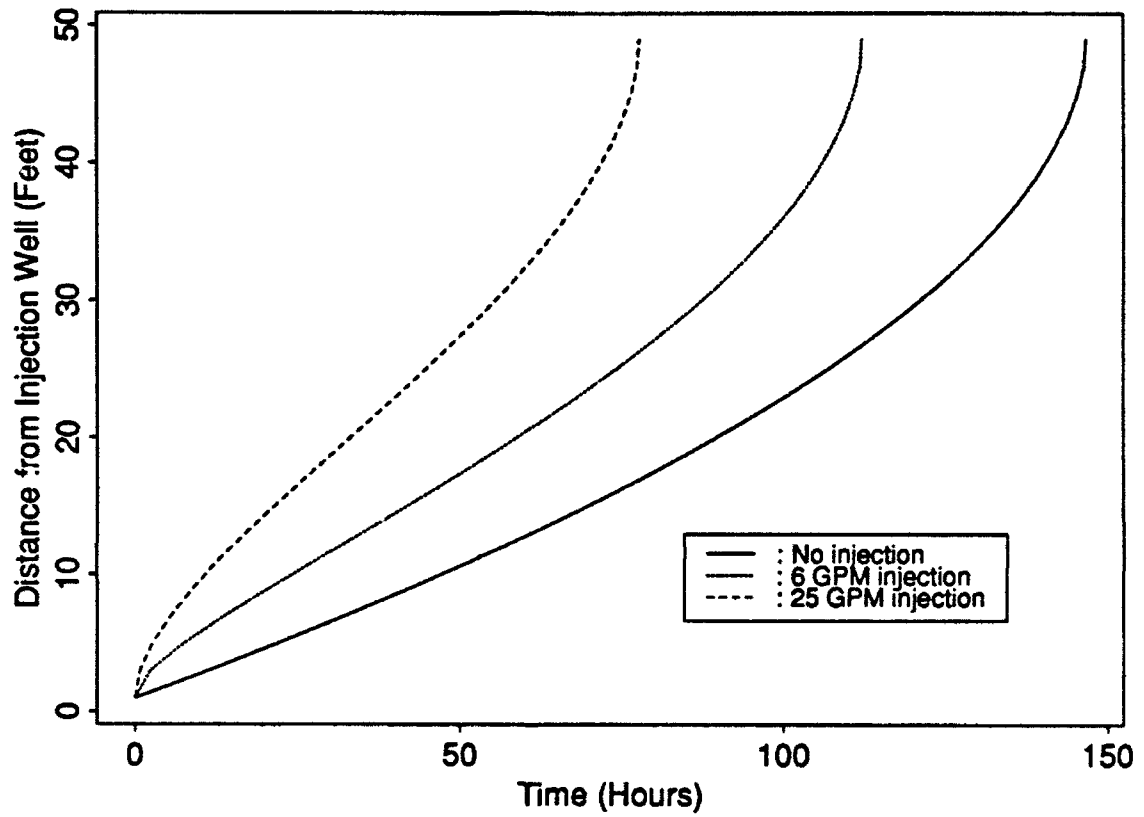
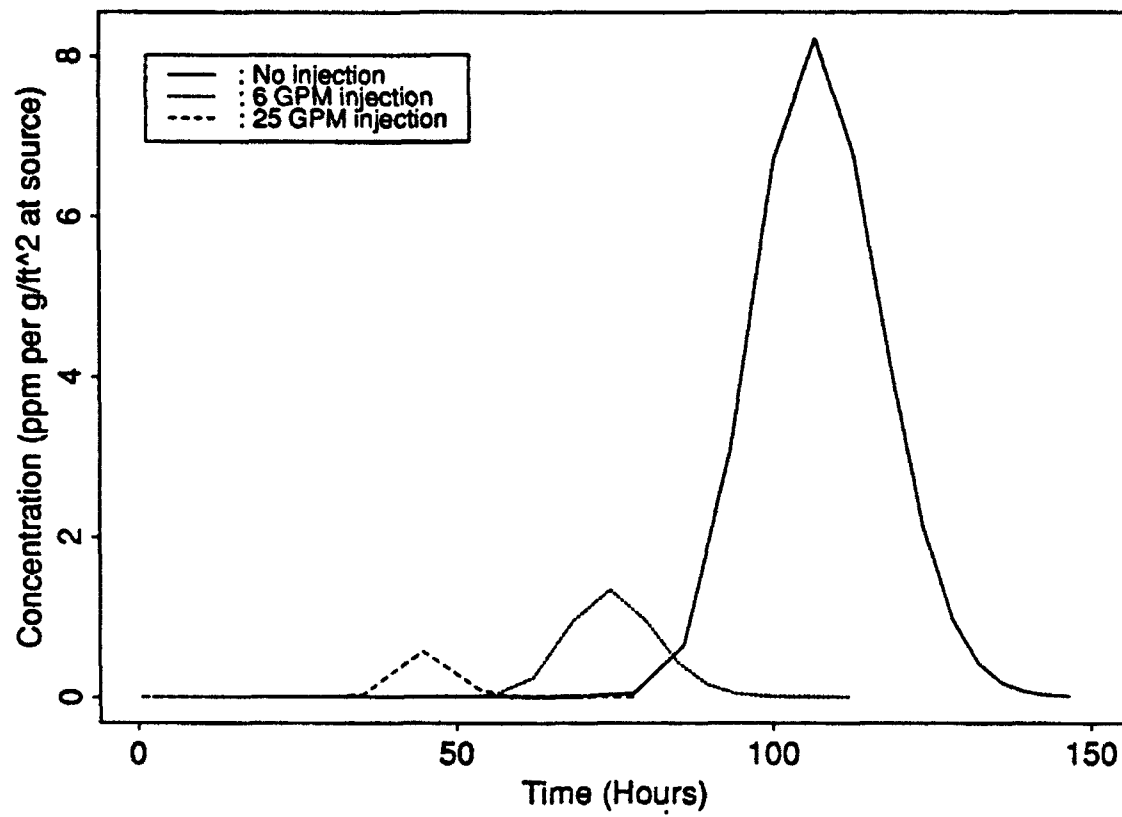


Figure 10: Breakthrough Curves for Three Test Scenarios



### **III. FIELD INVESTIGATIONS OF MULTILEVEL SLUG TESTS**

#### **A. IMPROVING THE RELIABILITY OF PARAMETER ESTIMATES OBTAINED FROM SLUG TESTS**

##### **Abstract**

The slug test is one of the most commonly used field methods for obtaining in-situ estimates of hydraulic conductivity. Despite its prevalence, this method has received criticism from many quarters in the groundwater community. This criticism emphasizes the poor reliability of the estimated parameters, a condition that is primarily a product of the somewhat casual approach that is often employed in slug tests. Recently, the Kansas Geological Survey (KGS) has pursued research directed at improving methods for the performance and analysis of slug tests. Based on extensive theoretical and field research, a series of guidelines have been proposed that should enable the reliability of parameter estimates to be improved. The most significant of these guidelines are: 1) three or more slug tests should be performed at each well during a given test period; 2) two or more different initial heads ( $H_0$ ) should be used at each well during a test period; 3) the method used to initiate a test should allow a good estimate of  $H_0$  to be obtained; 4) data acquisition equipment that enables a large quantity of high quality data to be collected should be employed; 5) if an estimate of the storage parameter is needed, an observation well other than the test well should be employed; 6) the method chosen for analysis of the slug-test data should be appropriate for site conditions; 7) use of pre- and post-analysis plots should be an integral component of the analysis procedure, and 8) appropriate well-construction parameters should be employed. Data from slug tests performed at a number of KGS field sites demonstrate the importance of these guidelines.

##### **Introduction**

The slug test is a widely used technique for the in-situ estimation of hydraulic conductivity at sites of suspected groundwater contamination (Kruseman and de Ridder, 1989; Chirlin, 1990). Parameter estimates obtained from slug tests can be used for a variety of purposes including prediction of contaminant transport, design of large-scale pumping tests and remediation schemes, etc. Recently, however, this technique has received a considerable amount of criticism in the groundwater literature (e.g., Osborne, 1993). A primary cause of this criticism is the discrepancy that is often observed between estimates obtained from slug tests and those obtained from other information collected as part of the site investigation (e.g., geologic and geophysical logs, core samples, estimates

from pumping tests, etc.). Although spatial variability and the different scales at which the various information was obtained can explain a portion of the observed discrepancy (e.g., Butler, 1990), a significant component of this difference undoubtedly arises as a result of the somewhat casual attitude that is often directed at the performance and analysis of slug tests. Since slug tests have considerable logistical and economic advantages over alternative approaches, it is imperative that these tests be done in such a manner so as to yield parameter estimates of as high a reliability as possible. The purpose of this paper is to propose practices for the performance and analysis of slug tests that should increase the reliability of the resulting parameter estimates.

Since 1989, the Kansas Geological Survey (KGS) has pursued extensive theoretical and experimental research on slug tests in porous formations. A major component of this effort has been a thorough examination of currently accepted practices. This work has resulted in the definition of a series of guidelines for the performance and analysis of slug tests. We have found that adherence to these guidelines will greatly improve the reliability of the parameter estimates obtained from a program of slug testing. The major purpose of this paper is to describe the most significant of these guidelines. In the following sections, each of the proposed guidelines is explained in detail. Tests from a variety of KGS field sites are used as examples to demonstrate the importance of the proposed guidelines.

### **Proposed Slug-Test Guidelines**

#### **1. Three or More Slug Tests Should be Performed at a Given Well**

According to conventional theory (e.g., Cooper et al., 1967), data from repeat slug tests at the same well should coincide when graphed in a normalized format (measured deviations from static normalized by the magnitude of the initial displacement, i.e. the size of the slug ( $H_0$ )). Figure 1 is a plot of a series of slug tests from a well in Lincoln County, Kansas in which the response data conform to conventional theory, despite a variation of almost a factor of four in the magnitude of the initial displacement ( $H_0$ ). Unfortunately, however, data from repeat slug tests at the same well will often not plot in this ideal manner. Figure 2 displays data from a series of slug tests from another well at the same site in Lincoln County in which there was considerable variation in test responses. Since the pattern of responses shown on Figure 2 does not indicate a strong dependence on  $H_0$  (test 3 on 5/21 and test 11 on 6/26 have similar  $H_0$  but yield Cooper et al. parameter estimates that differ by a factor of two), this behavior is most likely an indication that the gravel pack or a portion of the formation in the vicinity of the well is

being altered during the course of testing. One possible explanation is that some fine material is being mobilized by the introduction of the slug and is moving in a manner that produces progressive decreases in formation permeability during the course of testing. Without doing a series of tests at a given well, this behavior would not be identified and thus properties reflective of the skin could inadvertently be assigned to the formation. A minimum of three tests is suggested in order that the effects of an evolving skin can be separated from a dependence on  $H_0$  (discussed in the next section). Clearly, considerable attention must be given to well construction and development in order to minimize the possibility of skin development during the course of testing. Note that Dax (1987) describes results from a series of slug tests in which the wells are gradually clogged through time as a result of accumulation of material in the well and incrustation of the well screen. The test responses displayed on Figure 2 are not thought to be a result of such a process of gradual clogging. The large differences in response time that are seen between tests performed on the same day are strong evidence in support of the hypothesis of mobilization of fine material leading to a decrease in near-well permeability.

## 2. Two or More Different Slug Sizes Should be Used During Testing at a Given Well

As stated in the preceding section, conventional theory maintains that slug-test responses should be independent of the magnitude of the initial displacement ( $H_0$ ). In confined formations of moderate to low permeability ( $Kb < 15\text{--}20 \text{ m}^2/\text{d}$ , where  $K$  is hydraulic conductivity and  $b$  is screen length), this assumption appears quite sound (e.g., Figure 1 of this paper and Herzog (1994)). In very permeable systems, however, a dependence on  $H_0$  is often seen. Figure 3 is a plot from a series of tests in the semiconfined alluvial aquifer underlying the Geohydrologic Experimental and Monitoring Site (GEMS) in Douglas County, Kansas. A very strong dependence on  $H_0$  is seen in these data, producing an inverse relationship between  $H_0$  and hydraulic conductivity estimates obtained using conventional methods (i.e. Hvorslev (1951) and Cooper et al. (1967)). The tests displayed on Figure 3 were performed in a series of cycles from low to high  $H_0$ . As shown in the figure, repeat tests with the same approximate  $H_0$  from different cycles coincided, verifying that the observed behavior is a reproducible function of  $H_0$  and not a result of an evolving skin. In order to identify a dependence on  $H_0$ , a series of tests in which  $H_0$  varies between tests should be performed. The first and last tests should use the same  $H_0$  so that the effects of an evolving skin can be separated from the  $H_0$  dependence. Figures 4A and 4B display response data from such a test series in the alluvial aquifer underlying the Great Bend Prairie region of south central Kansas. The coincidence of the normalized plots on Figure

4B indicates that the test responses are independent of  $H_0$ , the formation is not being altered during testing, and that the responses are independent of whether the slug was induced by raising or lowering the water level in the well. It is strongly recommended that such a series of tests always be performed. Failure to do so can potentially introduce considerable error into the hydraulic conductivity estimates obtained from a program of slug tests.

The first and last tests in the series shown in Figure 4 employed initial displacements of similar magnitude but differing signs. According to conventional theory, responses should be independent of whether the test was initiated by an injection (slug in) or withdrawal (slug out) mechanism. The results of the tests shown in Figure 4 (and all other slug tests performed by the authors in wells screened in formations of moderate to low permeability) indicate that, as long as the water level in the test well is not driven below the top of the screen during the test, the responses will be essentially independent of the mechanism used for test initiation (i.e. injection versus withdrawal). However, in wells screened in very permeable formations, it is possible that test responses are dependent on whether the test was initiated by an injection or withdrawal mechanism. Current ongoing work is attempting to clarify this issue.

The above discussion of the dependence of test responses on the magnitude of  $H_0$  is appropriate for wells in confined formations and those in unconfined formations screened at least a certain minimum distance below the water table. In wells screened close to or across the water table, one may observe a dependence on  $H_0$  as a result of differences in the length of the screen through which water flows into/out of the test well. In such wells, one may also observe a dependence of test responses on the mechanism of test initiation (i.e. injection versus withdrawal). Dahl and Jones (1993) report a series of tests in which there is a clear dependence on  $H_0$  and the mechanism of test initiation. Figure 5 reproduces one set of tests reported by Dahl and Jones (1993). These tests were performed at the same well using different initial displacements and different mechanisms of test initiation. Hyder et al. (1993) have recently proposed an approximate analytical solution that can model the dependence both on  $H_0$  and on the mechanism of test initiation for such situations. Butler et al. (1994) provide estimates of the necessary minimum distance below the water table for test responses to be independent of  $H_0$ .

### 3. A Good Estimate of the Initial Displacement Should be Obtained

Conventional methodology for the analysis of slug-test data requires that the magnitude of the initial displacement ( $H_0$ ) be known. Thus, the method used to initiate a slug test must allow a good estimate of  $H_0$  to be obtained. In systems of moderate to low



permeability, measurements taken immediately after test initiation should yield a good estimate of  $H_0$ . In very rapidly responding systems, however, such measurements will not be sufficient.

Figure 6 displays data from a series of tests performed in the same permeable alluvial aquifer as in Figure 3. In this case, the slug was introduced by pneumatic means (i.e. pressurizing the air column in the well casing (producing a depression of the water level) followed by a near-instantaneous depressurization (e.g., McLane et al., 1990; Levy and Pannell, 1991)). The actual  $H_0$  values shown in Figure 6 (1.03 m and 4.20 m for tests 1 and 4, respectively) are based on measurement of the air pressure in the well casing using a high-accuracy gas pressure transducer, while the head readings were taken using submersible pressure transducers. The difference between the  $H_0$  readings taken with the gas pressure transducer and the submersible pressure transducer (0.20 m and 1.03 m for tests 1 and 4, respectively) leads to a lower-than-actual estimate of hydraulic conductivity when only the submersible transducer readings are used. Further testing at the same site showed that the difference between the  $H_0$  readings did not exist at wells screened in material of moderate to low permeability.

Although the example displayed in Figure 6 was from a pneumatic slug test, similar or greater uncertainty regarding  $H_0$  will arise in tests initiated by the addition or removal of a solid slug. Packer-based systems, in which the slug is introduced by opening the central pipe upon which the packer is mounted (e.g., Figure 4a of this paper and McElwee and Butler, 1989), provide one means of obtaining good estimates of  $H_0$  in very permeable systems. Note that Orient et al. (1987) and McLane et al. (1990), among others, suggest use of electric water level indicators (electric tapes) to estimate  $H_0$  for pneumatic slug tests. Although this approach can provide an approximate value of  $H_0$ , a high-accuracy gas pressure transducer will provide a better estimate. Since high-accuracy gas pressure transducers are inexpensive, can be readily added to the standard pneumatic slug-test well head assembly, and can be readily connected to standard data acquisition equipment, their use is strongly recommended for pneumatic slug tests.

#### 4. Appropriate Data Acquisition Equipment Should be Employed

Responses to a slug-induced disturbance can be measured either manually (electric tape, plopper, etc.) or electronically (pressure transducers connected to a data logger). For tests in wells screened in formations of moderate to low permeability, such as shown in Figure 1, manual methods can provide measurements of sufficient quality as long as a good estimate of  $H_0$  is available. However, for tests in more permeable systems ( $K_b > 15\text{-}20 \text{ m}^2/\text{d}$ ), such as shown in Figures 3-6, electronic methods must be employed,

as manual methods will not provide measurements of sufficient density or accuracy. Earlier theoretical work (McElwee et al., 1989) has shown that the reliability of parameter estimates is closely tied to the density and accuracy of measurements. In very rapidly responding wells (e.g., Figures 3 and 6), data acquisition rates of at least several hertz are needed in order to clearly define the nature of the responses. Note that the need for rapid acquisition rates is of special concern in oscillating systems where slow collection rates will produce aliasing and other effects that may make data interpretation and analysis difficult. Given the capabilities of currently available data acquisition equipment, data collection rates of several hertz are easily obtainable and, therefore, should always be used when rapid responses are expected.

#### 5. An Observation Well Should be Employed for Estimation of the Storage Parameter

It has frequently been observed that slug-induced responses at the test well are relatively insensitive to the value of the storage parameter (e.g., Cooper et al., 1967). McElwee et al. (1989) have used sensitivity analysis to demonstrate that reliable estimates of the storage parameter will be difficult to obtain using the density and quality of data that are normally collected during a single-well slug test. A primary reason for this condition is that the measured responses at the test well are much more sensitive to transmissivity than to the storage parameter. The limited sensitivity to the storage parameter that does exist is highly correlated with the sensitivity to transmissivity. In addition, any uncertainties about the effective screen radius (nominal screen radius or radius of gravel pack or radius of developed zone) will have a much larger effect on estimates of the storage parameter than on estimates of transmissivity. Use of an observation well during a slug test can greatly improve this situation as the insensitivity and correlation effects are dramatically lessened (McElwee et al., 1991). Uncertainties about the effective screen radius also have much less of an effect when data from an observation well are used (Butler, 1994).

Figure 7 displays data from a multi-well slug test at the same site as in Figure 1. The two wells, which are screened over similar intervals, are 6.45 m apart. Owing primarily to uncertainty about the effective screen radius, the estimate of specific storage obtained using data from well Ln-2 alone is too large by a factor of four. When the analysis is performed using data from both wells, a specific storage estimate compatible with other information is obtained. Note that measurements from the observation well were taken using a transducer placed below a packer located just above the screen. The observation well was packed off in order to remove the lagging and damping of responses that occurs due to wellbore storage at the observation well (Novakowski, 1989).

Although it may not be practical to install observation wells solely for use in slug tests, the density of pre-existing monitoring wells is often such that this technique can be readily employed. Generally, the observation well must be fairly close (within  $\approx 10$  m) to the test well in order that the responses to the slug-induced disturbance can be discerned from background noise. The storage parameter must be quite small in order to employ wells at greater distances from the test well (Sageev, 1986; Novakowski, 1989; McElwee et al., 1991).

#### 6. Method Chosen for Data Analysis Should be Appropriate for Site Conditions

Most analyses of slug-test data are performed using one of four techniques: 1) the method of Hvorslev (1951) for fully and partially penetrating wells in confined aquifers; 2) the method of Bouwer and Rice (1976) for wells in unconfined aquifers screened below the water table; 3) the method of Cooper et al. (1967) for fully penetrating wells in confined aquifers; and 4) the method of Nguyen and Pinder (1984) for partially penetrating wells in confined aquifers. Recent theoretical work at the KGS has focussed on the quality of the estimates provided by these techniques.

Figure 8 displays the results of a theoretical analysis of the error introduced into hydraulic conductivity estimates when applying the Cooper et al. model to data from a partially penetrating well. The  $\Psi$  quantity plotted on the x axis is the square root of the anisotropy ratio ( $K_z/K_r$ ) over the aspect ratio ( $b/r_w$ , where  $b$  is the screen length and  $r_w$  is the screen radius). The quantity plotted on the y axis is the hydraulic conductivity estimate provided by the Cooper et al. model over the actual conductivity value. A series of curves are shown for different values of the dimensionless storage parameter ( $\alpha$ , where  $r_c$  and  $S_s$  are the casing radius and specific storage, respectively). Note that the  $\alpha$  parameter used here is twice that defined by Cooper et al. (1967). Figure 8 shows that Cooper et al. estimates improve as  $\Psi$  decreases, i.e. the proportion of vertical flow in response to the slug test decreases. However, these results also indicate that, for tests in wells of moderate to low aspect ratios sited in isotropic formations (i.e. the upper end of the plotted  $\Psi$  range) having a low value for the dimensionless storage parameter ( $\alpha$ ), the Cooper et al. model will provide estimates that are significantly greater than the actual value.

Figure 9 displays results of a similar analysis for the Hvorslev technique. In this case, an anisotropy ratio must be assumed, producing a  $\Psi^*$  value (square root of assumed anisotropy ratio over the aspect ratio) that is used in the analysis. In most cases, the Hvorslev analysis is performed assuming an isotropic formation (e.g., Freeze and Cherry, 1979). Clearly, the results displayed in Figure 9 indicate that this approach will produce

a significant underestimation of hydraulic conductivity in anisotropic formations ( $K_r > K_z$ ).

Figure 10 displays results for a similar analysis of the Bouwer and Rice method. In this case, two plots are given so that the effect of aspect ratio and anisotropy can be evaluated separately. Again, anisotropy ( $K_r > K_z$ ) will produce a considerable underestimation of hydraulic conductivity. Hyder et al. (in press) and Hyder and Butler (in press) provide further details of the theoretical analyses of the Cooper et al., Hvorslev, and Bouwer and Rice techniques. It is strongly recommended that plots such as Figures 8-10 be employed for the selection of the appropriate method for the analysis of slug-test data. Use of these plots should considerably improve the reliability of the estimated parameters.

The fourth method for data analysis listed above, the Nguyen and Pinder method, is not recommended for the analysis of slug-test data. Butler and Hyder (1993) have recently shown that parameter estimates obtained using the Nguyen and Pinder method must be viewed with skepticism owing to an error in the analytical solution upon which that model is based. For slug tests performed in partially penetrating wells under conditions where Figures 8-10 indicate that the standard methods do not appear capable of providing acceptable parameter estimates, the recently introduced KGS model for slug tests in partially penetrating wells (Hyder et al., in press; Hyder and Butler, in press) can be employed for the analysis of the response data.

The above discussion pertains to conditions where conventional slug-test theory is applicable. However, in cases where test responses are dependent on  $H_0$  and the mechanism of test initiation (e.g., Figures 3 and 5), conventional theory is no longer viable. We (section III.B, this report) propose a model for the analysis of slug tests in highly permeable systems where a dependence on  $H_0$  is observed. The model proposed by Hyder et al. (1993) can be used for the analysis of data from slug tests performed in wells screened near or across the water table if a dependence on  $H_0$  and/or the mechanism of test initiation is observed. As emphasized earlier, it is critical that the series of slug tests performed at a well be designed so as to assess whether conventional theory is applicable.

#### 7. Use of Pre- and Post-Analysis Plots Should be an Integral Component of the Analysis

Currently, the vast majority of analyses of slug-test data are performed using automated fitting programs or procedures involving manual fitting of straight lines to test data. Unfortunately, all too often, the analysis is performed by rote, with little attention paid to the form of the plots and the nature of the fit of the theoretical model to the test

data. If the reliability of parameter estimates from slug tests is to be improved, more attention must be paid to all aspects of the analysis. Three examples are briefly given here to demonstrate the importance of these issues. Further details about the tests used for these examples can be found in Butler et al. (1993) and Butler and Liu (1994).

Figure 11 displays data and the best-fit Cooper et al. model from a test at the Lincoln County site (screen radius ( $r_w$ ) = 0.07 m, casing radius ( $r_c$ ) = 0.025 m, screen length ( $b$ ) = 3.96 m). Note that a constant specific storage of  $3.28 \times 10^{-6} \text{ m}^{-1}$  was assumed for the analysis based on an estimate obtained from a test at a higher interval at this site (Figure 7). The model fit in this case must be considered quite poor. The systematic deviation between the theoretical model and test data can be readily explained by an assumed specific storage that is too low. Justification for a higher specific storage can be found in Figure 12, which is a plot of the data in a semilog Hvorslev format. The distinct concave upward curvature seen on this plot is strong evidence (for a well of this aspect ratio) that the specific storage for the test interval is quite large (e.g., Chirlin, 1989). Therefore, the analysis was repeated without constraining the value of specific storage. Figure 13 displays the very good fit that was then obtained (estimated specific storage =  $0.00041 \text{ m}^{-1}$  corresponding to an a value of 0.025). Note that the hydraulic conductivity estimate decreased by over a factor of two between the analyses of Figures 11 and 13, a further indication of the importance that must be paid to deviations between the fitted theoretical model and the test data. Also note that the good agreement shown in Figure 13 between the Cooper et al. model and the test data would be predicted from Figure 8 for a well of this aspect ratio ( $b/r_w=57$ ), given the large  $a$  value. Since this well is of a moderate aspect ratio, the test data were also analyzed using the isotropic form of the earlier described KGS model for slug tests in partially penetrating wells (note that the isotropic version of the KGS model is equivalent to the model of Dougherty and Babu (1984)). The resulting conductivity estimate was the same as that obtained from the Cooper et al. model. This is in keeping with theoretical results of Hayashi et al. (1987) and Hyder et al. (in press) who found that vertical flow due to a slug-induced disturbance decreases with increases in the storage parameter (i.e. at large values of the storage parameter, responses from fully penetrating well models and partially penetrating well models will coincide).

Figure 14 displays data and the best-fit Cooper et al. model from a test at a site in Pratt County, Kansas ( $r_w=0.125 \text{ m}$ ,  $r_c=0.064 \text{ m}$ ,  $b=1.52 \text{ m}$ , assumed  $S_s$  of  $3.28 \times 10^{-6} \text{ m}^{-1}$ ). Again, a systematic deviation between the measured data and the Cooper et al. model is shown. This type of deviation is often seen when applying a fully penetrating well model to data from a test in a partially penetrating well. The near-linear Hvorslev

plot of the data shown in Figure 15 can be considered further support for the hypothesis of a deviation produced by a significant component of vertical flow. Hyder et al. (in press) state that a near-linear Hvorslev plot can be an indication of a significant component of vertical flow in response to a slug test in a partially penetrating well or of a low permeability well skin. Given the small aspect ratio ( $b/r_w=12$ ) and the coincidence of plots of normalized responses from five repeat tests at this well, the partially penetrating well explanation was considered the most likely. The data were therefore reanalyzed using the KGS model for slug tests in a partially penetrating well. Figure 16 displays the fit resulting from an analysis with the isotropic form of the KGS model. It is important to emphasize that the dramatic improvement in model fit between Figures 14 and 16 was not accompanied by an increase in the number of estimated parameters. Note that the hydraulic conductivity estimate provided by the Cooper et al. model is 2.4 times larger than the KGS model conductivity estimate, an overprediction by the Cooper et al. model very close to what would be theoretically predicted from Figure 8 for a well of this aspect ratio in an isotropic formation, given the assumed  $\alpha$  of  $3.8 \times 10^{-5}$ . Also note that this value of the dimensionless storage parameter ( $\alpha$ ) is much smaller than that of the previous example.

A final example illustrates the effect of an evolving low-conductivity well skin. Figure 17 displays data in a semilog Hvorslev format from two tests in the series shown on Figure 2. Note that the degree of curvature of the plotted data is significantly smaller in test 11 than in test 3. Figure 18 is a plot of the test data and the best-fit Cooper et al. models (assumed  $S_g=6.56 \times 10^{-6} \text{ m}^{-1}$ ). As shown in the figure, the nature of the deviation between the test data and the best-fit model changes between the two tests. The greater response time of the later test, the decrease in the degree of curvature on Figure 17, and the change in the nature of the deviation seen on Figure 18 are very strong evidence of a developing low-permeability skin. In the case of an evolving skin, the best option is to analyze data from tests before the skin becomes too pronounced. Test 3 of 5/21 was the first slug test performed at this well, so it should be the best test for analysis. The most likely explanation for the deviation shown on Figure 18 is that the assumed storage parameter is too low. The curvature of test 3 data seen in Figure 17 is strong support for this explanation. The results of a reanalysis of test 3 allowing the storage parameter to vary are shown in Figure 19. The agreement between the fitted model and the test data is significantly better in this case. Note that the conductivity estimate obtained from this analysis is within 5% of the value obtained from the analysis of a multiwell slug test centered at the nearby well Ln-2 (see Figure 7). The estimated specific storage ( $S_g=5.36 \times 10^{-5} \text{ m}^{-1}$ ), however, appears too large by a factor of six when compared to the

value obtained from the multiwell test. This larger specific storage estimate is thought to be a result of the earlier-discussed lack of sensitivity of test responses to the storage parameter and uncertainty concerning the effective screen radius.

Although the analysis of Test 3 appears to have been somewhat successful, analysis of tests in wells that display an evolving skin will, in general, be very difficult, as all available test data may be affected by the skin. Clearly, proper well construction and well development are essential in order to minimize the potential for the development of a well skin during a program of slug tests. Note that the normalized head data in Figure 19 and a number of the other figures used in this article show a good deal of fluctuation at very early times. These fluctuations are related to test initiation and should be ignored when considering the quality of the match between the best-fit model and the test data.

#### 8. Appropriate Well-Construction Parameters Should be Employed

One of the more significant sources of uncertainty in the analysis of slug-test data is introduced through the well-construction parameters. Specifically, the selection of values to use for the effective screen length and radius can inject considerable error into the analysis. Although the effective screen length has a much larger impact on parameter estimates, both quantities will influence estimates from slug tests through the dimensionless storage parameter ( $\alpha$ ) and, in partially penetrating wells, the aspect ratio (effective screen length/effective screen radius). In formations of moderate to low permeability ( $K_b < 15\text{-}20 \text{ m}^2/\text{d}$ ), the gravel pack will usually be considerably more permeable than the formation itself. Therefore, the effective screen length should be the length of the gravel pack and the effective screen radius should be the radius of the gravel pack. In very rapidly responding systems, however, the nominal screen radius and length will be more appropriate. There may be some uncertainty concerning the appropriate quantities to employ in wells screened in material of moderately high permeability. Appropriate sizing of the gravel pack, however, can largely remove this uncertainty from the analysis. In the examples of the preceding section, the radius of the gravel pack and the length of the gravel pack were used for  $r_w$  and  $b$ , respectively, in the analyses because the gravel pack was considerably more permeable than the formation in all cases. Butler (1994) provides further details concerning the effect of well-construction parameters on slug tests.

#### **Conclusions**

The slug test has the potential to provide very useful information about the transmissive and storage properties of a formation. In order for the potential of this

technique to be fully realized, however, considerable care must be given to all phases of test design, performance, and analysis. A series of guidelines have been outlined here that should allow parameter estimates of greater reliability to be obtained from a program of slug testing. Two very important points arising from this series of guidelines cannot be overemphasized: 1) it is critical that a series of slug tests at a given well be designed so as to assess whether conventional theory is applicable (i.e. is there a dependence on initial head or mechanism of test initiation, is there a well skin that is developing during the course of testing, etc.); and 2) the analysis of the response data must be done using the most appropriate model and with considerable care. Unfortunately, the authors have found through repeated experience that inattention to the issues discussed in this article will produce parameter estimates that differ considerably from reality. Finally, it should be stressed that these guidelines developed out of research performed in flow systems for which a porous media representation is valid. Although these guidelines will be applicable to slug tests in fractured systems, the complexities of tests in fractured systems may give rise to additional guidelines of equal or greater importance to those outlined here.



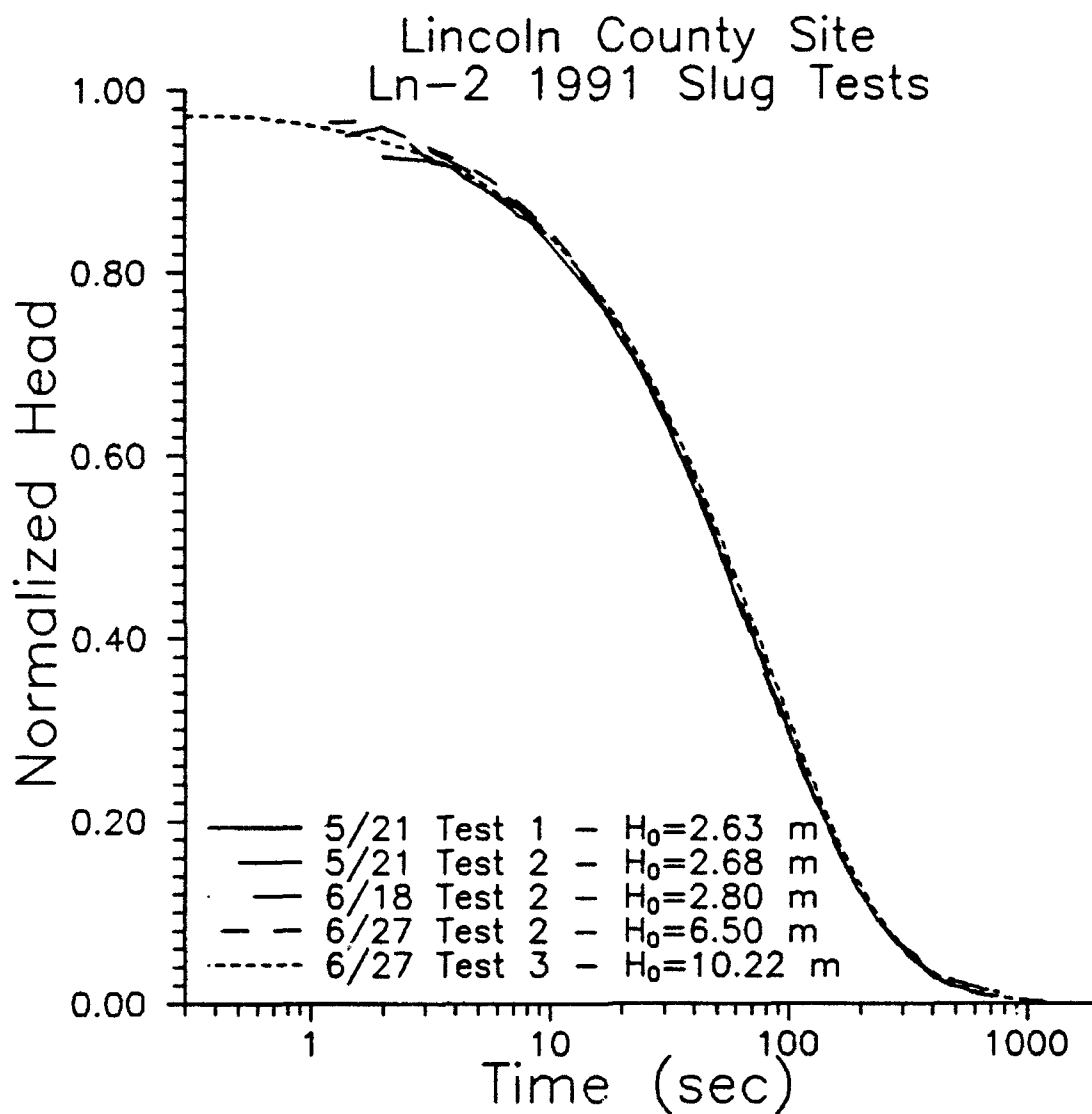


Figure III.A.1 - Normalized head ( $H(t)/H_0$ ) versus log time plot of a series of slug tests performed during May and June of 1991 in well Ln-2 at a site in Lincoln County, Kansas.

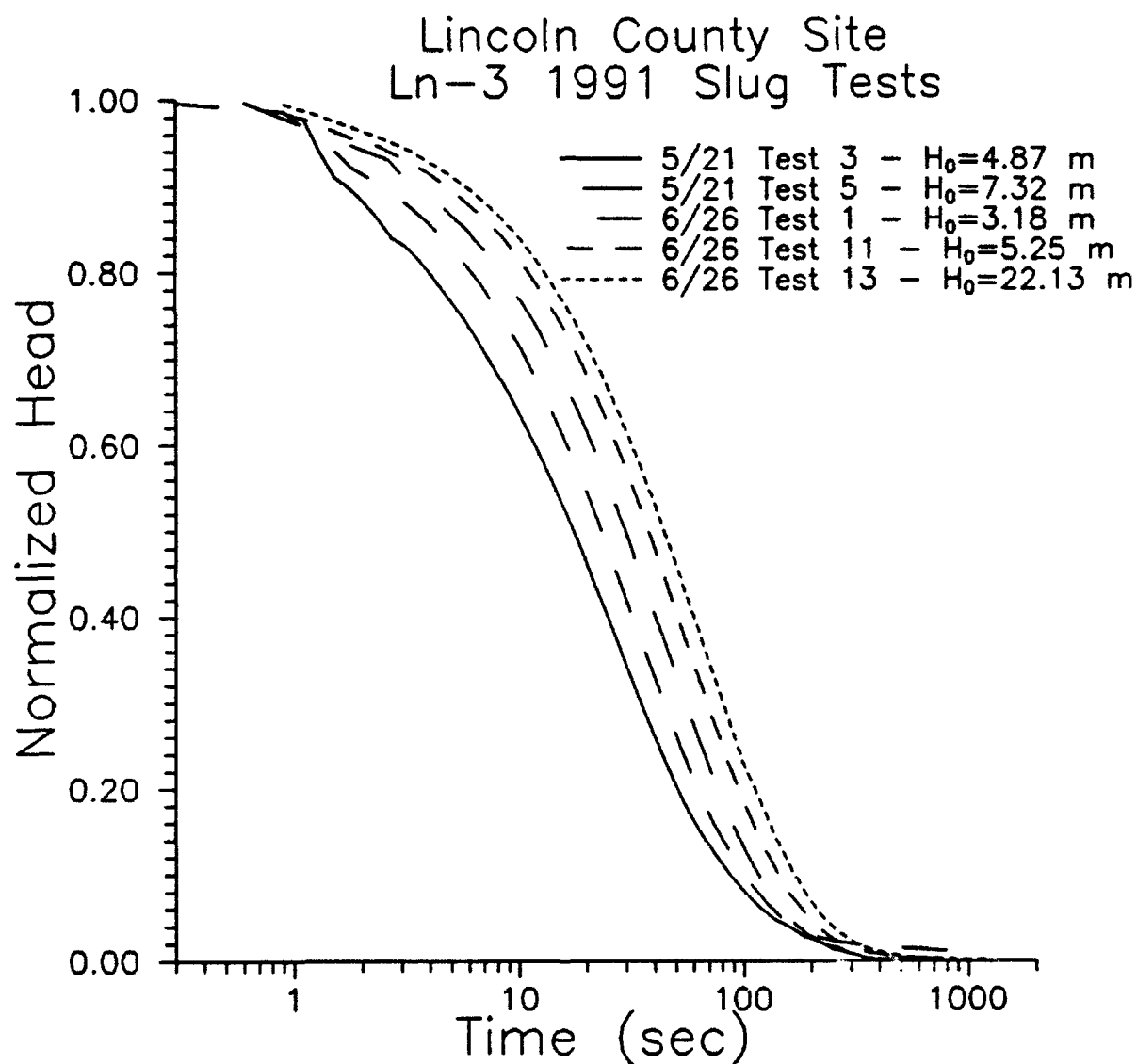


Figure III.A.2 - Normalized head ( $H(t)/H_0$ ) versus log time plot of a series of slug tests performed during May and June of 1991 in well Ln-3 at a site in Lincoln County, Kansas.

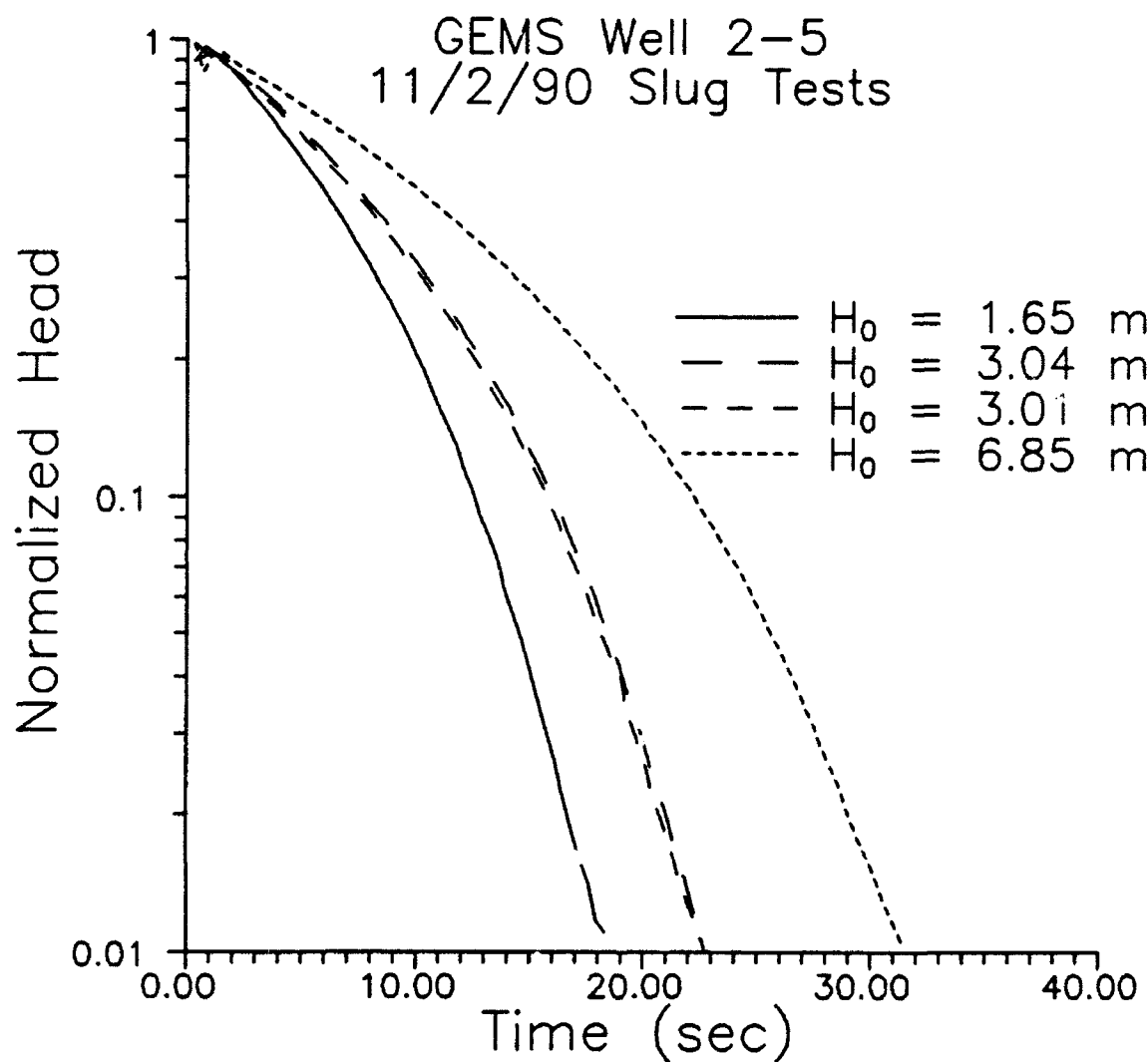


Figure III.A.3 - Normalized head ( $H(t)/H_0$ ) versus log time plot of a series of slug tests performed during November of 1990 in well 2-5 at the Geohydrologic and Experimental Site (GEMS) in Douglas County, Kansas.

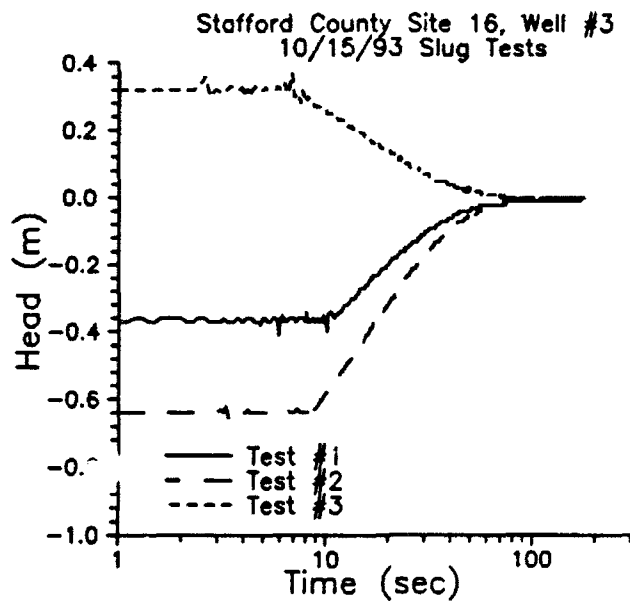
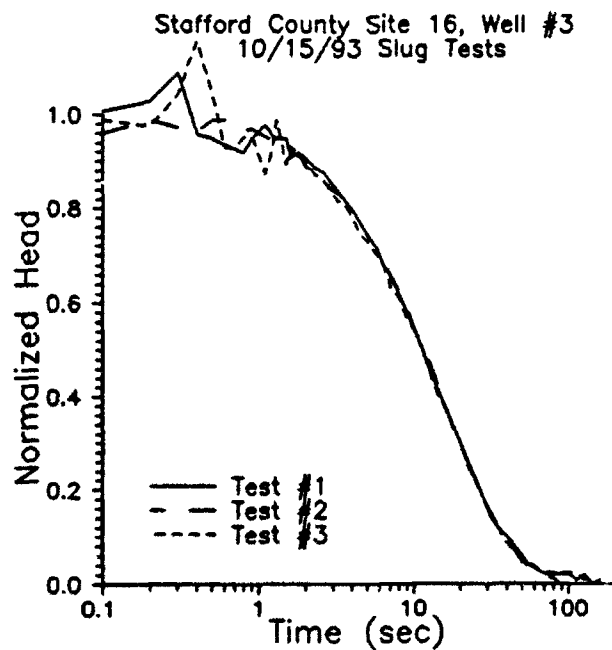


Figure III.A.4 - Plots of a series of slug tests performed during October of 1993 in well 3 at site 16 in Stafford County, Kansas: a) Head versus log time plot of slug-test data;



b) Normalized absolute head versus log time plot of slug-test data.

### MW11, 8' Slug, Injection and Withdrawal Tests

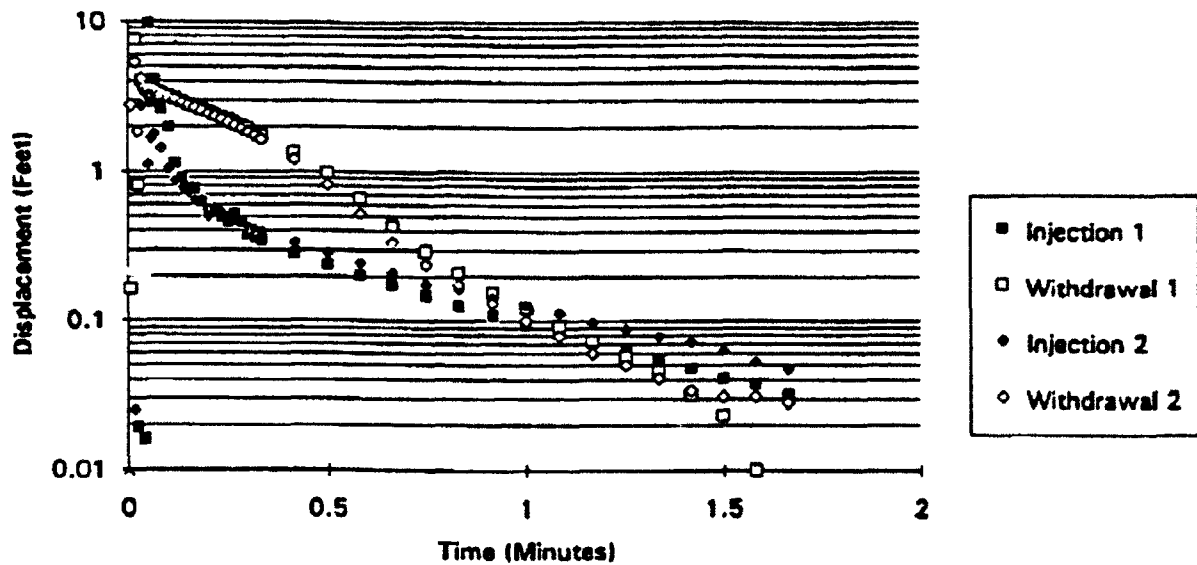
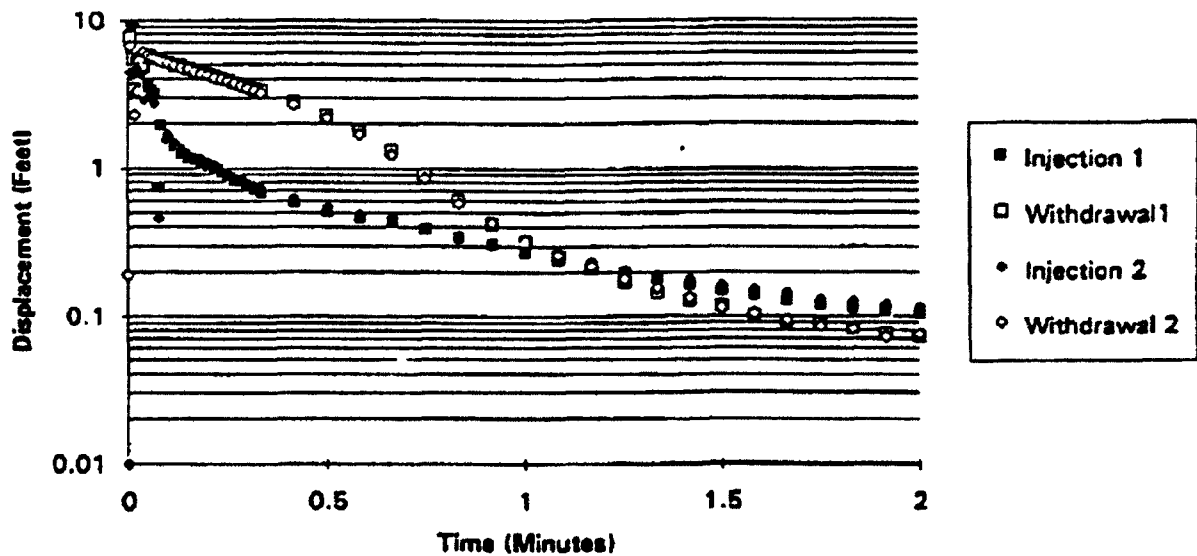


Figure III.A.5 - Log head versus time plot of a series of slug tests reported by Dahl and Jones (1993): a) Injection and withdrawal slug tests using  $H_0=1.07$  m;

### MW11, 12' Slug, Injection and Withdrawal Tests



b) Injection and withdrawal slug tests using  $H_0=1.59$  m.

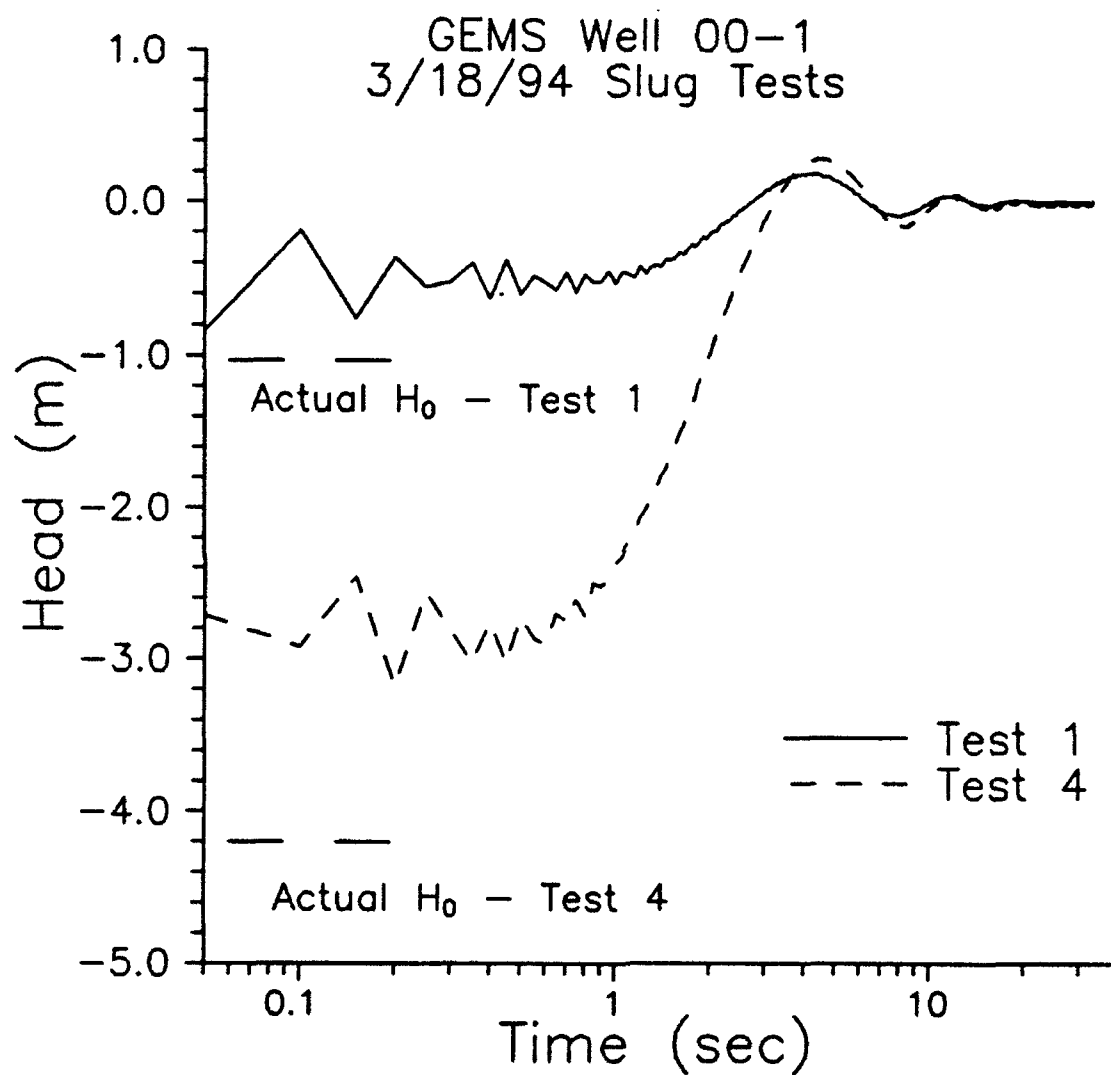


Figure III.A.6 - Head versus log time plot of a pair of slug tests performed during March of 1994 in well 00-1 at GEMS in Douglas County, Kansas ("actual  $H_0$ " estimated from gas pressure transducer).

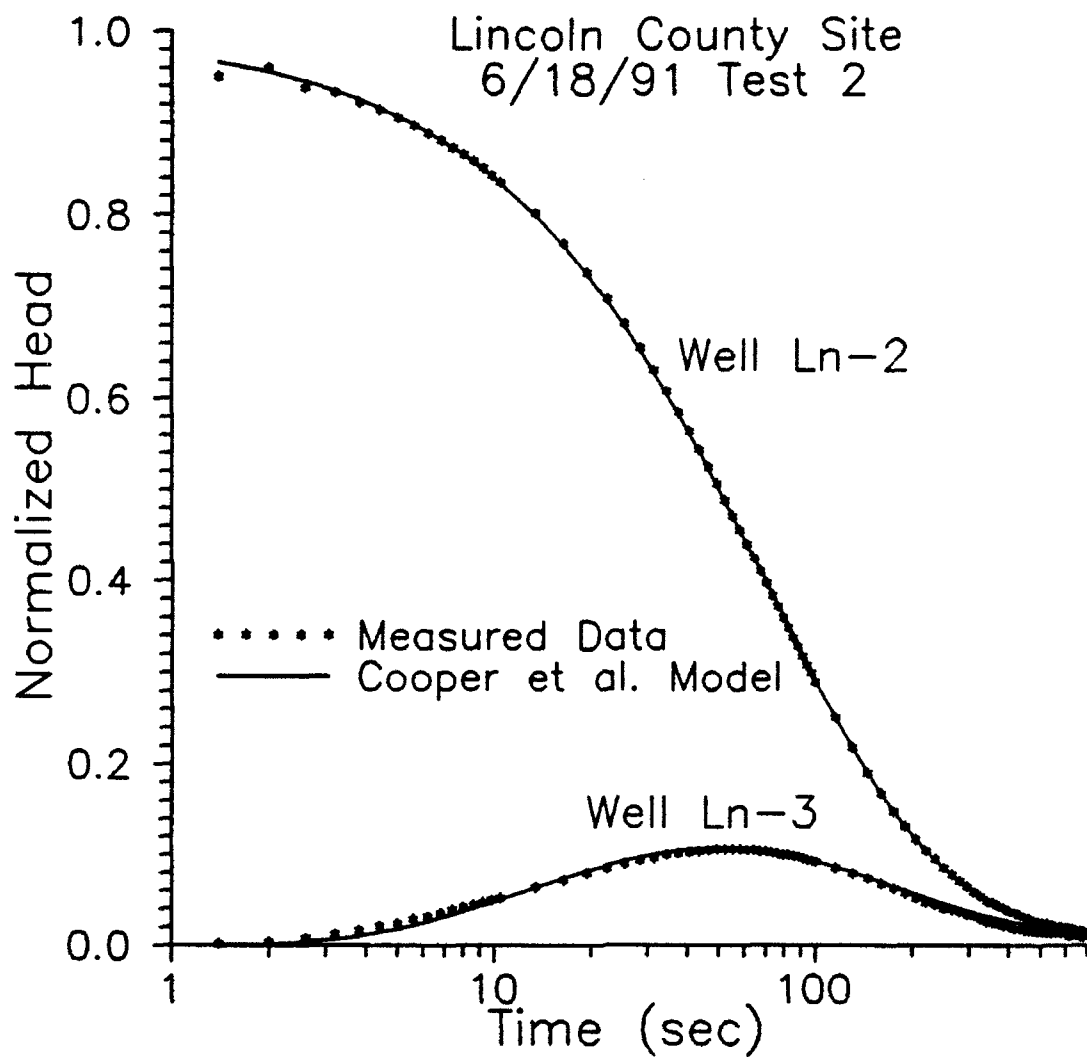


Figure III.A.7 - Normalized head ( $H(t)/H_0$ ) versus log time plot of Lincoln County slug-test data and best-fit Cooper et al. model.

Error Introduced by Cooper et al. Model  
When Applied to Case of Partially  
Penetrating Well

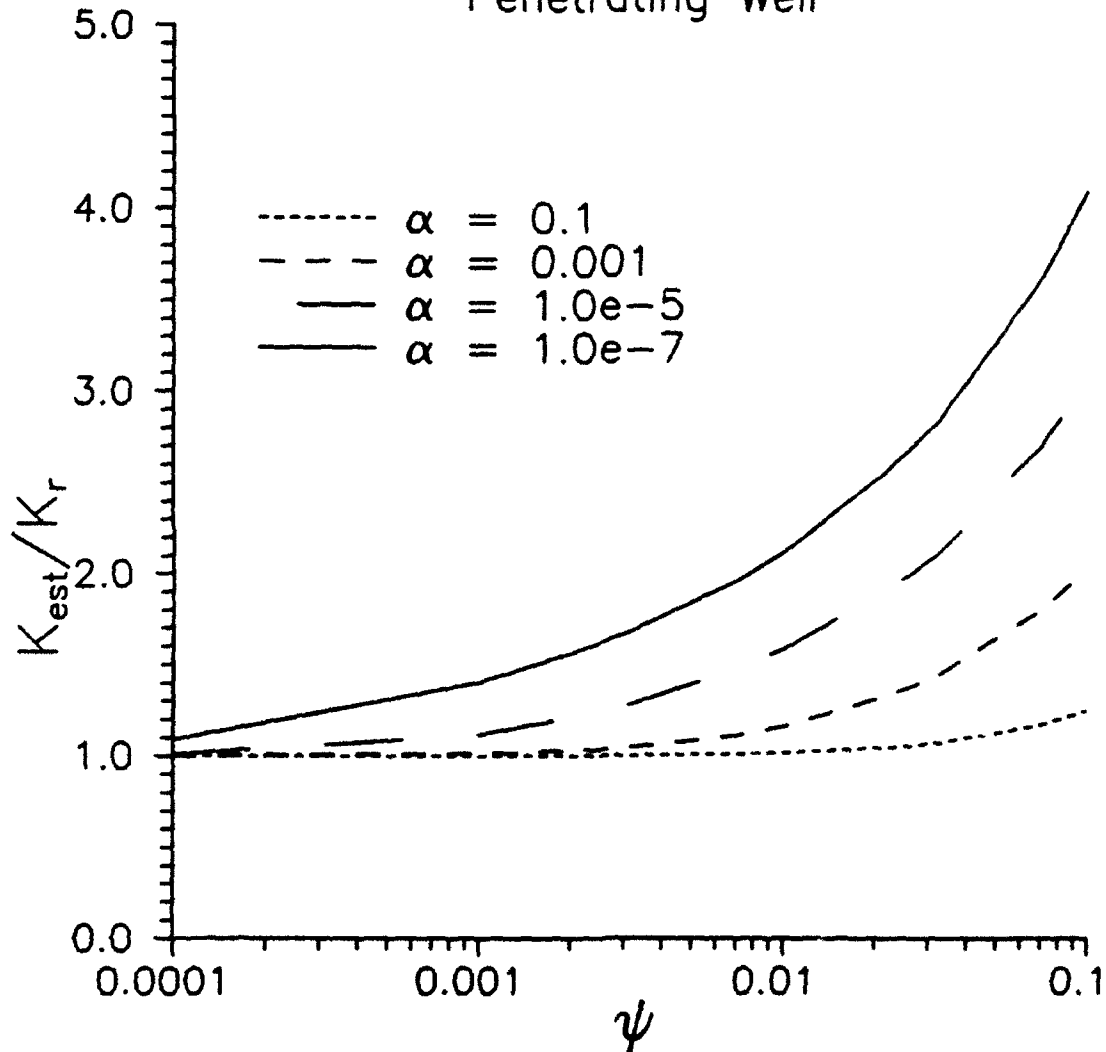


Figure III.A.8 - Plot of conductivity ratio (Cooper et al. estimate ( $K_{est}$ ) over actual conductivity ( $K_r$ )) versus  $\psi$  ( $\sqrt{K_r/K_e} / (b/r_w)$ ) as a function of  $\alpha$  ( $(2r_w^2 S_e b)/r_e^2$ ) for the case of a well screened near the center of a very thick aquifer (after Hyder et al. (in press)).



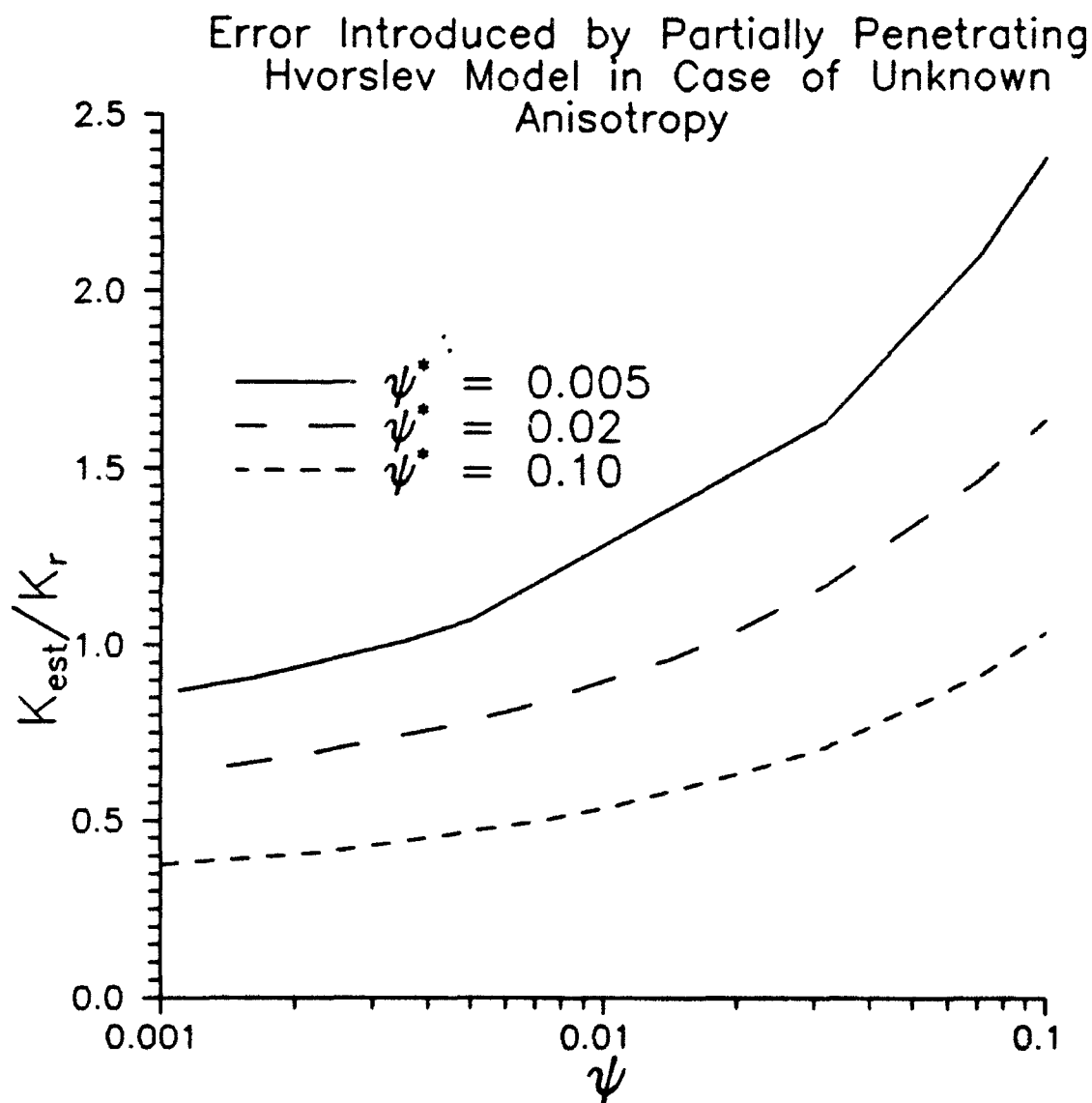


Figure III.A.9 - Plot of conductivity ratio (Hvorslev estimate ( $K_{est}$ ) over actual conductivity ( $K_r$ )) versus  $\psi$  ( $\sqrt{K_r/K_r} / (b/r_w)$ ) as a function of  $\psi^*$  ( $\psi$  term with an assumed anisotropy ratio) for the case of a well screened near the center of a very thick aquifer and  $\alpha = 1.0e^{-5}$  (after Hyder et al. (in press)).

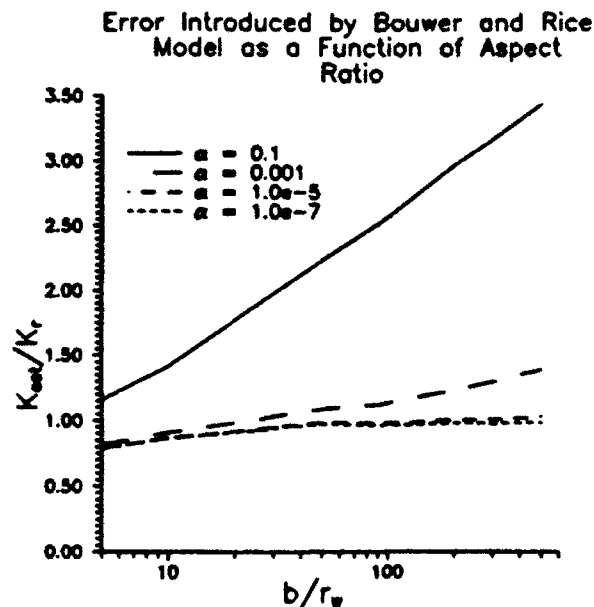
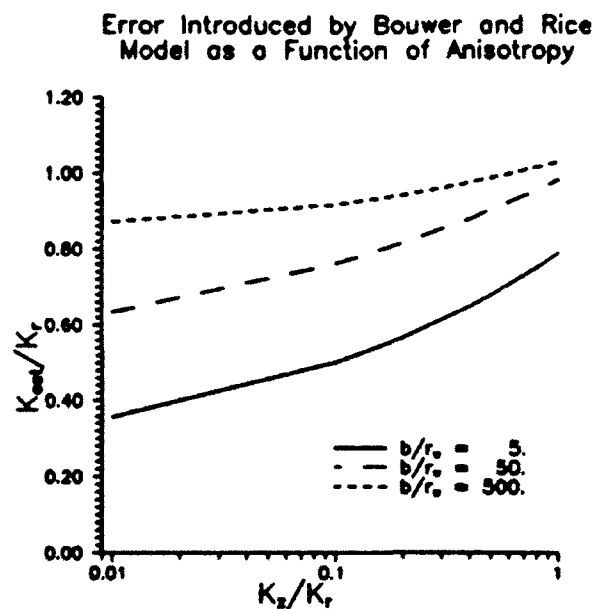


Figure III.A.10 - Plots illustrating the error introduced by the Bouwer and Rice model for the case of a well screened near the center of a very thick aquifer (after Hyder and Butler (in press)): a) Plot of conductivity ratio (Bouwer and Rice estimate ( $K_{Bouwer}$ ) over actual conductivity ( $K_r$ )) versus aspect ratio ( $b/r_w$ ) as a function of  $\alpha$  ( $(2r_w^2 S_b)/r_c^2$ );



b) Plot of conductivity ratio (Bouwer and Rice estimate ( $K_{Bouwer}$ ) over actual conductivity ( $K_r$ )) versus anisotropy ratio ( $K_z/K_r$ ) as a function of aspect ratio for  $\alpha = 1.0e^{-5}$ .

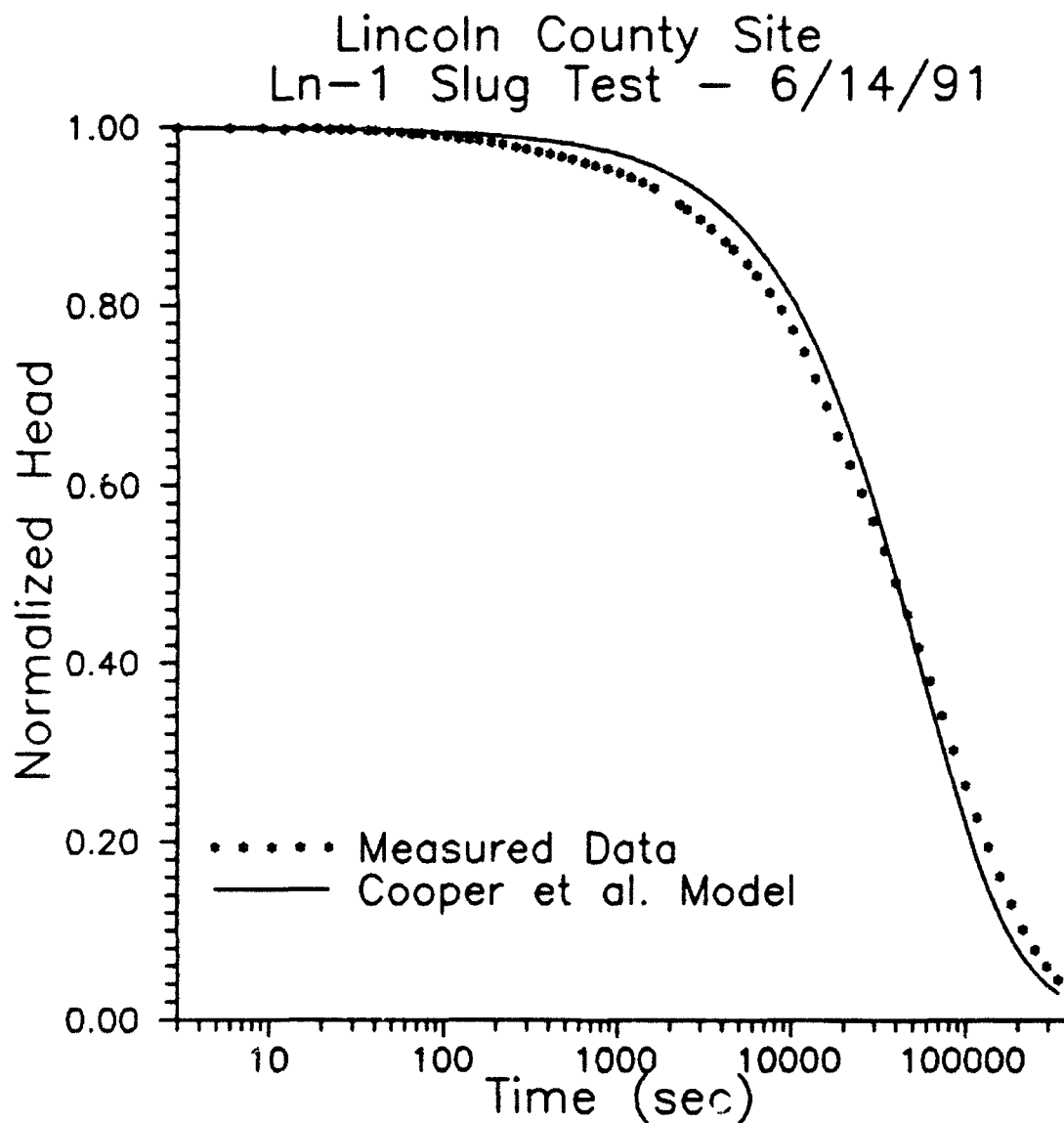


Figure III.A.11 - Normalized head ( $H(t)/H_0$ ) versus log time plot of 6/14/91 slug-test data from well Ln-1 at the Lincoln County site and the best-fit Cooper et al. model assuming  $\alpha=2.04 \times 10^{-4}$  ( $H_0=10.35$  m).

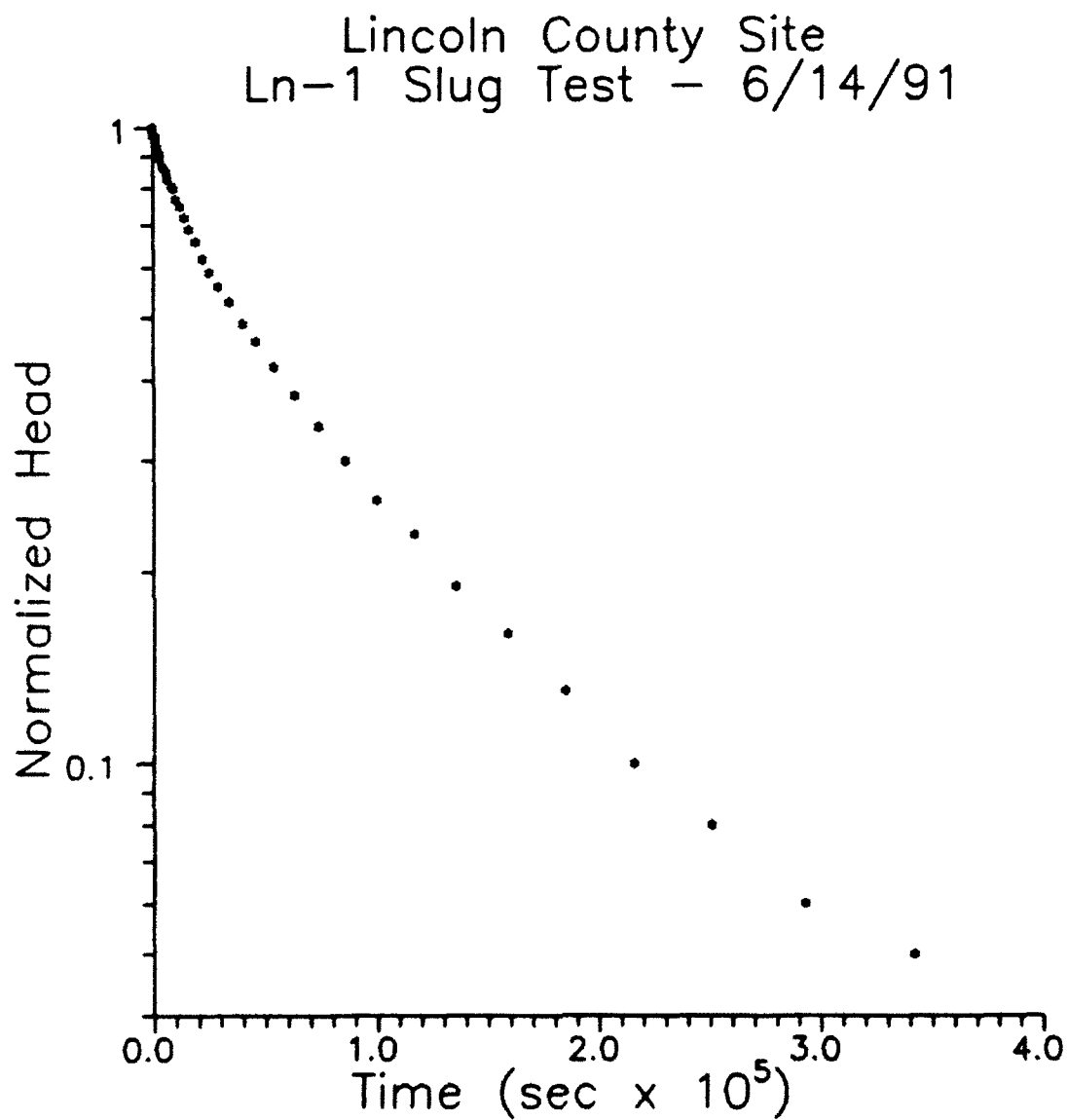


Figure III.A.12 - Log normalized head ( $H(t)/H_0$ ) versus time plot of 6/14/91 slug-test data from well Ln-1 at the Lincoln County site.

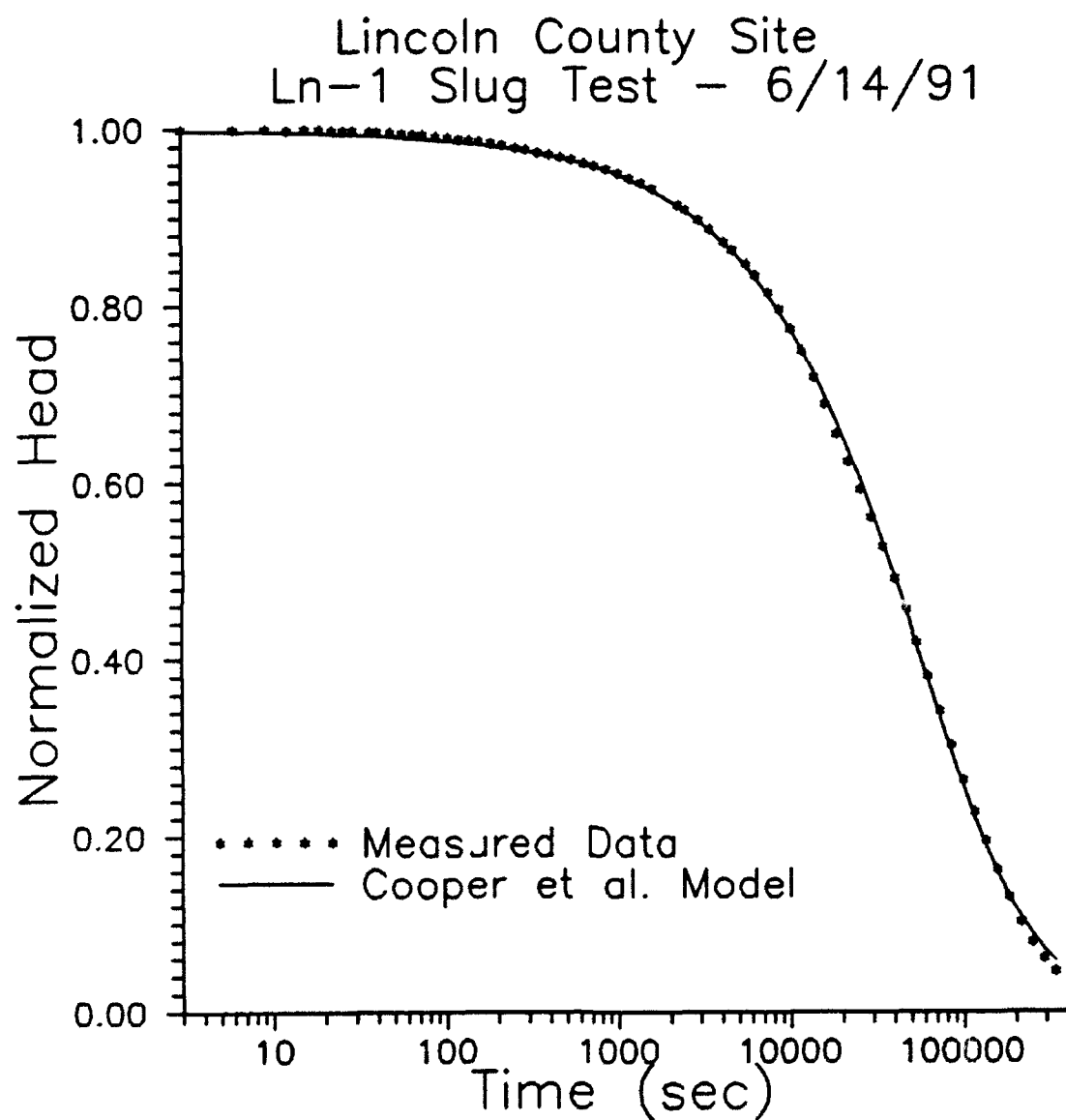


Figure III.A.13 - Normalized head ( $H(t)/H_0$ ) versus log time plot of 6/14/91 slug-test data from well Ln-1 at the Lincoln County site and the best-fit Cooper et al. model.

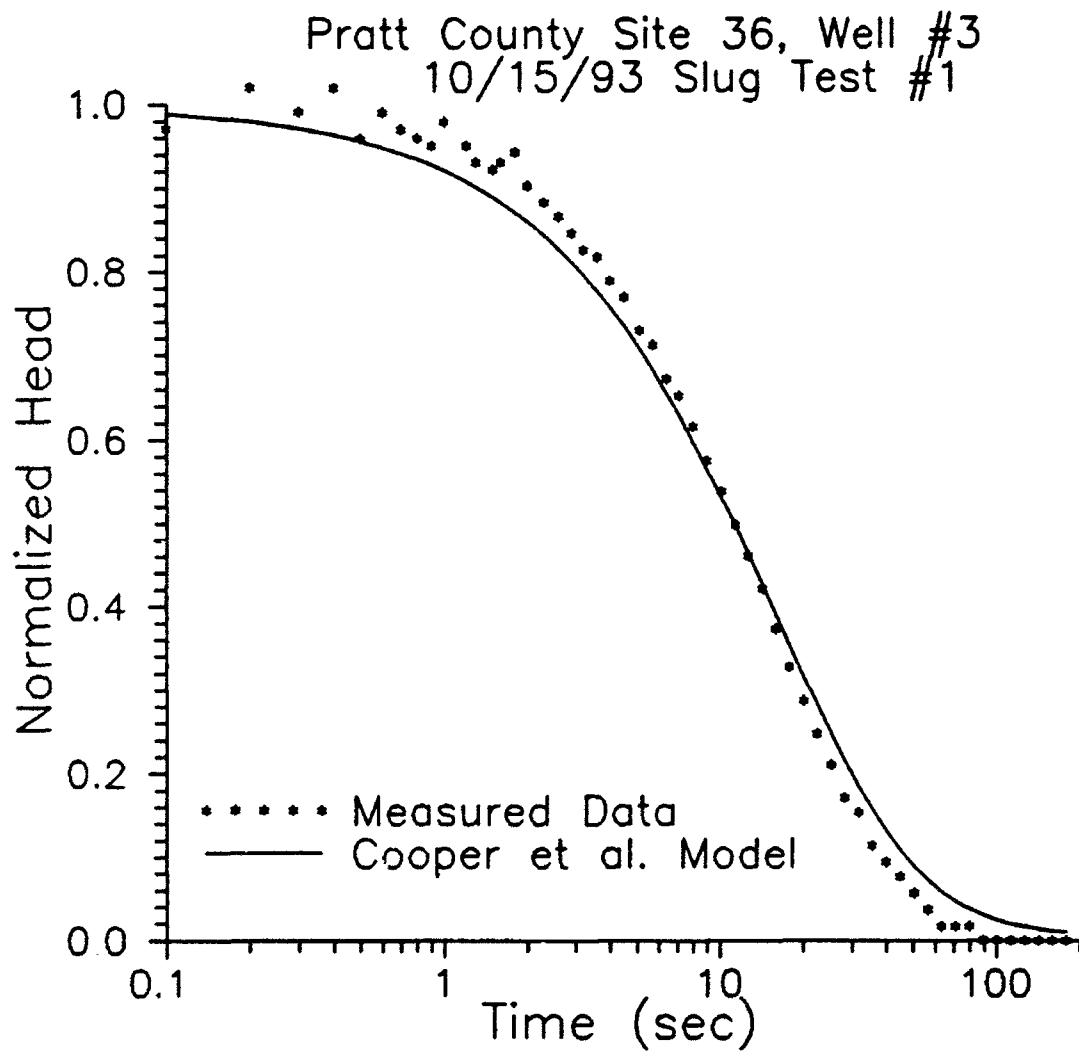


Figure III.A.14 - Normalized head ( $H(t)/H_0$ ) versus log time plot of 10/15/93 test #1 slug-test data from well 3 at site 36 in Pratt County, Kansas and the best-fit Cooper et al. model assuming  $\alpha=2.10 \times 10^{-4}$  ( $H_0=0.38$  m).

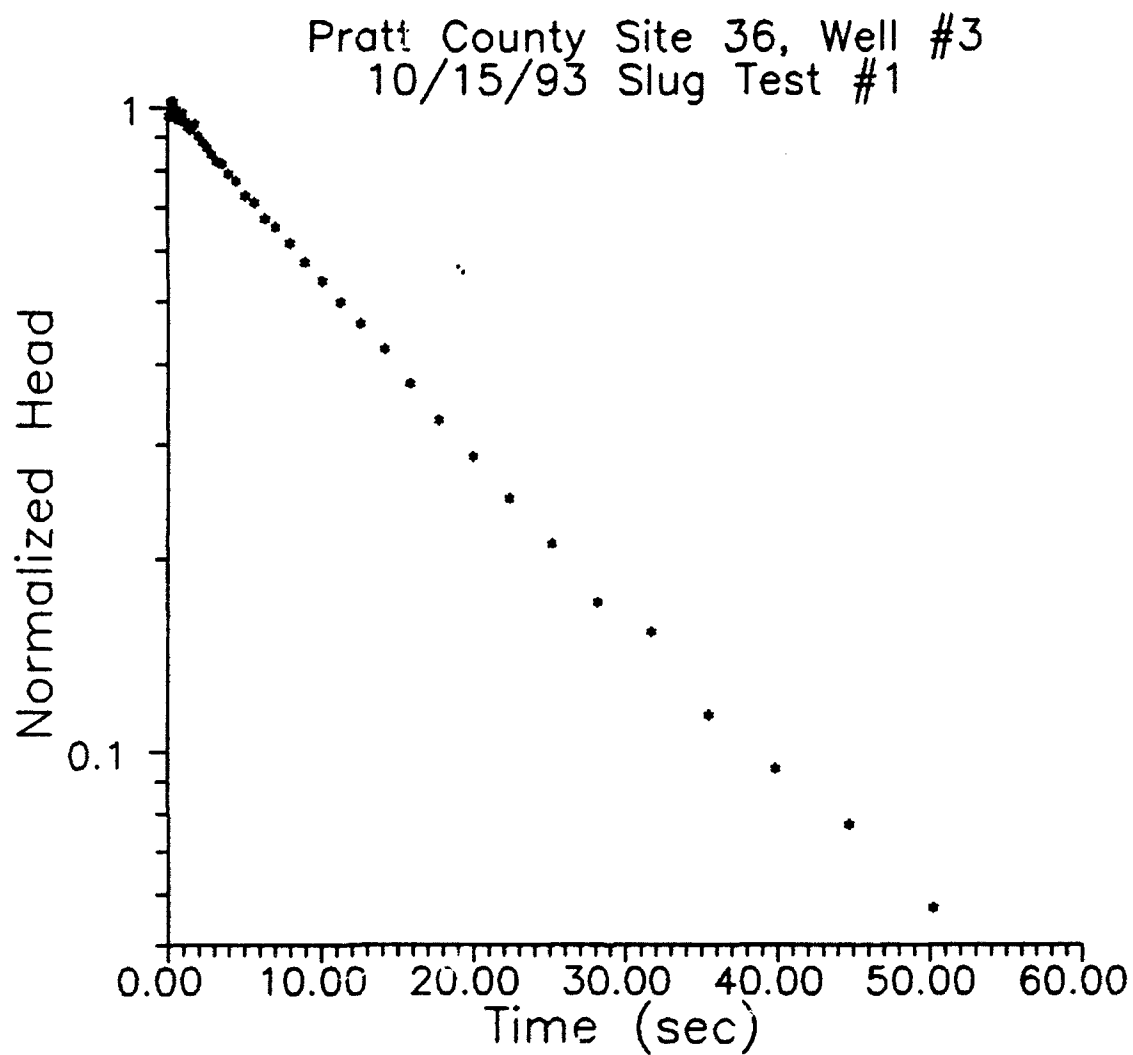


Figure III.A.15 - Log normalized head ( $H(t)/H_0$ ) versus time plot of 10/15/93 test #1 slug-test data from well 3 at site 36 in Pratt County, Kansas.

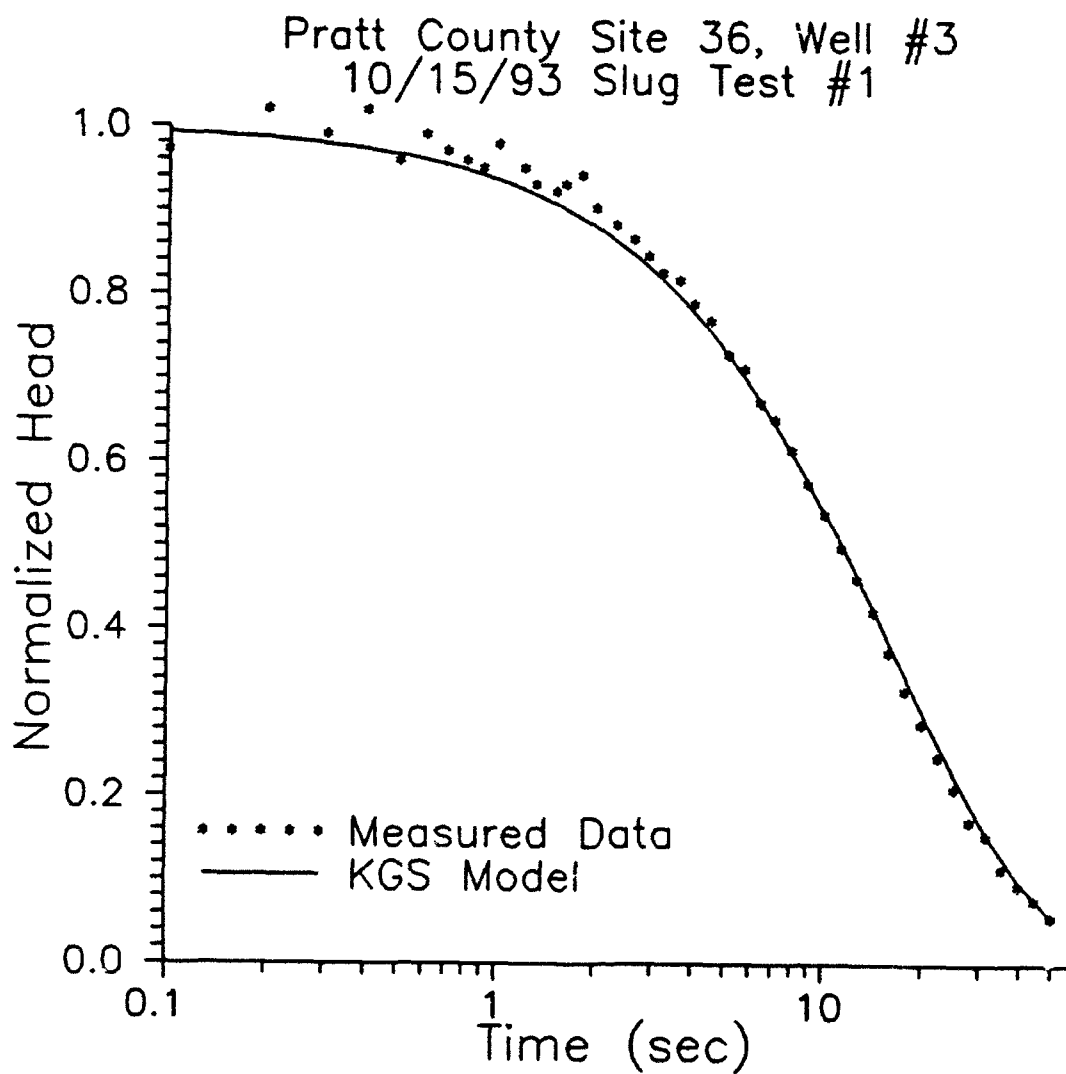


Figure III.A.16 - Normalized head ( $H(t)/H_0$ ) versus log time plot of 10/15/93 test #1 slug-test data from well 3 at site 36 in Pratt County, Kansas and the best-fit Cooper et al. model (no prior assumption concerning  $\alpha$ ).



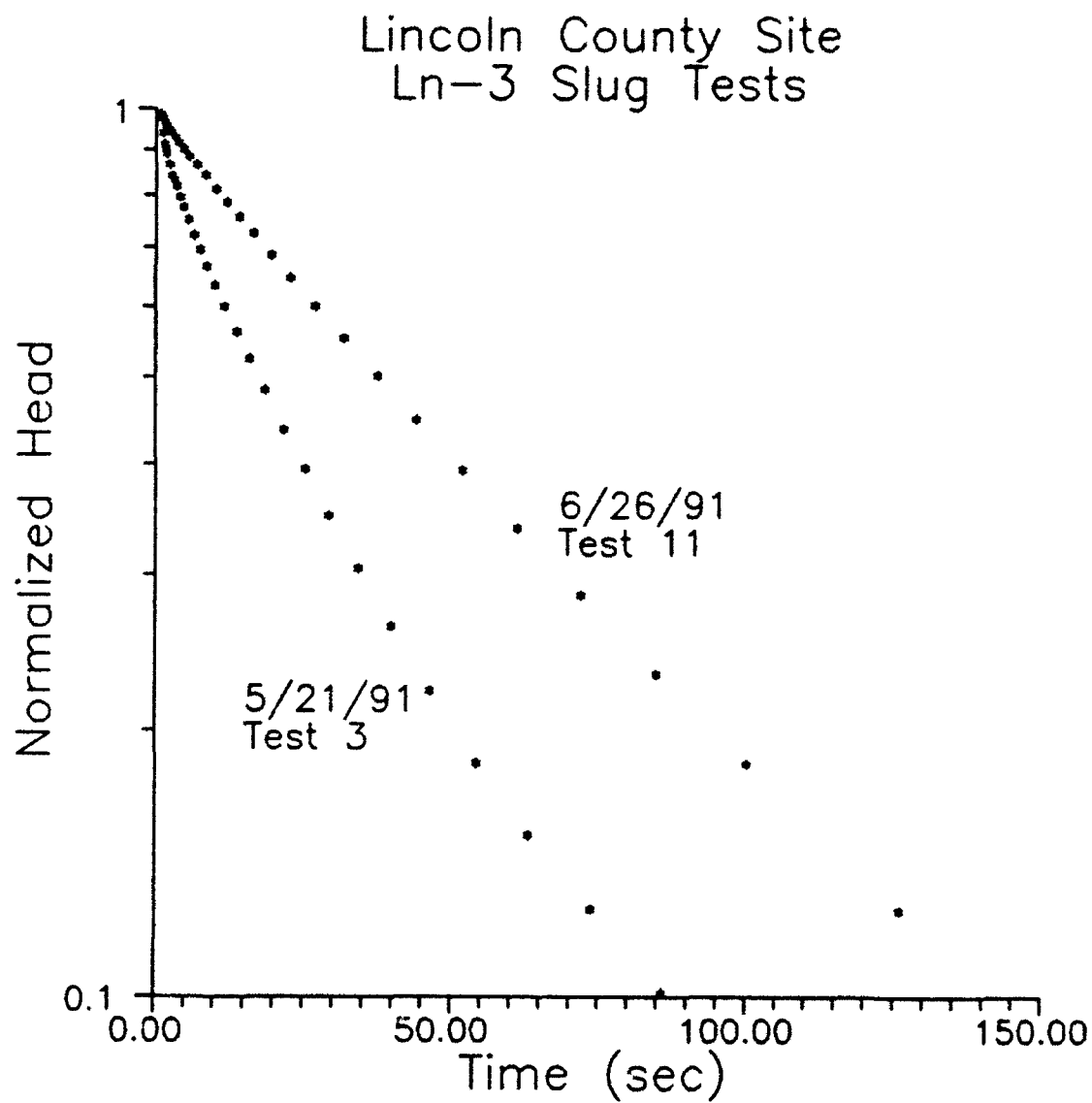


Figure III.A.17 - Log normalized head ( $H(t)/H_0$ ) versus time plot of 5/21/91 test #3 ( $H_0=4.87$  m) and 6/26/91 test #11 ( $H_0=5.25$  m) slug tests performed in well Ln-3 at Lincoln County site.

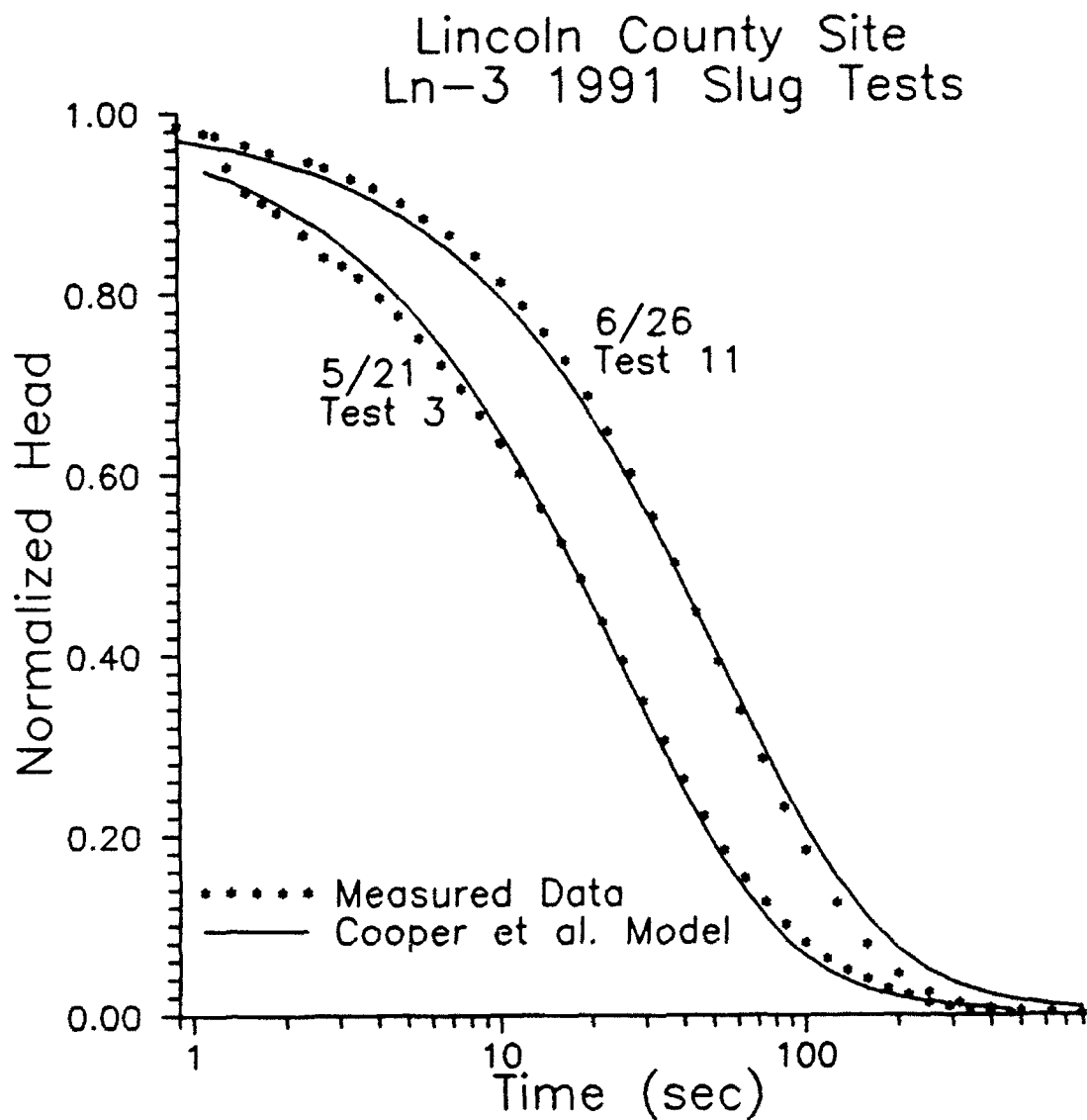


Figure III.A.18 - Normalized head ( $H(t)/H_0$ ) versus log time plot of 5/21/91 test #3 and 6/26/91 test #11 slug tests from well Ln-3 at Lincoln County site and the best-fit Cooper et al. models assuming  $\alpha = 3.87 \times 10^{-4}$

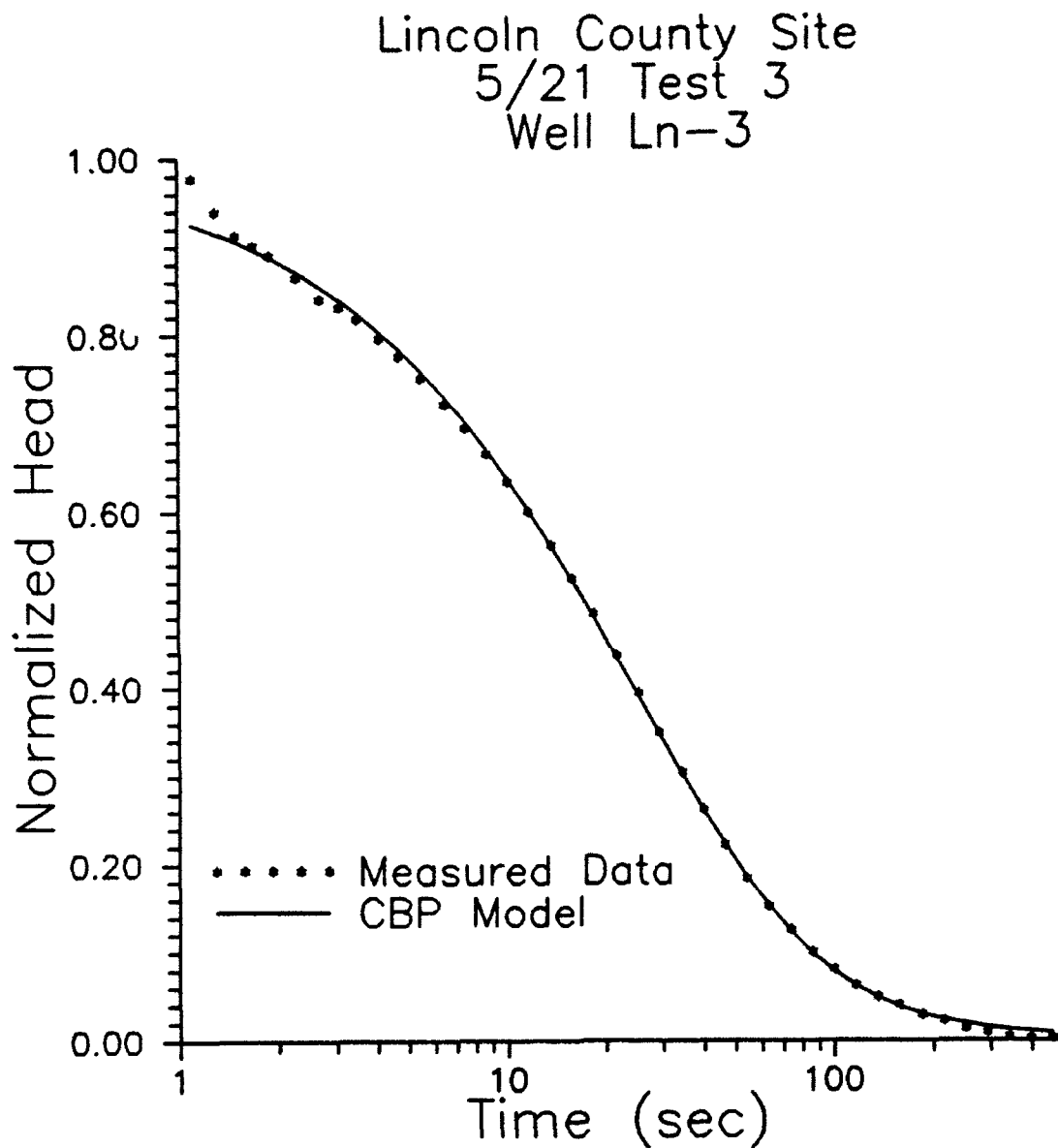


Figure III.A.19 - Normalized head ( $H(t)/H_0$ ) versus log time plot of 5/21/91 test #3 slug test from well Ln-3 at Lincoln County site and the best-fit Cooper et al. model (no prior assumption concerning  $\alpha$ ).

## **B. A GENERAL NONLINEAR MODEL FOR ANALYSIS OF SLUG-TEST DATA**

### **Introduction**

Slug tests are frequently used to characterize the transmissivity of an aquifer. In highly permeable aquifers however, problems arise when conventional analytical techniques are applied. At one of our field sites (GEMS, Geohydrologic Experimental and Monitoring Site) in an aquifer consisting of coarse sand and gravel overlain by silt and clay, we have consistently seen deviations from the expected response of linear theoretical models. Typically, we see a systematic lack of fit to traditional models and a dramatic dependence of the slug test on the magnitude of the initial displacement (Figures III.B.1. and III.B.2.).

Figure III.B.1 shows some typical slug test data from a GEMS well that does not oscillate, however, the conventional theories do not adequately explain this data. The main problems shown in the data of Figure III.B.1 are: first, the response is dependent on the initial head and second, the Hvorslev (1951) and Cooper, Bredehoeft, and Papadopoulos (CBP, 1967) models show a systematic lack of fit. In all linear theories the normalized responses for various initial slug heights should collapse onto one curve. Clearly, this is not the case in Figure III.B.1. As we shall see later, a typical Hvorslev plot of the field data does not yield a straight line, but instead we see a pronounced downward curvature. This is in contrast to the upward curvature Chirlin (1989) shows should result from the transient CBP model. The implication is that this well is exhibiting behavior in the "critically damped" region. The Hvorslev and CBP theories are supposed to be valid in the "overdamped" region. These concepts will be discussed later in the paper in connection with the theory presented.

In some wells we have also observed oscillatory behavior (Figure III.B.2). Although there are some theories describing oscillatory behavior in slug tests, until now it has been difficult to analyze tests which are in the so-called "critically damped" region. One of the earliest attempts to analyze oscillatory data was by van der Kamp (1976); however, he invoked a number of assumptions to make the theory linear. Kipp (1985) has also dealt with the linear theory of oscillatory slug test responses by using Laplace transforms and numerical inversions to calculate type curves. Kabala et al. (1985) are among the first to consider the use of a nonlinear equation to describe the oscillatory slug test behavior. However, after considerable numerical study, they state that "the linear

model is sufficiently accurate in all practical cases." The data in Figure III.B.2 show that their conclusion is not valid for this well. Very recently Stone and Clarke (in press) have used a nonlinear model to study hydraulic properties in glacial flow systems.

We have developed a unified model for slug tests that includes the effects of nonlinear terms, inertia, turbulence (spatial velocity distributions), viscosity and differing casing and screen radii. We have developed a numerical solution under Hvorslev type assumptions that should be valid over the whole range from "overdamped" to "underdamped" conditions. There are a couple of surprises that come to light in analyzing the GEMS data. First, most investigators (van der Kamp, Kabala et al., and Stone and Clarke) find that the effective water column height may be different than that measured in the field. We think we may have found an explanation for this phenomena. Second, some nonlinear effects are much stronger than most investigators have suggested and the magnitude of their strength is not easily predicted with the theory. For this reason, we use the magnitude as a fitted parameter.

### Navier-Stokes Equation for the Borehole

The motion of the water in the borehole can be described by the Navier-Stokes equations (Eskinazi, 1967). If we consider the borehole as a streamtube with average flow in the z direction the z component equation is

$$\frac{\partial V}{\partial t} + V \frac{\partial V}{\partial z} = -g - \frac{\nabla P}{\rho} + \frac{\mu}{\rho} \nabla^2 V \quad (\text{III.B.1})$$

V is the average velocity of the water in the borehole in the z direction, g is the acceleration of gravity, P is the pressure,  $\rho$  is the density and  $\mu$  is the viscosity. This equation is basically a force balance equation per unit fluid mass and can be integrated in the z direction over the length of the borehole shown in Figure III.B.3 to obtain an energy or work balance equation. We assume that the length of the screen (b) is negligible in comparison with the water column length,

$$b \ll z_o + h(t) \quad (\text{III.B.2})$$

$$\int \frac{\partial V}{\partial t} dz + \int V dV = -g(h + z_o + b) - \int \frac{dP}{\rho} + \int \frac{\mu}{\rho} \nabla^2 V dz \quad (\text{III.B.3})$$

We will assume that the water is incompressible ( $\rho$  is constant) and that the viscosity is constant. Integrating from the bottom of the screen to the top of the water in the borehole gives

$$\int \frac{\partial V}{\partial t} dz + \frac{V_T^2 - V_s^2}{2} = -g(h + z_o + b) + \frac{P_s - P_a}{\rho} + \int \frac{\mu}{\rho} \nabla^2 V dz \quad (\text{III.B.4})$$

$P_s$  and  $P_a$  are the pressures at the screen and the top of the water column, respectively and  $V_T$  and  $V_s$  are the water velocities at the top of the column and at the screen, respectively. These velocities are related by the conservation of mass flow while the average velocity at the top of the water column is simply  $dh/dt$ .

$$\pi r_c^2 V_T = \pi r_s^2 \frac{dh}{dt} = 2\pi r_s b V_s \quad (\text{III.B.5})$$

$r_c$  and  $r_s$  are the casing and screen radii, respectively. Using equation (III.B.5) in equation (III.B.4) results in

$$\int \frac{\partial V}{\partial t} dz + \frac{1}{2} \left[ 1 - \left( \frac{r_c^2}{2r_s b} \right)^2 \right] \left( \frac{dh}{dt} \right)^2 = -g(h + z_o + b) + \frac{P_s - P_a}{\rho} + \int \frac{\mu}{\rho} \nabla^2 V dz \quad (\text{III.B.6})$$

The first and last terms of equation (III.B.6) require a little more explanation.

The last term in equation (III.B.6) is the work done by viscous forces in the fluid column. Writing out the Laplacian operator gives

$$\int \frac{\mu}{\rho} \nabla^2 V dz = \frac{\mu}{\rho} \int \left[ \frac{\partial^2 V}{\partial r^2} + \frac{1}{r} \frac{\partial V}{\partial r} + \frac{1}{r^2} \frac{\partial^2 V}{\partial \theta^2} + \frac{\partial^2 V}{\partial z^2} \right] dz \quad (\text{III.B.7})$$

If we assume that the flow is unchanging in the  $\theta$  direction and that the cross section of the borehole is uniform and the fluid is incompressible then

$$\frac{\partial^2 V}{\partial \theta^2} = 0, \quad \frac{\partial^2 V}{\partial z^2} = 0 \quad (\text{III.B.8})$$

and equation (III.B.7) becomes

$$\int \frac{\mu}{\rho} \nabla^2 V dz = \frac{\mu}{\rho} \int \left[ \frac{\partial^2 V}{\partial r^2} + \frac{1}{r} \frac{\partial V}{\partial r} \right] dz \quad (\text{III.B.9})$$

Of course if we have varying radii in the borehole due to changes in casing radius or the presence of an obstruction such as a packer or other equipment, then equation (III.B.8) is no longer true and additional terms need to be added to equation (III.B.9) due to viscous work being performed at those locations. If we assume a parabolic distribution of velocities across the borehole radius as shown in Figure III.B.4, we can write

$$V = V_o \left[ 1 - \frac{r^2}{r_c^2} \right]. \quad (\text{III.B.10})$$

This allows equation (III.B.9) to be written as

$$\int \frac{\mu}{\rho} \nabla^2 V dz = -\frac{4\mu}{r_c^2 \rho} V_o \int dz = -\frac{4\mu}{r_c^2 \rho} V_o (h + z_o + b) \quad (\text{III.B.11})$$

The average vertical water velocity is given by the rate of change of the height of the water column and is related to the maximum of the parabolic velocity distribution as follows

$$Q = \pi r_c^2 \frac{dh}{dt} = \int V dA = 2\pi \int_0^{r_c} V_o \left[ 1 - \frac{r^2}{r_c^2} \right] r dr = \frac{\pi r_c^2 V_o}{2} \quad (\text{III.B.12})$$

$$V_o = 2 \frac{dh}{dt}$$

where Q is the rate of water flow through the borehole. The final form for equation (III.B.11) is

$$\int \frac{\mu}{\rho} \nabla^2 V dz = -\frac{8\mu}{r_c^2 \rho} (h + z_o + b) \frac{dh}{dt} \quad (\text{III.B.13})$$

The first term in equation (III.B.6) can be manipulated as follows

$$\int \frac{\partial V}{\partial t} dz = \frac{\partial}{\partial t} \int V dz = \frac{\partial}{\partial t} \left[ \frac{dh}{dt} \int \frac{\pi r_c^2}{A(z)} dz \right] \quad (\text{III.B.14})$$

by remembering that conservation of water flow requires that

$$\pi r_c^2 \frac{dh}{dt} = A(z) V(z) \quad (\text{III.B.15})$$

where  $dh/dt$  is the velocity in the casing with normal radius  $r_c$  and  $V(z)$  is the velocity where the cross sectional area is  $A(z)$ . If the cross sectional areas do not change with time and if the cross sectional area is uniform in the  $z$  direction then equation (III.B.14) becomes

$$\int \frac{\partial V}{\partial t} dz = (h + z_o + b) \frac{d^2 h}{dt^2} \quad (\text{III.B.16})$$

Additional acceleration work terms must be added to this equation if there are significant restrictions in the cross sectional area in the borehole. Our calculations show that these additional terms are usually negligible if the restrictions in cross sectional area are not too great.

Using equations (III.B.16) and (III.B.13) in equation (III.B.6) allows us to write the form

$$(h + z_o + b) \frac{d^2 h}{dt^2} + \frac{1}{2} \left[ 1 - \left( \frac{r_c^2}{2r_s b} \right)^2 \right] \left( \frac{dh}{dt} \right)^2 = -g(h + z_o + b) + \frac{P_s - P_a}{\rho} - \frac{8\mu}{r_c^2 \rho} (h + z_o + b) \frac{dh}{dt} \quad (\text{III.B.17})$$



which is an ordinary differential equation for the height of the water column in the borehole as a function of time. Notice that the equation is nonlinear in  $h$ .

### Borehole and Aquifer Interaction

The pressure at the screen will depend on the head in the aquifer, which in turn depends on the aquifer parameters. If  $H(r)$  is the head in the aquifer relative to the static level shown in Figure III.B.3, we can write

$$P_s = P_a + g\rho[H(r_s, t) + z_o + b] \quad (\text{III.B.18})$$

(assuming that  $b$  is small so that the pressure across the screen is nearly constant in the vertical). With the use of equation (III.B.18) in equation (III.B.17) we obtain the final form for the borehole equation which couples to the aquifer equation through  $H(r, t)$ .

$$\begin{aligned} (h + z_o + b) \frac{d^2 h}{dt^2} + \frac{1}{2} \left[ 1 - \left( \frac{r_c^2}{2r_s b} \right)^2 \right] \left( \frac{dh}{dt} \right)^2 + \frac{8\mu}{r_c^2 \rho} (h + z_o + b) \frac{dh}{dt} \\ + g[h - H(r_s, t)] = 0 \end{aligned} \quad (\text{III.B.19})$$

The general aquifer equation

$$\nabla \cdot [bK \nabla H(r, t)] = S \frac{\partial H}{\partial t} \quad (\text{III.B.20})$$

must be solved for  $H(r, t)$  concurrently with equation (III.B.19) to obtain the complete solution, where  $K$  and  $S$  are the aquifer conductivity and storage, respectively. The screen is the boundary between these two solutions and the following boundary condition applies.

$$Q(t) = -\pi r_c^2 \frac{dh(t)}{dt} = -2\pi bK \left[ r \frac{\partial H(r, t)}{\partial r} \right]_{r_s} \quad (\text{III.B.21})$$

### Hvorslev Style Approximation

The system of equations (III.B.19)-(III.B.21) is difficult to solve in general, so an approximation which simplifies the solution would be welcome. In the spirit of the Hvorslev (1951) and Bouer and Rice (1976) methods we can assume that the storage in the aquifer is negligible and consider the aquifer as going through a series of quasi steady states in response to the slug in the borehole. With this assumption, equation (III.B.21) can be taken to hold at any radius, not just at the screen. In that case the following equation describing  $H(r,t)$  can be obtained by integrating equation (III.B.21) over  $r$ .

$$H(r,t) = \left( \frac{r_c^2}{2bK} \right) \left( \frac{dh}{dt} \right) \ln \left( \frac{r}{r_c} \right) \quad (\text{III.B.22})$$

$r_c$  is an empirical parameter, which is the effective radius at which the effect of the slug goes to zero. Evaluating equation (III.B.22) at  $r_s$  and substituting in equation (III.B.19) gives a single ordinary differential equation which must be solved for  $h(t)$ .

$$\begin{aligned} (h + z_o + b) \frac{d^2 h}{dt^2} + \frac{1}{2} \left[ 1 - \left( \frac{r_c^2}{2r_s b} \right)^2 \right] \left( \frac{dh}{dt} \right)^2 \\ + \left[ \frac{8\mu}{r_c^2 \rho} (h + z_o + b) + g \left( \frac{r_c^2}{2bK} \right) \ln \left( \frac{r_s}{r_c} \right) \right] \left( \frac{dh}{dt} \right) + gh = 0 \end{aligned} \quad (\text{III.B.23})$$

Equation (III.B.23) is the nonlinear equivalent to the usual linear Hvorslev equation. Dropping the nonlinear, inertial, and viscous terms in equation (III.B.23) gives

$$\left[ g \left( \frac{r_c^2}{2bK} \right) \ln \left( \frac{r_s}{r_c} \right) \right] \left( \frac{dh}{dt} \right) + gh = 0 \quad (\text{III.B.24})$$

which is equivalent to the Hvorslev equation

$$Q = -\pi r_c^2 \frac{dh}{dt} = FK h \quad (\text{III.B.25})$$

if we identify the Hvorslev form factor (F) as

$$F = \frac{2\pi b}{\ln\left(\frac{r_e}{r_s}\right)} \quad (\text{III.B.26})$$

Both F and  $r_e$  are empirical factors, so it does not matter which we use. In order to stay consistent with the Hvorslev theory which is widely used, we will write equation (III.B.23) as

$$\begin{aligned} (h + z_o + b) \frac{d^2 h}{dt^2} + \frac{1}{2} \left[ 1 - \left( \frac{r_e^2}{2r_s b} \right)^2 \right] \left( \frac{dh}{dt} \right)^2 \\ + \left[ \frac{8\mu}{r_e^2 \rho} (h + z_o + b) + g \left( \frac{\pi r_e^2}{FK} \right) \right] \left( \frac{dh}{dt} \right) + gh = 0 \end{aligned} \quad (\text{III.B.27})$$

This equation only has one unknown parameter which is K, if we use the usual Hvorslev expressions for F. The rest of the physical parameters in equation (III.B.27) can be measured directly in the field or laboratory. Therefore, a least squares fit of the numerical solution of equation (III.B.27) to field data for  $h(t)$  should yield a value for K, the aquifer conductivity.

To conserve writing effort we use the usual definition of the Hvorslev time lag

$$t_o = \frac{\pi r_e^2}{FK} \quad (\text{III.B.28})$$

and define two more quantities

$$A = \frac{\left[ 1 - \left( \frac{r_e^2}{2r_s b} \right)^2 \right]}{2g\pi r_e^2} \quad (\text{III.B.29})$$

and

$$M = \frac{8\mu}{gt_o r_c^2 \rho} \quad (\text{III.B.30})$$

With these definitions and dividing by  $gt_o$ , equation (III.B.27) can be written as

$$\frac{(h + z_o + b)}{gt_o} \frac{d^2 h}{dt^2} + FKA \left( \frac{dh}{dt} \right)^2 + [M(h + z_o + b) + 1] \left( \frac{dh}{dt} \right) + \frac{h}{t_o} = 0 \quad (\text{III.B.31})$$

When the acceleration term is negligible and  $M = 0$  this is the same model presented by McElwee et al.(1992) for the nonoscillating case.

### Limiting Case Solutions

Analytical solutions to equation (III.B.31) can be obtained in a couple of limiting cases. At  $t = 0$  the water column is at rest and  $dh/dt = 0$ . The velocity of the water column will be small at early times, so the velocity dependent terms of equation (III.B.31) can be dropped to give

$$(h_o + z_o + b) \frac{d^2 h}{dt^2} + gh_o = 0 \quad (\text{III.B.32})$$

where  $h_o$  is the initial height. Equation (III.B.32) can only be used for very early times before the water column has moved much because we are assuming the height is approximately constant at  $h_o$ . With these assumptions the solution to equation (III.B.32) is

$$h = h_o - \frac{g}{2} \left( \frac{h_o}{h_o + z_o + b} \right) t^2. \quad (\text{III.B.33})$$

This is simply the normal equation for a falling body under the action of gravity; however, the acceleration is not  $g$  but some fraction based on the quantities  $h_o$ ,  $z_o$ , and  $b$ . In the case where  $h_o \gg z_o + b$ , the column acceleration approaches  $g$  at early times.

Dropping only the velocity squared term (assuming small velocities) in equation (III.B.31) gives

$$(h + z_o + b) \frac{d^2 h}{dt^2} + g t_o [M(h + z_o + b) + 1] \left( \frac{dh}{dt} \right) + gh = 0 \quad (\text{III.B.34})$$

which would be the usual damped harmonic oscillator equation except for the expression  $(h + z_o + b)$  which occurs in the coefficients and makes the equation nonlinear. In the case where  $h_o \ll z_o + b$  (initial displacements are small), equation (III.B.34) can be approximated by

$$(z_o + b) \frac{d^2 h}{dt^2} + g t_o [M(z_o + b) + 1] \left( \frac{dh}{dt} \right) + gh = 0 \quad (\text{III.B.35})$$

which is exactly the damped harmonic oscillator equation (Kreyszig, 1983). Three cases can be identified. The overdamped case is the classical one usually treated in older geohydrology papers and texts.

$$g^2 t_o^2 [M(z_o + b) + 1]^2 > 4g(z_o + b) \quad (\text{III.B.36})$$

In this case the water column does not oscillate at all. In these overdamped cases the viscosity effects represented by  $M$  are usually much smaller than the damping due to the low aquifer conductivity, and can usually be ignored. If the quantities on both sides of equation (III.B.36) are equal, then critical damping is said to occur and there is no oscillation.

The third case to be identified is underdamping and occurs when

$$g^2 t_o^2 [M(z_o + b) + 1]^2 < 4g(z_o + b) \quad (\text{III.B.37})$$

In this case we have an exponentially decaying oscillation given by

$$h(t) = C \text{Exp}[-\alpha t] \cos(\omega^* t - \delta) \quad (\text{III.B.38})$$

where

$$\alpha = \frac{gt_o[M(z_o + b) + 1]}{2(z_o + b)} \quad (\text{III.B.39})$$

and

$$\omega^* = \sqrt{\frac{g}{z_o + b} - \alpha^2} \quad (\text{III.B.40})$$

C and  $\delta$  are given by the initial conditions on the displacement and the velocity of the water column. If  $\alpha = 0$  in equation (III.B.40), which corresponds to no damping either by viscous forces or the aquifer, then  $\omega^*$  is just the natural frequency of an undamped water column. A number of papers in recent years have dealt with this case (Van der Kamp, Kabala et al., etc.). However, little has been done to treat the general case which might lie anywhere in the domain from overdamped to underdamped. Clearly what is needed is a general solution to equation (III.B.31).

### Numerical Solution

Since the fully nonlinear equation (III.B.31) can not be solved analytically, we must resort to numerical techniques. Evaluating equation (III.B.31) at time  $n$  and using central difference formulas for the time derivatives results in

$$\begin{aligned} \frac{(h^n + z_o + b)}{gt_o} \left[ \frac{h^{n+1} - 2h^n + h^{n-1}}{\Delta t^2} \right] + FKA \left( \frac{h^{n+1} - h^{n-1}}{2\Delta t} \right)^2 + \\ [M(h^n + z_o + b) + 1] \left( \frac{h^{n+1} - h^{n-1}}{2\Delta t} \right) + \frac{h^n}{t_o} = 0 \end{aligned} \quad (\text{III.B.41})$$

We have had good results applying a point iterative method to equation (III.B.41). In order to apply this iterative method an iteration index ( $m+1$ ) will be introduced as a superscript in all single appearances of  $h$  at time level  $n+1$ . In all terms where  $h$  squared at time level  $n+1$  appears we must evaluate one  $h$  at the new iteration level ( $m+1$ ) and one  $h$  at the old iteration level ( $m$ ).

$$\begin{aligned}
& \frac{(h^n + z_o + b)}{gt_o} \left[ \frac{h^{n+1(m+1)} - 2h^n + h^{n-1}}{\Delta t^2} \right] \\
& + FKA \left( \frac{h^{n+1(m)} - h^{n-1}}{2\Delta t} \right) \left( \frac{h^{n+1(m+1)} - h^{n-1}}{2\Delta t} \right) \\
& + [M(h^n + z_o + b) + 1] \left( \frac{h^{n+1(m+1)} - h^{n-1}}{2\Delta t} \right) + \frac{h^n}{t_o} = 0
\end{aligned}
\tag{III.B.42}$$

Rearranging equation (III.B.42) gives

$$h^{n+1(m+1)} = \frac{\text{coef}(n-1, m)h^{n-1} + \text{coef}(n)h^n}{\text{coef}(n+1, m)}
\tag{III.B.43}$$

where

$$\text{coef}(n+1, m) = \left[ 1 + \left( M + \frac{2}{gt_o \Delta t} \right) (h^n + z_o + b) + FKA \left( \frac{h^{n+1(m)} - h^{n-1}}{2\Delta t} \right) \right],
\tag{III.B.44}$$

$$\text{coef}(n-1, m) = \left[ 1 + \left( M - \frac{2}{gt_o \Delta t} \right) (h^n + z_o + b) + FKA \left( \frac{h^{n+1(m)} - h^{n-1}}{2\Delta t} \right) \right],
\tag{III.B.45}$$

and

$$\text{coef}(n) = \left[ \frac{4(h^n + z_o + b)}{gt_o \Delta t} - \frac{2\Delta t}{t_o} \right].
\tag{III.B.46}$$

Equation (III.B.43) can now be solved iteratively for  $h$  at the new time level  $n+1$ .

This numerical solution has been incorporated into an automated hydraulic test analysis package called SUPRPUMP (Bohling and McElwee, 1992). As mentioned

earlier there is really only one parameter available for fitting in equation (III.B.31); and that is K, the hydraulic conductivity of the aquifer. We discovered a number of things when we tried to fit the field data. First of all, it was impossible to fit the overall shape of the oscillatory field data with only one available parameter. The values of A and M in equations (III.B.29) and (III.B.30) were quite small and did not seem to fit the field data. The value of A calculated from equation (III.B.29) for our field data was about .7 sec<sup>2</sup>/ft<sup>2</sup>. The kinematic viscosity ( $\mu/\rho$ ) is about 10<sup>-5</sup> ft<sup>2</sup>/sec. Therefore, neither of these parameters played an important role in the analysis of our data. We decided to treat A as an adjustable parameter to be determined by fitting the data. McElwee et al. (1992) had pretty good success using this kind of model when no oscillating water column was observed. Unfortunately, when applied to oscillatory data the model with two parameters (A and K) still did not give a good overall fit to the shape of the curve and most troubling of all, a constant set of values for A and K did not seem to predict the head dependence of the slug test properly. In the process of trying to fit the data it was observed that if the length of the water column in the borehole was adjusted to larger values the general shape of the field data could be fit much better. So, it seemed that something was missing in the physical model.

### Revision of the Model

An alternate method of deriving the equation of motion of the water column in a slug test can be obtained by considering an energy balance equation (Hansen, 1967). Consider the water column inside the borehole (Figure III.B.3) to be a control volume. The change of energy within the control volume over time is determined by the work done at the free surface and the amount of energy that flows out the screen. In equation form this is

$$\frac{d}{dt} \int_{V_{cv}} \left( \frac{V^2}{2} + gz \right) \rho dV_{cv} + \int_{A_s} \left( \frac{P_s}{\rho} + \frac{V_s^2}{2} \right) V_{rn} \rho dA_s + \int_{A_T} P_a V_a dA_T = 0 \quad (\text{III.B.47})$$

The first term is the rate of change of kinetic and potential energy in the borehole (control volume,  $V_{cv}$ ). The second term is the rate at which energy flows out the screen area ( $A_s$ ) due to a radial velocity ( $V_{rn}$ ), where  $P_s$  and  $V_s$  are the screen pressure and velocity respectively. The third term is the rate at which work is done by atmospheric pressure ( $P_a$ ) on the moving upper surface. This equation neglects viscous forces.



Assume that the pressure is constant over the screen area ( $2\pi r_s b$ ) and on the upper surface ( $\pi r_c^2$ ). In addition, assume that the velocity is uniform over the screen area ( $V_s$ ) and the upper free surface ( $V_a$ ). If we consider the water incompressible, the average screen velocity is related to the average borehole velocity ( $dh/dt$ ).

$$V_s = -\frac{r_c^2}{2r_s b} V_a = -\frac{r_c^2}{2r_s b} \frac{dh}{dt} \quad (\text{III.B.48})$$

Using the mean value theorem to average equation (III.B.47) over the control volume gives the result

$$\begin{aligned} \frac{d}{dt} \left\{ \left[ \frac{\overline{V^2}}{2} + \frac{g}{2}(h + z_o + b) \right] \pi r_c^2 \rho (h + z_o + b) \right\} \\ - \left\{ \frac{P_s}{\rho} + \left( \frac{r_c^2}{2r_s b} \right)^2 \frac{1}{2} \left( \frac{dh}{dt} \right)^2 \right\} \left( \frac{r_c^2}{2r_s b} \frac{dh}{dt} \right) 2\pi r_s b \rho + P_a \pi r_c^2 \frac{dh}{dt} = 0 \end{aligned} \quad (\text{III.B.49})$$

The term involving  $\overline{V^2}$  is the average kinetic energy per unit volume of the borehole and needs further consideration. In actual fact there will be other velocity components inside the borehole other than the average vertical velocity describing the drop of the water column. These velocity components may be random in nature (turbulence) or axially circular (curl of velocity not zero) but when averaged over the borehole they do not contribute to the net flow of water out the screen. However, these velocity components may carry significant energy and must be considered when averaging the kinetic energy over the control volume, which is the entire borehole. Assume that the velocity field can be represented by a vertical component and a random component.

$$V = V_z + V_r \quad (\text{III.B.50})$$

Using this form for the velocity in equation (III.B.49) gives

$$\begin{aligned}
\overline{V^2} \rho \pi r_c^2 (h + z_o + b) &= \int_{V_{cv}} V^2 \rho dV_{cv} = \int_{V_{cv}} (V_z + V_r)^2 \rho dV_{cv} \\
&= \int_{V_{cv}} (V_z^2 + 2V_z V_r + V_r^2) \rho dV_{cv}
\end{aligned}
\tag{III.B.51}$$

Since  $V_r$  is a random velocity component, we assume that the following integral will average to zero over the control volume.

$$\int_{V_{cv}} V_z V_r \rho dV_{cv} = 0 \tag{III.B.52}$$

Assume that  $V_z$  is given by a radial velocity distribution defined by equations (III.B.10) and (III.B.12).

$$V_z = 2 \frac{dh}{dt} \left[ 1 - \frac{r^2}{r_c^2} \right] \tag{III.B.53}$$

The first term in equation (III.B.51) can now be evaluated. The last term in equation (III.B.51) requires some addition assumptions about the random component. Since the random component is zero in a static situation and could logically be expected to increase proportionally to the average vertical velocity, it is reasonable to assume that

$$V_r = \alpha \frac{dh}{dt} \tag{III.B.54}$$

With these assumptions equation (III.B.51) can be written as

$$\begin{aligned}
\overline{V^2} \rho \pi r_c^2 (h + z_o + b) &= \left( \frac{dh}{dt} \right)^2 \int_{V_{cv}} \left( 4 \left[ 1 - \frac{r^2}{r_c^2} \right]^2 + \alpha^2 \right) \rho dV_{cv} \\
&= \left( \frac{dh}{dt} \right)^2 \left[ \frac{4}{3} + \alpha^2 \right] \rho \pi r_c^2 (h + z_o + b)
\end{aligned}
\tag{III.B.55}$$

which shows that the average square velocity is larger than the square of the average velocity by a factor greater than one.

$$\overline{V^2} = \left( \frac{dh}{dt} \right)^2 \left[ \frac{4}{3} + \alpha^2 \right] \quad (\text{III.B.56})$$

This implies that the kinetic energy of the water column can be significantly larger than one might suspect based on the average vertical velocity ( $dh/dt$ ).

With the above considerations, equation (III.B.49) can now be written as

$$\begin{aligned} \frac{d}{dt} \left\{ \left[ \frac{1}{2} \left( \frac{dh}{dt} \right)^2 \left( \frac{4}{3} + \alpha^2 \right) + \frac{g}{2} (h + z_o + b) \right] \pi r_c^2 \rho (h + z_o + b) \right\} \\ - \left\{ \frac{P_s}{\rho} + \left( \frac{r_c^2}{2r_s b} \right)^2 \frac{1}{2} \left( \frac{dh}{dt} \right)^2 \right\} \left( \frac{r_c^2}{2r_s b} \frac{dh}{dt} \right) 2\pi r_s b \rho + P_a \pi r_c^2 \frac{dh}{dt} = 0 \end{aligned} \quad (\text{III.B.57})$$

Performing the differentiation and rearranging slightly shows that this is identical to equation (III.B.17) except for the viscous terms which have been neglected and the factor multiplying the kinetic energy.

$$\left( \frac{dh}{dt} \right) \left\{ (h + z_o + b) \left[ \frac{4}{3} + \alpha^2 \right] \frac{d^2 h}{dt^2} + \frac{1}{2} \left[ \frac{4}{3} + \alpha^2 - \left( \frac{r_c^2}{2r_s b} \right)^2 \right] \left( \frac{dh}{dt} \right)^2 \right. \\ \left. + g(h + z_o + b) - \frac{P_s - P_a}{\rho} \right\} = 0 \quad (\text{III.B.58})$$

By considering an energy based equation we have derived the same basic equations as are obtained starting from the Navier-Stokes equation; however, the kinetic energy contribution of velocity components other than those in the vertical direction may be considerable and a new parameter ( $\alpha$ ) has been added to the model. The generalization of equation (III.B.58) to include a viscous term or the addition of the factor multiplying

the acceleration term into equation (III.B.17) gives the final form for the mathematical model.

$$(h + z_o + b) \left[ \frac{4}{3} + \alpha^2 \right] \frac{d^2 h}{dt^2} + \frac{1}{2} \left[ \frac{4}{3} + \alpha^2 - \left( \frac{r_c^2}{2r_s b} \right)^2 \right] \left( \frac{dh}{dt} \right)^2 + g(h + z_o + b) - \frac{P_s - P_a}{\rho} + \frac{8\mu}{r_c^2 \rho} (h + z_o + b) \frac{dh}{dt} = 0 \quad (\text{III.B.59})$$

The definition of A given in equation (III.B.29) now needs to be changed slightly, with the 1 in the numerator replaced by  $4/3 + \alpha^2$ . Since A is used as an empirical factor which is fitted to the field data, this redefinition of A does not change the form of the earlier model.

### Data Analysis

The numerical method presented earlier can easily be adapted to the model presented by equation (III.B.59) simply by adding the factor which multiplies the acceleration term. The point iterative formula for the head at the latest time level is still given by equation (III.B.43).

$$h^{n+1(m+1)} = \frac{\text{coef}(n-1, m) h^{n-1} + \text{coef}(n) h^n}{\text{coef}(n+1, m)} \quad (\text{III.B.43})$$

Only the coefficients are changed slightly.

$$\text{coef}(n+1, m) = 1 + \left( M + \frac{2 \left( \frac{4}{3} + \alpha^2 \right)}{g t_o \Delta t} \right) (h^n + z_o + b) + FKA \left( \frac{h^{n+1(m)} - h^{n-1}}{2 \Delta t} \right) \quad (\text{III.B.60})$$

$$\begin{aligned}
 coef(n-1, m) = 1 + & \left( M - \frac{2\left(\frac{4}{3} + \alpha^2\right)}{gt_o \Delta t} \right) (h^n + z_o + b) \\
 & + FKA \left( \frac{h^{n+1(m)} - h^{n-1}}{2\Delta t} \right)
 \end{aligned}
 \tag{III.B.61}$$

and

$$coef(n) = \frac{4\left(\frac{4}{3} + \alpha^2\right)(h^n + z_o + b)}{gt_o \Delta t} - \frac{2\Delta t}{t_o} .
 \tag{III.B.62}$$

The model represented by equation (III.B.43) and equations (III.B.60)-(III.B.62) has three parameters ( $\alpha$ , A, K) which may be adjusted to fit the field data. We have had good results fitting this model to the GEMS data. Figures III.B.5 and III.B.6 show the fitted theoretical values as stars on the field data plots. The theory describes the head dependence and general shape of the field data very well. Both the nonoscillatory (Figure III.B.5) and oscillatory (Figure III.B.6) data are predicted very well with the fitted values. Field data for a variety of initial slug heights are reproduced well for a single set of parameters ( $\alpha$ , A, K). Earlier models (McElwee et al., 1992) fit the non oscillatory data pretty well but the parameters had some dependence on the initial slug height. In general, the effect of the viscosity term in the model appears to be insignificant. The factor  $(4/3 + \alpha^2)$  in the model implies that the velocity components not in the z direction carry about 15% of the kinetic energy since  $\alpha = .5$  is the best fit value. The 4/3 is given by assuming there is a parabolic distribution of velocities along the radius. Any other radial distribution will give a slightly different result; however, the important point is that the column is usually carrying more kinetic energy than would be predicted by simply using the average vertical velocity ( $dh/dt$ ). These two contributions together increase the kinetic energy about 60% over the uniform velocity case. The other parameter, A, was fitted with a magnitude of 55-70 for this field data. This is much larger than would be calculated from equation (III.B.29) for A. Clearly, some physical mechanism has been left out of the model, apparently with the same mathematical form as the term involving

A in equation (III.B.31), but with a much larger magnitude. Further research is needed to shed light on the nature of this mechanism.

Figures III.B.7 and III.B.8 are simply single plots of the field data and theory for one particular value of the initial slug height. These plots allow one to better access the quality of the fit of theory to experiment. In general the fit is very good. Figure III.B.9 is a Hvorslev type plot of the field data and theory for the non oscillatory well. Notice that the data is becoming very noisy after about 12 seconds, so little quantitative information is available in that region. Also notice that the theory curve is approaching a straight line whose slope is proportional to  $K$  at large time (McElwee et al., 1992). However, there is no hope that data could ever be collected in this region since the response is so small. Only in the overdamped case will this straight line portion move into the range where it is measureable. In the case of wells in the critically damped region, we will see this characteristic downward curvature on a Hvorslev plot, in that case an appropriate model must be used to analyze the data.

## Conclusions

Generally, the effects of viscosity and changing casing-screen radii are negligible on slug test responses. However, the effects of nonlinearities, inertia, and velocity distributions can be quite important. The nonlinear terms make slug test results dependent on the initial head, inertial effects are important when oscillatory behavior is observed, and nonuniform velocity distributions cause the effective water column length to be greater than expected. We have developed a general model incorporating all these features. This general model can be reduced to a Hvorslev type model by assuming no storage in the aquifer. We have obtained an iterative numerical solution to this model and have applied it to field data from our research site. The results are quite good both for oscillatory and non oscillatory situations and give consistent values of the physical parameters for various initial displacements. The theory predicts the general shape and head dependence observed in the field data. Further research is needed to identify the source of the strong nonlinearity represented by one parameter.

Figure 1.  
Slug Test Response at GEMS Well 02

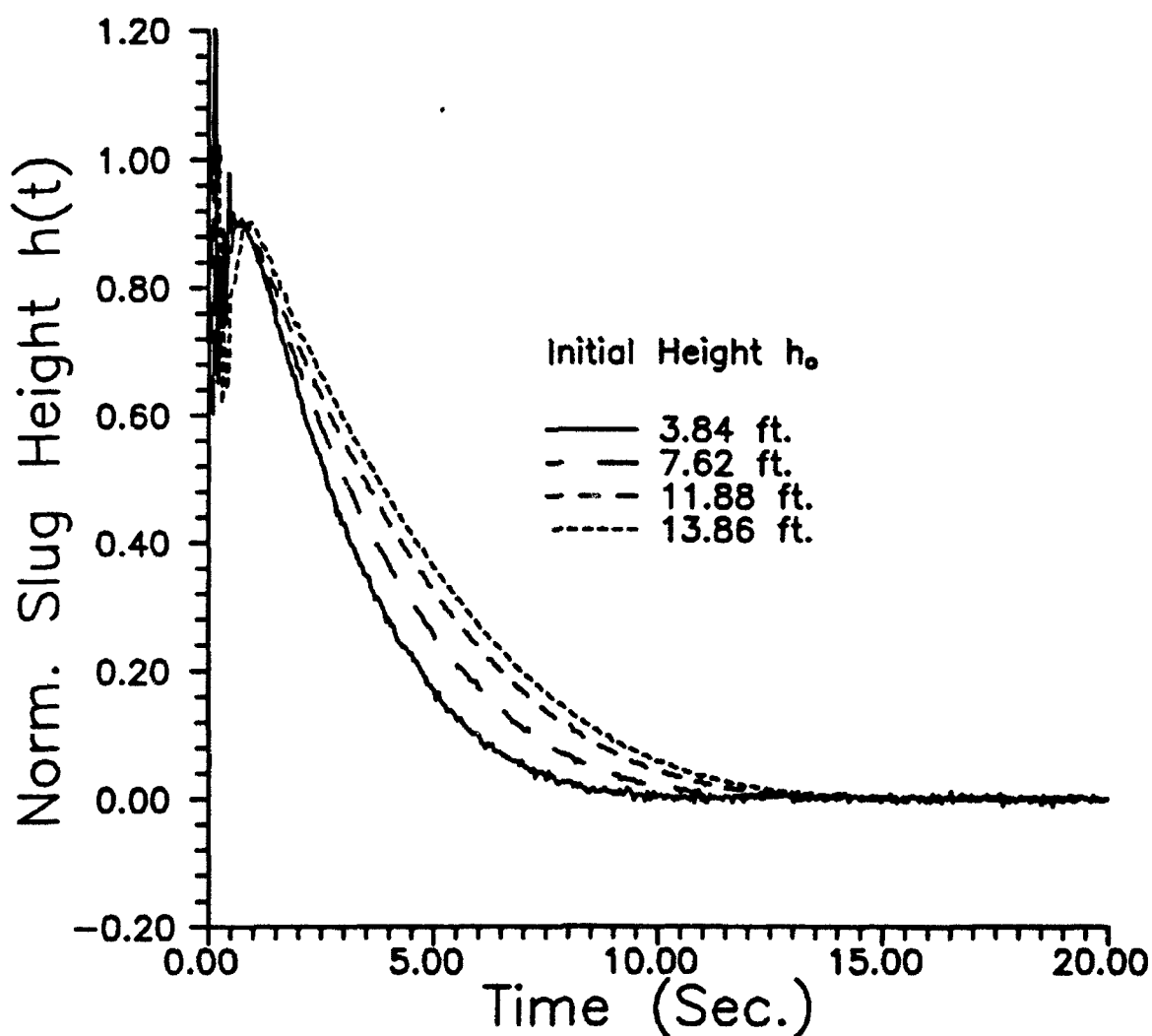


Figure 2.

Slug Test Response at GEMS Well 07

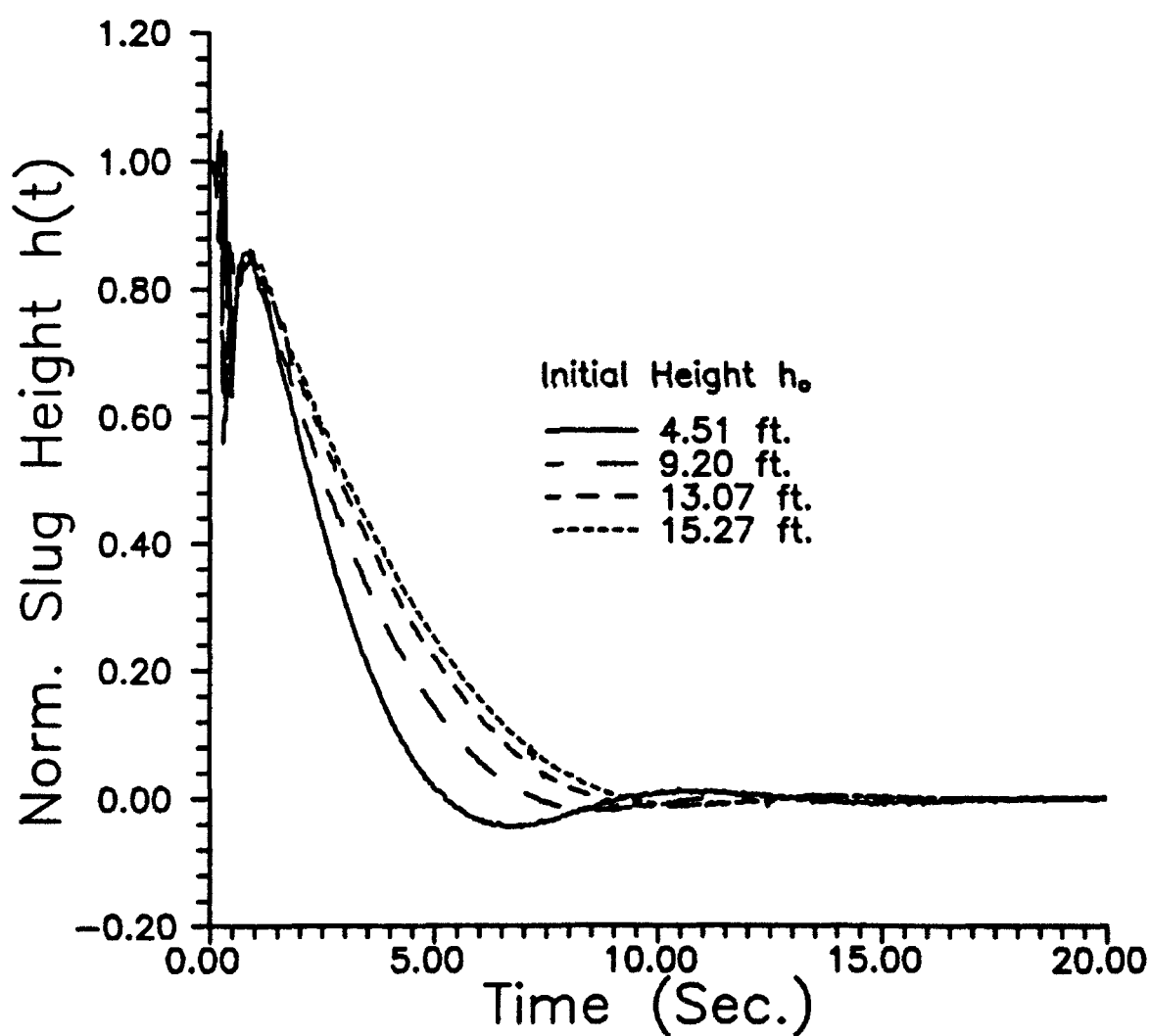
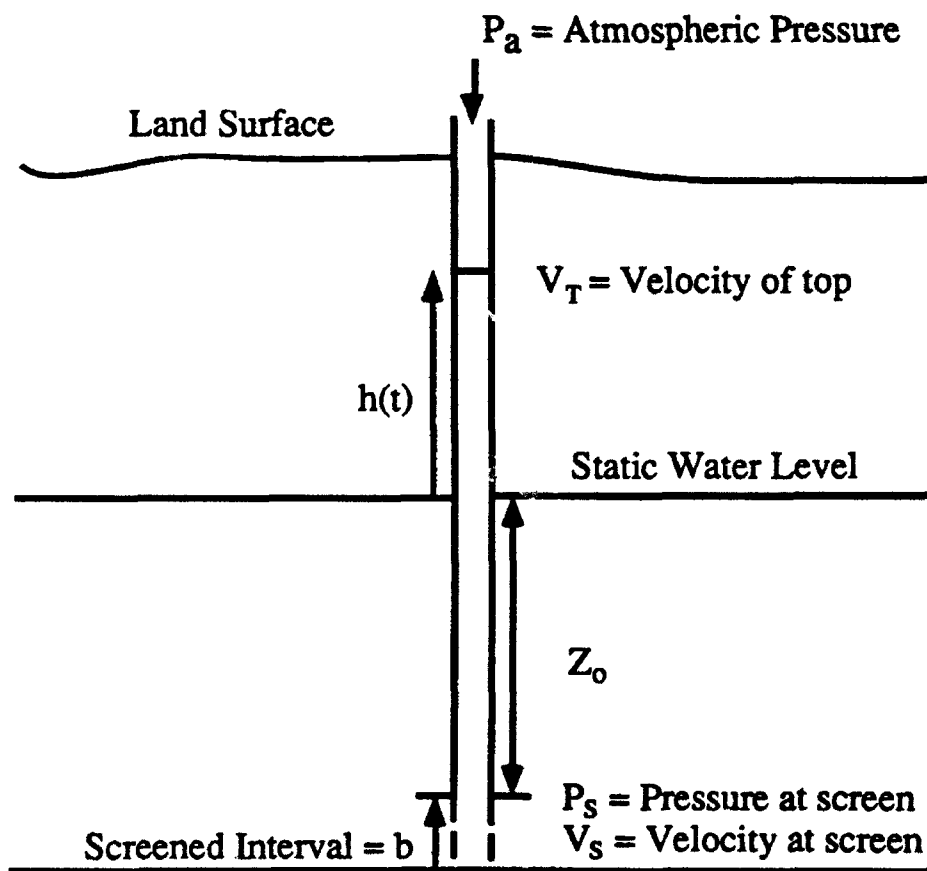




Figure III.B.3. Schematic of the Slug Test Wellbore



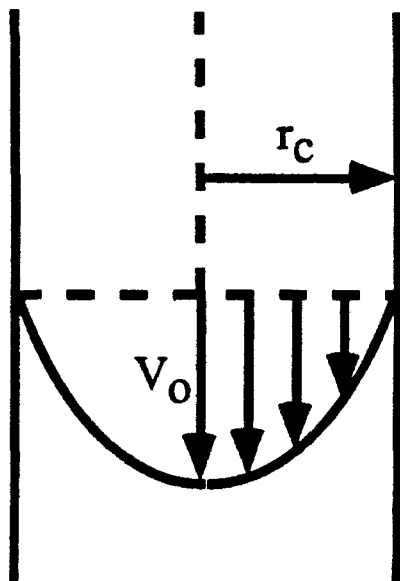


Figure III.B.4. Assumed Radial Velocity Distribution

Figure 5.  
Slug Test Response at GEMS Well 02

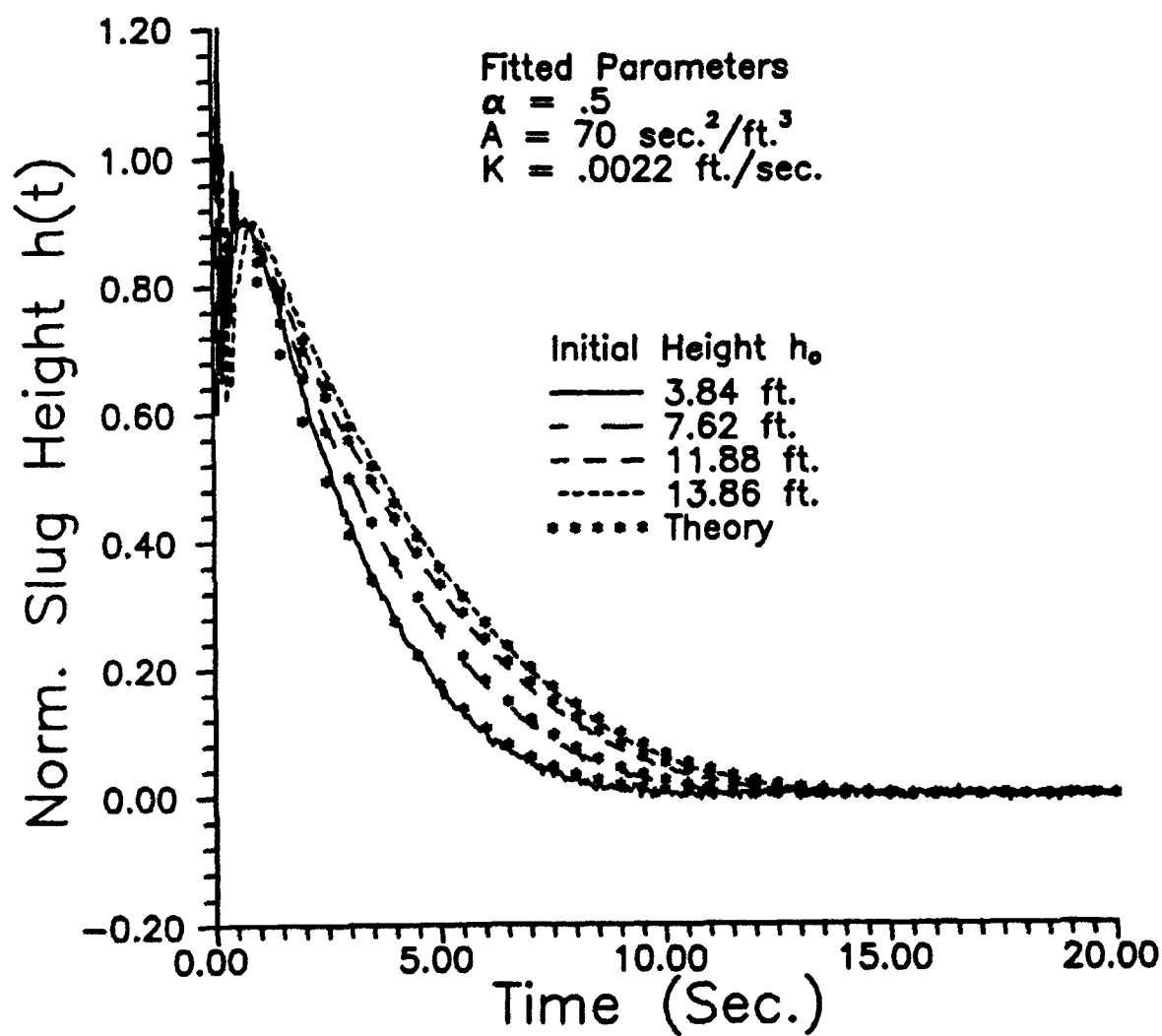


Figure 6.  
Slug Test Response at GEMS Well 07

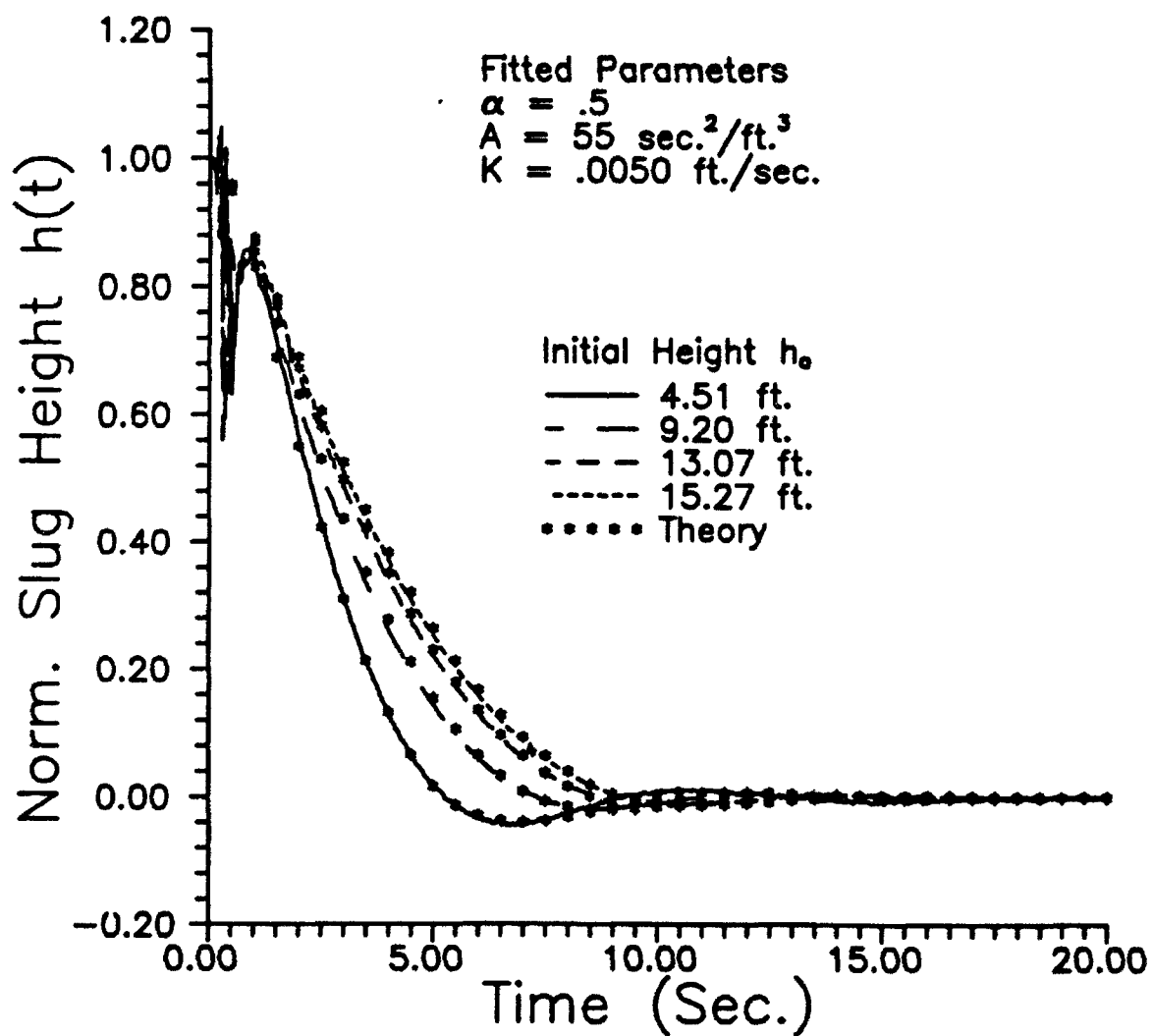


Figure 7.  
Slug Test Response at GEMS Well 02

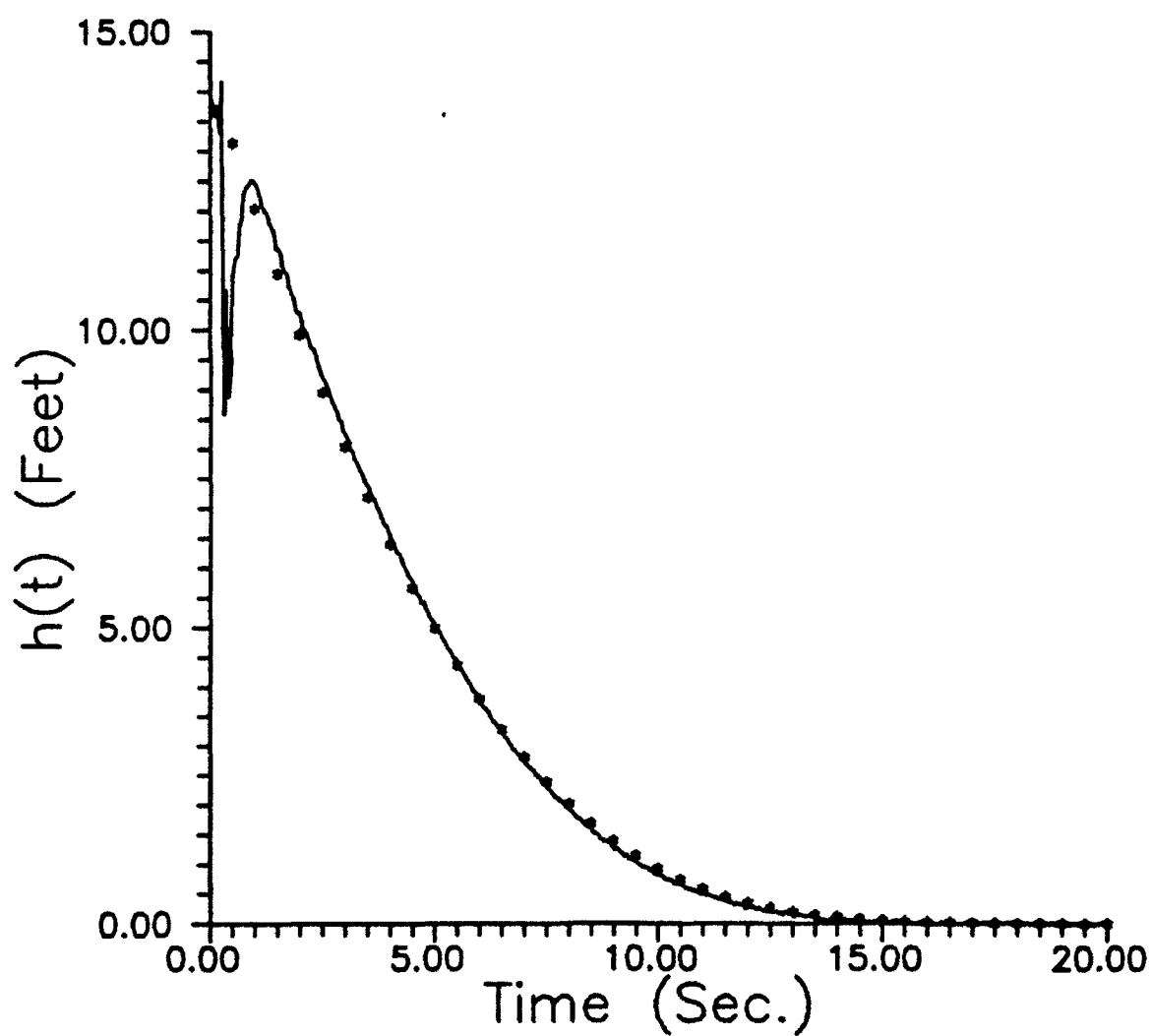


Figure 8.  
Slug Test Response at GEMS Well 07

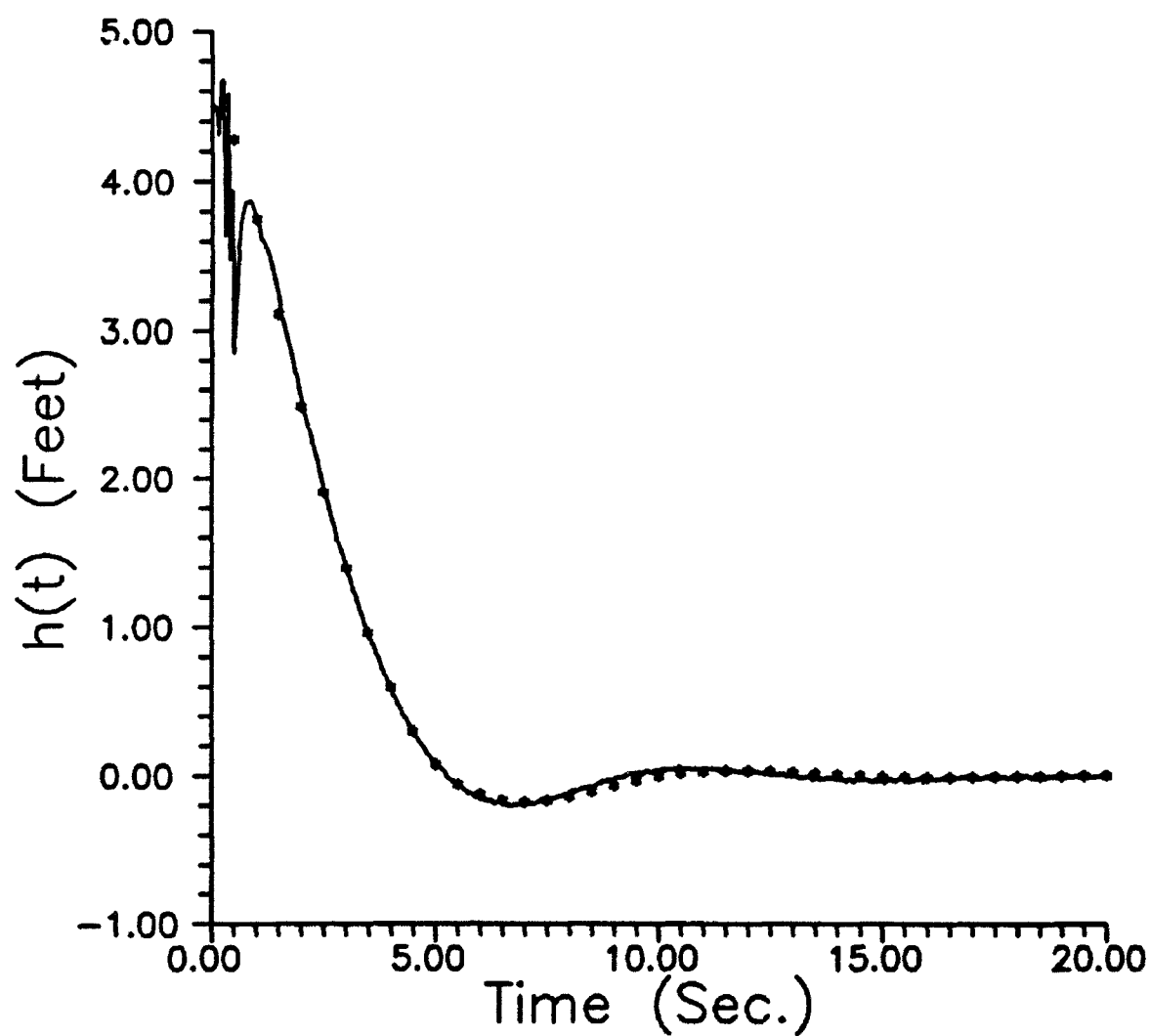
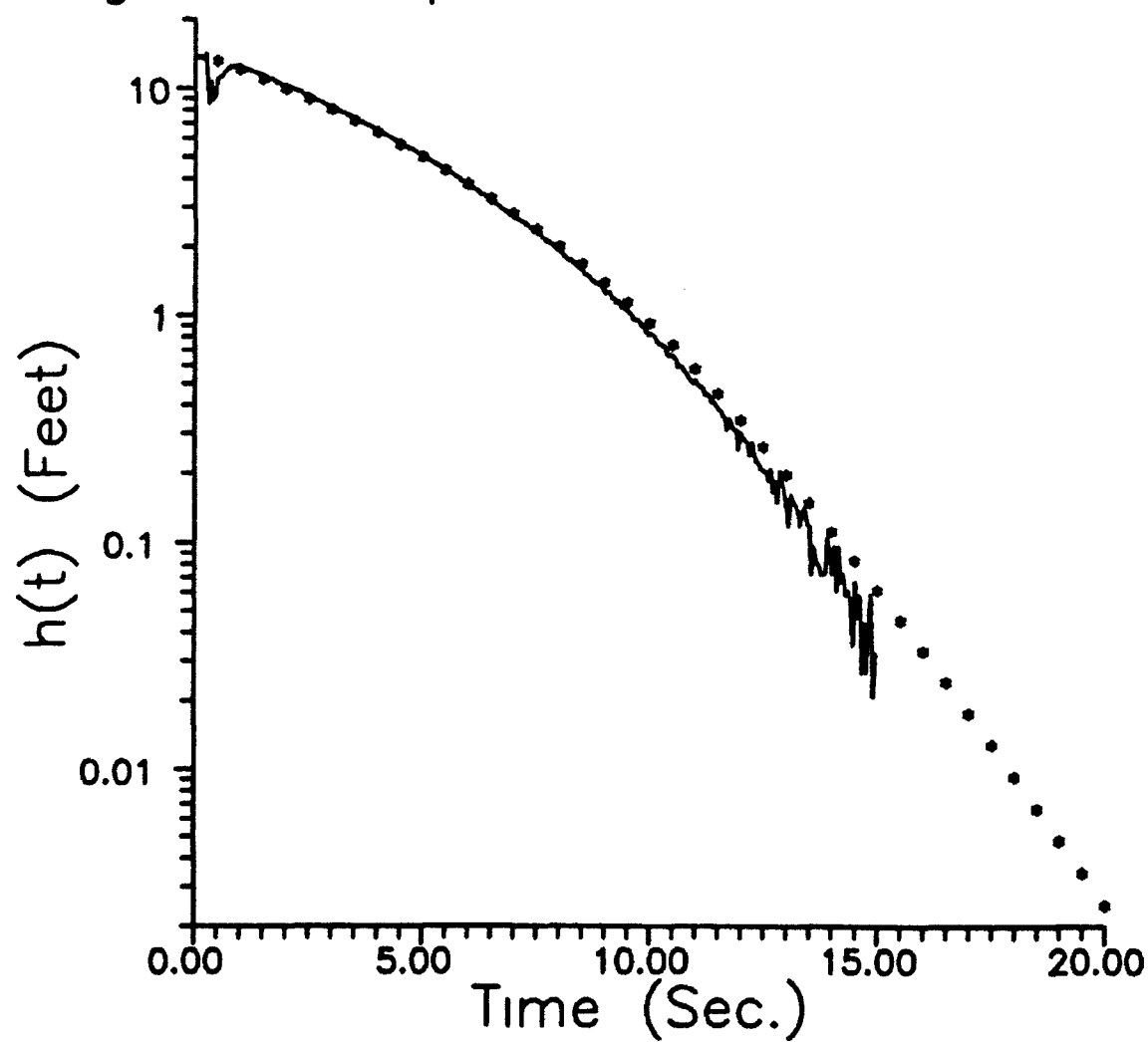


Figure 9.  
Slug Test Response at GEMS Well 02



## **IV. SITE CHARACTERIZATION ACTIVITIES**

### **A. DRILLING AND SAMPLING ACTIVITIES**

#### **Introduction**

At the end of the last report period, May 31, 1993, forty wells had been installed at GEMS in the Kansas River alluvium. Fourteen of these wells have been cored through 30-35 feet of coarse sand and gravel at depths of 35-70 feet using various techniques (eight of these core holes have been reported on in detail in the reports for years one and two of this project). In this report period (ending May 31, 1994), seventeen new holes have been drilled at GEMS bringing the total to 57 observation or monitoring wells. One hole (TMO-1) was cored from 35 feet to the bedrock. Cores in the sand and gravel section were taken using the new sampler design (McElwee et al., 1991) which incorporates an inflatable bladder, located in the drive shoe, which closes off the end of the sampler during recovery. Fifteen new multilevel sampling (MLS) wells were drilled (14 just north and a little east of the 00 nest site, and one near nest 1). The 14 wells started the installation of an array of wells to be used for conducting a series of tracer tests at GEMS; twenty-three wells are planned for the total array. One new 4 inch well (0-9) was drilled with the new large diameter auger flights that were obtained as part of this research effort in year two.

#### **Drilling Procedure**

All except a few of the wells at GEMS have been installed with hollow-stem auger techniques. A review of hollow-stem auger techniques and equipment is given by Hackett (1987). Auger flights with 3 1/4 inch inside diameter and 6 5/8 inch outside diameter were used for most holes (2 inch wells). New larger diameter auger flights were purchased as part of the year two research effort, and have been used to install two four inch wells. These auger flight have an inside diameter of 6 1/2 inches and an outside diameter of 10 inches. The deepest alluvial wells at the site are about 70 feet. One bedrock well, which was installed with mud rotary techniques, is about 80 feet deep and extends into bedrock about 10 feet. A typical nonsampling installation (with either set of auger flights) would proceed by drilling to the desired depth with a knock-out plate installed in the auger head in place of a pilot bit (Perry and Hart, 1985; Hackett, 1987). At that point, the well casing would be installed through the hollow flights and the plate would be knocked out .



Heaving sands or sandblows (Minning, 1982; Perry and Hart, 1985; Keely and Boateng, 1987; and Hackett, 1987) are a severe problem at this site in the zone of sand and gravel (35-70 ft.). It is absolutely essential to maintain greater hydrostatic pressure inside the auger flights than in the formation when drilling or coring in heaving sands. The water level inside the auger flights is maintained higher than the ambient water table by adding water at critical times (mainly, when tools are moved within the flights or the flights are moved). If a greater hydrostatic head within the auger flights is not maintained at critical times, several feet of sediment may quickly enter the flights, with the result that the possibility of obtaining an undisturbed sample at that depth is lost. Adding water to maintain a higher head in the flights may affect the chemistry and biota of an aquifer, so an investigator must balance this concern with the need to control heaving sands.

Typically, when sampling the sand and gravel portion the new bladder sampler design is used (McElwee et al., 1991). The sampler is driven 5 feet and then a flexible bladder is inflated on the end to hold the sediments in place during recovery. Water is added during recovery to prevent heaving sands. After each 5 foot sample collection, the hole is advanced 5 feet by continued augering. Typically, we take 7 of these 5 foot sections in each cored well. Usually the last sample is less than 5 feet due to reaching consolidated bedrock. Due to the physical construction of the sampler (length and position of the bladder), six inches is always lost on the end of each sample. This means that 90% is the maximum recovery under ideal conditions. We usually lose another several percent due to compaction, premature piston movement, and wall friction or large cobbles preventing material from moving into the sampler. This usually shows up as head space above the sample in the sampler tube.

This year we instituted a new procedure; it is for installing the multilevel sampling (MLS) wells. The first part is similar to the old procedure, in that we drill to 35 feet with a pilot bit in the end of the auger flights. At this point, we add water and pull the pilot bit slowly to obtain an open hole. Seventy-five feet of new drive casing with a 3 inch O.D. has been obtained this year. After drilling thirty-five feet we place a plastic end cap on the drive casing and proceed to drive it to bedrock (about 70 feet) with a pneumatic jack hammer. The endcap keeps the inside of the drive casing clean and is much better than trying to wash out an open ended drive string after it has been driven (an earlier version of this installation procedure). With the plastic cap on or near bedrock, drill rods are lowered into the casing to gently push out the plastic cap as the drill casing is raised slightly. When the casing is free of the plastic cap we pull the drill rods while adding water to prevent heaving sands. The MLS wells are made of 1 1/4 inch PVC pipe

with 17 polyethylene tubes (14 inch O.D.) running through the middle to each port location (see section V for construction details). After the drill rods are out, an MLS well is lowered into place ten feet at a time. Each section must be screwed together and the small tubing threaded through each piece ( the first few ten foot pieces containing ports are already threaded with the small tubing at construction time, the others are threaded on site as lowered). This lowering and threading procedure is awkward and required a crew of four or five people to be done efficiently. When the MLS well is in place we add water and carefully pull the drive casing from around the MLS. We have only had one problem with heaving sands locking the MLS into the drive casing and we were able to wash it out. The auger flights are pulled after all the drive casing has been re'rieved. On a very good long day (nothing goes wrong) we can install two of these MLS wells. However, our long term average so far is closer to one per day. Others have reported in the literature various installation procedures for MLS wells with either augering techniques or driving techniques (Pickens et al., 1978; Morin et al., 1988; Boggs et al., 1988; and Stites and Chambers, 1991 ). However, we have refined and combined the two techniques into a procedure that appears to work quite well.

#### **Drilling and Sampling - Third Year**

During the 1993-94 field season one additional well was drilled, cored and completed (the last of nine which were required by the terms of this project), fifteen MLS wells were installed, and one additional 4 inch well was completed with the new larger diameter flights. This brings the total to 57 monitoring wells at GEMS.

The well cored during this period was cored from about 35 feet to the bedrock, using the bladder sampler techniques outlined above. This well (TMO-1) was cored near the center of the proposed tracer test array of MLS wells. Starting at approximately thirty-five feet, the bladder sampler was used to collect samples of the sand and gravel. After recovery, the sand and gravel cores were x-rayed for structure determination and then taken to the laboratory to be cut up and processed for storage until measurement of hydraulic conductivity, porosity, density and particle-size fraction can be done. The sample recovery for this hole was good; we did not lose any large sections and the equipment did not malfunction. The cores are now being processed but the exact data are not yet available.

Fifteen MLS wells have been installed (see section V for construction details) according to the procedure outlined above. One well was installed near nest 1 to aid in the single well injection testing of section IV.D. The other 14 MLS wells were installed according to the array designed in section II.C and located just north and slightly east of

nest 00. Nine more are planned to complete the array as designed. Each of these 15 wells have been completed by cutting the casing back to a known distance above the top port. There are two kinds of wells as detailed in the construction section (V); one has two feet spacing between ports (regular) and one has one foot spacing of ports (detailed). The regular MLS wells were cut back to 38 feet above the top port. The detailed samplers were cut back to 53 feet above the top port. We have yet to measure the elevations of the top of each casing; when this is done we will accurately know the depth of each port relative to others. The 1/4 tubing was cut back and permanently labeled three ways to avoid confusion: First, the tubes are uniformly color coded for depth; Second, they are marked with a sequential port number; and Third, they are labeled with the depth below top of casing. The marking are done with a permanent marker and covered with clear heat shrink tubing for durability. For completion, the well tops are covered with 2 inch PVC casing using a water tight neopreme connector between the 1 1/4 inch and 2 inch PVC casings. After the well installations were complete a comprehensive program of developing the ports was begun using multichannel peristaltic pumps (two ten-channel pumps). If a port did not develop quickly and give the desired flow ( approximately 150ml per min.) of clear water then a repeated sequence of backflushing followed by pumping was performed. Of the 255 ports in 15 MLS wells only 4 ports have problems of insufficient or no flow. Overall we are very pleased with this success rate.

The remaining hole (0-9) was a large diameter well to be used for future hydraulic testing. It was drilled in June of 1993 and completed with 4" well casing and a wirewrapped screen (Sch 40, .020 slot size) of length 2.5 feet. The completion depth was approximately 55 feet. The larger casing means that larger pumps can be used and the aquifer can be stressed more than from a 2 inch well. This should make it invaluable in some pulse testing work, allowing a larger volume per unit time to be pumped. In addition, we plan to use this well with a number of slug tests, since the larger diameter will allow much more instrumentation to be placed in the well. The two 4 inch diameter wells have been used extensively as high volume sources of water for drilling and the injection testing described in section IV.D.

## **B. LABORATORY ACTIVITIES**

### **Laboratory Procedures and Methods**

The cores recovered from the drilling and sampling summarized in the previous section of this report were taken to the laboratory for measurement of core properties. The procedures and methods used in analyzing the core samples are essentially the same as those described in the reports of the first and second years of this project (McElwee and Butler, 1992, 1993).

As noted in the report of the second year of this project, the decrease in hydraulic conductivity with time that was observed for many of the cores could be a result of the deposition of calcite in pore throats. Another possible explanation would be the expansion and/or dispersion of clays, which would also produce a clogging of pore throats. In an attempt to identify the primary mechanism responsible for the observed decreases in conductivity with time, a series of experiments was conducted using a single core in the permeameter. The chemistry of the water prior to passage through the core and after passage through the core was carefully monitored with the assistance of the Analytical Services Section of the Kansas Geological Survey.

As described in the report of year two, the water circulated in the permeameter is obtained from wells at GEMS that are screened close to or over the same interval from which the core was taken. At the same time water was collected for use in the permeameter experiments, samples were taken in the field for analysis by the Analytical Services Section. The collected water was then transported to the laboratory where it was allowed to sit for two weeks in order to equilibrate with laboratory temperatures and pressures. Additional water samples were taken during this period in order to assess changes occurring with equilibration to laboratory conditions. Once the water was placed in the permeameter, samples were taken several times a day from the water that had passed through the core and once a day from the permeameter water that had not passed through the core. A subset of these samples was chosen for major cation analysis by the Analytical Services Section using observed changes in hydraulic conductivity as the selection criterion. Note that the permeameter setup used here involves recirculating the water that has passed through the cores. For these experiments, however, no recirculation was allowed so that any chemistry changes occurring in the water passing through a core could be readily identified and not be masked by mixing.

In addition to the major cation analyses performed by the Analytical Services Section, the pH and dissolved oxygen of the water prior to passage through the core (henceforth designated as permeameter water) and after passage through the core

(henceforth designated as outflow-tube water) were monitored in the laboratory. The pH was determined using a CARDY Twin pH meter (Horiba Instruments). Measurement of the pH of the outflow-tube water was done several times a day, while measurement of the pH of the permeameter water was done at least once a day. Dissolved oxygen (DO) was measured using a K-7512 CHEMets colorimetric kit (CHEMetrics). DO was determined for outflow-tube water once a day and once every 3 to 4 days for the permeameter water.

Sediment samples from the cores used in these experiments were collected for x-ray analysis of clay mineralogy both before and after being processed in the permeameter.

As a result of the findings of the water chemistry and clay analysis, two further modifications have been made to the laboratory procedure: 1) carbon dioxide gas is being bubbled into the water of the upper reservoir to maintain the pH, which is monitored daily, at a level comparable to that of the water at GEMS; and 2) a different biocide (dichlorophene) is being used to inhibit biologic growth in the system.

## **Results and Discussion**

### **Core Analyses**

Graphs of the original and repacked hydraulic conductivities and porosities, the percent fines (<53 microns), and the mean grain size of core segments from wells 7-1 and 9-1 are presented in Figures IV.B.1 - IV.B.14. The hydraulic conductivities and porosities for original and repacked core segments from GEMS well 11-1 are presented in Figures IV.B.15 - IV.B.19. The grain size statistics for that well will be given in the final report of this project.

#### **GEMS 7-1**

Sample #1 was not recovered due to the sampler malfunctioning.

The undisturbed cores of well 7-1 (not including the cores through which no water flowed) have an arithmetic mean hydraulic conductivity of 32.38 m/day, with a sample standard deviation of 48.85 m/day (Figure IV.B.1). Values range from a minimum of 0.28 m/day to a maximum of 261.78 m/day. There is no apparent trend in hydraulic conductivity with depth. There was no flow through three segments from this well: sample #6, segments #1, #4, and #5 (18.41-18.56 m, 18.86-19.01 m and 19.01-19.17 m).

The repacked cores of well 7-1 have a higher mean conductivity but less

variability than the undisturbed cores (Figure IV.B.2). Values range from 0.18 m/day to 153.65 m/day with a mean of 39.91 m/day and a standard deviation of 36.94 m/day. For 27 of the 35 processed segments, the repacked hydraulic conductivity is greater than the original measurement (Figure IV.B.3). Sample #5, segment #7 (17.93-18.09 m) and the three cores mentioned in the preceding paragraph were not repacked because of their very low original permeability. They will be processed when the low permeability permeameter cell described in the report of year two is fully operational.

The original cores have porosities ranging from 19.8% to 36.4% with an arithmetic mean of 25.8% and a standard deviation of 3.4% (Figure IV.B.4). The porosity of the repacked cores ranges from 20.2% to 36.0% with an arithmetic mean of 26.5% and a standard deviation of 3.3% (Figure IV.B.5).

The differences between the original and repacked porosities range from 0.01% to 2.83% with an arithmetic mean of 0.87%. For 25 of the 35 processed cores, the repacked porosity is greater than the original porosity; 10 of the repacked cores have lower porosities than the original cores.

The percent fines for well 7-1 ranges from 0.4% to 20.28% with an arithmetic mean of 3.3% and a standard deviation of 4.1% (Figure IV.B.6). The phi sizes for well 7-1 range from -0.73 to 0.98 with an arithmetic mean of 0.02 and a standard deviation of 0.45 (Figure IV.B.7). Grain size data are not available for segments that have not yet been repacked.

#### GEMS 9-1

The undisturbed cores of well 9-1 have an arithmetic mean hydraulic conductivity of 27.19 m/day, with a sample standard deviation of 32.59 m/day (Figure IV.B.8). Values range from a minimum of 0.19 m/day to a maximum of 134.73 m/day.

The repacked cores of well 9-1 have a higher mean conductivity and greater variability than the undisturbed cores (Figure IV.B.9). Values range from 0.16 m/day to 233.27 m/day with a mean of 49.19 m/day and a standard deviation of 43.36 m/day. For 44 of the 47 processed segments, the repacked hydraulic conductivity is greater than the original measurement (Figure IV.B.10). Sample #1, segment #1 was not repacked because it was used for x-ray analysis of clay mineralogy.

The original cores have porosities ranging from 21.3% to 36.3% with an arithmetic mean of 26.4% and a standard deviation of 2.8% (Figure IV.B.11). The porosity of the repacked cores ranges from 21.5% to 37.2% with an arithmetic mean of 27.6% and a standard deviation of 3.0% (Figure IV.B.12).

The differences between the original and repacked porosities range from 0.05%

to 4.74% with an arithmetic mean of 1.51%. For 35 of the 47 processed cores, the repacked porosity is greater than the original porosity; 12 of the repacked cores have lower porosities than the original cores.

The percent fines for the segments from well 9-1 ranges from 0.2% to 33.43% with an arithmetic mean of 2.7% and a standard deviation of 5.9% (Figure IV.B.13). The phi sizes for well 9-1 range from -1.05 to 2.07 with an arithmetic mean of 0.19 and a standard deviation of 0.69 (Figure IV.B.14). Grain size and porosity data for sample #1 segment #1 (10.81-10.98 m) are not available because the core was used for x-ray analysis of clay mineralogy. Grain size data for sample #2, segment #3 are not included in the calculations since an error was made in the sieve analysis.

#### GEMS 11-1

The undisturbed cores of well 11-1 have an arithmetic mean hydraulic conductivity of 29.6 m/day, with a sample standard deviation of 32.51 m/day (Figure IV.B.15). Values range from a minimum of 0.41 m/day to a maximum of 118.57 m/day. Hydraulic conductivity values were not obtained for sample #1, segments #1, #2 and #5 (10.92-11.07, 11.07-11.19 and 11.47-11.61 m); sample #5, segment #6 (17.66-17.81 m); and sample #6, segment #1 (18.50-18.64 m), as there was no flow through these cores under the head gradient produced in the permeameter.

The repacked cores of well 11-1 have a higher mean conductivity and greater variability than the undisturbed cores (Figure IV.B.16). Values range from 1.20 m/day to 166.72 m/day with a mean of 63.93 m/day and a standard deviation of 45.26 m/day. For 30 of 36 processed segments, the repacked hydraulic conductivity is greater than the original measurement (Figure IV.B.17). The samples mentioned in the preceding paragraph, as well as sample #6, segments #5 and #6, were not repacked and have been set aside to process in the low permeability cell. Sample #3, segment #3 and sample #5, segments #3 and #8 were not repacked because they were used for x-ray analysis of clay mineralogy. The repack information from sample #3, segment #4; sample #4 segments #1, #4 and #7; sample #5, segment #4; and sample #7, segment #3 were not included in the graphs and statistics, since a mistake was made when the method of securing the cores in the permeameter was modified, and the sediment from these cores was repacked to a length approximately 1 to 2 cm longer than the original cores.

The original cores have porosities ranging from 22.2% to 33.0% with an arithmetic mean of 26.4% and a standard deviation of 2.7% (Figure IV.B.18). The porosity of the repacked cores ranges from 21.2% to 31.7% with an arithmetic mean of 26.8% and a standard deviation of 3.7% (Figure IV.B.19).

The differences between the original and repacked porosities range from 0.09% to 2.03% with an arithmetic mean of 1.06%. For 20 of the 29 cores considered, the repacked porosity is greater than the original porosity; 9 of the repacked cores have lower porosities than the original cores.

Grain size data for well 11-1 are still being analyzed.

#### Chemistry Analyses

The pH of GEMS water measured in the field is approximately 7. Monitoring of the pH of water collected for use in the permeameter did not reveal any trend with time while equilibrating to laboratory conditions over a 19 day period. After the water was introduced into the permeameter, the pH rose fairly rapidly to approximately 8 and fluctuated between 8 and 9 while circulating through the permeameter with no apparent trend with time (Figure IV.B.20). There was no significant change in pH after the water had passed through the cores. The measured differences are within the limit of accuracy of the pH meter. The rise in pH when the water started circulating through the permeameter was most likely due to the loss of CO<sub>2</sub>. Bubbling CO<sub>2</sub> through the upper reservoir has been successful in maintaining a pH close to 7.

Dissolved oxygen (DO) measurements indicate that the oxygen content of the water increases after the water is placed in the permeameter. Before the water is placed in the permeameter, it has a DO content of 1 to 2 ppm. After the water has been placed in the permeameter, the DO content increases to 5 to 8 ppm. There is no significant change in DO content after the water has passed through a sediment core.

Major cation analyses of the water in the permeameter and outflow-tube for the three cores employed in these experiments indicate that the calcium content of the water generally decreases with time (Figure IV.B.21), further demonstrating that precipitation of calcite is occurring within the permeameter apparatus.

The first core placed in the apparatus (GEMS 9-1 sample #1, segment #1) shows a consistently lower calcium content in the outflow-tube water as compared to that in the permeameter (the accuracy of the chemical analysis is better than 1 ppm for calcium). This indicates that calcite is being precipitated in the core and perhaps contributing to a decrease in hydraulic conductivity. The pH rose at the beginning of the period that this core was in the permeameter and the calcium content of the permeameter water remained fairly high.

GEMS 11-1, sample #5, segment #3 was the next core placed in the permeameter. During the period of time that water was flowing through this core the calcium content of the water decreased. No conclusions concerning the relative calcium content of the



outflow tube and permeameter water can be made. Only three analyses of the permeameter water were done, with one having a higher calcium content than the outflow-tube water, one having a lower calcium content, and a third sample (marked by an asterisk) that is probably not representative of the system because circulation had been very slow for some time.

The third core placed in the permeameter for this experiment was GEMS 11-1, sample #3, segment #3. The outflow-tube water from this core had a calcium content consistently higher than that of the permeameter water, suggesting that calcite was being dissolved out of the core. However, the hydraulic conductivity of this core decreased with time, which indicates that deposition of calcite is not the controlling mechanism in reducing hydraulic conductivity during this time period.

X-ray analyses of the clays have determined that the clays are composed primarily of smectite, with some kaolinite and some illite (which is fairly crystalline, bordering on mica). There is no change in the composition of the clays while they are in the permeameter, but there was some deposition of calcite on the clays.

It was noted during preparation of the clays for x-ray analysis, that the clays are easily flocculated and dispersed, and that thymol, which had been used in the system as a biocide, caused the clays to flocculate. This tendency to readily flocculate and disperse could result in the clogging of pore throats and decreases in hydraulic conductivity. Fogler and Vaidya (1993) suggested that if the hydraulic conductivity of a core was reduced due to fines blocking the pore throats, reversing the flow direction through the core should flush out the clogged pore throats and produce an increase in hydraulic conductivity. GEMS 7-1, sample #4, segment #3, which experienced a decrease in hydraulic conductivity, was turned upside down in the permeameter, but no increase in conductivity was observed.

Using a different biocide, dichlorophene, appears to have reduced, but not eliminated, the decreases in hydraulic conductivity with time. Whether this is due to more effective biocidal action in the core (though it appears to be less effective in the permeameter tubing), or due to the fact that the dichlorophene is not reacting with the clays is unclear at this time.

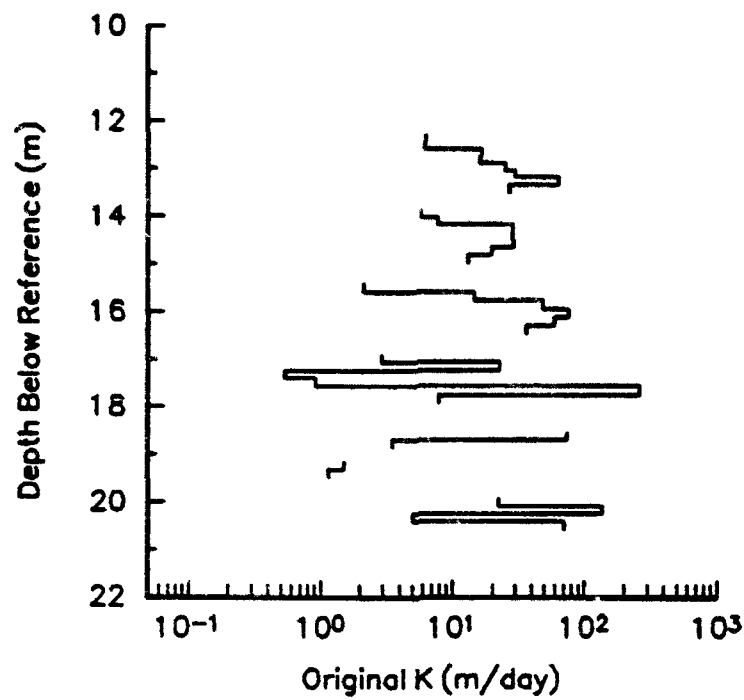


Figure IV.B.1 - Original hydraulic conductivity vs. depth for GEMS well 7-1.

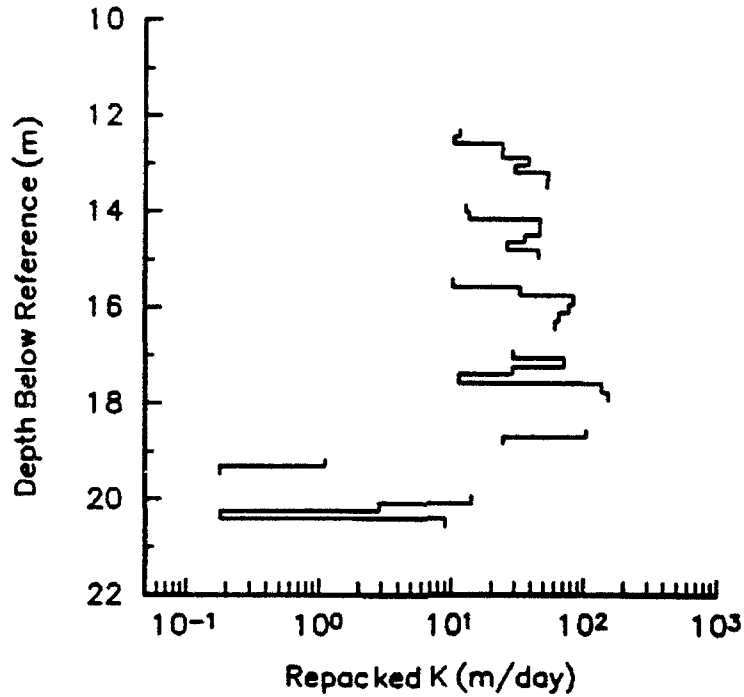


Figure IV.B.2 - Repacked hydraulic conductivity vs. depth for GEMS well 7-1.

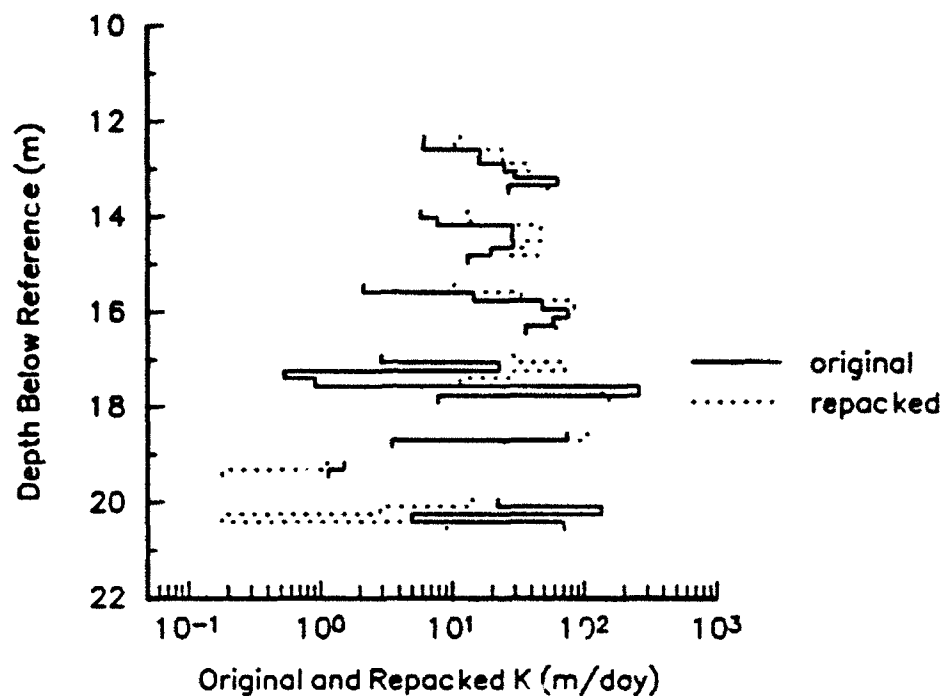


Figure IV.B.3 - Original and repacked conductivity vs. depth for GEMS well 7-1.

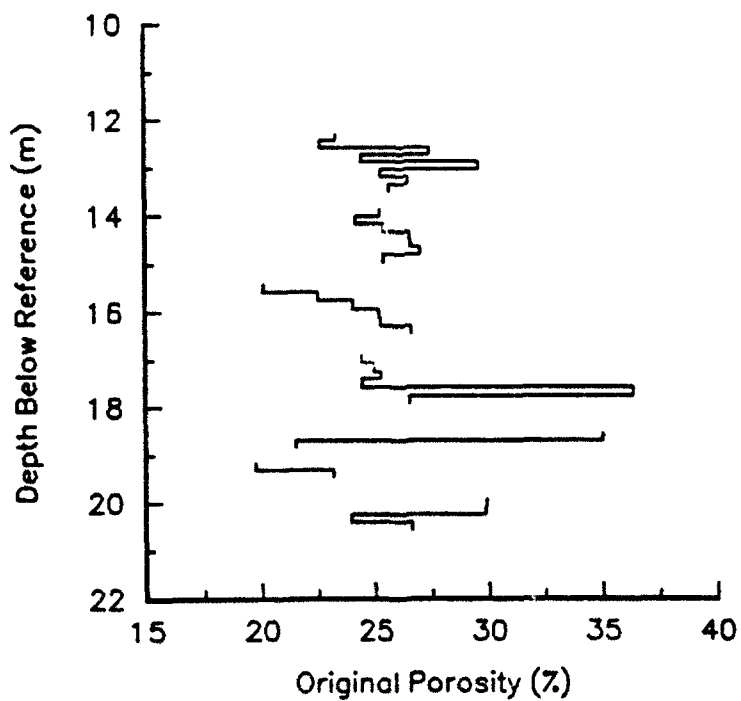


Figure IV.B.4 - Original porosity vs. depth for GEMS well 7-1.

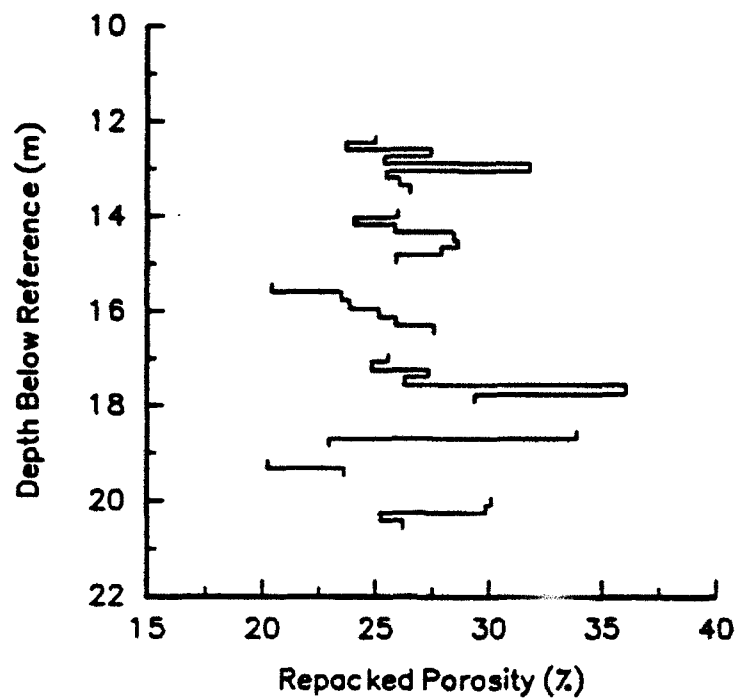


Figure IV.B.5 - Repacked porosity vs. depth for GEMS well 7-1.

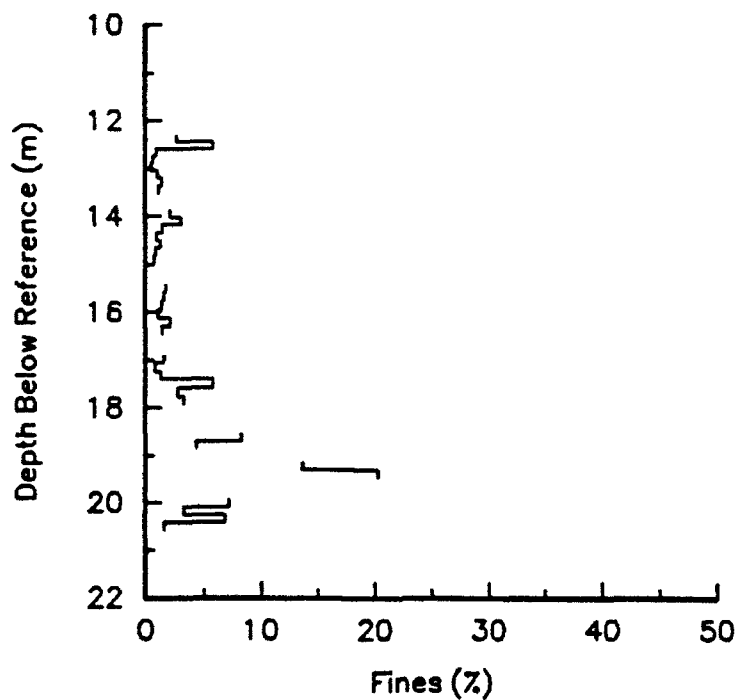


Figure IV.B.6 - Percent fines (<.053 mm) vs. depth for GEMS well 7-1.

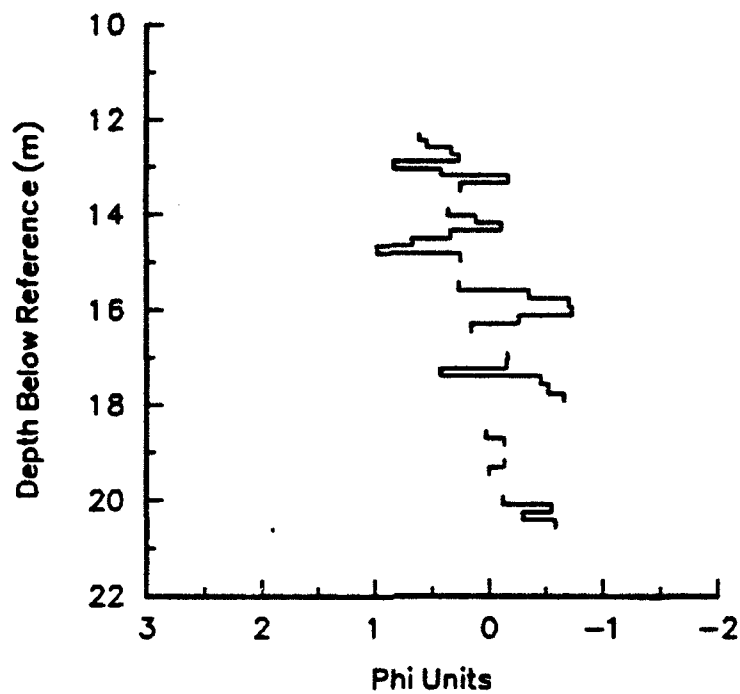


Figure IV.B.7 - Mean grain size (in phi units) vs. depth for GEMS well 7-1.

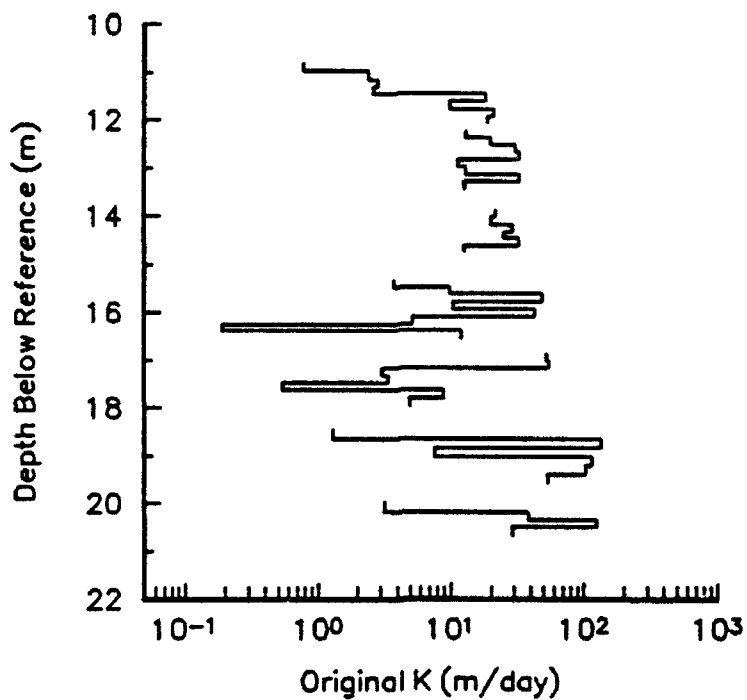


Figure IV.B.8 - Original hydraulic conductivity vs. depth for GEMS well 9-1.

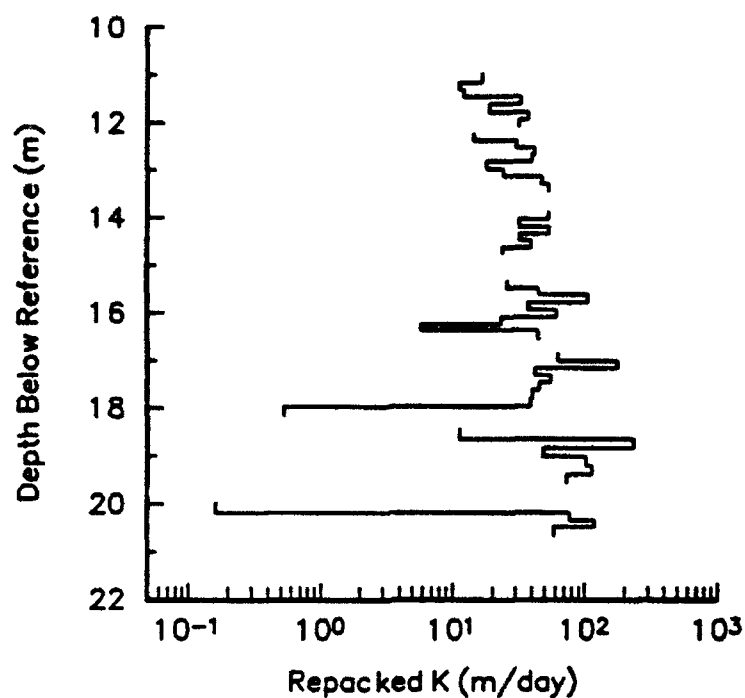


Figure IV.B.9 - Repacked hydraulic conductivity vs. depth for GEMS well 9-1.

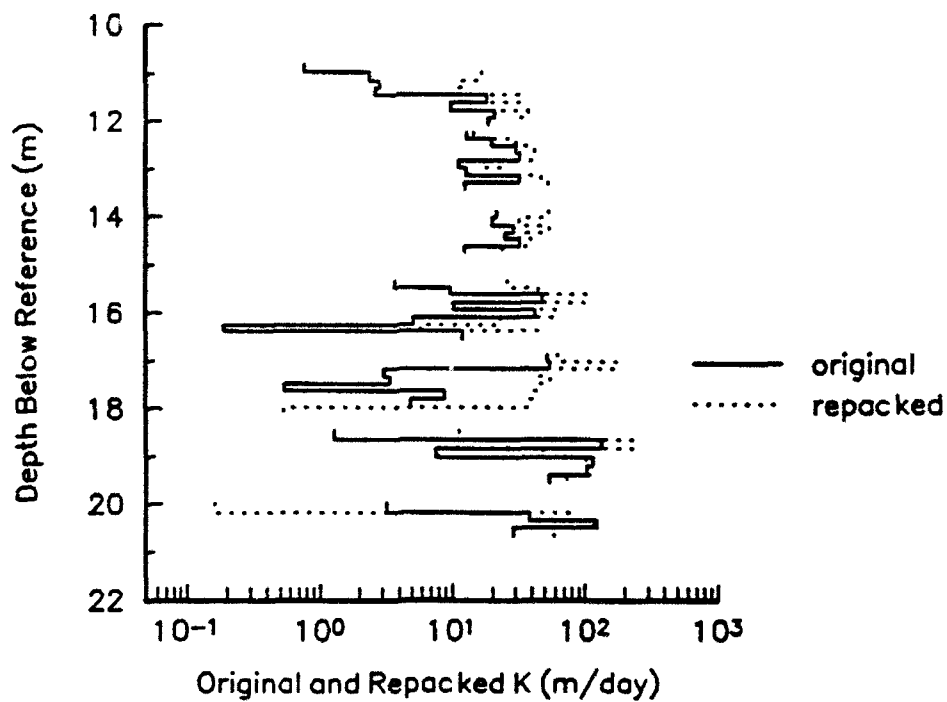


Figure IV.B.10 - Original and repacked conductivity vs. depth for GEMS well 9-1.

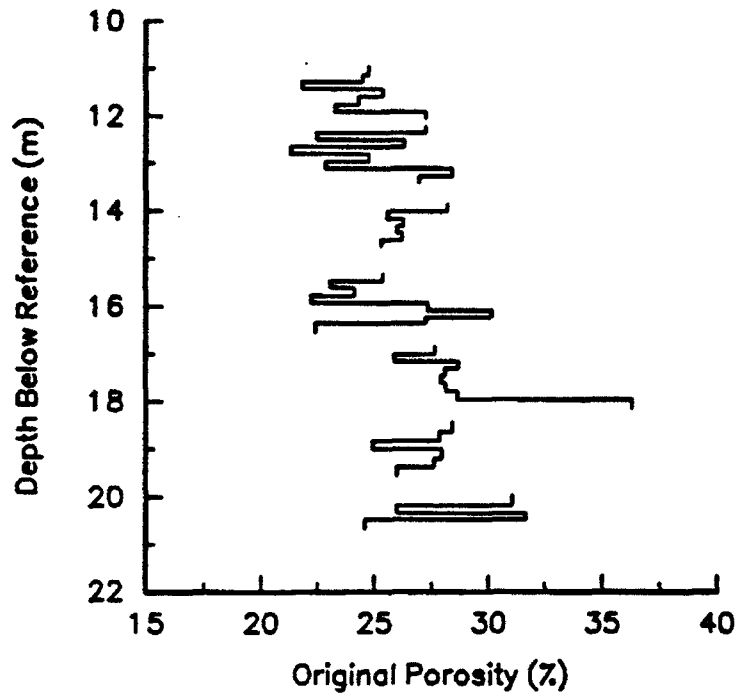


Figure IV.B.11 - Original porosity vs. depth for GEMS well 9-1.

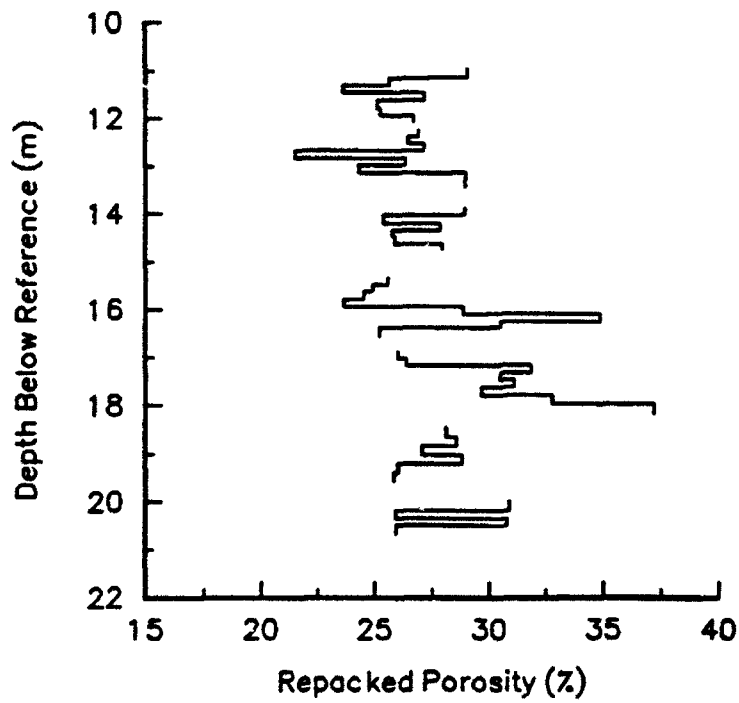


Figure IV.B.12 - Repacked porosity vs. depth for GEMS well 9-1.

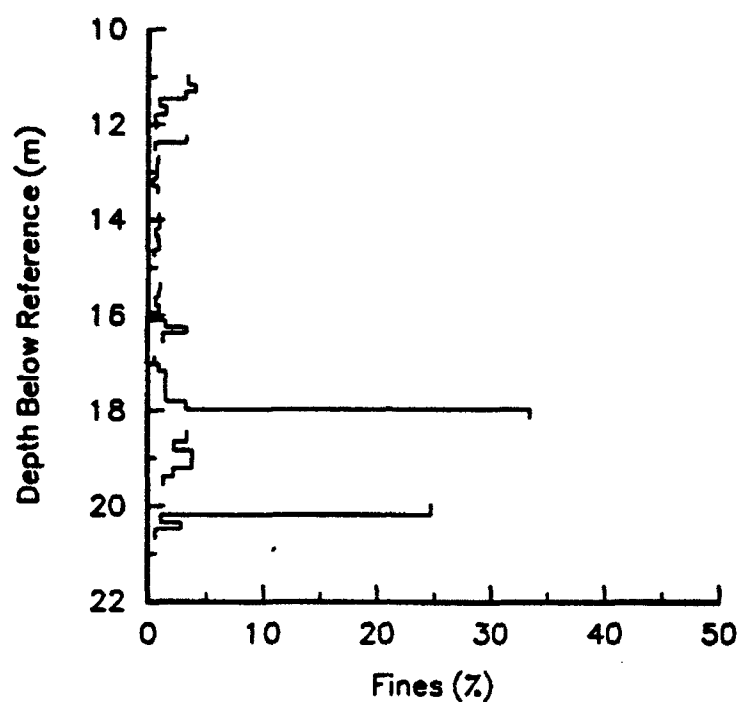


Figure IV.B.13 - Percent fines (<.053 mm) vs. depth for GEMS well 9-1.

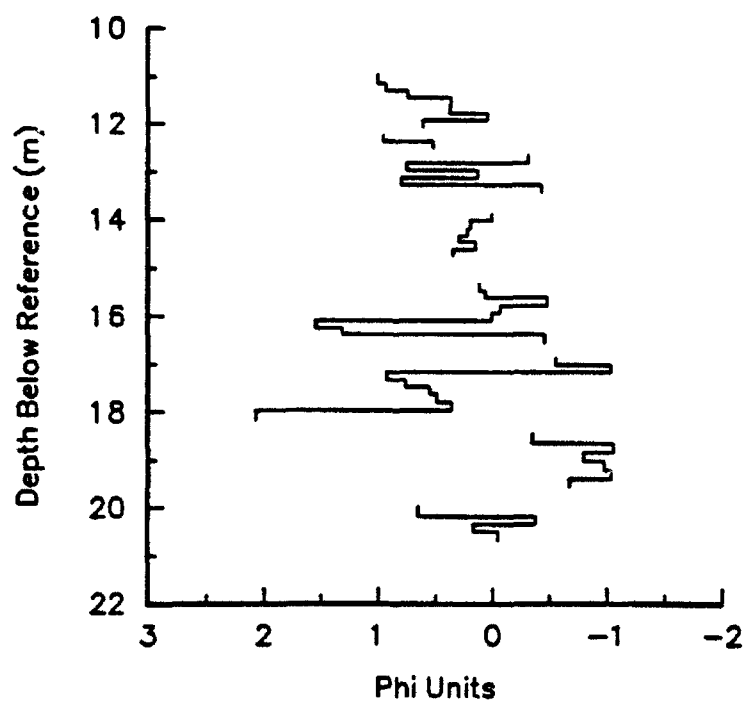


Figure IV.B.14 - Mean grain size (in phi units) vs. depth for GEMS well 9-1.



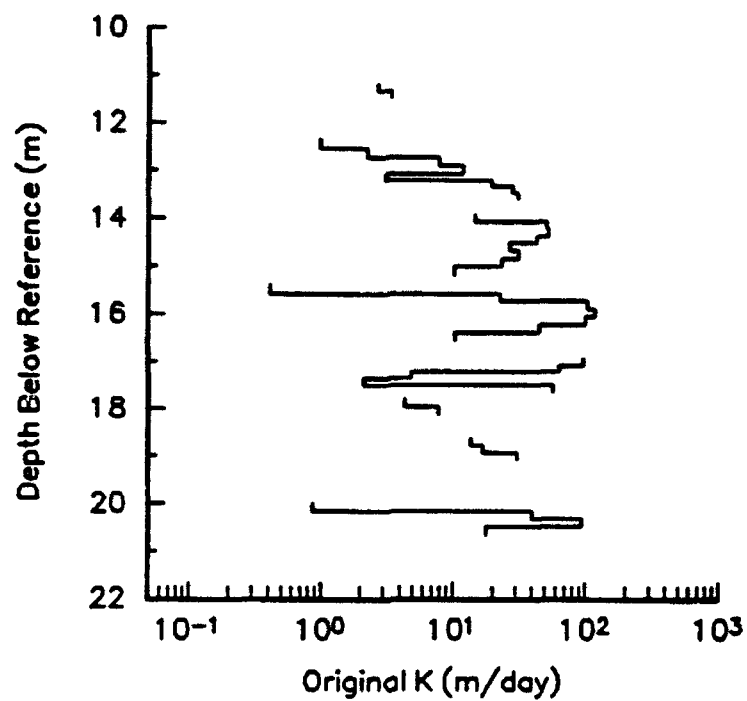


Figure IV.B.15 - Original hydraulic conductivity vs. depth for GEMS well 11-1.

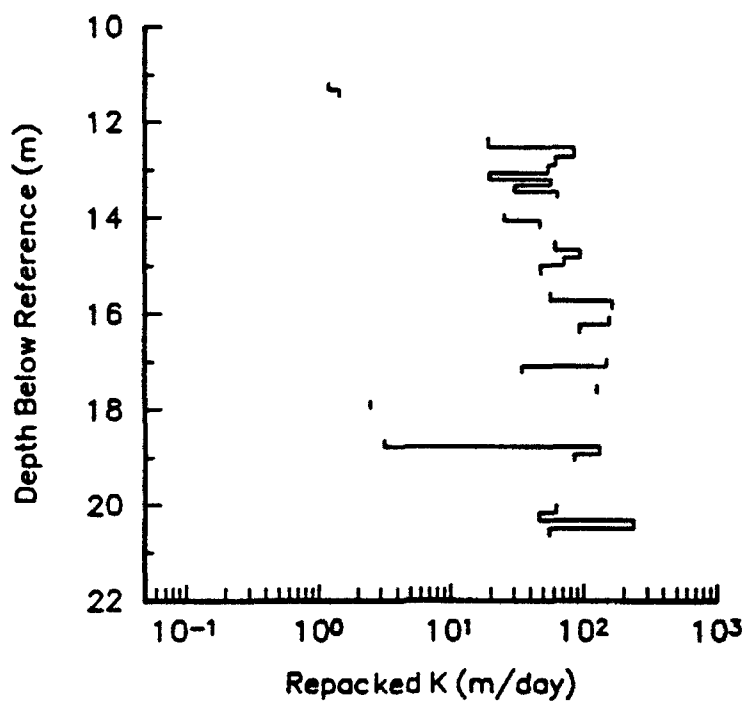


Figure IV.B.16 - Repacked hydraulic conductivity vs. depth for GEMS well 11-1.

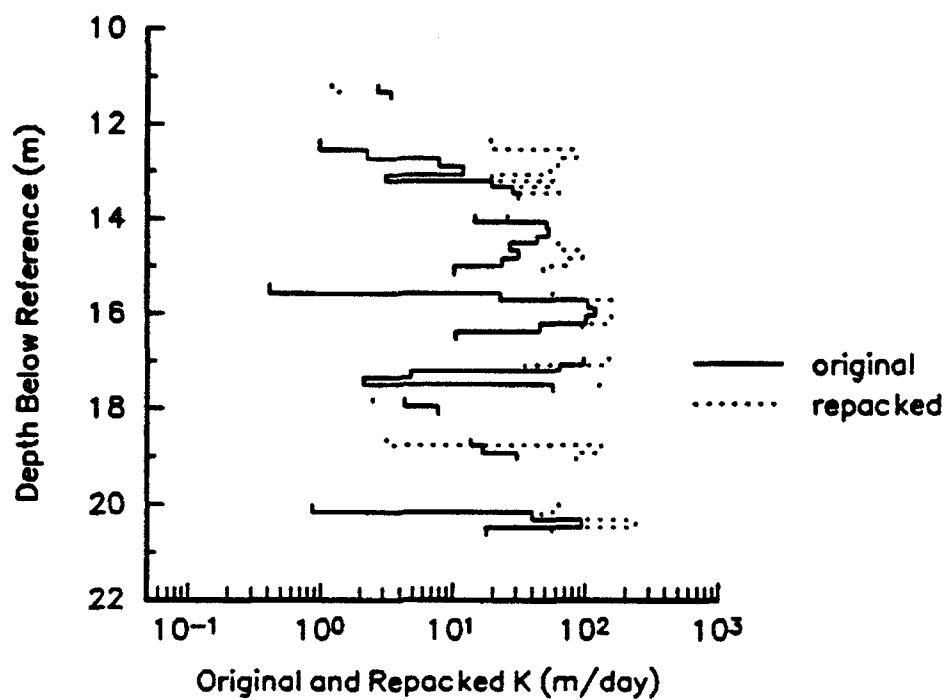


Figure IV.B.17 - Original and repacked conductivity vs. depth for GEMS well 11-1.

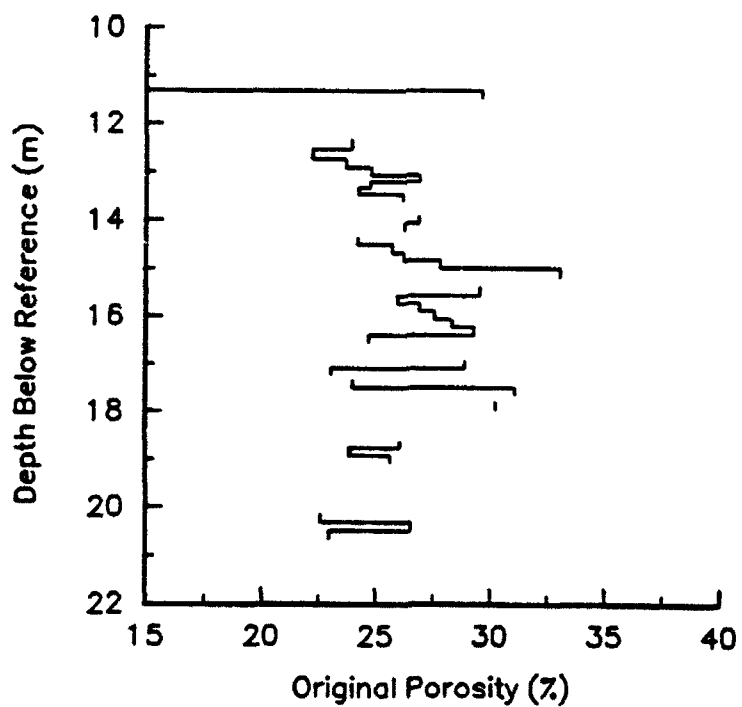


Figure IV.B.18 - Original porosity vs. depth for GEMS well 11-1.

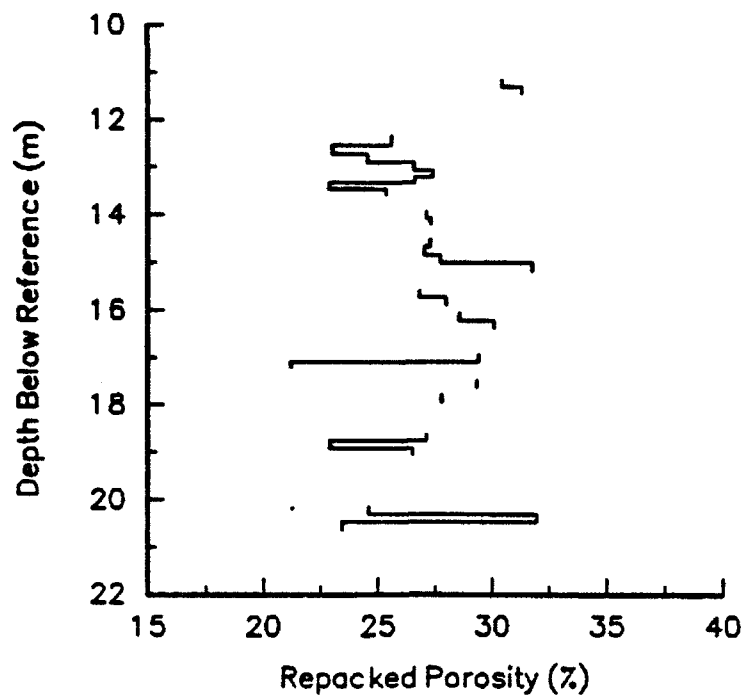


Figure IV.B.19 - Repacked porosity vs. depth for GEMS well 11-1.

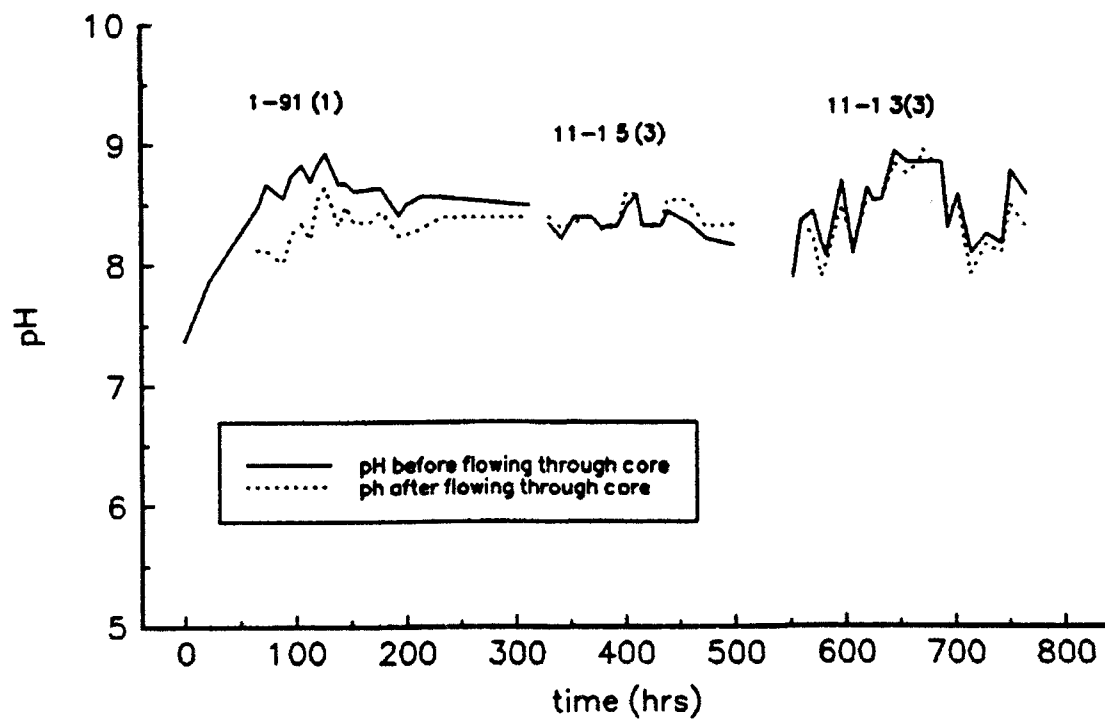


Figure IV.B.20 - pH of water vs. time.

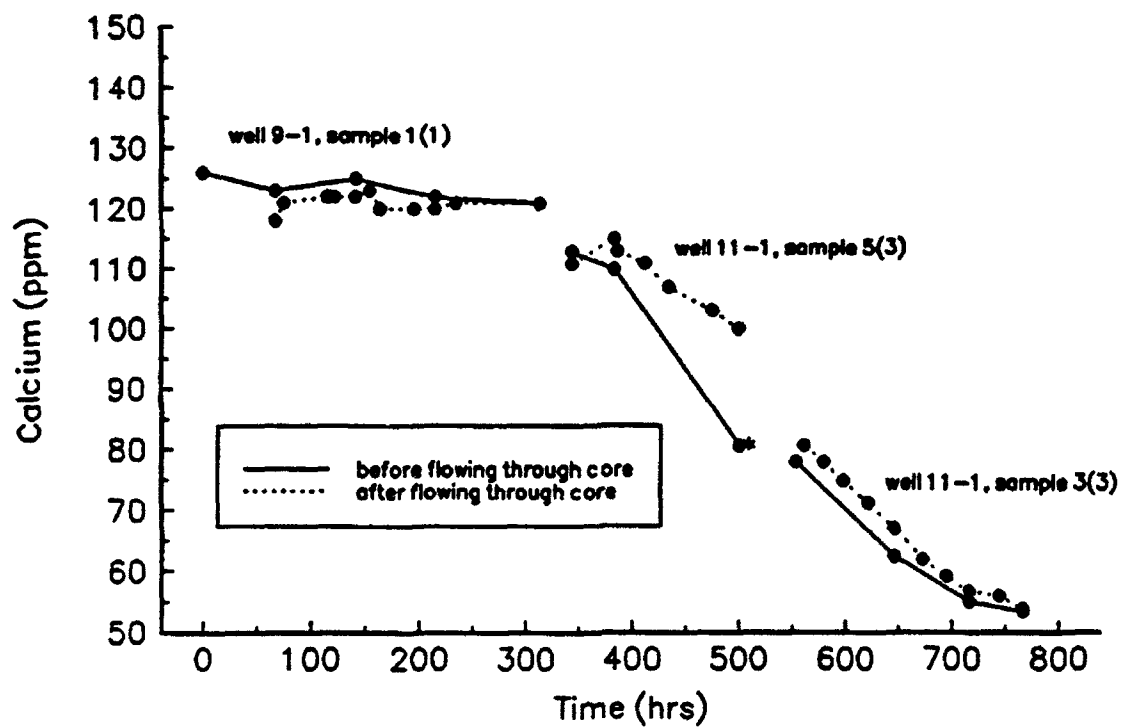


Figure IV.B.21 - Calcium content of water vs. time.

## **C. AQUEOUS GEOCHEMISTRY AT GEMS**

### **INTRODUCTION**

Characterization of the aqueous geochemistry at GEMS has included determination of the major ion chemistry of the ground water and estimation of the effect of leakage between the bedrock and overlying alluvial aquifer. From 1992 to 1994, as many as five samples from many of the wells at GEMS have been collected and analyzed in order to assess the magnitude of spatial and temporal variability of the aqueous geochemistry. This section of the report discusses the variability of ground-water chemistry at GEMS and the implications that chemical variability has to tracer test methodology.

### **SAMPLE SUITE**

Water samples have been collected primarily from the #0 nest and the #2 nest, with fewer samples collected from the #00 and #1 nests. Sampling dates were September, 1992; May, 1993; August, 1993; November, 1993; and March, 1994. Sampling times include all four seasons (Macpherson and Schulmeister, 1994).

### **RESULTS**

A summary of the mean, one standard deviation, and coefficient of variation is found in Table 1. Only two parameters are shown, nitrate-nitrogen ( $\text{NO}_3\text{-N}$ ) and sulfate ( $\text{SO}_4$ ) because these are sufficient to demonstrate the variability at the site.

The nitrate content of the ground water at GEMS is quite variable, with means from individual wells ranging from less than 0.01 mg/L to nearly 8 mg/L. The coefficient of variations for the means from each of the wells is quite high, and ranges from 12 to 200%.

The sulfate content of the ground water at GEMS is much less variable, with means from individual wells ranging from about 30 to 68 mg/L. The highest mean is the result of one sample which was twice as high as all others from that well, and may be incorrect. Excluding this well, means range from about 30 to 47 mg/L. Coefficients of variation are lower than for nitrate, but are still typically greater than 5%, and thus are significant relative to the precision of the method (2%).

### **DISCUSSION**

The large variability in chemistry of ground water at GEMS has serious implications to the successful interpretation of tracer tests in the alluvial aquifer. The

variability in the chemistry translates to variability in density of the fluids, which in turn influences movement of a tracer fluid. In order to complete the tracer test in the most rigorous manner, it will be important that an assessment of ground-water chemistry be done soon before the test is initiated. This will allow assessment of the variability of water density around the expected flow path of the tracer and more accurate calculations of aquifer properties can be done.

## CONCLUSIONS

The temporal and spatial variability of water chemistry in the alluvial aquifer at GEMS requires that an assessment of the chemistry be done just before any tracer test is initiated. The multi-level samplers, during development in preparation for the test, can be used to collect samples for this purpose.

Table 1: Statistics on Times-Series Sampling  
of Selected GEMS Wells  
(1992 - 1994)

	Well depth, m	NO3-N, mg/L Mean	n	Std Dev	Coef Var
Nest #0					
Well 0-4	7.6	7.63	5	0.9195	12.1
Well 0-3	11.0	1.65	5	0.7641	104
Well 0-2	14.0	0.324	5	0.2438	75.2
Well 0-8	15.3	1.02	2	0.3536	34.7
Well 0-7	16.5	3.07	4	3.53	115
Well 0-5	19.8	2.07	5	1.236	59.7
Well 0-1	21.6	6.26	4	2.087	33.3
Well 0-6 (Bedrock)	24.4	0.105	4	0.1666	159
Nest #2					
Well 2-4	6.0	0.173	3	0.1185	68.3
Well 2-3	8.2	1.25	4	0.8386	67.1
Well 2-1	11.6	0.0075	4	0.015	200
Well 2-2	14.6	0.0075	4	0.015	200
Well 2-7	17.1	0.2325	4	0.1159	49.8
	Well depth, m	SO4, mg/L Mean	n	Std Dev	Coef Var
Nest #0					
Well 0-4	7.6	31.7	5	1.7936	5.65
Well 0-3	11.0	44.8	5	11.2108	25.05
Well 0-2	14.0	45.0	5	4.4869	9.98
Well 0-8	15.3	34.4	2	0.3536	1.03
Well 0-7	16.5	47.1	4	15.8144	33.61
Well 0-5	19.8	33.9	5	3.7501	11.05
Well 0-1	21.6	29.8	4	2.4636	8.27
Well 0-6 (Bedrock)	24.4	47.8	4	20.2684	42.38
Nest #2					
Well 2-4	6.0	45.1	3	3.4385	7.63
Well 2-3	8.2	45.7	4	3.0768	6.73
Well 2-1	11.6	67.5	4	45.8974	67.97
Well 2-2	14.6	38.9	4	0.1732	0.45
Well 2-7	17.1	34.7	4	5.1075	14.72

## **D. WIRELINE LOGGING ACTIVITIES - AN EVALUATION OF A BOREHOLE INDUCTION SINGLE-WELL TRACER TEST TO CHARACTERIZE THE DISTRIBUTION OF HYDRAULIC PROPERTIES IN AN ALLUVIAL AQUIFER**

### **ABSTRACT**

In order to assess the potential of a borehole induction single-well tracer test to characterize the vertical distribution of hydraulic properties, a series of tracer tests was performed at a field site in the Kansas River alluvium. The procedure involves the injection of a nonreactive, electrically conductive tracer into a well under artificially induced, steady-state flow conditions. Vertical variations in the rate of the horizontal invasion of the injected tracer solution are computed from repeated logs using a focussed induction borehole probe. These data are employed to construct vertical profiles of effective porosity and hydraulic conductivity at the injection well. Although modification of the procedure was necessary in order to ensure that model assumptions are valid, to reduce monitoring error, and to remove the effects of a near-well drilling-induced disturbed zone, the tracer test appears to have considerable potential for accurate characterization of alluvial aquifers.

### **Introduction**

#### **Background**

In order to predict the movement of water and pollutants accurately in the subsurface, it is necessary to understand the factors controlling their transport. Spatial variability in aquifer hydraulic parameters may produce differential flow (contrasting flow rates), greatly influencing groundwater flow and transport (Freeze and Cherry, 1979). Therefore, accurate characterization of parameter spatial variability is critical if reliable predictions of contaminant transport are to be made.

Taylor *et al.* (1990) recently evaluated commonly employed methods for estimating spatially varying hydraulic properties in unconsolidated geologic formations. They conclude that due to near-hole drilling disturbances, inadequate sediment sampling techniques, and sampling bias, current methods have significant limitations. Clearly, refinement of current methods or the development of new methods is needed if hydrogeologists are to keep pace with increasing demands for reliable predictions of contaminant transport.



The borehole induction single-well tracer test is a new method of aquifer characterization apparently first reported in the groundwater literature by Taylor and Molz (1990). The method provides estimates of vertical variations in horizontal hydraulic properties at a scale that has been difficult to obtain in the past. Detailed information of this kind can greatly improve the understanding of the primary controls on subsurface flow and transport at a site.

To date, there have been no published evaluations of the borehole induction single-well tracer test method. Although the study of Taylor and Molz (1990) produced reasonable results, a more thorough evaluation of the method is needed. The following subsection summarizes the tracer test method, its application at a research site of the Kansas Geological Survey, and important refinements that are required in the originally proposed approach.

#### Field Site

Five tracer tests were conducted at the Geohydrologic Experimental and Monitoring Site (GEMS). The bedrock beneath GEMS is a silty sandstone of the Pennsylvanian Douglas Group (Davis and Carlson, 1952). The bedrock at the site is covered by approximately 22 m of unconsolidated Kansas River alluvium of the early Wisconsin Newman terrace (Davis and Carlson, 1952). The alluvium is composed of approximately 11 m of sand and gravel overlain by 11 m of silt and clay. The sand and gravel unit, the focus of this study, is composed primarily of quartz, feldspar, and chert grains and contains an average of 2 to 3 weight percent silt and clay (McElwee *et al.*, 1993). Cores from this unit display cross-bedding, variable grain size and clay content, and clay drapes, measuring approximately 1 to 3 cm in thickness. The average phi size and hydraulic conductivity determined from repacked core material are -0.02 and 58.26 m/day, respectively (McElwee *et al.*, 1993).

The underlying Pennsylvanian bedrock and the overlying silt and clay unit hydraulically restrict groundwater flow in the sand and gravel, forming a leaky confined aquifer. Water levels in the sand and gravel and the silt and clay intervals are approximately 7 m and 5 m from the land surface, respectively. The lateral hydraulic gradient in the confined aquifer ranges from approximately  $2E-3$  to  $4E-3$  throughout the year and is directed approximately  $S20^{\circ}E$ . The four injection wells used for the five tests are constructed of 0.051 m diameter PVC pipe and are fully screened across the sand and gravel interval.

## Tracer Test Methodology

### Summary of Method

The Taylor and Molz (1990) tracer test method involves the injection of a nonreactive, electrically conductive tracer solution into a well under artificially induced, steady-state flow conditions (Figure 1). As the tracer solution enters the aquifer through the well screen, it moves radially outward, displacing the native pore fluid. Since the electrical conductivity of a formation is significantly controlled by porosity and pore fluid chemistry (Dobrin and Savit, 1988), a considerable increase in the formation conductivity occurs as the tracer advances radially outward from the well. The invasion of the tracer is monitored by repeated logs using a focussed induction borehole probe. The rate of invasion as a function of depth is determined from the induction logs. Detailed vertical profiles of the effective porosity and hydraulic conductivity are constructed using the tracer invasion rates, the induced hydraulic gradient, and the observed change in formation electrical conductivity as the tracer solution invades the aquifer.

### Tracer Injection

Induced steady-state flow conditions were produced in the injection well prior to the introduction of the tracer solution. This was accomplished by pumping native GEMS groundwater using a 0.089 m diameter submersible pump (*Simer*, model 9BC) from a 0.102 m diameter PVC well (0-8, see section IV.A for a well map) screened in the sand and gravel aquifer, and directly discharging it into the injection well. The pumping well was located far enough from the injection well (> 20 m) that drawdown at the injection well due to pumping was negligible. A constant injection rate of 14 - 45 gal./min. (depending on the test) was used for input to the injection well. When the water level in the injection well stabilized, flow within the volume of the aquifer adjacent to the well was assumed to be at steady state.

Once steady-state flow conditions were achieved, a concentrated saline solution was pumped from a storage tank directly into the line between the pumping and injection wells. The tracer solution (water from pumping well and concentrated saline solution) discharged into the injection well at the land surface, cascaded down the well, and entered the aquifer through the well screen. The tracer replaced the native pore fluid as it was transported radially outward under the induced hydraulic gradient. As the tracer advanced, the conductivity of the formation increased. This change was monitored throughout the test with repeated surveys using a borehole induction tool.

Tracer injection continued until the tracer traveled a radial distance of roughly 2.5 m from the well (the approximate radial detection limit of the induction tool). During

this time, 21,600 - 38,000 L (5700 - 10,000 gal.) of tracer solution were injected into the aquifer. The exact volume depended on the porosity of the media and the length of the screened interval. Injection periods lasted about 4 to 8 hours.

#### Tracer Solution

A dilute NaCl solution was used for the tracer due to the high solubility, relative inertness, low cost, and low toxicity of NaCl. The specific conductivity of the tracer solution (115 - 200 mS/m) was roughly 2 to 3 times the specific conductivity of the native groundwater (64.5 mS/m). During each test, approximately 7 - 37 kg of NaCl was pumped into the aquifer.

The saline solution was prepared and stored in a 1988 L (525 gal.) polyolefin storage tank. GEMS native groundwater, used as the solvent, was pumped from the pumping well prior to injection. To ensure complete dissolution of the solute and thorough mixing throughout the test, a small submersible pump (*Little Giant*, model 2E) was used to continuously circulate the solution. A second submersible pump (*Grundfos*, model MP1) was used to pump the concentrated saline solution from the tank, into the main injection line.

#### Induction logging

The electrical conductivity of the formation adjacent to the injection well was logged before, during, and after tracer injection with a focussed induction borehole probe manufactured by *Century Geophysical Corporation* (model 9510). The borehole probe contains a pair of transmitter coils carrying an alternating electric current. This current produces an alternating magnetic field in the formation surrounding the tool. The magnetic field induces current loops in the formation outside the well. This current creates a magnetic field that induces an electric current in a pair of receiver coils inside the induction probe. The magnitude of the current in the receiver coils is a function of the initial current in the transmitter coils and the ability of the formation to conduct the current loops. As the electrically conductive tracer solution invades the formation, the ability of the formation to conduct an electric current increases. The borehole induction tool measures this change and enables the position of the tracer front with respect to the injection well to be estimated. During the tracer tests, the conductivity of the formation was measured at 0.030 m intervals as the induction tool was slowly raised in the injection well. The conductivity readings (units of mS/m) were transmitted in digital form to the land surface and stored in a computer.

The injection well was logged with the induction probe four times prior to the initiation of tracer injection. Pretest experiments show that statistical variability in log values is reduced by computing average logs from repeated measurements. Four was chosen for the number of repeat logs as a compromise between logging time and variability reduction in log values. Following the initiation of tracer injection, the injection well was initially logged every 20-35 minutes to monitor the radial invasion of the tracer solution into the aquifer. Logging continued at increasing time intervals until the tracer solution approached the radial detection limit of the induction probe. This state was assumed to have been reached when conductivity logs showed little change with continued injection. At that time, the injection well was logged four more times and tracer injection was terminated.

### Test Monitoring

During practice injection tests and the first tracer test, pressure transducers (*Instrumentation Northwest*) were placed in the pumping, injection, and observation wells to monitor water levels. These data were recorded by a data logger (analog - digital converter: *Iotech*, model ADC488/16; P.C.: *Zenith*, model ZW-241-82; software: *Scentech*, Turbolab 1.0) and used to determine the induced hydraulic gradient in the vicinity of the injection well. For the remaining tests, the water level in the injection well was monitored with an electric water level tape (*Solinst*) and sometimes with pressure transducers.

A flow meter (*Omega*, model FP-5800) attached to a 0.025 m inner diameter PVC flow-through pipe fitting monitored the tracer solution injection rate. The meter was inserted into the main injection line downstream of the point of introduction of the concentrated saline solution. The meter was monitored with a data logger or by visual inspection.

A fluid conductivity cell (*Hach*, model 44600) monitored the electrical conductivity of the tracer solution in the injection line. This meter also served as a check to ensure that the pumping well and tracer tank pumps were operating properly. A second conductivity cell (*Solomat*, Chemistry Module 4007) identified the appearance of the tracer solution at the bottom of the screened interval of the injection well in three of the initial four tests. During two tests, the tracer solution reached the bottom of the well within three minutes of the start of tracer injection. In the third test, the tracer solution reached the bottom of the well within 10 minutes.

## Remediation

Following the completion of each test, the injection well was pumped to remove the tracer from the aquifer. The injection well was pumped using an air-lift system (air compressor: *Curtis*, model ES-20) at a rate approximately equal to or greater than the tracer injection rate. Pumping from the injection well continued until 1.5 - 3.1 pore volumes (one pore volume is defined here as a volume equivalent to the volume of tracer solution injected) were removed. During this time, the specific conductivity of the discharge returned to the pretest level. The water pumped out during remediation was transported off site (> 50 m) using irrigation pipe and discharged onto the land surface. Most of the discharge contained  $\text{Cl}^-$  levels below EPA specified drinking water standards and offered no threat to the natural environment. The tracer was removed primarily because of potential interference with future tests at the site.

During tracer removal the specific conductivity of the discharge was periodically measured at the surface. An approximate mass balance (comparison of tracer injected to tracer removed) showed that between 20 and 60 percent of the tracer was removed. Repeated formation conductivity logs suggested that some of the tracer was still present near the injection well following remedial pumping. Further pumping, however, removed no additional detectable tracer. It is suspected that during tracer injection a significant volume of tracer solution moved preferentially in some intervals, traveling beyond the influence of remedial pumping.

## **Theory of Tracer Test Data Analysis**

### Porosity Estimation

It has been shown experimentally that a relationship exists between formation electrical conductivity, native pore water electrical conductivity, and porosity (Archie, 1942). This relation, Archie's Law, is described in most geophysical logging texts (e.g., Bateman, 1985; Dewan, 1983; Ellis, 1987; Schlumberger, 1989). The Taylor and Molz (1990) tracer test method employs this relation to construct a model of formation conductivity that is used to estimate the effective porosity of the formation from the induction logs.

This model defines the electrical conductivity of the formation ( $\sigma_{fm}$ ) as a sum of a contribution from the matrix ( $\sigma_m$ ) and that from the pore fluid ( $\sigma_{pf}$ ):

$$\sigma_{fm} = \sigma_m + \sigma_{pf} \quad (\text{IV.D.1})$$

The contribution from the pore fluid can be represented by Archie's Law:

$$\sigma_p = (\sigma_f \theta^m) / \alpha \quad (\text{IV.D.2})$$

where  $\sigma_f$  = electrical conductivity of the pore fluid,  $\theta$  = porosity,  $m$  = cementation factor, and  $\alpha$  = tortuosity.

Substituting Archie's Law into Equation (IV.D.1) yields:

$$\sigma_m = \sigma_m + (\sigma_f \theta^m) / \alpha \quad (\text{IV.D.3})$$

From the induction logs taken before tracer injection and those taken after the tracer moves beyond the radial detection of the tool (henceforth termed tracer saturation), the formation conductivity when the aquifer is saturated with pore fluid of two different electrical conductivities is known. Equation (IV.D.3) can therefore be written as 2 equations:

$$\sigma_{fm1} = \sigma_m + \frac{(\sigma_{f1} \theta^m)}{\alpha} \quad (\text{IV.D.4})$$

$$\sigma_{fm2} = \sigma_m + \frac{(\sigma_{f2} \theta^m)}{\alpha} \quad (\text{IV.D.5})$$

where  $\sigma_{fm1}$  and  $\sigma_{fm2}$  are the formation conductivity before and after tracer saturation, respectively, and  $\sigma_{f1}$  and  $\sigma_{f2}$  are the conductivity of the native pore water and the tracer solution, respectively. Subtracting Equation (IV.D.4) from (IV.D.5) and solving for porosity yields:

$$\theta = \left[ \frac{(\sigma_{fm2} - \sigma_{fm1})}{(\sigma_{f2} - \sigma_{f1})} \alpha \right]^{1/m} \quad (\text{IV.D.6})$$

The cementation factor ( $m$ ) and tortuosity ( $\alpha$ ) are empirical factors dependant on lithology and pore structure. It has been shown that for unconsolidated sands these variables are approximately 1.4 and 1.0, respectively (Jackson et al., 1978).

### Radius of Tracer Invasion

The radius of tracer invasion is determined for each induction log using the radial dependence relationship for the induction probe response. The formation conductivity at a single interval is a weighted average of the conductivity adjacent to that interval. The relationship between the magnitude of contribution and the radial distance from the probe is called the response function. Figure 2 displays the normalized theoretical radial response function for the probe used for this work (*Century Geophysical Corporation*, unpublished). This curve displays how the probe weights the conductivity of specific portions of the formation around the probe to determine an average formation conductivity for each interval. The shape of this curve is a function of receiver and transmitter coil geometry and can be theoretically determined (Saito, 1982).

Figure 3 is a plot of the cumulative sum of the theoretical radial responses. This function,  $Z(R)$ , can be used to relate changes in formation conductivity during tracer injection to the depth of tracer invasion. This function is related to the formation conductivity measured during the injection tests in the following way:

$$Z(R) = \frac{(\sigma_a - \sigma_{fm1})}{(\sigma_{fm2} - \sigma_{fm1})} \quad (IV.D.7)$$

where  $\sigma_a$  is a formation electrical conductivity measured at a specific time during tracer injection. Given  $\sigma_a$ ,  $\sigma_{fm1}$ , and  $\sigma_{fm2}$ , a value for  $Z(R)$  is calculated, and Figure 3 is used to determine the position of the tracer solution front at the time of a particular induction log.

### Hydraulic Conductivity Estimation

Knowing the radial position of the tracer solution front as a function of time and the effective porosity, Taylor and Molz (1990) estimate hydraulic conductivity by equating a simple geometric representation of radial plug flow and Darcy's Law. The volume of pore fluid within a vertical segment of an aquifer can be represented by a cylinder with the well at the center:

$$V = \pi R^2 b \theta \quad (IV.D.8)$$

where  $V$  = volume,  $R$  = radius of cylinder,  $b$  = height of cylinder, and  $\theta$  = porosity. The discharge into this volume can be written as:

$$Q = \pi R^2 b \theta / t \quad (\text{IV.D.9})$$

where  $Q$  = discharge, and  $t$  = time since initiation of tracer injection.

Discharge into this segment can also be written using Darcy's Law:

$$Q = -2\pi r b K (dh / dr) \quad (\text{IV.D.10})$$

where  $r$  = arbitrary radius for head evaluation (not related to  $R$ ),  $K$  = hydraulic conductivity, and  $h$  = hydraulic head.

Equation (IV.D.10) is a separable differential equation which can be integrated with respect to  $r$  and  $h$ :

$$\int_{h_e}^{h_w} dh = -\frac{Q}{2\pi b K} \int_{r_e}^{r_w} \frac{dr}{r} \quad (\text{IV.D.11})$$

where  $h_w$  is the induced hydraulic head (difference between static and steady-state water levels) at  $r_w$ , the radius of the injection well, and  $r_e$  is the minimum radius where the induced head is near zero ( $h_e$ ). The solution for this equation is:

$$h_w - h_e = -\frac{Q}{2\pi b K} [\ln r_w - \ln r_e] \quad (\text{IV.D.12})$$

Equation (IV.D.12) reduces to:

$$Q = \frac{2\pi b K H}{\ln\left(\frac{r_e}{r_w}\right)} \quad (\text{IV.D.13})$$

where  $H = h_w$ .

Equating Equations (IV.D.9) and (IV.D.13), and solving for  $K$  yields:



$$K = \frac{R^2 \theta}{2Ht} \ln \frac{r_e}{r_w} \quad (\text{IV.D.14})$$

Given  $R$  (radius of tracer invasion) and  $\theta$  determined for each induction tool sample interval (0.03 m) from time  $t$ , and  $r_e/r_w$  and  $H$ , Equation (IV.D.14) can be used to estimate  $K$  for each log interval.

## Application Problems

### Data Interpretation

The results from the first four tracer tests (in injection wells 1-7, 5-1, 9-1, and 11-1, see section IV.A for a well map) did not agree with results from previous studies at the site. Figure 4 contains formation electrical conductivity logs obtained before, during, and after tracer injection in well 5-1. The interval from 16 - 17 m shows little change in formation conductivity during tracer injection. This observation suggests the permeability in this interval is very small. Permeameter and grain-size analyses of cores from this well, however, do not display the pronounced low permeability interval.

Figure 5 contains porosity profiles determined from the tracer test and the analysis of core sediment from well 5-1 (Butler and McElwee, 1994). Note the relative magnitude of the estimates determined from the two methods. The average tracer test effective porosity and core total porosity are 0.121 and 0.264, respectively. Mackay *et al.* (1986) report tracer test and core porosity estimates from an unconsolidated alluvial aquifer near Borden, Ontario. The estimates of effective and total porosity for this aquifer are 0.30 and 0.33, respectively. The ratio of effective to total porosity for GEMS and the Borden site is 0.46 and 0.90, respectively. The GEMS data suggests that less than half of the pores in the aquifer are continuous. This observation seemed unlikely, considering that the aquifer is composed of unconsolidated sand and gravel. It was expected that the effective to total porosity ratio would be closer to that observed at the Borden site.

Figure 6 contains hydraulic conductivity ( $K$ ) profiles determined from the tracer test and the permeameter analysis of repacked core material from well 5-1 (Butler and McElwee, 1994). Again, note the relative magnitude of the estimates determined from the two methods. The average tracer test and permeameter  $K$  estimates are 2.04 and 48.2 m/day, respectively. The permeameter  $K$  represents disturbed samples because the original formation pore geometry was destroyed. The tracer test  $K$  represents groundwater movement in the principle flow direction and in the natural undisturbed environment. Therefore, the tracer test  $K$  should be greater than the permeameter  $K$ . The

fact that the average tracer test K is over an order of magnitude lower than the average permeameter K suggested that the tracer test data was in error.

All of the first four tracer tests produced similar questionable results. A simple sensitivity analysis of the tracer test model suggested that the primary controls on the parameter estimates were the induced hydraulic gradient, rate of tracer advance, and observations from the induction probe. These controls were studied to determine how they were contributing to the underestimation of the hydraulic parameters.

#### Tracer Solution Aeration

The tracer solution discharged into the injection well at land surface and cascaded down the well. It was hypothesized that during this descent, air bubbles entrapped in the turbulent column of water moved into the aquifer with the injected water. Once in the aquifer, the bubbles could clog pores, reducing the hydraulic conductivity of the near-well material and therefore increasing the induced hydraulic head in the injection well.

Field experiments were conducted to determine if air was introduced into the aquifer during tracer injection. In order to minimize air entrapment, a drop pipe (0.032 m ID) was placed inside the well (0.051 m ID). Water was pumped to the injection well, where it entered the drop pipe. The pipe housed the injected water during its descent in the well. The water discharged from the drop pipe approximately 2.4 m below the static water level in the well. The drop pipe was completely filled with tracer solution during injection, thereby minimizing contact between the injected water and the atmosphere.

Injection tests were performed with and without the drop pipe in order to assess if there was a difference in the induced head produced by the two approaches. Water was pumped from well 0-8 using a 0.089 m diameter submersible pump (*Simer*, model 9BC). The water entered injection well 1-7 at a constant rate of approximately 51 L/min. (13.6 gal./min.) for both tests. Pressure transducers, positioned 6.7 m below the static water level, were used to monitor the induced head. Figure 7 is a plot of the induced head versus time in injection well 1-7 for the two approaches. This plot displays greater induced head during the test without the drop pipe, suggesting air entered the aquifer and reduced the hydraulic conductivity of the near-well formation.

The possible presence of air in the formation presents serious problems for this tracer test method. Not only does the air clog pores, altering the hydraulic properties that are the subject of the investigation, but also the presence of air reduces the formation conductivity observed during tracer injection (air is less conductive than saline tracer solution). This decrease in formation conductivity alters the relationship between the induction readings and the hydraulic properties. As a result of these experiments, it was

concluded that a drop pipe must be used during tracer injection in order to eliminate aeration of the injection solution and subsequent introduction of air into the aquifer.

#### Aquifer and Well Head Losses

In addition to tracer aeration, head losses also contributed to the large induced heads observed during the first series of tracer tests. Head changes in an injection or pumping well result from phenomena in both the aquifer and well (Kruseman and de Ridder, 1990). Aquifer head losses result from gradient-induced laminar flow. They are time-dependant and linearly proportional to discharge. Well head losses consist of both linear and non-linear components. Linear well head losses result from well installation disturbances (skin) and friction in the well casing and screen. Non-linear well head losses result from turbulent flow in the well screen, casing, and aquifer near the screen.

Field experiments were performed to assess aquifer and well head losses during injection. Water was pumped from well 0-8 using a 0.089 m diameter submersible pump (*Franklin Electric*, model 2443050117). The water was discharged at 57 L/min. (15 gal./min.) into well 5-1 via the injection drop pipe. The discharge end of the drop pipe was 0.070 m above the static water level. Following the initiation of injection, the discharge end of the drop pipe was continuously below the water level in the well. Pressure transducers, placed at the bottom of the well and above the screen, monitored changes in water levels during injection. Once steady-state flow conditions were achieved, the lower pressure transducer was raised at 0.305 to 0.610 m (1.0 to 2.0 ft.) intervals in an attempt to observe vertical variations in the induced head. Pressure transducer observations from each interval were recorded with a data logger. Figure 8 is a plot of the induced head versus depth. The induced head at the top and bottom of the water column is 0.95 and 0.05 m, respectively. The plot displays rapid head loss in the top 10 m of the water column. The initial head loss, in the interval from 5 to 12 m, is slightly non-linear (concave downward) and is attributed to friction between the turbulent injection fluid and the well casing. The Reynolds number determined for this interval is 22,700 (well above the criteria for turbulent flow), providing support for this interpretation. The most significant head loss occurred in the interval from 12 to 15 m (just below the top of the well screen) and is attributed to linear aquifer and well losses and non-linear well losses in the screen. The induced head in the lower 6 m of the screen is small, but constant.

These observations have important implications for the tracer tests because the induced head measured during the tracer tests is likely to be inflated due to head losses above the screen. The results also imply that most of the injected tracer solution entered

the aquifer through the upper portion of the screened interval (12 to 15 m). Although the induction logs show that the tracer entered the lower portion of the aquifer during tracer injection, the tracer solution did not appear at the bottom of injection well 9-1 until 10 minutes after the initiation of tracer injection. Since the volume injected during the first 10 minutes represents several well volumes, this observation supports the hypothesis that most of the tracer entered the aquifer through the upper portion of the screened interval.

In an attempt to eliminate the observed vertical head variations in the injection well, the above injection test was repeated several times with a perforated drop pipe that extended to the bottom of the well. The drop pipe, perforated only in the screened interval, was constructed to distribute the injection solution throughout the entire interval. Several experiments were conducted with different perforation distributions and sizes to produce a vertical head profile that was sustainable, reproducible, and quantifiable. The final drop pipe design is illustrated in Figure 9. The pipe is perforated in the lower 4.6 m of the 9.1 m screened interval. The perforations increase in size and frequency with depth.

During the final drop pipe experiments, an injection rate of 106 l/min. (28 gal./min.) was used to induce an average head of 0.09 m in injection well 5-1. Figure 10 is a plot of the vertical distribution of induced head after 1.5 hr. of injection. Note that the head above and below the top of the screen is relatively constant. This implies the head losses observed in Figure 8 have been eliminated, and that a uniform distribution of injection solution exists with depth.

#### Tracer Solution Concentration

It is important that the change in formation electrical conductivity during tracer injection is large relative to the resolution of the borehole induction tool. If a weak saline solution is used, the increase in formation conductivity during tracer injection may be masked by noise in the readings from the induction tool. The accuracy of the induction tool used in this study, as defined by the manufacturer, is  $\pm 5\%$  at 30 mS/m. Assuming an average value of 30 mS/m for formation conductivity during tracer injection, this error corresponds to a range of approximately  $\pm 1.50$  mS/m.

The total maximum change in formation conductivity during the injection of solutions of electrical conductivity two and three times that of the background pore fluid was 6 and 14 mS/m, respectively. Clearly, the measured changes during the test conducted using a tracer solution with a conductivity twice that of background contains considerable error. To reduce the impact of measurement error, the electrical conductivity of the tracer solution should be at least three times that of the background

pore fluid conductivity. Error in induction measurements can also be reduced if averaged values of formation conductivity from repeat logs are used rather than values obtained from a single log.

Note that increasing the salinity of the tracer solution in order to increase the signal to noise ratio may induce chemical reactions within the aquifer. Significant changes in the cation ratios may initiate cation exchange on clay particles. Dissolution or precipitation of minerals such as calcite and aragonite may occur due to the common ion effect (if a Ca salt is used) or to an increase in ionic strength. Some of these reactions are kinetically fast and may alter the hydraulic properties of the aquifer during injection.

Permeameter analyses of cores from GEMS were conducted in the Kansas Geological Survey Core Properties Laboratory to determine the extent of hydraulic property alteration due to tracer-induced chemical reactions (laboratory protocol for the permeameter analysis is described in McElwee and Butler 1993). Hydraulic conductivity was measured for seven cores saturated with GEMS native pore water. The measurements were repeated with a saline solution similar to that used during the tracer tests. The two sets of measurements showed no change in hydraulic conductivity that could be attributed to chemical reactions between the tracer solution and the aquifer material. As a result, it was concluded that no changes in hydraulic properties occurred during the tracer tests due to the introduction of the tracer solution into the aquifer.

## **Repeated Tracer Test**

### **Introduction**

Based on the results of the above-described investigations, a second tracer test was conducted in GEMS well 5-1 using the revised procedure. Refinements were also made to the Taylor and Molz (1990) method of data analysis in order to improve the reliability of the parameter estimates. The results obtained from this tracer test are reasonable considering the nature of the aquifer material and are consistent with laboratory permeameter results from the same well.

### **Tracer Test Methodology**

With the exception of the use of the perforated drop pipe, the repeated test followed the procedure described earlier. The tracer solvent was pumped from well 0-8 using a 0.089 m diameter submersible pump (*Franklin Electric*, model 2443050117). The tracer injection rate (including water from the pumping well and the concentrated saline solution) was 112 L/min. (29.5 gal./min.). The head in the injection well was monitored with pressure transducers positioned at the bottom of the well and above the

top of the well screen. The induced head was determined from static and steady-state water levels observed each time the injection pumps were turned on and off. The average induced head at the bottom and top of the screened interval was 0.104 and 0.087 m, respectively. The slope from this vertical gradient was used to estimate the induced head for each 0.03 m section of the screened interval.

Prior to each induction logging period, tracer injection was terminated, and the drop pipe and pressure transducers were removed from the injection well. This procedure was necessary because there was not room in the injection well for all of the equipment at the same time. Termination of injection is assumed to have little influence on the movement of the tracer due to the low relative regional gradient, the short time required to log the well (approximately 15 min.), and the very short time necessary to achieve steady-state flow conditions following the initiation of injection (determined from pressure transducer data to be approximately 1.5 min.). The well was logged four times before and at the end of tracer injection and twice during six intervals during injection. Between logs, the induction probe was lowered in a nearby well in order to keep the probe in thermal equilibrium with the aquifer temperature. The specific conductivity of the background groundwater and injection solution was 60.8 and 193 mS/m, respectively. Tracer injection lasted for 5.70 hr. During this time, 38,240 L (10,100 gal.) of tracer solution, amounting to approximately 37 kg of NaCl, discharged into the well. Remedial pumping removed approximately 60 % of the NaCl.

### Data Analysis

#### Tracer Injection:

Figure 11 displays average formation electrical conductivity logs obtained before, during, and after tracer injection (Huettl, 1994). As the tracer invaded the aquifer, the measured formation conductivity increased. Note that much of the variation existing prior to injection (log at 0.00 hr.) remains after the tracer solution approached the radial detection limit of the induction tool (log at 5.70 hr.). This implies that even when the aquifer is saturated with the saline tracer, the contribution of the matrix conductivity to the total formation conductivity dominates over the combined contribution from porosity and pore fluid.

The Taylor and Molz (1990) method of parameter estimation summarized earlier assumes that tracer injection continues until the invading solution moves beyond the radial detection limit of the induction tool. After that time, the formation conductivity will not change with continued injection. Figure 12 displays the change in formation conductivity during tracer injection at four arbitrarily chosen intervals in well 5-1. In all

four intervals, the formation conductivity appears to be asymptotically approaching an upper limit. This suggests that the tracer solution is close to the induction probe's radial detection limit at 5.70 hr. and the assumption of tracer saturation is reasonable.

#### Porosity Estimation:

As stated earlier, the Taylor and Molz (1990) method of porosity estimation adopts a model of the relationship that exists between formation conductivity, pore water conductivity, and porosity. Equation (IV.D.6) provides a means of estimating effective porosity using this model. Figure 13 contains calculated and measured porosity profiles for well 5-1. The solid curve is data determined by the tracer test assuming tracer solution saturation at 5.70 hr and empirical factors  $m = 1.4$  and  $\alpha = 1.0$ . The dotted curves are confidence intervals determined by assuming 10 % error in the empirical factors. The dashed curve is data determined from grain-size analysis of sediment from cores from the same well (Butler and McElwee 1994). The average effective and total porosity estimates are 0.19 and 0.26, respectively. Note that the tracer test effective porosity is a minimum estimate because the tracer solution may not have entirely reached the radial detection limit of the induction probe. Figure 12 shows that the formation conductivity may have increased approximately 1 mS/m if injection had continued. This change would result in an increase of 0.010 in effective porosity.

Although the tracer test values are considerably lower than the permeameter values, the tracer test values are reasonable because they represent only the interconnected pores that were filled with tracer solution during injection.

#### Radius of Tracer Invasion:

The radial sensitivity of the induction probe (Figure 2) is determined theoretically from knowledge of magnetostatics and the induction probe coil geometry (Saito, 1982). The cumulative sum of these radial contributions (Figure 3) and Equation (IV.D.7) were used to estimate the radial position of the tracer solution front for each induction log displayed on Figure 11.

Figure 14 displays the estimated radius of tracer invasion at several times during injection using the theoretical cumulative radial response function. Empirical estimates of the average radius of tracer invasion for the entire screened interval were also made for each time that an induction log was taken during tracer injection. These estimates were made by determining the volume of aquifer invaded by the injected tracer solution assuming an average effective porosity of 0.193 and a constant tracer injection rate of 112 l/min. Figure 15 displays these estimates along with the average theoretical radius of

tracer invasion determined for each curve in Figure 14. These plots show that the radius of tracer invasion determined using the theoretical model is underestimated during early injection times and overestimated during later times. This observation suggests that the theoretical response function may be inappropriate in this field environment.

Assuming that the tracer reached the detection limit of the induction probe prior to the termination of injection during the repeated tracer test, an empirical cumulative radial response function can be generated. The average cumulative radial response,  $Z(R)$  [Equation (IV.D.7)], was determined for each induction log obtained during tracer injection. This value represents the percent of the total injection-induced change in formation conductivity that occurred by the time that induction log was obtained. When these values are plotted against the empirically determined average radius of tracer invasion for that time, the resulting plot is an empirically derived cumulative radial response function. Figure 16 displays computed empirical cumulative radial response functions. The solid curve represents a function determined assuming the empirical estimates of tracer invasion shown in Figure 15. The dotted curves represent "confidence interval" functions. They were determined from empirical estimates of tracer invasion derived from the porosity confidence intervals in Figure 13. The theoretical function is provided for comparison.

Figure 17 displays the radius of tracer invasion determined with the empirical response function. These values directly correlate with the empirical estimates in Figure 15. Figure 17 shows that the tracer invaded the aquifer uniformly in the interval from 13 to 16 m. Differential flow is observed in the lower portion of the screened interval, represented by a zone of relative rapid invasion centered at 18 m.

#### Hydraulic Conductivity Estimation:

Equation (IV.D.14), which is used to estimate hydraulic conductivity ( $K$ ), defines a linear relationship between  $R^2$  and  $t$  (where  $R$  = radius of tracer invasion determined at 0.03 m intervals for each induction log from time  $t$  since initiation of tracer injection). Figure 18 is a plot of  $R^2$  versus  $t$  determined at a depth of 17.98 m in well 5-1 using the theoretical and empirical response functions. The non-linearity observed in the theoretically determined values further demonstrates the previously discussed inappropriateness of the theoretical function.

According to equation (IV.D.14), all plots of  $R^2$  versus  $t$  should be straight lines passing through the origin. A linear regression of  $R^2$  (determined using the empirical response function) and  $t$  was performed to determine the slope and y-intercept for each 0.03 m interval of well 5-1. Figure 19 displays the y-intercept values. The intervals from



the upper 5/8 of the screened section have consistently negative intercepts, while the lower 3/8 have consistently positive intercepts.

The empirical radial response function (Figure 16) used to determine the radius of tracer invasion is a cumulative sum of the contributions of formation conductivity from all zones within the radial detection limit of the induction tool. Therefore, the contribution to formation conductivity from a drilling-induced disturbed zone (skin) adjacent to the borehole will influence every estimate of tracer radial invasion. As a result, all estimates of tracer invasion will be shifted by a constant factor that is a function of the hydraulic properties and size of the disturbed zone. This shift is represented by the non-zero y-intercepts shown in Figure 19. This constant factor is amplified by squaring  $R$  for the determination of  $K$  [Equation (IV.D.14)]. The non-zero y-intercept produces a changing slope and thus a time dependence in the  $K$  values determined from each  $R$  at a specific interval. Figure 20 displays the time dependence in  $K$  values produced by these effects using the data in Figure 18.

The positive and negative intercepts represent high and low permeability skins, respectively. These disturbances result from sediment churning, compaction, collapse, and smearing during drilling and development operations. The change from a low to a high permeability skin observed in Figure 19 is likely due to smearing of silt and clay from the upper alluvial unit on the inside of the borehole as the drilling flights penetrated the underlying sand and gravel.

These observations suggest that, contrary to the Taylor and Molz (1990) procedure, the application of Equation (IV.D.14) with individual values of  $R^2$  and  $t$  for  $K$  estimation is not appropriate for wells with a drilling-induced disturbed zone. Individual values for  $R^2$  and  $t$  in Equation (IV.D.14) must be replaced with the slope of  $R^2$  versus  $t$ , which will eliminate the influence of a near-well disturbed zone on the estimated  $K$  values. Although this slope method produces only one value of  $K$  for each depth interval, it is clearly more accurate than averaging several values determined by the Taylor and Molz (1990) method.

Figure 21 displays hydraulic conductivity profiles for well 5-1. The solid and dotted curves are smoothed data (nine point running average) estimated with the  $R^2$  and  $t$  slope method. The solid curve data was computed using values of  $R$  estimated with an empirical response function derived assuming the tracer-test-determined effective porosity (0.193). The dotted curve was computed using  $R$  values estimated with an empirical response function derived assuming the average laboratory-determined total core porosity (0.264). The dashed curve is data determined from permeameter tests performed on repacked core material from the same well (Butler and McElwee, 1994).

The average tracer test and permeameter K estimates are 137 and 48.2 m/day, respectively. As expected, the tracer test values are greater than those determined from repacked sediment samples. This is due to the orientation of the sediment particles and structures relative to the lateral radial flow of the tracer. The tracer test and permeameter data show good correlation of relative spatial trends in K. Both data sets display a relatively low permeability zone centered at approximately 16.0 - 16.5 m.

The average tracer test K estimates determined with different empirical response functions are very similar. The K values, assuming tracer-test-determined effective porosity and laboratory-determined core total porosity, are 137 and 134 m/day, respectively. K values were also determined (but not displayed) using values of R computed from the "confidence interval" response functions in Figure 16. The average porosity values used to construct these response functions are 0.148 and 0.238. The corresponding K estimates are 154 and 136 m/day, respectively. These average K estimates represent a wide range of porosity values (coefficient of variation = 24.2 %), but display little variation (coefficient of variation = 6.6 %). This observation suggests that the tracer test model for K estimation is not sensitive to variations in porosity.

It is important to note that the tracer test parameter estimates are not discrete observations. Figure 3 displays the manner in which conductivity contributions from zones at different radial distances are averaged by the induction tool. This averaging masks some natural variation. Permeameter tests performed on cores and repacked sediment samples produce parameter estimates for a much smaller volume. These parameter estimates show considerably more variation, but are biased because they either represent flow normal to bedding planes or flow through disturbed samples. In short, the tracer test parameters are averages from a larger aquifer volume than the permeameter parameters, but are more accurate because they represent *in situ* observations made under flow conditions similar to those that exist in nature.

A final check on the absolute magnitude of the tracer test K estimates can be conducted by comparing them to an average K determined for the whole screened interval by the Thiem Equation (Kruseman and de Ridder, 1990):

$$K = \frac{Q}{2\pi bH} \ln\left(\frac{r_e}{r_w}\right) \quad (\text{IV.D.15})$$

If Q (discharge) = 161 m<sup>3</sup>/day, b (aquifer thickness) = 9.14 m, H (induced head) = 0.096 m,  $r_e$  (effective radius) = 2.62 m (assumed to equal the average maximum extent of tracer invasion), and  $r_w$  (radius of well) = 0.025 m, then K = 136 m/day. This value compares

very well to the value of 137 m/day determined by averaging the K values determined for each vertical interval. The similarity in these estimates suggests that the magnitude of the tracer test K estimates is accurate.

### Geologic Interpretation

The results of the final tracer test and data from cores retrieved during the installation of the injection well provide insight into the near-surface geology at GEMS. The formation conductivity and natural gamma logs obtained during a pre-tracer test survey reveal a fining-upward sequence composed of two distinct units of roughly equal thickness (approximately 11 m) for well 5-1.

X-rays of core display cross-bedded sand and gravel and clay drapes in the lower unit, indicating fluvial deposition (Blatt *et al.*, 1980). Sieve analyses of unconsolidated core sediment from this unit (McElwee and Butler, 1993) display a fining-upward trend, typical of fluvial channel deposits (Allen, 1965). The fining-upward trend, however, is not observed as a decreasing-upward trend in tracer test K. This may be the result of variations in particle sorting and packing during deposition. The mean K for the tracer test data is 137 m/day, typical of silty to clean sands (Freeze and Cherry, 1979). The mean tracer test effective porosity is 0.19. This value is low for unconsolidated sands (typically 0.25 - 0.50, Freeze and Cherry, 1979) and may be attributed to exceptionally poor particle sorting and tight particle packing. There appears to be no consistent correlation between effective porosity, K, and grain size.

Cores from the upper unit are composed of silt and clay. This interval appears homogenized by bioturbation, and contains rootlets and organic matter. These observations indicate subaerial exposure.

The basal sand and gravel alluvial unit is interpreted as laterally accreted river channel deposits. The overlying silt and clay alluvial unit is interpreted as vertically accreted floodplain deposits. It is likely that the two units represent a single lateral migration of the Kansas River.

### Conclusion

The borehole induction single-well tracer test appears to be theoretically sound. It has considerable potential for accurate and detailed characterization of vertical variations in effective porosity and the radial component of hydraulic conductivity. Modifications of the originally proposed procedure have been made in order to ensure that the model assumptions are valid, to reduce monitoring error, and to remove the effects of a near-well, drilling-induced disturbed zone. These modifications include the use of a perforated

drop pipe to eliminate the introduction of air into the aquifer during tracer injection and to create a quantifiable head distribution in the injection well. Averaged induction logs were used for parameter estimation in order to increase accuracy by decreasing the impact of noise in the induction probe readings. The theoretically determined cumulative radial response function was replaced with an empirically derived function that preserved mathematical relationships defined by the theoretical analysis model. Finally, refinements have been made in the method of data analysis such that the technique can be used for wells with both high and low permeability skins.

The method has advantages over traditional aquifer characterization methods. It is superior to other *in situ* single-well methods, such as slug and pumping tests, in that it is relatively insensitive to drilling-induced disturbances and may have higher vertical resolution. The tracer test parameter estimates are superior to permeameter estimates because the parameters are determined for the principle flow direction and in the natural undisturbed environment. The only major drawback of the tracer test method is the high cost of the borehole induction probe.

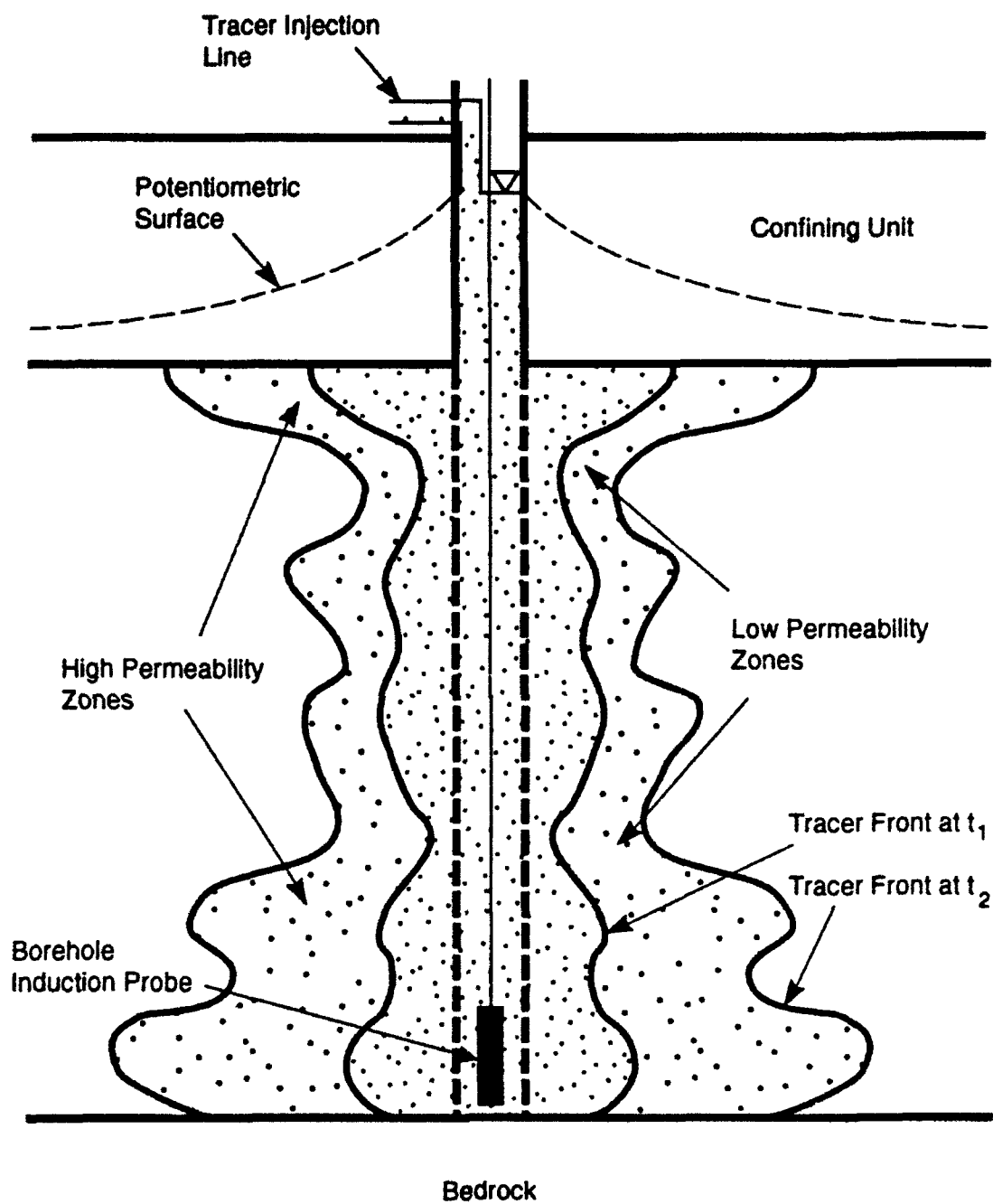


Figure 1. Illustration of single-well tracer test (modified from Huettl *et al.*, 1993).

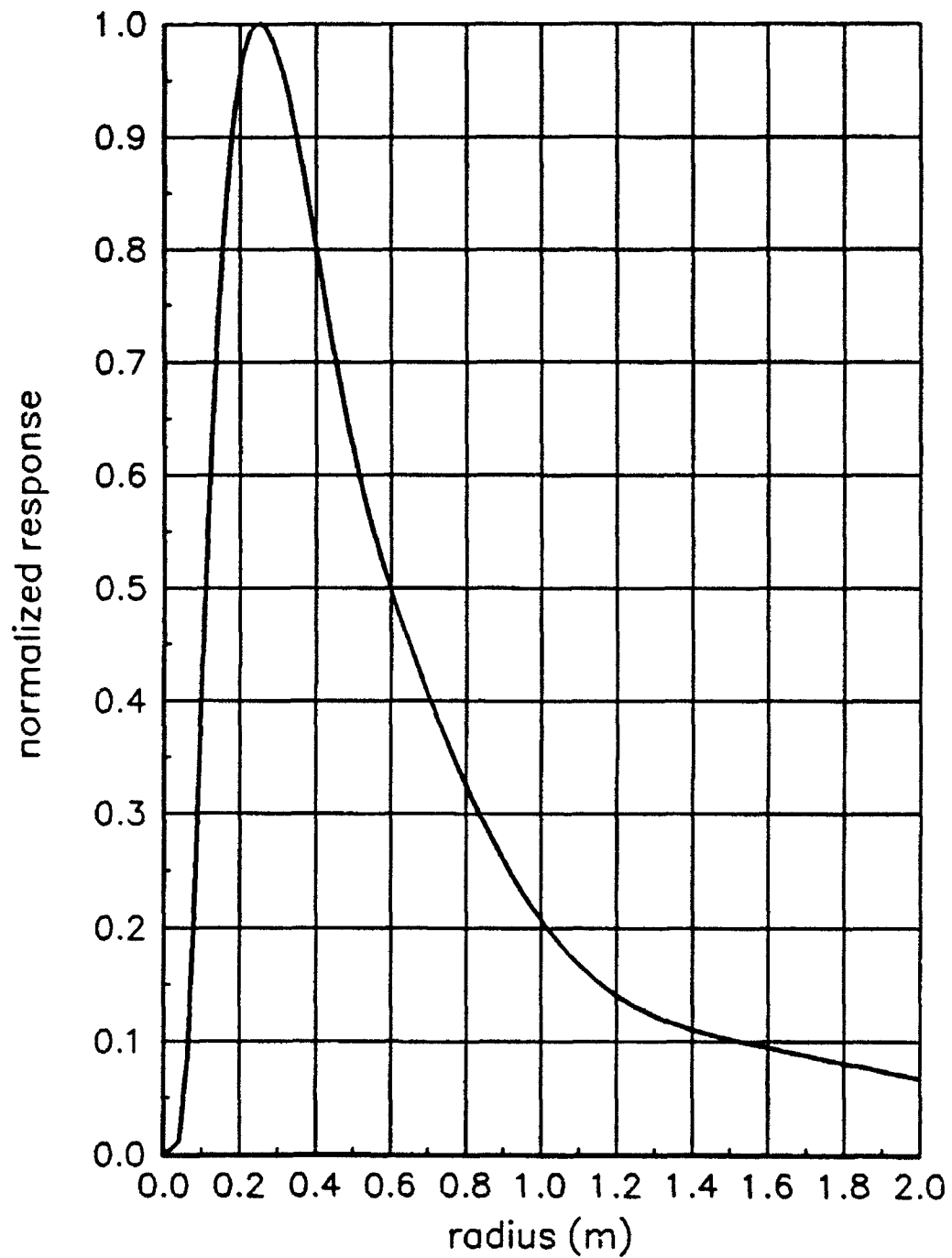


Figure 2. Induction probe theoretical radial response function (modified from *Century Geophysical Corporation*, unpublished).

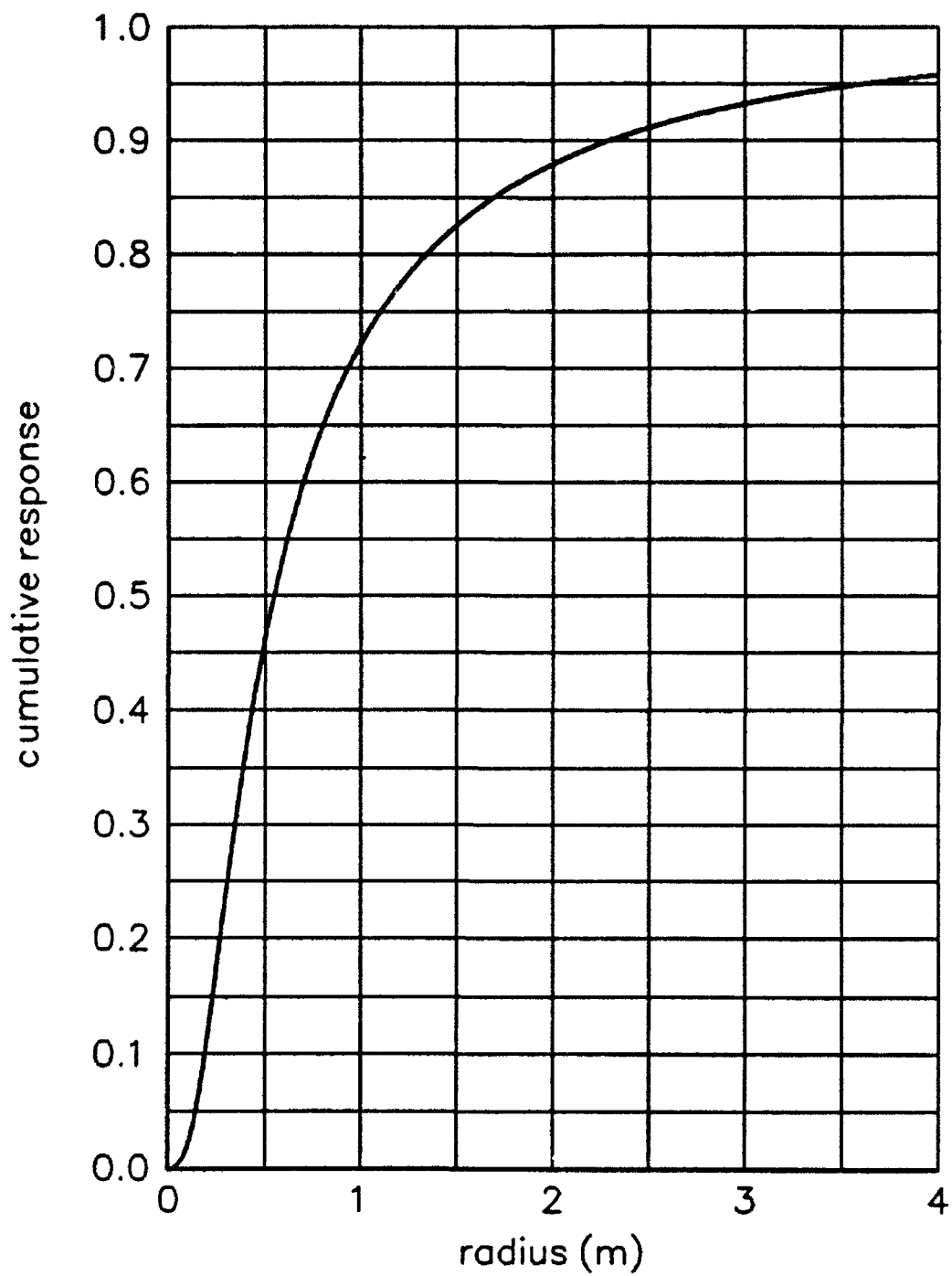


Figure 3. Induction probe theoretical cumulative radial response function (modified from *Century Geophysical Corporation*, unpublished).

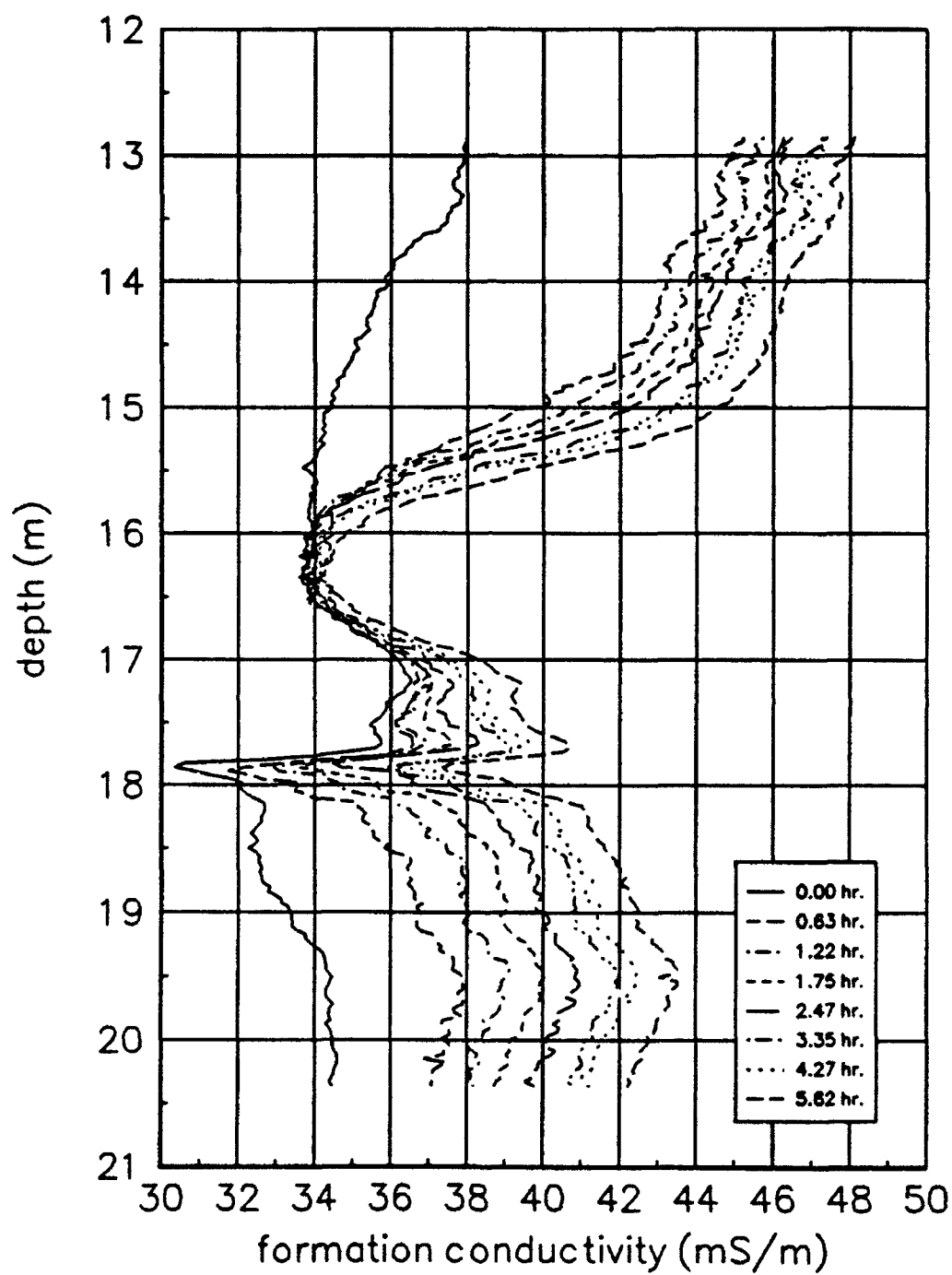


Figure 4. Formation conductivity before, during, and after tracer injection in well 5-1.



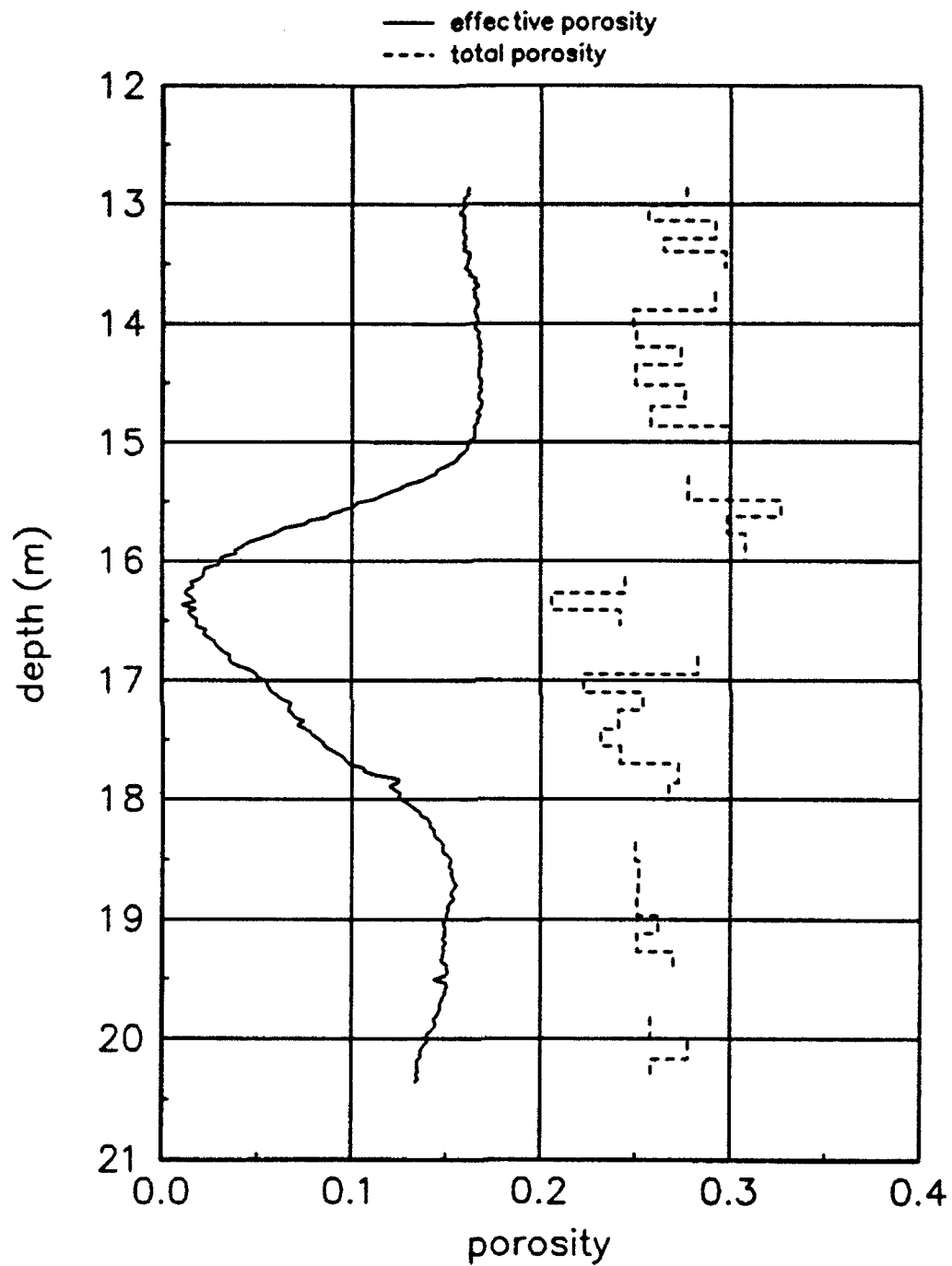


Figure 5. Porosity profiles from well 5-1. Total porosity from Butler and McElwee (1994).

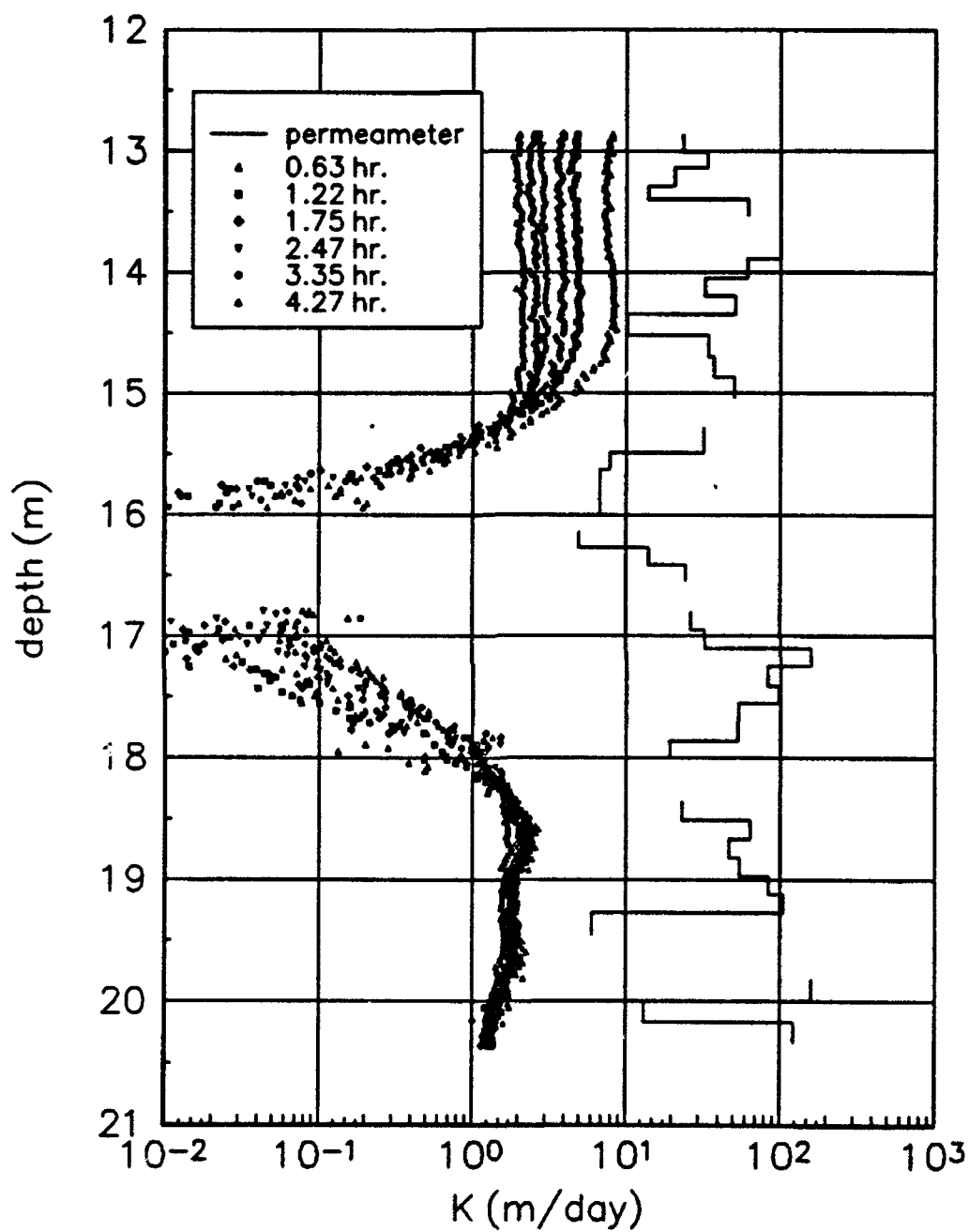


Figure 6. Hydraulic conductivity profiles from well 5-1. Permeameter data from Butler and McElwee (1994).

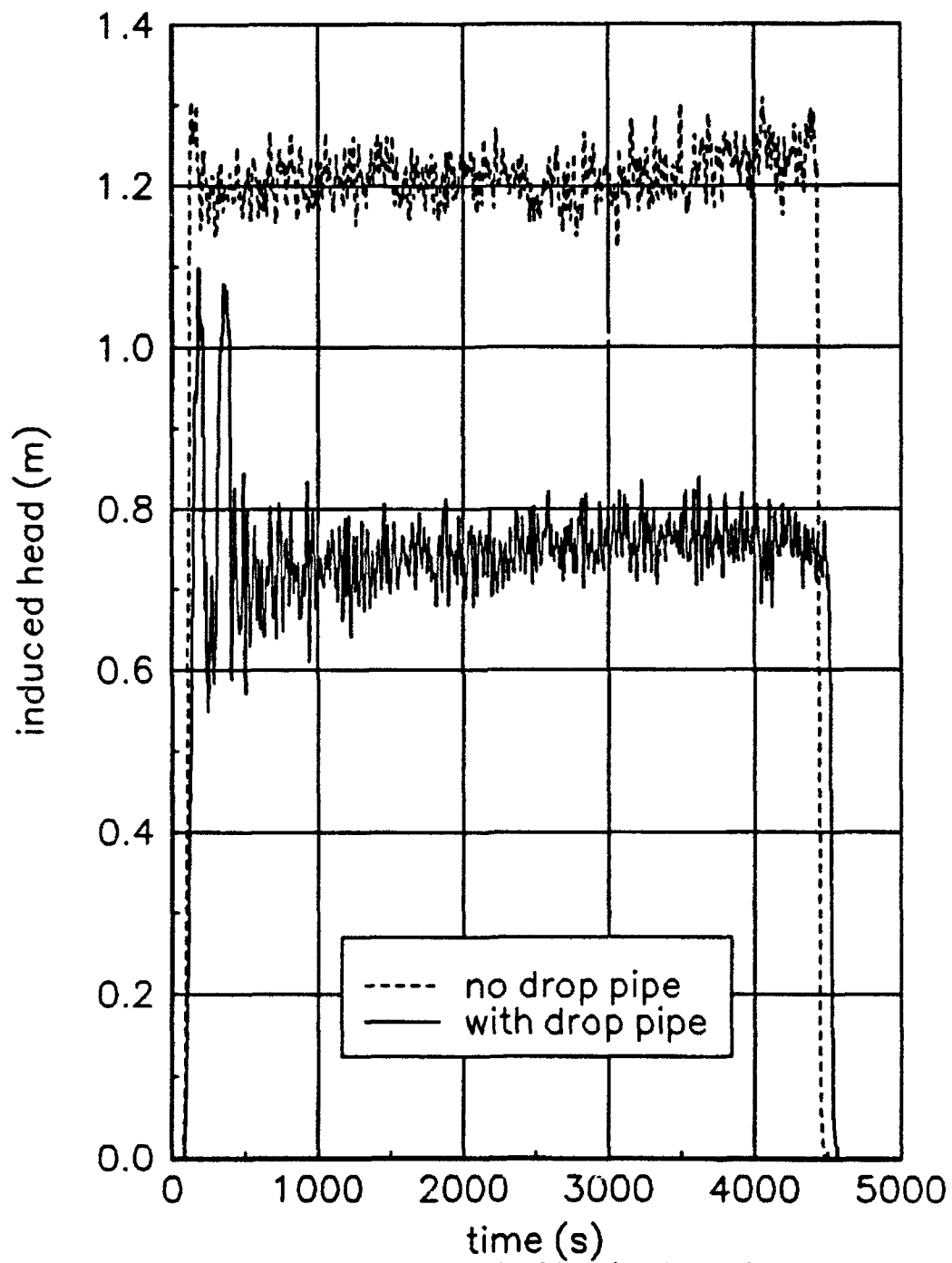


Figure 7. Induced head versus time in well 1-7 with and without injection drop pipe ( $Q = 51 \text{ L/min}$ ).

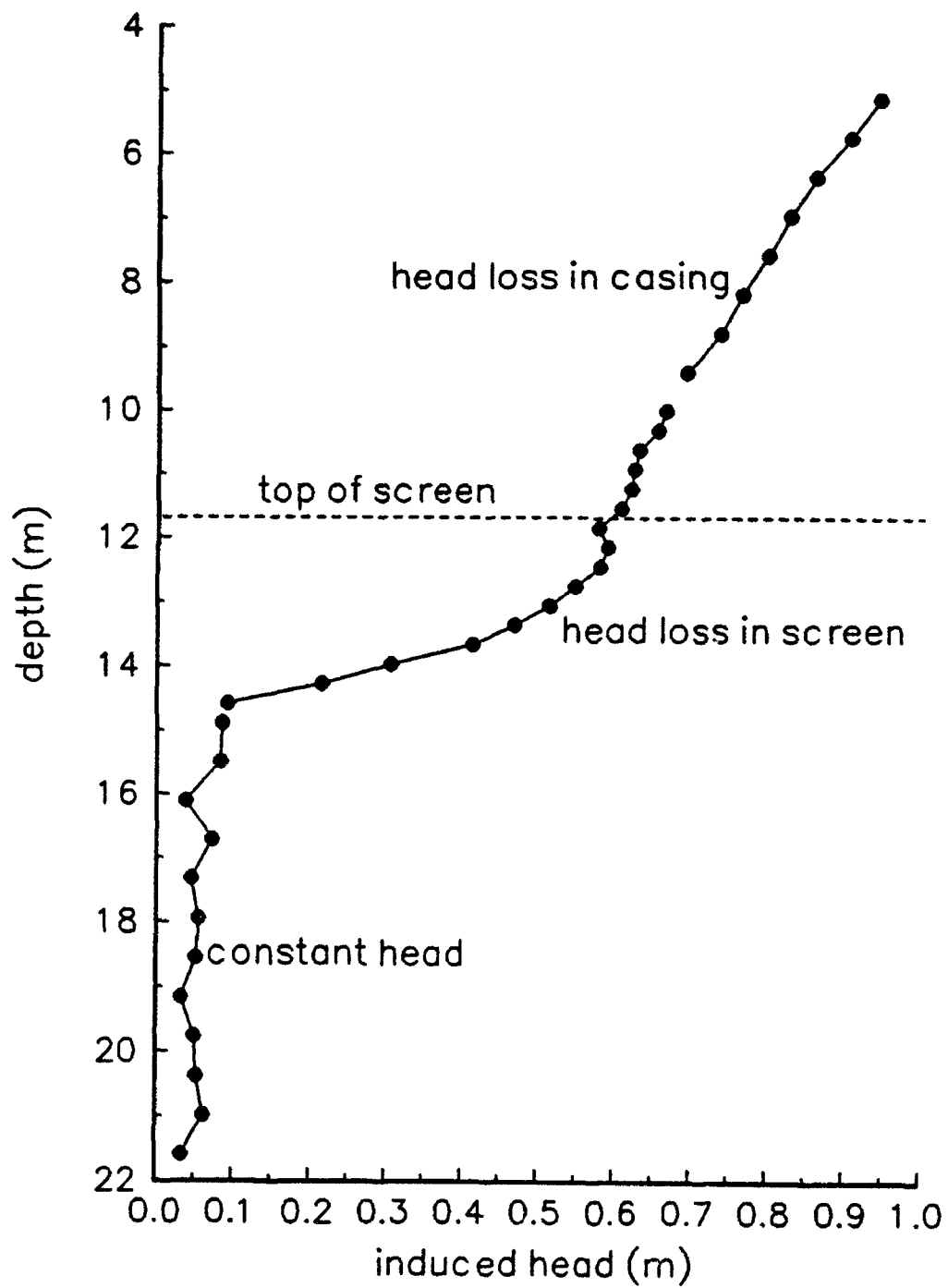


Figure 8. Head loss during injection in well 5-1 ( $Q = 57 \text{ L/min.}$ ).

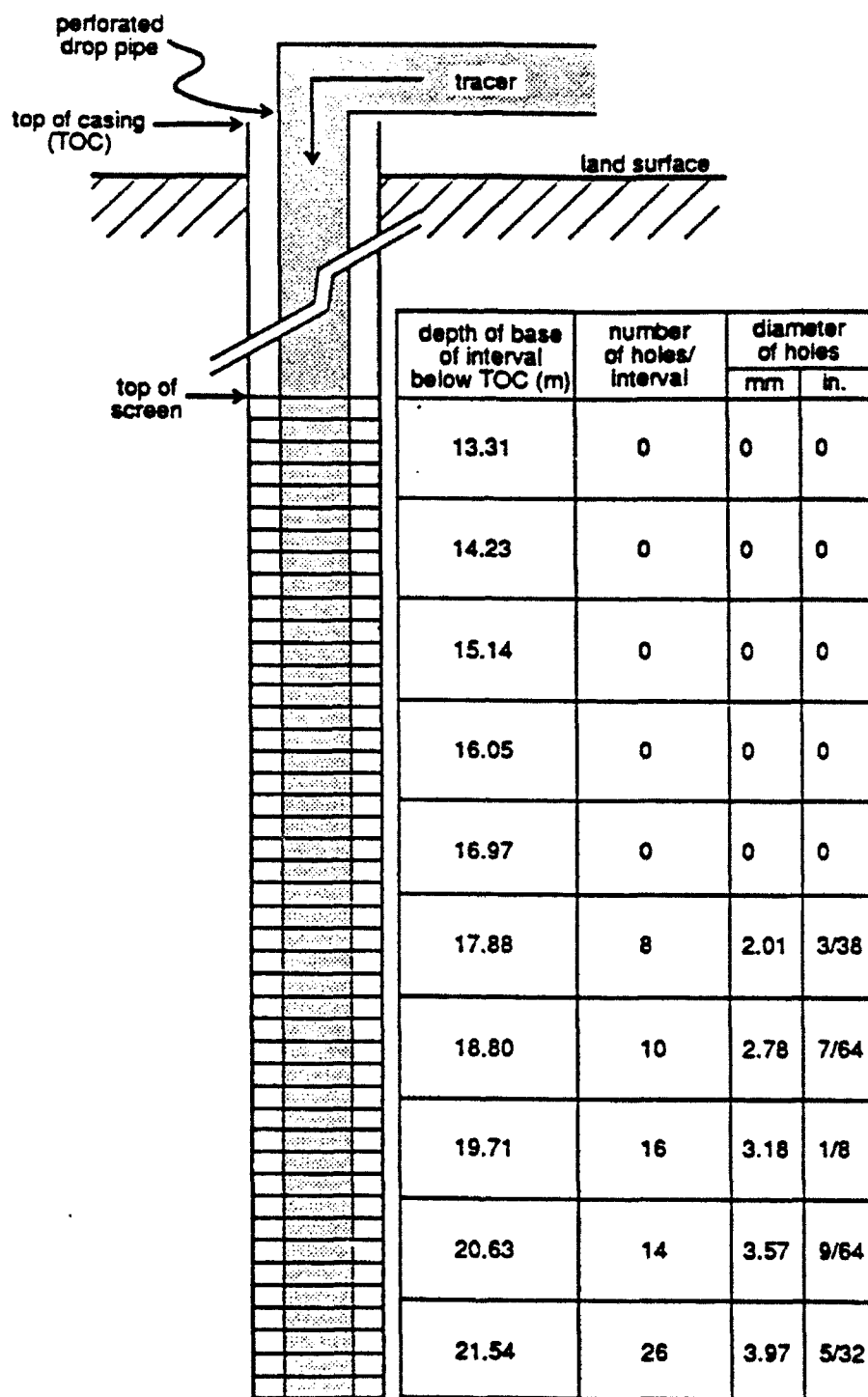


Figure 9. Illustration of the final drop pipe design, including the size and distribution of the perforations.

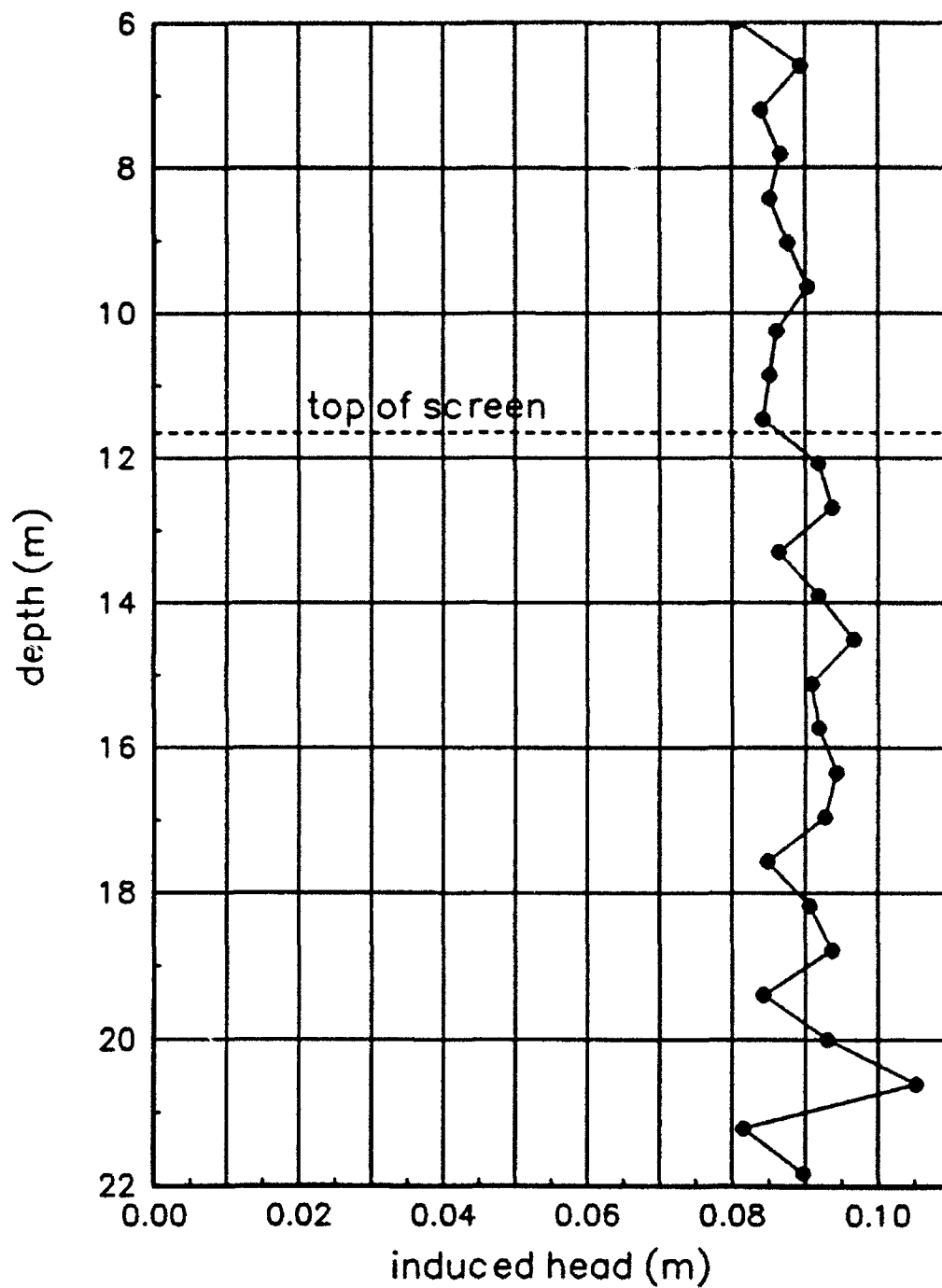


Figure 10. Vertical distribution of induced head in well 5-1 with final injection drop pipe design ( $Q = 106 \text{ L/min.}$ ).

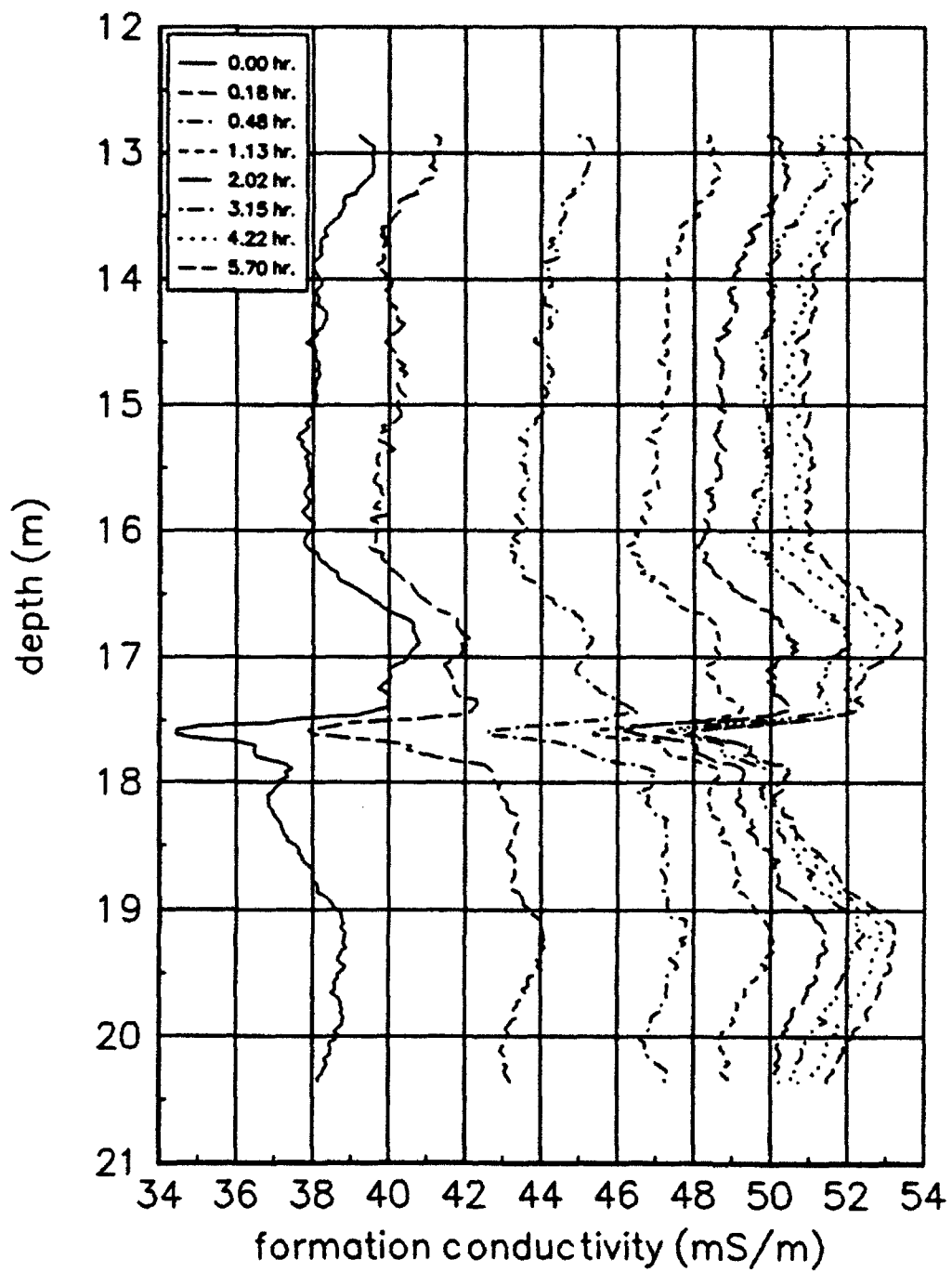


Figure 11. Average formation conductivity before, during, and after the second tracer test in well 5-1.

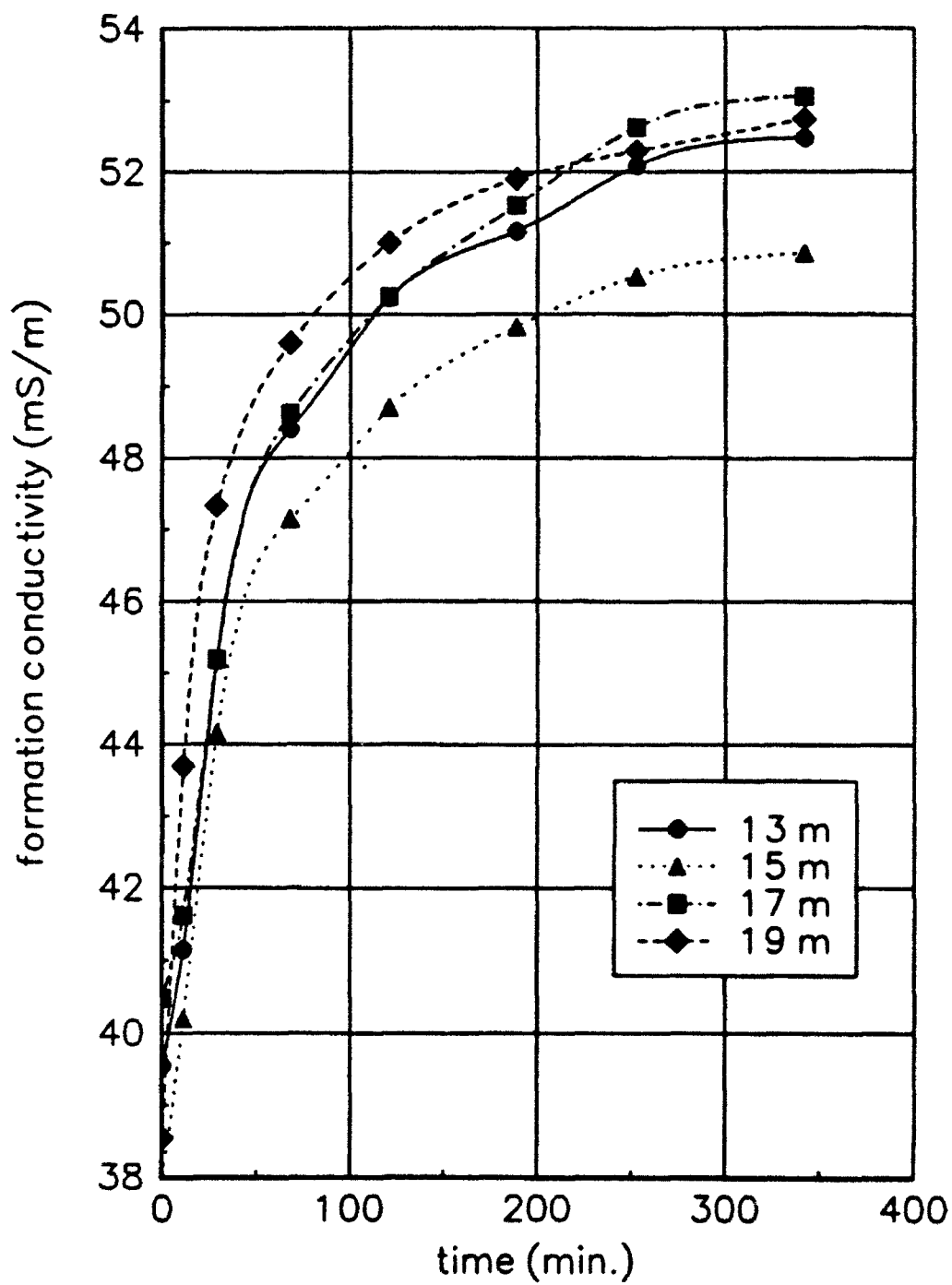


Figure 12. Formation conductivity during tracer injection in well 5-1 at arbitrarily chosen intervals.



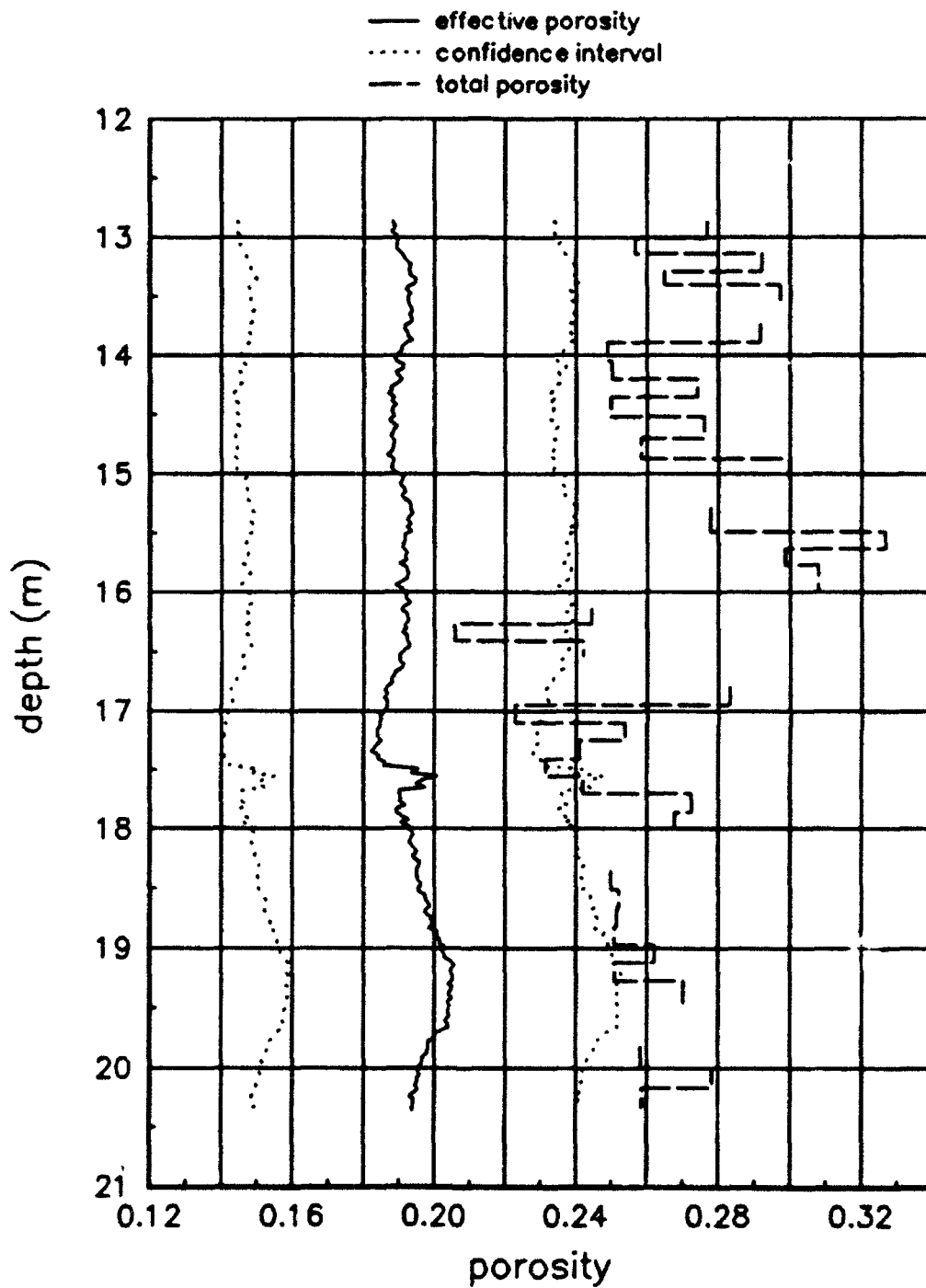


Figure 13. Porosity profiles for well 5-1. Total porosity from Butler and McElwee (1994).

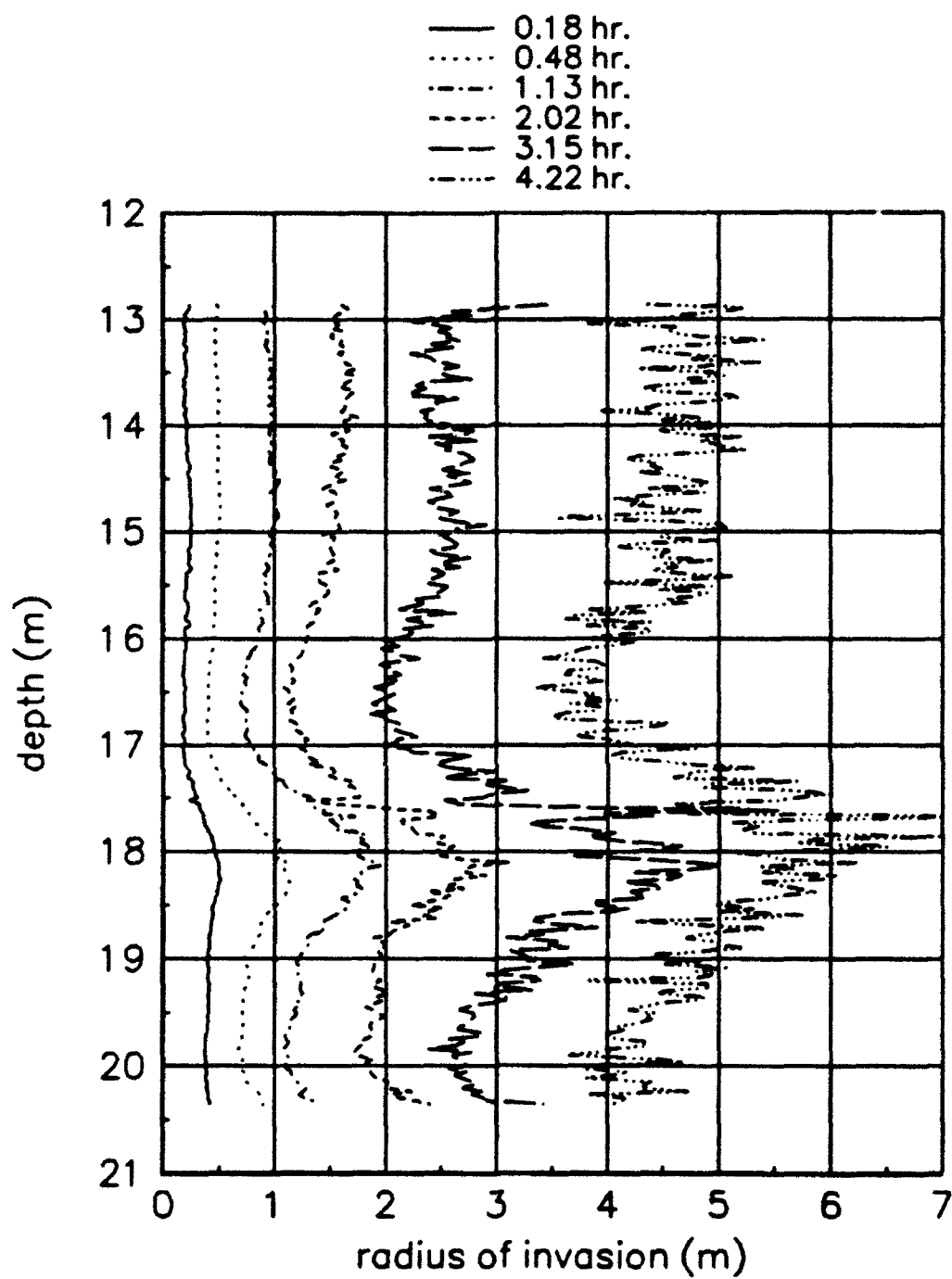


Figure 14. Radius of tracer invasion in well 5-1 determined with the theoretical cumulative radial response function.

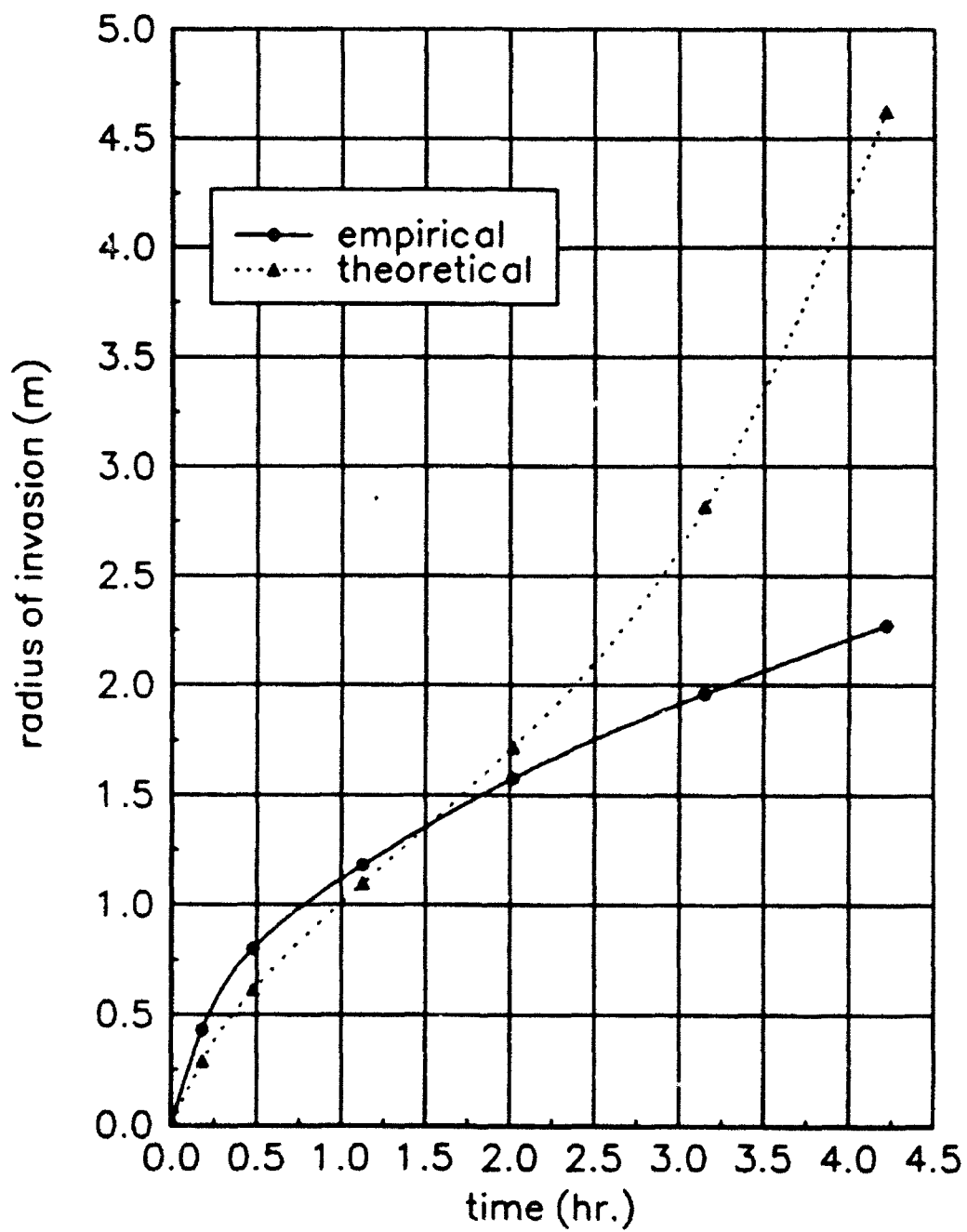


Figure 15. Theoretical and empirical estimates of the average radius of tracer invasion determined for the entire screened interval of well 5-1.

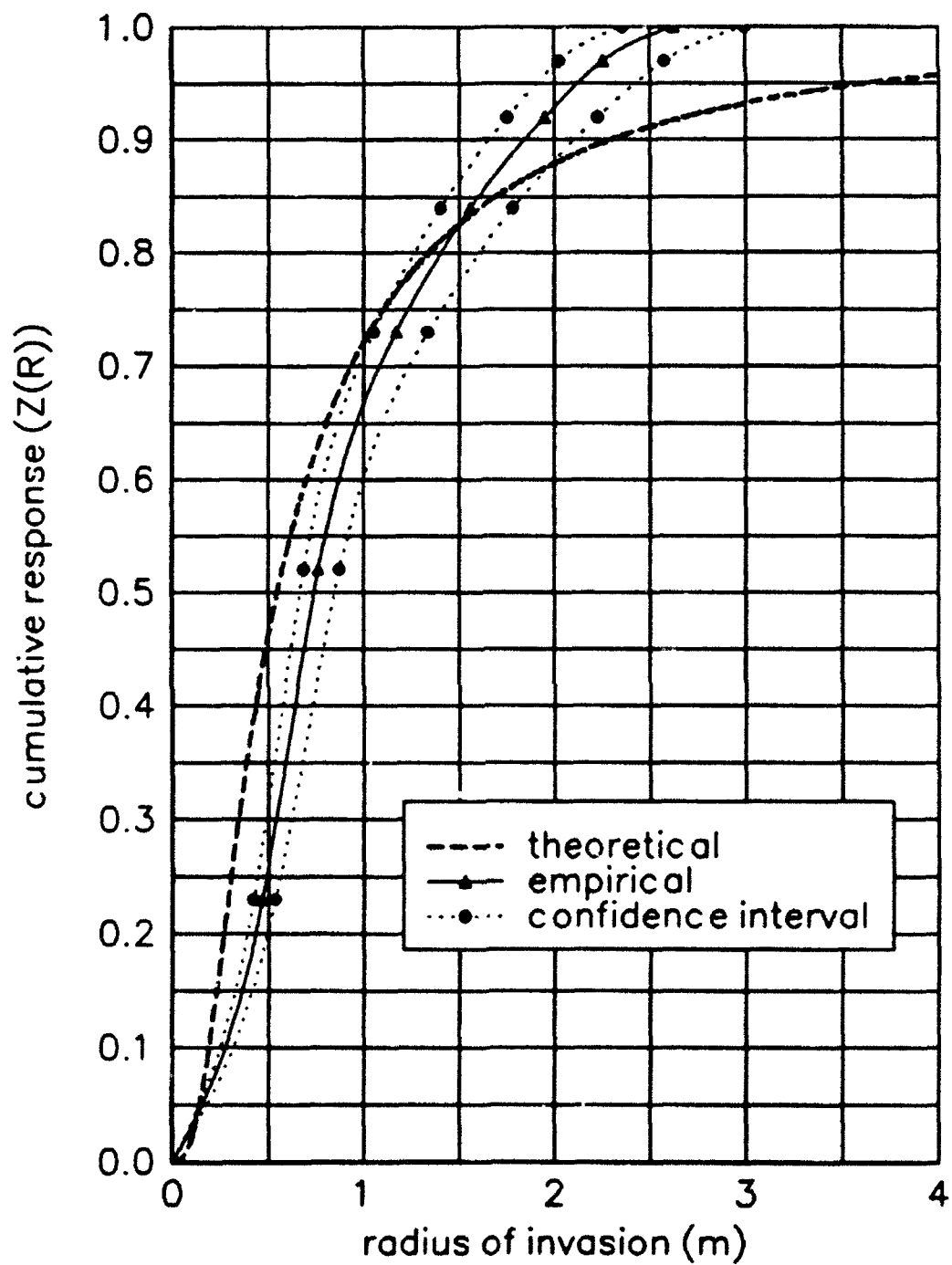


Figure 16. Induction tool empirical cumulative radial response functions.

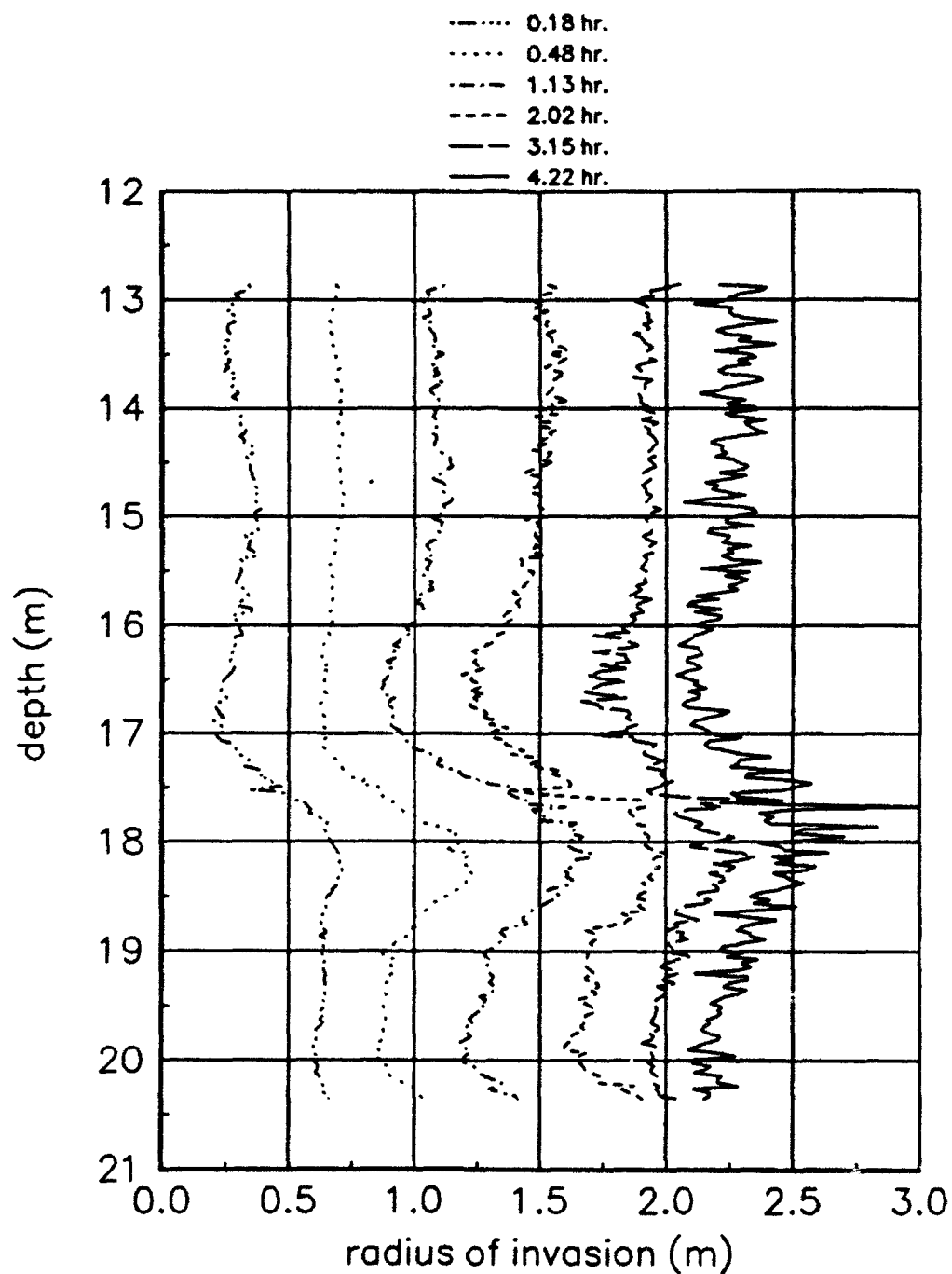


Figure 17. Radius of tracer invasion in well 5-1 determined with the empirical cumulative radial response function.

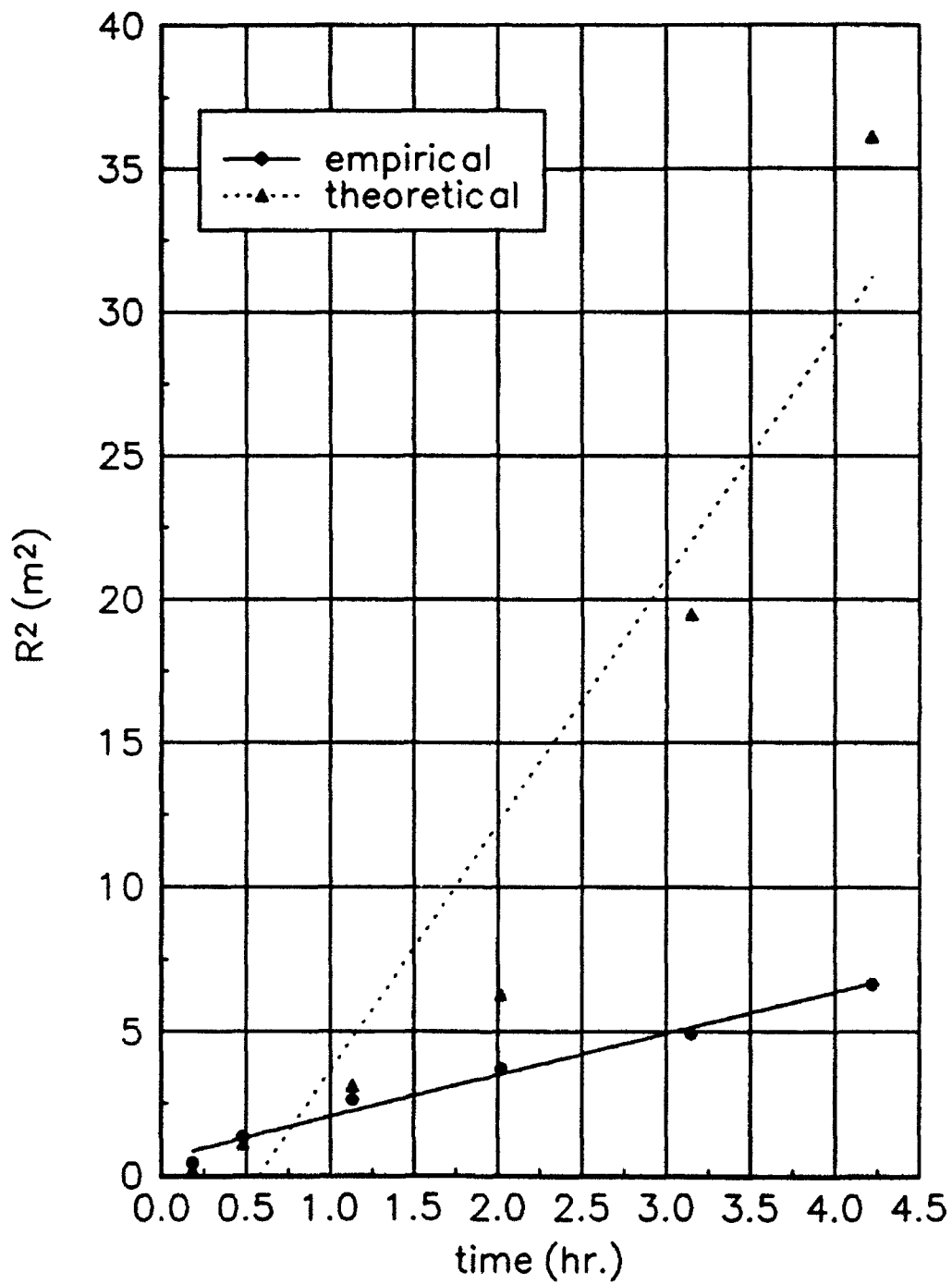


Figure 18. Radius of tracer invasion squared versus time determined at 17.98 m in well 5-1.

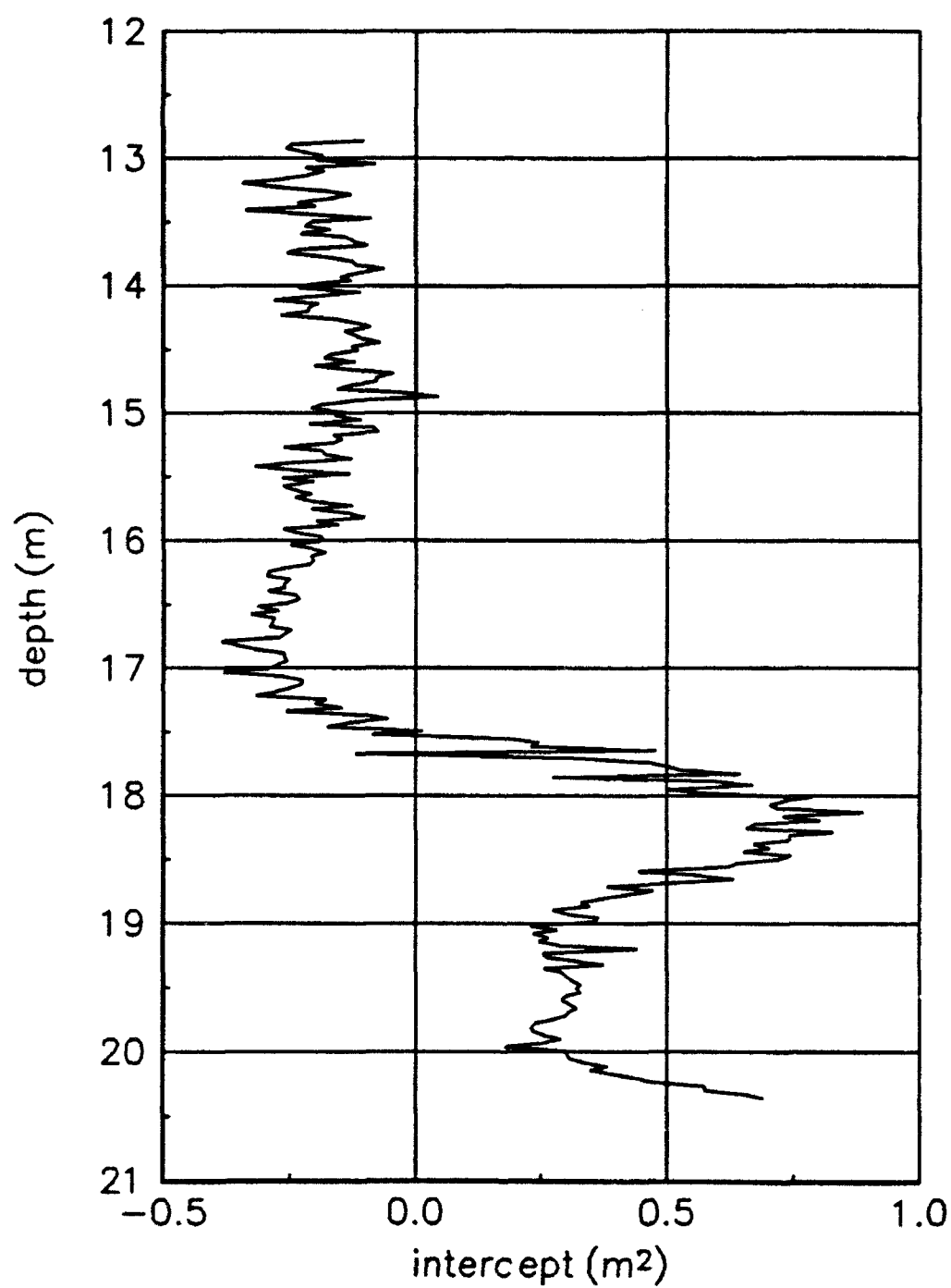


Figure 19. Y-intercept values from  $R^2$  versus  $t$  plots determined for each 0.03 m interval of well 5-1.

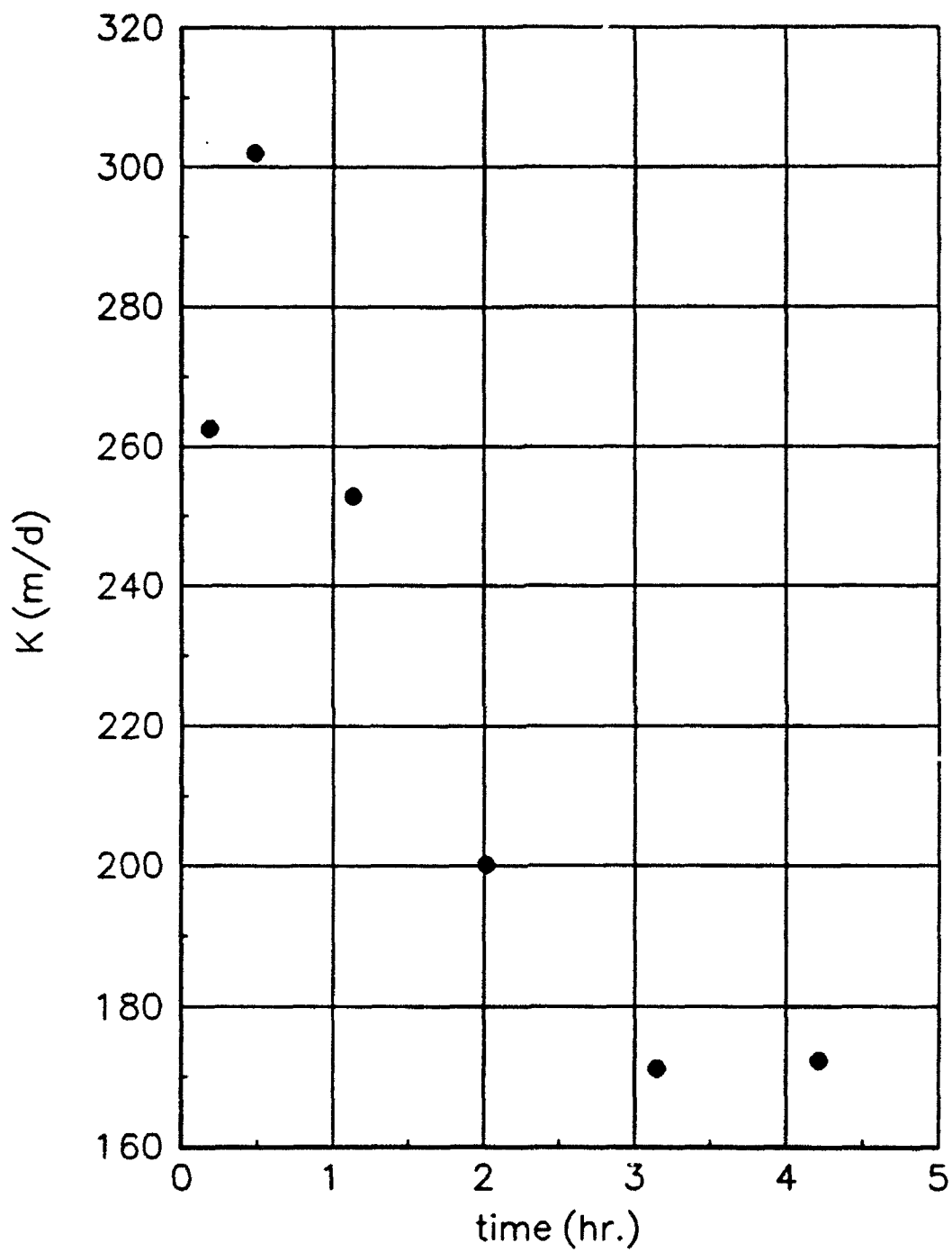


Figure 20. Time dependence in calculated hydraulic conductivity at 17.98 m in well 5-1 due to the presence of a skin.



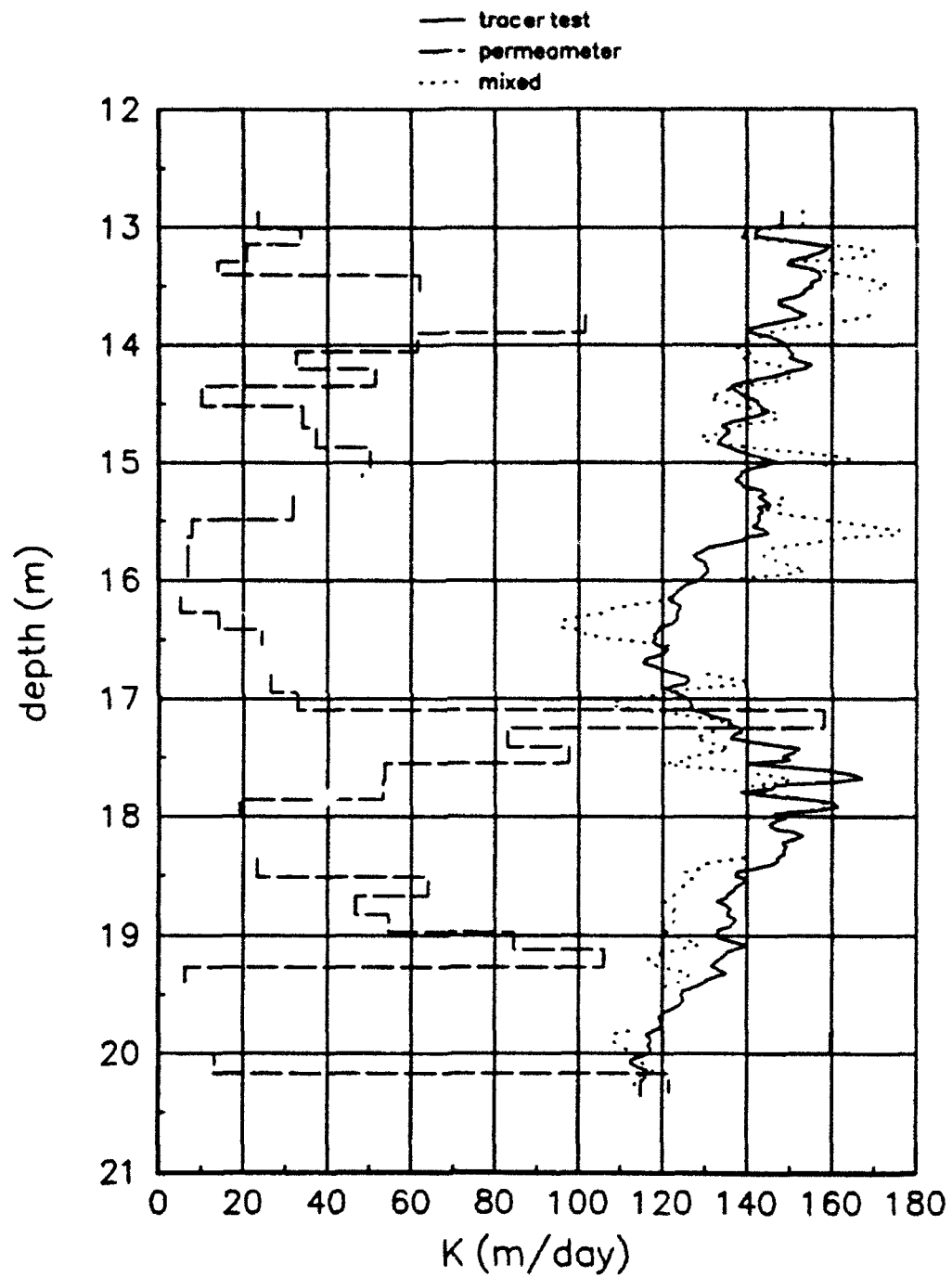


Figure 21. Hydraulic conductivity profiles for well 5-1. Permeameter data from Butler and McElwee (1994).

## **V. CONSTRUCTION PROJECTS AND EQUIPMENT PURCHASES**

### **Laboratory Equipment**

The laboratory apparatus for measuring hydraulic conductivity on sand and gravel cores was upgraded for greater efficiency and the number of stations doubled to eight during year two of this project. The backlog of sand and gravel samples to be run in the laboratory has been eliminated. All the stored cores have now been run except for the one well (TMO-1) that was cored May 5 and 6 of 1994. We project the lab work on the high conductivity cores from this well to be done by the end of summer.

Equipment to measure the hydraulic conductivity of low permeability samples, such as silt and clay, was acquired in previous project years. This equipment will allow us to measure the hydraulic conductivity of silt and clay samples that were acquired in year two from the upper 35 foot portions of four cored wells. In addition we have been saving some samples from the lower 35 foot region of sand and gravel that had a significant percentage of fine material. These samples were obtained with the bladder sampler in the lower region, but would not flow significantly when mounted in our permeameter designed for sand and gravel samples. The new equipment contains a flexible wall permeability cell which will handle sample sizes up to 4 inches. It is currently set up for 2.5 inch diameter samples; but, we have also equipped it for 1 3/8 inch samples. The system also includes a triaxial permeability panel for accurate measurement of volume changes and flow rates with regulators and burettes. In addition, the system has digital transducer readout with an RS-232 serial port for computer interface. We have gotten it set up and the appropriate supply lines such as air and water run, but have not yet begun measurements on the collected low conductivity samples. The plan is to complete the analysis of the sand and gravel cores before starting up the low permeability apparatus. We do not have sufficient personnel to run both simultaneously.

### **Field Equipment**

The single well tracer test work described in section IV.D required a mechanism to pump 2 inch PVC wells at high volumes (30-45 gal/min). It was determined that an air lifting arrangement would perform satisfactorily. Therefore, a 3 HP 230 volt air compressor was purchased. This compressor performed well and was used for the remediation phase of the single well tracer test work.

The work of section III.B dealing with nonlinear slug tests reveals that the response of these nonlinear slug tests depends on the magnitude of the initial slug. The

initial slug is usually placed on top of an inflated and closed packer. The packer is then opened and the response measured versus time. There is a continuing question of how important the packer is in all this. We wonder if some of the nonlinearity is due to frictional forces in the packer flow-through pipe. This pipe is the smallest diameter in the system and could be a significant agent of nonlinear head loss. To investigate this possibility we have built an alternate system of inducing slug tests using either pressurized gas (nitrogen) or a vacuum. Since the packer is absent, we can compare data from the same well with and without the packer to see if there is a significant difference. In building this apparatus it was necessary to buy a gas pressure transducer and a high accuracy gas pressure test gauge. Together, these allow the gas or vacuum pressures applied to the well to be measured very accurately. This system is operational and has been used to collect data twice in the field. However, the data analysis is very preliminary (some preliminary results are presented in section III.A) and additional field work needs to be done. We are confident that this system will be of great help to us in finishing the research on nonlinear slug testing.

A major focus of the effort during this project year has been to design and perform a tracer test at GEMS. This has required numerous purchases and construction projects. The area at GEMS chosen for the tracer test was north of nest 00 and the array is oriented a little west of the north-south line (see section II.C) approximately along the local groundwater gradient. This area is a bit lower than other areas and it tends to be wet for a considerable time after rains. We were concerned about our ability to develop the site for the tracer test in its original state. Therefore, we spent \$3000 on site preparation, bringing in fill dirt and large gravel. This expenditure was split between state and federal funding. The site is now accessible in almost all weather for light vehicles and can be accessed with heavy equipment soon after rains.

We have manufactured 24 MLS well casings to be used in the tracer monitoring array. Over 25,000 feet of 1/4 inch polyethylene tubing was used in constructing the 24 samplers and about 1680 feet of 1 1/4 inch PVC casing. Each MLS well has 17 ports connected to the surface by 1/4 inch polyethylene tubing. All seventeen of these tubes must be threaded (a difficult task) through each section (10 foot standard length) of PVC casing. There are two kinds of MLS wells as detailed in Figure 1; one has two feet spacing between ports (regular) and one has one foot spacing of ports (detailed). The regular samplers contain 5 ports in each of the first three sections of casing and 2 ports in the fourth section. The detailed samplers have 9 ports in the first section and 8 in the second section. These section divisions are shown in Figure 1. Originally, the 1/4 inch tubing was cut 5 feet longer than shown in Figure 1, for the purposes of construction.

The color sequence for the 1/4 inch tubing is a mirror image around port location 8; this was done to make the most efficient use of material from 500 foot reels.

The 1/4 inch tubes run through the center of the 1 1/4 inch casing and come out the side of the casing to form ports periodically ( every 2 feet for regular samplers and every 1 foot for detailed samplers). These ports are formed by about 3 inches of the 1/4 inch tubing protruding from the larger casing and tied to it with two stainless steel wires. The tubing has been cut at approximately a 45 degree angle and the end covered with a screen material consisting of a piece of nylon hose. The screen material is held in place by the two stainless steel wires which also secure the port to the larger casing. Figure 2 shows the details of a typical port in a schematic way.

After the hole has been drilled, an MLS well casing is lowered into place. The regular MLS well casings were cut back to 38 feet above the top port. The detailed MLS well casings were cut back to 53 feet above the top port. Generally, this left about a foot or less of 1 1/4 inch PVC casing sticking out of the ground. The 1/4 tubing was cut back to a convenient length (about 14 inches above the top of casing) and permanently labeled three ways to avoid confusion: First, the tubes are uniformly color coded for depth (as shown in Figure 1); Second, they are marked with a sequential port number (also shown in Figure 1); and Third, they are labeled with the depth below top of casing (also shown in Figure 1). The marking are done with a permanent marker and covered with clear heat shrink tubing for durability. For completion, the well tops are covered with 2 inch PVC casing using a water tight neopreme connector between the 1 1/4 inch and 2 inch PVC casings. All 24 MLS well casings have been manufactured but only 15 have been installed at this time.

We have purchased two ten-channel peristaltic pumps for pumping each of the 17 ports of each MLS well. This means that all ports on a given well can be pumped simultaneously. After the ports have been developed properly and are yielding 150 ml/min or more (all except 4 out of 255), it should be possible to sample one well completely in approximately 10 minutes allowing for sample storage and changeover time to the next well. During the tracer test it will be necessary to sample all affected wells several times during the duration of the tracer test. This necessity will make it imperative that we are able to complete sampling a given well in as little time as possible. This is the justification for buying two multichannel peristaltic pumps. To further improve our sampling efficiency we have built a cart to hold the pumps, the associated tubing, and the sample bottles. This cart is on wheels and can easily be pushed from one well to the next. The full sample bottles can be unloaded quickly from the sample bottle shelf and it can be reloaded with empty sample bottles rapidly. Ion specific electrodes

(ISE) have been purchased for rapid analysis of the water samples for the bromide tracer. However, the analyses will not be able to keep up with the sampling schedule, so some samples will need to be stored for later analysis. With this purchased and constructed equipment, we feel it will be possible to conduct the tracer test rapidly, efficiently, and with quality control.

### **Computer Laboratory**

A computationally intensive project like this one needs the benefit of state-of-the-art computers. A computer laboratory has been set up to give access to the computers for both research and teaching. We acquired three additional machines this year to upgrade our computing capabilities. Two 486 machines running at 66 MHz and easily upgradable to Pentium technology have been obtained this project year. The third machine purchased this project year is a Power Macintosh running at 80 MHz. The laboratory currently contains six computers: two 486 machine running at 66 MHz, two 486 machines running at 33 MHz, and two 386 machines running at 25 MHz. Some of our older 286 and 386 machines have been removed from the computer lab and have been used in the field or permeability lab for data acquisition. In the computer lab a network for printer sharing has been set up so that every computer has access to a high quality laser printer. Two laser printers are available in the computer laboratory. In addition, the Power Macintosh machine is available in the office of the PI and a 486 machine running at 33 MHz is used in the office of the CoPI. Each computer is connected to our mainframe computer (Data General machine) either by direct cable or through an Ethernet card. In this way each computer can act as a terminal into the mainframe and information can be shared between all systems. The computers with Ethernet cards are attached to the University Ethernet Backbone network. This connection allows direct access to the internet and many other computing networks across the US. Miscellaneous software has been purchased to allow the computers to function efficiently or perform specialized tasks.

**Figure 1.**  
**Polyethylene Tubing Detail**  
**Multilevel Sampler Construction**

Regular MLS Depth Below Top of Casing	Port number and Color		Detailed MLS Depth Below Top of Casing
70 feet	First Section	1. Natural	First Section 70 feet
68 "		2. Black	69 "
66 "		3. Blue	68 "
64 "		4. Green	67 "
62 "		5. Orange	66 "
60 "	Second Section	6. Red	65 "
58 "		7. Yellow	64 "
56 "		8. Natural	63 "
54 "		9. Yellow	62 "
52 "		10. Red	60 "
50 "	Third Section	11. Orange	59 "
48 "		12. Green	58 "
46 "		13. Blue	57 "
44 "		14. Black	56 "
42 "		15. Natural	55 "
40 "	Fourth Section	16. Natural	54 "
38 "		17. Natural	53 "

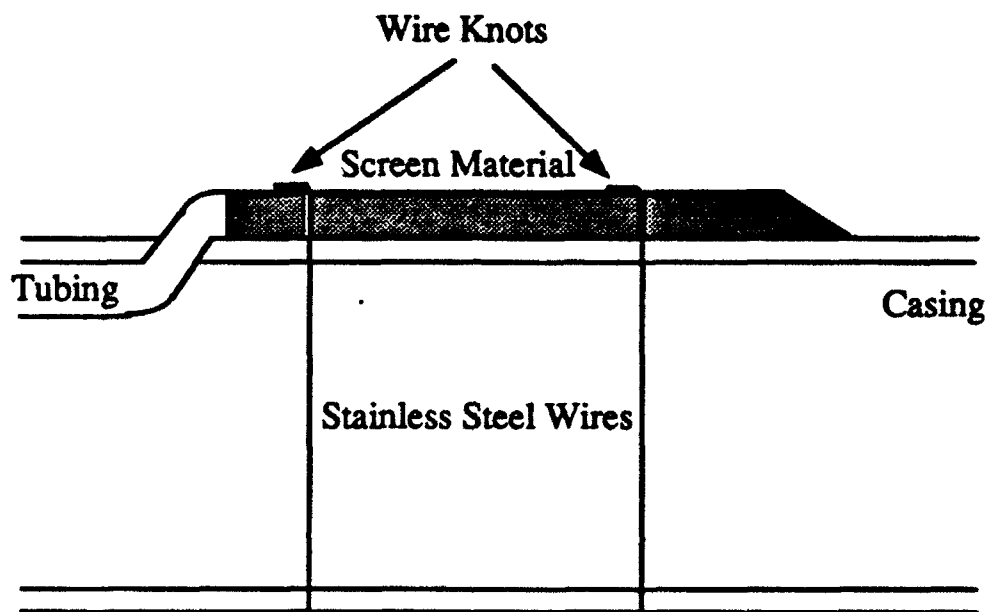


Figure 2. MLS Sampler port detail.

## **VI. PERSONNEL AND PRODUCTIVITY ISSUES**

### **A. PUBLISHED AND PLANNED PAPERS**

#### **Published Papers**

The following four papers were published or accepted for publication in this grant period by professional journals.

McElwee, C.D., Bohling, G.C., and Butler, J.J., Jr., Sensitivity analysis of slug tests: *Journal of Hydrology*, accepted for publication.

Hyder, Z., Butler, J.J., Jr., McElwee, C.D., and Liu, W.Z., Slug tests in partially penetrating wells, *Water Resources Research*., accepted for publication.

Butler, J.J., Jr., G.C. Bohling, Z. Hyder, and C.D. McElwee, The use of slug tests to describe vertical variations in hydraulic conductivity: *Journal of Hydrology*, v. 156, pp.137-162.

McElwee, C.D., Butler, J.J., Jr., Bohling, G.C., and Liu, W.Z., The use of observation wells with slug tests: *Journal of Hydrology*, accepted for publication.

The following three abstracts dealing with our DoD sponsored work were published this grant year. The material also exists as KGS open file reports.

McElwee, C.D., Zenner, Z., Butler, J.J., Jr. and Bohling, G.C., 1993, Unified analysis of slug tests including nonlinearities, inertial effects and turbulence: *Eos, Trans. Amer. Geophys. Union*, v. 74, no. 43, p. 235. Also KGS Open-File Report no. 93-45, 23 pp..

Huettl, T.J., Butler, J.J., Jr., and McElwee, C.D., 1993, A borehole induction single-well tracer test to characterize spatial variations in aquifer flow properties: *Eos, Trans. Amer. Geophys. Union*, v. 74, no. 43, p. 319. Also KGS Open-File Report no. 93-48, 19 pp.

Butler, J.J., Jr. and McElwee, C.D., 1994, Improving the reliability of parameter estimates obtained from slug tests: *Eos, Trans. Amer. Geophys. Union*, v. 75, no. 16, p. 151. Also KGS Open-File Report no. 94-21, 29 pp.

#### **Papers Submitted for Publication**

The following papers have been or very soon will be submitted for publication in professional journals.

Bohling, G.C. and McElwee, C.D., Hydraulic tomography in two-dimensional groundwater flow: has been submitted to *Water Resources Research*..

McElwee, C.D., Zenner, Z., Butler, J.J., Jr. and Bohling, G.C., Unified analysis of slug tests including nonlinearities, inertial effects and turbulence: to be submitted to *Water Resources Research*..



Butler, J.J., Jr. and McElwee, C.D., Improving the reliability of parameter estimates obtained from slug tests: to be submitted to *Ground Water*.

#### **Papers Planned or in Preparation**

The following papers are planned for future publication in professional journals. Currently they exist as informal Kansas Geological Survey Open File Reports.

Liu and Butler, A time-continuous numerical model for well tests in heterogeneous aquifers, *Journal of Hydrology*.

McElwee, C.D. and Butler, J.J., 1992, Effective Transmissivities from slug tests in wells with a skin: KGS Open-File Report no. 92-12, 31 pp.

#### **B. LIST OF PARTICIPATING PERSONNEL**

McElwee, C.D.- PI, is a Senior Scientist at the Kansas Geological Survey ( KGS) in the Mathematical Geology Section and is also an Adjunct Professor in the Geology and Physics Departments of the University of Kansas (KU).

Butler, J.J. Jr. - Co-PI, is an Associate Scientist at the KGS in the Geohydrology Section and is also an Adjunct Assistant Professor in the KU Geology Department.

Bohling, G.C. - Investigator, is a Research Assistant in the Mathematical Geology Section at KGS.

Macpherson, G.L. - Investigator, is an Assistant Professor in the KU Geology Department.

The following three students have been fully supported by this grant.

Mennicke, C.M. - was a student Research Assistant in the Mathematical Geology Section at KGS and is working on a Ph.D. degree in the KU Geology Department. She is currently employed by the Kansas Department of Health and Environment.

Huettl, T. - was a student Research Assistant in the Mathematical Geology Section at KGS and has finished a Master's degree in the KU Geology Department.

Beilfuss, M.L.- is a student hourly employee who is an undergraduate student in the KU Geology Department.

The following students have contributed to this work in substantial ways, however they have not been primarily supported by this grant.

Liu, W. - is a student Research Assistant in the Geohydrology Section at KGS and is working on a Ph.D. degree in the KU Civil Engineering Department.

Hyder, Z. - is a student Research Assistant in the Mathematical Geology Section at KGS and is working on a Ph.D. degree in the KU Civil Engineering Department.

Zenner, M. - is a student Research Assistant in the Geohydrology Section at KGS and is working on a Ph.D. degree in the KU Civil Engineering Department.

Orcutt, M. - is a student Research Assistant in the Geohydrology Section at KGS and is working on a Master's degree in the Architectural Engineering Department at KU.

### **C. INTERACTIONS WITH OTHER RESEARCH GROUPS**

#### **Professional Meetings Attended and Papers Presented**

Carl McElwee attended the National Convention of the National GroundWater Association, Kansas City, MO, Oct. 17-20, 1993.

Carl McElwee, Jim Butler, Terrance Huettl, and Zafar Hyder attended the Fall AGU (American Geophysical Union) meeting in San Francisco in December 93 and gave three papers:

McElwee, C.D., Zenner, Z., Butler, J.J., Jr. and Bohling, G.C., 1993, Unified analysis of slug tests including nonlinearities, inertial effects and turbulence: *Eos, Trans. Amer. Geophys. Union*, v. 74, no. 43, p. 235. Also KGS Open-File Report no. 93-45, 23 pp..

Hyder, Z., Butler, J.J., Jr., and, McElwee, C.D., 1993, An approximate technique for analysis of slug tests in wells screened across the water table: *Eos, Trans. Amer. Geophys. Union*, v. 74, no. 43, p. 235. Also KGS Open-File Report no. 93-44, 25 pp.

Huettl, T.J., Butler, J.J., Jr., and McElwee, C.D., 1993, A borehole induction single-well tracer test to characterize spatial variations in aquifer flow properties: *Eos, Trans. Amer. Geophys. Union*, v. 74, no. 43, p. 319. Also KGS Open-File Report no. 93-48, 19 pp.

Jim Butler attended the Spring AGU meeting in Baltimore in May 94 and gave the paper:

Butler, J.J., Jr. and McElwee, C.D., 1994, Improving the reliability of parameter estimates obtained from slug tests: *Eos, Trans. Amer. Geophys. Union*, v. 75, no. 16, p. 151. Also KGS Open-File Report no. 94-21, 29 pp.

#### **University of Nebraska Research Group**

Dr. Vitaly Zlotnik is the leader of a research group working on well testing at the University of Nebraska at Lincoln. Jim Butler and Carl McElwee have had numerous discussions throughout the year with Dr. Zlotnik and his graduate students on various issues related to slug tests in alluvial aquifers. Carl McElwee was invited to give a talk on his recent work involving nonlinear slug test analysis on Feb. 18, 1994

#### **D. TEACHING ACTIVITIES**

In conjunction with the tracer test work we taught a seminar course called Geol 791, Dispersivity and Tracer Tests at GEMS for 3 hours credit. We had 3 students sign up for credit; but, numerous people audited the course including students and permanent staff at KGS. The course consisted of reviewing the groundwater literature on various aspects of tracer tests and practical application in the form of construction and installation of the MLS well casings.

The computer laboratory is used by our research group and other geohydrology graduate students. The computer laboratory allows hands on computer training to geohydrology graduate students through formal class work. We have taught two classes: Physics 727/Geology 771, Finite Difference Methods, fall semester 1993 (4 students), and Physics 727/Geology 771, Finite Element Methods, spring semester 1994 (5 students). In addition, we have made the laboratory available for other computer oriented classes taught by other hydrogeology faculty members. We expect this computer laboratory to continue to be a valuable asset to our research and graduate education in geohydrology.

## **VII. SUMMARY OF YEAR THREE RESEARCH AND OUTLOOK FOR THE EXTENSION PERIOD**

### **A. SUMMARY OF RESEARCH IN YEAR THREE**

There were two major thrusts of research in the third year of this project: 1) the use of well tests to describe spatial variations in hydraulic conductivity, and 2) preparation for a series of induced-gradient tracer tests at GEMS. The research in both areas had theoretical and field components.

The theoretical work on well tests was directed at developing a better understanding of the type of information that can be obtained from well tests in heterogeneous media. In order to assess the error that is introduced into parameter estimates by employing conventional methods for the analysis of data from slug tests performed in configurations not strictly addressed in the derivation of those methods, a semianalytical solution to a general mathematical model describing the flow of groundwater in response to a slug test was developed. This model incorporates the effects of partial penetration, anisotropy, finite-radius well skins, and upper and lower boundaries of either a constant-head or an impermeable form. This model was employed to develop a series of dimensionless plots that can be utilized by field practitioners to assess the amount of error introduced into parameter estimates through use of a particular method for data analysis. If it appears that conventional approaches will not provide acceptable parameter estimates for a test in a particular configuration, the semianalytical solution developed here can be used to analyze the response data. Theoretical work on pulse testing was carried out this year to extend the results obtained during the second year of this project. Both analytical and numerical approaches were explored in an attempt to assess whether discrete zones in heterogeneous formations could be characterized with pulsing (in this case sinusoidally varying) signals. There were two major results of this work: 1) a sinusoidal signal generated at a central well can be transmitted quite large distances relative to the dimensions of most sites of groundwater contamination, and 2) the sinusoidal signal can be analyzed for amplitude and phase to yield some useful information about heterogeneities, in particular the location of fairly discrete boundaries.

This year, the field components of this investigation of well tests in heterogeneous formations again concentrated on slug tests. Although the slug test has the potential to provide very useful information about the transmissive and storage properties of a formation, considerable care must be given to all phases of test design, performance, and

analysis if the potential of the technique is to be fully realized. In an attempt to improve the reliability of parameter estimates obtained from a program of slug tests, a series of practical guidelines for slug tests were proposed on the basis of the field and theoretical investigations of this research. Two very important points arise from this series of guidelines: 1) it is critical that a series of slug tests at a given well be performed in order to assess whether conventional theory is applicable (i.e. is there a dependence on initial head or mechanism of test initiation, is there a well skin that is developing during the course of testing, etc.); and 2) the analysis of the response data must be done using the most appropriate model and with considerable care. Results of slug tests at most of the wells in the alluvial aquifer at the Geohydrologic Experimental and Monitoring Site (GEMS) indicate that tests in the sand and gravel section at GEMS are being affected by mechanisms not accounted for in the conventional theory on which the standard methods for slug-test data analysis are based. This year, we have developed a general unified model incorporating the effects of nonlinearities, inertia, viscosity, changing casing radii, and velocity distributions to explain the anomalous behavior observed at GEMS. Although the effects of viscosity and changing casing radii are negligible in most cases, the effects of nonlinearities, inertia, and velocity distributions can be quite important. Application of this model to several sets of data from slug tests at GEMS produced very promising results.

The second major thrust of the work of the third year of this research involved preparation for a series of induced-gradient tracer tests to be performed at GEMS in late summer and fall of 1994. Twenty-four multilevel sampling wells (17 sampling ports per well) were constructed and fifteen of these wells were installed during an intensive field effort in the spring of 1994. Sampling well locations were based on a theoretical investigation of appropriate designs for the tracer-test monitoring well array. Various designs were assessed using a numerical streamline-tracing algorithm that was coupled with an analytical solution for the simulation of conservative transport along streamlines. The final design was a compromise between theoretical considerations and operational logistics (e.g., the minimum well spacing dictated by the size of the drilling rig, etc.).

As in the first two years of this research, a significant amount of the work in year three was directed at increasing our knowledge of the subsurface at GEMS. This work included continued drilling and sampling activities at GEMS; continued laboratory analysis of the cores obtained with the KGS bladder sampler; a continuing study of the aqueous geochemistry of the alluvium and underlying bedrock at GEMS; and experimentation with a new single-well tracer test method that involves using a wireline logging system and an electrically conductive tracer to delineate vertical variations in

hydraulic conductivity and porosity. These characterization efforts, which have continued throughout this project, are directed towards the development of a detailed picture of the subsurface at GEMS, so that we can better assess the results of the hydraulic and tracer tests that are being performed as part of this research.

A considerable amount of acquisition, construction, and modification of equipment took place during the third year of this project in support of the research effort. The purchased equipment included a high capacity air compressor for pumping small-diameter wells, two 10-channel peristaltic pumps for water-quality sampling, and three additional computers for data processing and analysis. A considerable amount of equipment for field and laboratory use was also constructed during the third year of this project. The constructed equipment included a field cart to hold the peristaltic pumps and associated equipment during sampling, and a well-head apparatus for the performance of pressurized slug tests. In addition, as a result of the prolonged waterlogging of GEMS that occurred due to the heavy rains in the spring and summer of 1993, access to all portions of GEMS was significantly improved during this year. Fill dirt was added and the site was leveled and covered with gravel to provide an all-weather surface.

## **B. OUTLOOK FOR RESEARCH IN THE EXTENSION PERIOD**

The primary purpose of the work in the requested extension period will be to bring this phase of our research on the characterization of spatial variations in hydraulic conductivity to a satisfactory conclusion. The research planned for the extension period can be classified into four major activities: 1) the preparation for and performance of an initial series of induced-gradient tracer tests at GEMS, 2) completion of the analysis of all remaining core samples from GEMS, 3) completion of the field verification of the general unified model for the analysis of slug tests performed in formations of high hydraulic conductivity, and 4) completion of the first phase of the field investigation of pulse tests. In the following paragraphs, each of these planned activities is briefly described. As with the research of the earlier years of this project, the ultimate goal of all of these activities is to improve our present capabilities for the prediction of contaminant movement in shallow alluvial aquifers.

The objective of the initial series of induced-gradient tracer tests at GEMS is to assess the utility of information obtained from various types of well tests for the prediction of the movement of a conservative tracer in a heterogeneous formation. Prior to the performance of the tracer tests, the remaining nine multilevel sampling wells and an injection and discharge well pair must be installed in the monitoring well array. The first of this initial series of tracer tests, all of which will employ a bromide tracer, is

planned for August of 1994. A number of additional pulse- and continuous-injection tracer tests are planned for the fall of 1994. The results of this first series of tests will be reported on at a Special Session entitled "Recent Field Experiments for the Investigation of Transport Processes in Heterogeneous Sand and Gravel Aquifers" at the Fall American Geophysical Union Meeting in San Francisco in early December. Although this first series of tests will employ a conservative tracer and is directed at assessing the utility of information obtained from well tests, future research is planned using tracers of different chemical mobility and biological susceptibility in order to assess how chemical and microbial processes are affected by formation heterogeneity. The network of multilevel sampling wells that is being established in this work should prove to be an excellent resource for future research and teaching activities in hydrogeology at the University of Kansas.

The second objective of work in the extension period will be to complete the laboratory analysis of all the core samples obtained from drilling at GEMS. The current laboratory permeameter is designed for cores of moderate to high permeability as a result of the coarse nature of the sediments that comprise the majority of the sand and gravel interval at GEMS. However, a considerable number of the core samples from GEMS are of quite low permeability. In order to analyze these cores, the recently purchased low-permeability permeameter apparatus must be made operational. It is important that reliable estimates of the hydraulic conductivity of core samples from the less-transmissive intervals be obtained so that we have a complete picture of the variability in hydraulic conductivity that exists in the subsurface at GEMS. An accurate characterization of the spatial variability at the scale of a core is an essential first step in developing an understanding of the relationship between measurement scale and spatial variations in effective flow parameters, which is an important long-term goal of this research.

The third objective of work in the extension period will be to complete the field verification of the general unified model for the analysis of slug tests performed in formations of high hydraulic conductivity. Although the theoretical work on the unified nonlinear slug-test model is nearing completion, we still need to do considerably more field work to further evaluate the proposed theory. An extensive series of field tests will be done in late summer and early fall of this year in order to thoroughly assess model performance under a wide range of conditions. The completion of the field verification of this model is a critical step in this research as it will allow us to obtain reliable estimates of hydraulic conductivity on the scale of a slug test.

The final objective of work in the extension period will be to complete the first phase of the field investigation of pulse tests. Although we have done considerable theoretical work on pulse tests in heterogeneous media, we have done relatively little field work as a result of the slug-test phase of this research taking considerably more time than originally planned. In the extension period, we will complete field work on the simplest form of pulse testing, the multiwell slug test. In addition, we plan to complete an initial evaluation of pulse-testing schemes involving the generation of a string of multiple pulses. In this work, we will examine if reliable pulsing signals can be produced and how far they can be propagated. Although this work will be a quite limited examination of pulse tests, we should be able to demonstrate the potential of the technique for use in estimation of flow properties at sites of groundwater contamination. Further research, however, will be required to thoroughly assess the potential of the approach.



## VIII. REFERENCES

- Allen, J.R.L., 1965, Fining-upward cycles in alluvial successions: *Geological Jour.*, v. 4, pp. 229-246.
- Amoozegar, A., and Warrick, A. W., 1986, Hydraulic conductivity of saturated soils: Field methods: in *Methods of Soil Analysis, Part 1, Physical and Mineralogical Methods*, Agronomy Monograph Series 9, edited by A. Klute, pp. 735-770, American Soc. of Agronomy, Madison, Wi.
- Archie, G.E., 1942, Electrical resistivity log as an aid in determining some reservoir characteristics: *Trans.*, AIME 146.
- Bateman, R.M., 1985, *Open-Hole Log Analysis and Formation Evaluation*: IHRDC, Boston, MA, 647 pp.
- Blatt, H., Middleton, G., and Murrey, R., 1980, *Origin of Sedimentary Rocks*: Prentice-Hall, Englewood, NJ, 782 pp.
- Bliss, J.C., and K.R. Rushton, 1984, The reliability of packer tests for estimating the hydraulic conductivity of aquifers: *Quart. Jour. of Eng. Geol.*, v. 17, pp. 81-91.
- Boggs, J.M., Young, S.C., Hemond, H.F., Richardson, L., and Schaefer, M.E., 1988, Evaluation of tracer sampling devices for the macrodispersion experiment: Electric Power Research Institute (EPRI), Research Project 2485-5, Interim Report.
- Bohling, G.C. and McElwee, C.D., 1992, SUPRPUMP: An interactive program for well test analysis and design: *Ground Water*, v. 30, no. 2, pp. 262-268.
- Bouwer, H. and Rice, R.C., 1976, A slug test for determining hydraulic conductivity of unconfined aquifers with completely or partially penetrating wells: *Water Resour. Res.*, v. 12, no. 3, pp. 423-428.
- Bouwer, H., 1989, The Bouwer and Rice slug test - an update: *Ground Water*, v. 27, no. 3, pp. 304-309.
- Brigham, E. O., 1974, *The Fast Fourier Transform* : Prentice-Hall, Inc, Englewood Cliffs, New Jersey, 252 pp.
- Butler, J.J., Jr., 1990, The role of pumping tests in site characterization: Some theoretical considerations: *Ground Water*, v. 28, no. 3, pp. 394-402.
- Butler, J.J., Jr., 1994, The effect of well-construction parameters on slug tests: Kansas Geological Survey Open-File Rept. 94-27.
- Butler, J.J., Jr., and McElwee, C.D., 1990, Hydrogeologic characterization of hazardous waste sites: Kansas Water Resources Research Inst. Contribution No. 283, 114 pp.
- Butler, J.J., Jr. and Hyder, Z., 1993, An assessment of the Nguyen and Pinder method for slug test analysis: Kansas Geological Survey Open-File Rept. 93-46, 25 pp. (also in press at Ground Water Monitoring and Remediation).

- Butler, J.J., Jr. and Liu, W.Z., 1994, Analysis of 1991-1992 slug tests in the Dakota Aquifer of central and western Kansas: Kansas Geological Survey Open-File Rept. 93-1C.
- Butler, J.J., Jr., Liu, W.Z., and Young, D.P., 1993a, Analysis of October, 1993 slug tests in Stafford, Pratt, and Reno counties, south-central Kansas: Kansas Geological Survey Open-File Report 93-52, 70 pp.
- Butler, J.J., Jr., McElwee, C.D., and Hyder, Z., 1993b, Slug tests in unconfined aquifers: Kansas Water Resources Research Inst. Contribution No. 303, 67 pp.
- Butler, J.J., Jr., McElwee, C.D., and Hyder, Z., 1994, Slug tests in unconfined aquifers - year two: Kansas Water Resources Research Inst. Contribution No. 310, Manhattan, Ks.
- Butler, J.J., Jr., Bohling, G.C., Hyder, Z., and McElwee, C.D., 1994a, The use of slug tests to describe vertical variations in hydraulic conductivity: *Jour. of Hydrology*, v. 156, pp. 137-162.
- Butler, J.J., Jr., McElwee, C.D., Mennicke, M., Hyder, Z., Liu, W., Orcutt, M., 1994, Well-testing methodologies for characterizing heterogeneities in alluvial-aquifer systems: Second year report: Kansas Geological Survey Open-File Report 94-16, 171 pp.
- Century Geophysical Corp., unpublished, Report describing the design and test of a prototype four coil slim induction tool, Century Geophysical Corp., Tulsa, OK, 12 pp.
- Chirlin, G.R., 1989, A critique of the Hvorslev method for slug test analysis: The fully penetrating well: *Ground Water Monitoring Review*, v. 9, no. 2, pp. 130-138.
- Chirlin, G.R., 1990, The slug test: the first four decades: *Ground Water Management*, v. 1, pp. 365-381.
- Churchill, R.V., 1972, *Operational Mathematics*, McGraw Hill, New York, 481 pp.
- Cooley, J. W., and Tukey, J. W., 1965, An algorithm for machine calculations of complex Fourier series: *Math. Computation*, v. 19, pp. 297-301.
- Cooper, H.H., Bredehoeft, J.D., and Papadopoulos, I.S., 1967, Response of a finite-diameter well to an instantaneous charge of water: *Water Resour. Res.*, v. 3, no.1, pp. 263-269.
- Dagan, G., 1978, A note on packer, slug, and recovery tests in unconfined aquifers: *Water Resour. Res.*, v. 14, no. 5, pp. 929-934.
- Dahl, S. and Jones J., 1993, Evaluation of slug test data under unconfined conditions with exposed screens, and low permeability filter pack: Proc. of the 7th National Outdoor Action Conf, NGWA, pp. 609-623.
- Davis, S.N., and Carlson, W.A., 1952, Geology and ground-water resources of the Kansas River valley between Lawrence and Topeka, Kansas: Kansas Geological Survey Bull. 96, pp. 201-276.

- Dax, A., 1987, A note on the analysis of slug tests: *Jour. of Hydrology*, v. 91, pp. 153-177.
- Dewan, J.T., 1983, *Essentials of Modern Open-Hole Log Interpretation*: Pennwell Books, Tulsa, OK, 361 pp.
- Dobrin, M.B., and Savit, C.H., 1988, *Introduction to Geophysical Prospecting*: McGraw-Hill, Inc., N.Y., NY, 842 pp.
- Dougherty, D.E., and Babu, D.K., 1984, Flow to a partially penetrating well in a double-porosity reservoir: *Water Resour. Res.*, v. 20, no. 8, pp. 1116-1122.
- Ellis, D.V., 1987, *Well Logging For Earth Scientists*: Elsevier Science Publishing Company, Inc., N.Y., NY, 519 pp.
- Eskinazi, S., 1967, *Vector Mechanics of Fluids and Magnetofluids*: Academic Press, New York, pp. 194-206.
- Fogler, H. S., and Vaidya, R.N., 1993, Effects of pH on fines migration and permeability reduction: in *Manipulation of Groundwater Colloids for Environmental Restoration*, J. F. McCarthy and F. J. Wobber (eds.), pp. 123-128.
- Freeze, R.A., and Cherry, J.A., 1979, *Groundwater*: Prentice-Hall, Inc., Englewood Cliffs, NJ, 604 pp.
- Haberman, R., 1987, *Elementary Applied Partial Differential Equations*: Prentice-Hall, Inc., Englewood Cliffs, N.J., 547 pp.
- Hackett, G., 1987, Drilling and constructing monitoring wells with hollow-stem augers Part 1: Drilling considerations: *Ground Water Monitoring Review*, v. VII, no. 4, pp. 51-62.
- Hansen, A.G., 1967, *Fluid Mechanics* : John Wiley and Sons, Inc., New York, pp. 134-137.
- Hantush, M. S., and Jacob, C. E., 1955, Non-steady radial flow in an infinite leaky aquifer: *Transactions, American Geophysical Union*, v. 36, no. 1, pp. 95-100.
- Hayashi, K., Ito, T., and Abe, H., 1987, A new method for the determination of in situ hydraulic properties by pressure pulse tests and application to the Higashi Hachimantai geothermal field: *J. Geophys. Res.*, v. 92, no. B9, pp. 9168-9174.
- Herzog, B.L., 1994, Slug tests for determining hydraulic conductivity of natural geologic deposits: in *Hydraulic Conductivity and Waste Contaminant Transport in Soils*, D.E. Daniel, and S.J. Trautwein (Editors), ASTM STP 1142, American Society for Testing and Materials.
- Huettl, T.J., 1994, An evaluation of a borehole induction single-well tracer test to characterize the distribution of hydraulic properties in an alluvial aquifer: Master's Thesis, Dept. of Geol., Univ. of Kansas, Lawrence, Ks.

- Huettl, T.J., Butler, J.J., Jr., McElwee, C.D., 1993, A borehole induction single-well tracer test to characterize spatial variations in aquifer flow properties: Kansas Geological Survey Open-File Report 93-48, 19 pp.
- Hvorslev, M.J., 1951, Time lag and soil permeability in ground-water observations, Bull no. 36, Waterways Exper. Sta., Corps of Engrs., U.S. Army, 50 pp.
- Hyder, Z., 1994, Analysis of slug tests in partially penetrating wells, Ph.D. thesis, Dept. of Civil Eng., Univ. of Kansas, Lawrence, Ks.
- Hyder, Z., and J.J. Butler, Jr., 1994, Slug tests in unconfined formations: An assessment of the Bouwer and Rice technique: *Ground Water*, in press.
- Hyder, Z., Butler, J.J., Jr., and McElwee, C.D., 1993, An approximate technique for analysis of slug tests in wells screened across the water table (abstract): *EOS*, v. 74, no. 43, p. 235.
- Hyder, Z., Butler, J.J., Jr., McElwee, C.D., and Liu, W.Z., 1994 Slug tests in partially penetrating wells: *Water Resour. Res.*, in press.
- Hyder, Z., Liu, W.Z., and Butler, J.J., Jr., 1993, Software for the evaluation of semianalytical solutions for slug tests in partially penetrating wells: KGS Comput. Program Ser. 93-1, Kansas Geol. Survey, 42 pp.
- Jackson, P.D., Taylor-Smith, D., and Stanford, P.N., 1978, Resistivity-porosity-particle shape for marine sands: *Geophysics*, v. 43, no. 6, pp. 1250-1268.
- Kabala, Z.J., Pinder, G.F., and Milly, P.C.D., 1985, Analysis of well-aquifer response to a slug test: *Water Resour. Res.*, v. 21, no.9, pp. 1433-1436.
- Keely, J.F., and Boateng K., 1987, Monitoring well installation, purging and sampling techniques, Part 1: Conceptualizations: *Ground Water*, v. 25, no. 3, pp. 300-313.
- Kipp, K.L., Jr., 1985, Type curve analysis of inertial effects in the response of a well to a slug test: *Water Resour. Res.*, v. 21, no.9, pp. 1397-1408.
- Kreyszig, E., 1983, *Advanced Engineering Mathematics*: John Wiley and Sons, New York, pp. 75-81.
- Kruseman, G.P., and de Ridder, N.A., 1990, *Analysis and Evaluation of Pumping Test Data*, International Institute for Land Reclamation and Improvement, Wageningen, The Netherlands, 287 pp.
- Kruseman, G.P., and de Ridder, N.A., 1989, *Analysis and Evaluation of Pumping Test Data* - ILRI publication 47, 377 pp., ILRI, The Netherlands.
- Levy, B.S. and Pannell, L., 1991, Evaluation of a pressure system for estimating in-situ hydraulic conductivity: Proc. of the 5th National Outdoor Action Conf, NWWA, pp. 131-146.
- Mackay, D.M., Freyberg, D.L., McCarthy, P.L., Roberts, P.V., and Cherry, J.A., 1986, A natural gradient experiment on solute transport in a sand aquifer, 1, Approach and overview of plume movement: *Water Resour. Res.*, v. 22, no. 13, pp. 2017-2029.

- Macpherson, G. L., and M. K. Schulmeister, 1994, Source(s), fate and residence time of nitrate in ground water at two sites in Kansas—A comparison of carbonate and alluvial aquifers: Kansas Water Resources Research Institute Report No. C2020-08, Contribution No. 312, 81 p.
- McElwee, C. D. and Butler, J.J., Jr., 1989, Slug testing in highly permeable aquifers (abstract): GSA 1989 Annual Meeting Abstracts with Program, p. A193.
- McElwee, C.D., and Butler, J.J., Jr., 1992, Effective transmissivities from slug tests in wells with a skin, Kansas Geol. Survey, Open-File Rept. 92-12, 31 pp.
- McElwee, C.D. and Butler, J.J., Jr., 1992, Characterization of heterogeneities controlling transport and fate of pollutants in unconsolidated sand and gravel aquifers: First year report: Project Report to Air Force Office of Scientific Research, University Research Initiative, Research Initiation Program, U.S. Dept. of Defense, Kansas Geological Survey Open-File Report 92-20, 209 pp.
- McElwee, C.D. and Butler, J.J., Jr., 1993, Characterization of heterogeneities controlling transport and fate of pollutants in unconsolidated sand and gravel aquifers: Second year report: Project Report to Air Force Office of Scientific Research, University Research Initiative, Research Initiation Program, U.S. Dept. of Defense, Kansas Geological Survey Open-File Report 93-21, 221 pp.
- McElwee, C. D., Bohling, G. C., and J. J. Butler, Jr., 1989, Sensitivity analysis of slug tests: Kansas Geological Survey, Open-File Report 89-33, 29 pp.
- McElwee, C.D., Butler, J.J., Jr., and Healey, J.M., 1991, A new sampling system for obtaining relatively undisturbed samples of unconsolidated coarse sand and gravel: *Ground Water Monitoring Review*, v. 11, no. 3, pp. 182-191.
- McElwee, C.D., Butler, J.J., Jr., Bohling, G.C., and Liu, W.Z., 1991, The use of observation wells with slug tests: Kansas Geological Survey, Open-File Report 91-63, 32 pp.
- McElwee, C.D., Butler, J.J., Jr., and Bohling, G.C., 1992, Nonlinear analysis of slug tests in highly-permeable aquifers using a Hvorslev-type approach: *Eos*, v. 73, no. 43, p. 164. Also Kansas Geologic Survey, Open File Report 92-39, 22 pp.
- McLane, G.A., Harrity, D.A., and Thomsen, K.O., 1990, A pneumatic method for conducting rising and falling head tests in highly permeable aquifers: Proc. of 4th Annual NWWA Outdoor Action Conf. , pp. 1219-1231.
- Minning, R.C. , 1982, Monitoring well design and installation: Proceedings of the Second National Symposium on Aquifer Restoration and Ground Water Monitoring, Columbus, Ohio, pp. 194-197.
- Moench, A., and Ogata, A., 1984, Analysis of constant discharge wells by numerical inversion of Laplace transform solutions, in: Rosenshein, J., and Bennett, G.D., ed., *Groundwater Hydraulics*, AGU Water Resour. Monogr. 9, AGU, Washington, DC., pp. 146-170.
- Moench, A.F., and Hsieh, P.A., 1985, Analysis of slug test data in a well with finite-thickness skin: in *Memoirs of the 17th Intern. Cong. on the Hydrogeology of Rocks of Low Permeability*, v. 17, pp. 17-29.

- Molz, F.J., Guven, O., and Melville, J.G., 1989, Characterization of the hydrogeologic properties of aquifers: The next step: in: *Proc. of the Conf. on New Field Techniques for Quantifying the Physical and Chemical Properties of Heterogeneous Aquifers*, National Water Well Association, pp. 407-418.
- Morin, R.H., LeBlanc, D.R., and Teasdale, W.E., 1988, A statistical evaluation of formation disturbance produced by well-casing installation methods: *Ground Water*, v. 26, no. 2, pp. 207-217.
- Nguyen, V., and Pinder, G.F., 1984, Direct calculation of aquifer parameters in slug test analysis: in *Groundwater Hydraulics*, J. Rosenshein and G.D. Bennett (Editors), AGU Water Resour. Monogr. No. 9, pp. 222-239.
- Novakowski, K.S., 1989, Analysis of pulse interference tests: *Water Resour. Res.*, v. 25, no. 11, pp. 2377-2387.
- Orient, J.P., Nazar, A., and Rice, R.C., 1987, Vacuum and pressure test methods for estimating hydraulic conductivity: *Ground Water Monitoring Review*, v. 7, no. 1, pp. 49-50.
- Osborne, P.S., 1993, Suggested operating procedures for aquifer pumping tests: EPA/540/S-93/503. U.S. EPA, Office of Research and Development, 23 pp.
- Perry, C.A. and Hart, R.J., 1985, Installation of observation wells on hazardous waste sites in Kansas using a hollow-stem auger: *Ground Water Monitoring Review*, v. V, no. 4, pp. 70-73.
- Pickens, J.F., Cherry, J.A., Grisak, G.E., Merritt, W.F., and Risto, B.A., 1978, A multilevel device for ground-water sampling and piezometric monitoring: *Ground Water*, v. 16, no. 5, pp. 322-327.
- Pollock, D. W., 1988, Semianalytical computation of path lines for finite-difference models: *Ground Water*, v. 26, no. 6, pp. 743-750.
- Press, W.H., Teukolsky, S.A., Vetterling, W.T., and Flannery, B.P., *Numerical Recipes in FORTRAN*, Cambridge Univ. Press, Cambridge, UK, 963 pp.
- Sageev, A., 1986, Slug test analysis: *Water Resour. Res.* v. 22, no. 8, pp. 1323-1333.
- Saito, A., 1982, Theory and application of induction logging for civil engineering: unpublished Masters Thesis, Colorado School of Mines, Golden, CO, 69 pp.
- Schafer-Perini, A. L., and Wilson, J.L., 1991, Efficient and accurate front tracking for two-dimensional groundwater flow models: *Water Resources Research*, v. 27, no. 7, pp. 1471-1485.
- Schlumberger, 1989, *Log Interpretation/Applications*, Schlumberger Educational Services, Houston, TX, 227 pp.
- Stehfest, H., 1970, Numerical inversion of Laplace transforms: *Commun. ACM.*, v. 13, no. 1, pp. 47-49.

- Stites, W., and Chamber, L., 1991, A method for installing miniature multilevel sampling wells: *Ground Water*, v. 29, no. 3, pp. 430-432.
- Stone, D.B. and Clarke, G.K.C., in press, Estimation of subglacial hydraulic properties from induced changes in basal water pressure: a theoretical framework for borehole response tests: *J. of Glaciology*.
- Streitsova, T.D., 1988, *Well Testing in Heterogeneous Formations*: John Wiley & Sons, Inc., New York, 413 pp.
- Taylor, K., and Molz, F., 1990, Determination of hydraulic conductivity and porosity logs in wells with a disturbed annulus: *Jour. of Contaminant Hydrology*, no. 5, pp. 317-332.
- Taylor, K., Wheatcraft, S., Hess, J., and Molz, F., 1990, Evaluation of methods for determining the vertical distributions of hydraulic conductivity: *Ground Water*, v. 28, no.1, pp. 88-98.
- U.S. Dept. of Navy, Bureau of Yards and Docks, 1961, Design Manual, Soil Mechanics, Foundations, and Earth Structures, DM-7, Chap. 4.
- Voss, C.I., 1984, A Finite-Element Simulation Model for Saturated-Unsaturated, Fluid-Density-Dependent Ground-Water Flow with Energy Transport or Chemically-Reactive Single-Species Solute Transport: U.S. Geological Survey, National Center, Reston, Virginia. Prepared in Cooperation with U.S. Air Force Engineering And Service Center, Tyndall A.F.B., Florida.
- Welty, C., and Gelhar, L.W., 1994, Evaluation of longitudinal dispersivity from nonuniform flow tracer tests: *Journal of Hydrology*: v. 153, pp. 71-102.

## IX. APPENDICES

### APPENDIX A

#### Derivation of Partially Penetrating Slug Test Solution

In this section, the mathematical derivations of the solutions discussed in Section II.A are presented. For the sake of generality, the solutions are obtained in a dimensionless form. The solutions will be presented here as transform-space expressions. Information concerning the scheme used to numerically invert these expression to real space is given in Appendix B. Note that the expressions given here are only for the head within the stressed well. Solutions for heads outside the stressed well are given in Butler and McElwee (1994).

#### Confined Aquifer Solution

Equations (1)-(9) of Section II.A describe the flow conditions of interest here. To work with the most general form of the solution, this derivation is performed using dimensionless forms of (1)-(9). The dimensionless analogues of (1)-(9) are as follows:

$$\frac{\partial^2 \phi_i}{\partial \xi^2} + \frac{1}{\xi} \frac{\partial \phi_i}{\partial \xi} + \psi_i^2 \frac{\partial^2 \phi_i}{\partial \eta^2} = R_i \frac{\partial \phi_i}{\partial \tau} \quad (\text{A1})$$

$$\phi_i(\xi, \eta, 0) = 0, \quad \xi > 1, \quad 0 \leq \eta \leq \beta \quad (\text{A2})$$

$$\begin{aligned} \phi_1(1, \eta, 0) &= \Phi(0) = 1, \quad \zeta \leq \eta \leq \zeta+1 \\ &= 0, \quad \text{elsewhere} \end{aligned} \quad (\text{A3})$$



$$\phi_2(\infty, \eta, \tau) = 0, \tau > 0, 0 \leq \eta \leq \beta \quad (\text{A4})$$

$$\frac{\partial \phi_i(\xi, 0, \tau)}{\partial \eta} = \frac{\partial \phi_i(\xi, \beta, \tau)}{\partial \eta} = 0, \xi > 1, \tau > 0 \quad (\text{A5})$$

$$\int_{\xi}^{\xi+1} \phi_1(1, \eta, \tau) d\eta = \Phi(\tau), \tau > 0 \quad (\text{A6})$$

$$\frac{\partial \phi_1(1, \eta, \tau)}{\partial \xi} = \frac{\gamma}{\alpha} \frac{d\Phi(\tau)}{d\tau} \square(\eta), \tau > 0 \quad (\text{A7})$$

$$\phi_1(\xi_{nk}, \eta, \tau) = \phi_2(\xi_{nk}, \eta, \tau), 0 \leq \eta \leq \beta, \tau > 0 \quad (\text{A8})$$

$$\frac{\partial \phi_1(\xi_{nk}, \eta, \tau)}{\partial \xi} = \gamma \frac{\partial \phi_2(\xi_{nk}, \eta, \tau)}{\partial \xi}, 0 \leq \eta \leq \beta, \tau > 0 \quad (\text{A9})$$

where

$$\begin{aligned} \phi_i &= h_i/H_0; \\ \xi &= r/r_w; \\ \eta &= z/b; \\ \tau &= (tbK_{r2})/(r_c^2); \\ \psi_i &= (A_i/a^2)^{.5}; \\ A_i &= K_z/K_n; \\ a &= b/r_w; \\ R_i &= \gamma\alpha/2\lambda, i = 1, \end{aligned}$$

$$\begin{aligned}
&= \alpha/2, i = 2; \\
\lambda &= S_{a2}/S_{a1}; \\
\beta &= B/b; \\
\Phi &= \text{head in the stressed well} = H/H_0; \\
\gamma &= K_{a2}/K_{a1}; \\
\alpha &= (2r_w^2 b S_{a2})/r_c^2; \\
\Box(\eta) &= \text{boxcar function} = 0, \eta < \varsigma, \eta > \varsigma + 1, \\
&= 1, \text{ elsewhere}; \\
\varsigma &= d/b; \\
\xi_{sk} &= r_{sk}/r_w.
\end{aligned}$$

A solution can be obtained for (A1)-(A9) through the use of integral transforms (Churchill, 1972). A Laplace transform in time followed by a finite Fourier cosine transform in the  $\eta$  direction produce a Fourier-Laplace space analogue to (A1) of the following form:

$$\frac{\partial^2 \bar{\phi}_i}{\partial \xi^2} + \frac{1}{\xi} \frac{\partial \bar{\phi}_i}{\partial \xi} - (\psi_i^2 \omega^2 + R_i p) \bar{\phi}_i = 0 \quad (\text{A10})$$

where

$$\begin{aligned}
\bar{\phi}_i &= \text{the Fourier-Laplace transform of } \phi_i, f(\xi, \omega, p); \\
\omega &= \text{the Fourier-transform variable} = (n\pi)/\beta, n=0,1,2,\dots; \\
p &= \text{the Laplace-transform variable.}
\end{aligned}$$

The Fourier-Laplace space solution to (A10) is quite straightforward, as (A10) is simply a form of the modified Bessel equation (Haberman, 1987). A solution can therefore be proposed in the form:

$$\bar{\phi}_i = C_i K_0(\nu_i \xi) + D_i I_0(\nu_i \xi) \quad (\text{A11})$$

where

$$\nu_i = (\psi_i^2 \omega^2 + R_i p)^{1/2};$$

$C_i, D_i = \text{constants};$

$K_i = \text{modified Bessel function of the second kind of order } i;$

$I_i = \text{modified Bessel function of the first kind of order } i.$

Using the transform-space analogues of auxiliary conditions (A4) and (A6)-(A9), the constants in (A11) can be evaluated. Since the focus of interest in most slug tests is responses in the stressed well, only the transform-space expression for head at a radial distance of  $\xi=1$  is given here:

$$\bar{\phi}_1(1, \omega, p) = \frac{\gamma}{\alpha} [1 - p\Phi(p)] F_c(\omega) f_1 \quad (\text{A12})$$

where

$\Phi(p) = \text{Laplace transform of } \Phi(t), \text{ the nondimensional form of } H(t);$

$F_c(\omega) = \text{finite Fourier cosine transform of } \square(z)$

$$= \frac{2}{\omega} \sin\left(\frac{\omega}{2}\right) \cos\left(\frac{\omega(1+2\zeta)}{2}\right), \quad \omega = n\pi/\beta, \quad n=1, 2, 3, \dots,$$

$$= 1, \quad \omega=0;$$

$$f_1 = \frac{[\Delta_2 K_0(\nu_1) - \Delta_1 I_0(\nu_1)]}{\nu_1 [\Delta_2 K_1(\nu_1) + \Delta_1 I_1(\nu_1)]};$$

$$\Delta_1 = K_0(\nu_1 \xi_{\bullet}) K_1(\nu_2 \xi_{\bullet}) - \left[\frac{N}{\gamma}\right] K_0(\nu_2 \xi_{\bullet}) K_1(\nu_1 \xi_{\bullet});$$

$$\Delta_2 = I_0(\nu_1 \xi_{\bullet}) K_1(\nu_2 \xi_{\bullet}) + \left[\frac{N}{\gamma}\right] K_0(\nu_2 \xi_{\bullet}) I_1(\nu_1 \xi_{\bullet});$$

$$N = \nu_1 / \nu_2.$$

The application of an inverse finite Fourier cosine transform to (A12) for  $\eta$  within

the screen and utilization of the Laplace-space analogue of (A6) produces the following expression for head in the stressed well:

$$\Phi(p) = \frac{\gamma}{\alpha} [1 - p\Phi(p)]\Omega \quad (\text{A13})$$

where

$$\Omega = \int_{\xi}^{\xi+1} (F_c^{-1}(F_c(\omega) f_1)) d\eta;$$

$F_c^{-1}$  = inverse finite Fourier cosine transform.

Solving for  $\Phi(p)$  yields

$$\Phi(p) = \frac{\frac{\gamma}{\alpha} \Omega}{[1 + \frac{\gamma}{\alpha} p \Omega]} \quad (\text{A14})$$

Appendix B provides details of the Fast Fourier Transform scheme used to invert the expression in the  $\Omega$  term. The algorithm of Stehfest (1970) was used to perform the numerical Laplace inversion of (A14).

#### Unconfined Aquifer Solution

For the unconfined case, (A5) is replaced by the dimensionless analogues of (11) and (12):

$$\phi_i(\xi, 0, \tau) = 0, \quad \xi > 1, \quad \tau > 0 \quad (\text{A15})$$

$$\frac{\partial \phi_i(\xi, \beta, \tau)}{\partial \eta} = 0, \quad \xi > 1, \quad \tau > 0 \quad (\text{A16})$$

A solution for (A1)-(A4), (A6)-(A9), and (A15)-(A16) is obtained using the same approach as in the confined case. The Fourier-Laplace expression for head at a radial distance of  $\xi=1$  in the unconfined case can be written as:

$$\overline{\phi}_{1u}(1, \omega^*, p) = \frac{\gamma}{\alpha} [1 - p\Phi_u(p)] F_s(\omega^*) f_1 \quad (\text{A17})$$

where

$\overline{\phi}_{1u}$  = the Fourier-Laplace transform of  $\phi_{1u}$ , the nondimensional form of  $h_1$  for the unconfined case;

$\Phi_u(p)$  = the Laplace transform of the nondimensional form of  $H(t)$  for the unconfined case;

$F_s(\omega^*)$  = modified finite Fourier sine transform of  $\square(z)$

$$= \frac{2}{\omega^*} \sin\left(\frac{\omega^* (2\zeta + 1)}{2}\right) \sin\left(\frac{\omega^*}{2}\right);$$

$\omega^*$  = Fourier transform variable for the modified sine transform  
 $= (n\pi)/2\beta, n=1,3,5,\dots$

The application of an inverse modified finite Fourier sine transform to (A17) for  $\eta$  within the screen and rewriting in terms of  $\Phi_u(p)$  produces the following expression:

$$\Phi_u(p) = \frac{\frac{\gamma \Omega^*}{\alpha}}{[1 + \frac{\gamma}{\alpha} p \Omega^*]} \quad (\text{A18})$$

where

$$\Omega^* = \int_{\zeta}^{\zeta+1} (F_s^{-1}(F_s(\omega^*) f_1)) d\eta.$$

The modified finite Fourier sine transform employed in the unconfined case requires a bit of discussion. The standard finite Fourier sine transform is quite useful when a constant head is maintained at both boundaries. In the unconfined case, the upper boundary ( $\eta=0$ ) is defined as a constant-head condition while the lower boundary ( $\eta=\beta$ ) is defined as a no-flow condition. Churchill (1972) presents the modified finite Fourier sine transform

$$F_s(n) = \int_0^\beta f(\eta) \sin\left(\frac{n\pi\eta}{2\beta}\right) d\eta, \quad n=1,3,5,\dots \quad (A19)$$

as an example of a Sturm-Liouville transformation. When this modified sine transform is applied to the second-order derivative with respect to  $\eta$ , integration by parts yields

$$\int_0^\beta \frac{\partial^2 \phi_i}{\partial \eta^2} \sin\left(\frac{n\pi\eta}{2\beta}\right) d\eta = -\omega^{*2} \overline{\phi_i} + \omega^* \phi_i(0) - (-1)^n \frac{\partial \phi_i(\beta)}{\partial \eta} \quad (A20)$$

where

$$\omega^* = (n\pi)/2\beta, \quad n=1,3,5,\dots$$

For the boundary conditions employed here, (A20) reduces to

$$-\omega^{*2} \overline{\phi_i} \quad (A21)$$

## APPENDIX B

### Numerical Inversion Procedures

In this section, details of the procedures employed to numerically invert the transform-space expressions derived in Appendix A are presented. As discussed in section II.A, the Fast Fourier Transform (FFT) procedure was employed to perform the required Fourier transforms/inversions in this work. In order to demonstrate that the Discrete Fourier Transforms introduced negligible error into the numerically inverted solution, a comparison between the discrete solution and the continuous form is discussed.

For the confined case (cf. (A14)), a finite Fourier cosine transform was employed. The continuous form of this transform can be written as

$$F_c(n) = \int_0^\beta f(\eta) \cos\left(\frac{n\pi\eta}{\beta}\right) d\eta \quad (B1)$$

where

$F_c$  = finite Fourier cosine transform;

$f(\eta) = F_c(\omega)f_1$ .

In order to utilize the FFT procedure, (B1) is approximated using a Discrete Fourier Transform:

$$F_c(n) \approx \Delta \sum_{k=0}^{N-1} f(\Delta k) \cos\left(\frac{n\pi k}{N}\right), \quad n=0,1,2,\dots,N-1 \quad (B2)$$

where

$N$  = number of equally spaced points between 0 and  $\beta$ , must be an integer power of 2;

$\Delta = \beta/N$  = interval between equally spaced points.

For the unconfined case (cf. (A18)), a modified finite Fourier sine transform was employed. The continuous form of this transform can be written as

$$F_s(n) = \int_0^\beta f_{\omega}(\eta) \sin\left(\frac{n\pi\eta}{2\beta}\right) d\eta, \quad n=1,3,5,\dots \quad (B3)$$

where

$F_s$  = modified finite Fourier sine transform;

$f_{\omega}(\eta) = F_s(\omega^*)f_1$ .

Equation (B3) is only defined for odd numbered  $n$ 's. For ready implementation with standard FFT algorithms, (B3) is rewritten in terms of a continuous sequence of  $n$ 's:

$$F_s(n) = \frac{[1+(-1)^{n+1}]}{2} \int_0^\beta f_{\omega}(\eta) \sin\left(\frac{n\pi\eta}{2\beta}\right) d\eta, \quad n=1,2,3,\dots \quad (B4)$$

Equation (B4) is now approximated using a Discrete Fourier Transform :

$$F_s(n) = \frac{[1+(-1)^{n+1}]}{2} \Delta \sum_{k=1}^{N-1} f_{\omega}(\Delta k) \sin\left(\frac{n\pi k}{2N}\right), \quad n=1,2,\dots,N-1 \quad (B5)$$

Equations (B2) and (B5) can be directly implemented in standard FFT algorithms. In this work, an FFT algorithm given in Press et al. (1992) was employed. The total number of sampling points ( $N$ ) in  $\eta$  was constrained such that there would always be at least ten points within the screened interval.

In order to check on the approach outlined above, an additional series of simulations was performed in which the continuous forms of the finite Fourier transforms were employed for the required transforms/inversions. The  $\Omega$  term that is employed in (A14) can be written in the continuous form as:

$$\Omega = \frac{f_1(n=0)}{\beta} + \frac{8\beta}{\pi^2} \sum_{n=1}^{\infty} \frac{f_1(n)}{n^2} \sin^2 \frac{n\pi}{2\beta} \cos^2 \left( \frac{n\pi(1+2\zeta)}{2\beta} \right) \quad (B6)$$

The  $\Omega^*$  that is employed in (A18) can be written in the continuous form as:



$$\Omega^* = \frac{16\beta}{\pi^2} \sum_{n=1}^{\infty} [1 + (-1)^{n+1}] \frac{f_1(n)}{n^2} \sin^2 \frac{n\pi}{4\beta} \sin^2 \left( \frac{n\pi(1+2\zeta)}{4\beta} \right) \quad (\text{B7})$$

In all cases, the inversion of (B6) and (B7) produced results that were virtually indistinguishable from those found using a FFT algorithm with (B2) and (B5). The computational time, however, was significantly greater.

The inverse Laplace transform, the final step of the numerical inversion procedure, was performed here using the algorithm of Stehfest (1970). Sixteen terms were used in the summation of the Stehfest algorithm for all the cases examined in this work. Note that the procedures discussed here are implemented in a series of Fortran programs found in Hyder et al. (1993).